A study of polyaniline membranes for gas separations

A STUDY OF POLYANILINE MEMBRANES FOR GAS SEPARATIONS

by

YOGESH GUPTA

A Doctoral Thesis submitted to the Faculty of Engineering at Loughborough University in the partial fulfilment of the requirement for the degree of

DOCTOR OF PHILOSOPHY

in

Chemical Engineering

Advanced Separation Technologies Group

Department of Chemical Engineering

Loughborough University

ABSTRACT

Membrane based gas separations are proven to be technically attractive because of their simplicity and low energy costs, although they are often limited by insufficient flux, selectivity and stability. During the past thirty years, major developments in this technology have been made by developing high flux asymmetric membranes, and large surface area membrane modules. Today, in the present market, the sales of the membrane gas separation equipments have grown to become a $150 million per year business, and substantial growth in the near future is likely.

More than 90% of membrane gas separation business involves the separation of non-condensable gases, i.e., nitrogen from air, carbon dioxide from methane, and hydrogen from nitrogen, argon, or methane. However, a large potential market for membrane gas separation lies in refineries. The separations of hydrogen/hydrocarbon and olefin/paraffin are regarded as import processes (although challenging ones) in the petrochemical industry. The membrane based separation process to separate olefins from paraffins is likely to be developed to the commercial state in the next few years. Industry's demands for increasing the separation effectiveness and productivity have encouraged conducting research into development of new membrane materials. Polyaniline is regarded as, so far, the best alternative for gas separations, since the molecular spacing of polymer chains can be controlled by its interesting doping/dedoping chemistry.

A novel method to make reproducible defect-free dense self-supported polyaniline films with the thicknesses between 2 and 6 μm, and polyaniline nano-film membranes with selective polyaniline layer thicknesses between 300 and 800 nm supported on a porous polyvinylidene fluoride (PVDF) substrate is developed. Various undoped self-supported polyaniline (EB) films (polyaniline film thickness = 2 to 6 μm), and polyaniline/PVDF composite membranes (selective polyaniline layer thickness = 300 to 800 nm) were tested to measure their transport properties for various pure gases such as H_2, CO_2, O_2, N_2, CH_4, C_2H_4, C_2H_6, C_3H_6 and C_3H_8. The ideal (pure gas) selectivities ($\alpha_{A/B}$) obtained for the gas pairs H_2/N_2 (348), H_2/O_2 (69.5), H_2/CO_2 (8.6), CO_2/O_2 (8.1), CO_2/N_2 (40.4), H_2/C_3H_8 (757), CO_2/C_3H_8 (256), in the case of undoped self supported

polyaniline films, were considerably higher than those obtained by other researchers, which surpass the selectivities of the majority of the conventional polymeric materials. The results obtained during this work were reproducible for both self-supported polyaniline films and ultrathin polyaniline films supported on a porous PVDF substrate.

The thickness of the polyaniline membrane seemed to have an effect on the productivity (pressure normalised flux) of the permeating gases. The productivity values obtained for all permeating gases were significantly higher in the case of ultrathin polyaniline membranes. The productivity increased almost linearly with decreasing polyaniline film thickness. The pure gas selectivity values for various gas pairs through ultrathin polyaniline membranes supported on porous PVDF substrate (selective polyaniline layer thickness = 0.4 to 1.37 μm) were similar to those of self-supported polyaniline membranes (selective polyaniline film thickness = 2 to 3 μm).

The permeation behaviour of binary gas mixtures (i.e. O_2-N_2, CO_2-O_2 and CO_2-N_2) through self-supported polyaniline membranes and polyaniline/PVDF composite membranes at various feed compositions was investigated. The pure gas and mixed gas selectivity values were similar for the non-polar mixed gas system (O_2-N_2 mixed gas system). The model suggested, to predict mixed gas permeance, is good for achieving the accurate permeance values for non-polar mixed gas systems.

Extraordinarily high gas transport rates (GTR) were obtained for polyaniline based nano-membranes. GTR for various gases were higher by a magnitude of 10^4 than those reported for self-supported polyaniline membranes.

From the industrial point of view, the productivity (permeance) can be significantly increased by using ultrathin polyaniline membranes having higher permeability and gas flux with the similar separation efficiency for various gas pairs.

Key words: Polyaniline, gas separation, polyaniline nano-membranes, composite membranes, productivity, permeance, separation efficiency.

ACKNOWLEDGEMENT

I would like to thank my supervisors, Prof. Richard J Wakeman and Dr. Klaus Hellgardt, for their constant supervision and guidance over the past three years. Their pursuit of excellence, enthusiasm and total commitment as educators have made this work possible. Special recognition is also paid to their incredible patience, fruitful discussions and excellent ideas throughout the research. Furthermore, I would like to thank Prof. Wakeman for his proof reading of this dissertation.

I would also like to express my utmost appreciation for the Postgraduate Studentship given by the Department of Chemical Engineering, Loughborough University, for making this research possible.

I am deeply indebted to the staff in the laboratory and the workshop, who were always available to help during the period of my experimental work.

A special thank to Mr. Peter Chapman at Imperial College, London (Prof. Andrew G Livingston's Research Group), for his help to analyse polymer samples with Gel Permeation Chromatography (GPC).

The support from all student colleagues is also acknowledged for their practical assistance, know-how and constantly providing creative ideas. I would also like to thank the staff members of Pilkington Library for their continuous help.

At the end I would like to extend my sincere regards and gratitude to my parents. This sojourn would have been tougher and endless had the love, support, affection, guidance and directive criticism not been there. Acknowledging their love and support is beyond my wits and words.

LIST OF CONTENTS

CHAPTER 1 – INTRODUCTION

CHAPTER 2 – LITERATURE REVIEW

CHAPTER 3 – EXPERIMENTAL TECHNIQUES

LIST OF APPENDICES

LIST OF FIGURES

CHAPTER 1 – INTRODUCTION

CHAPTER 2 – LITERATURE REVIEW

CHAPTER 3 – EXPERIMENTAL TECHNIQUES

CHAPTER 4 – RESULTS AND DISCUSSION

LIST OF TABLES

CHAPTER 1 – INTRODUCTION

CHAPTER 2 – LITERATURE REVIEW

CHAPTER 4 – RESULTS AND DISCUSSION

Chapter 1

INTRODUCTION

1. THE EARLY YEARS – *A SCIENTIFIC TOOL*

The earliest studies on transport of gases and vapours in polymeric membranes were necessarily concerned with natural polymers. The work which followed was mainly concerned with natural and synthetic elastomers, all well above their glass transition temperatures, mainly hydrocarbon in nature, and non-crystalline. Systematic studies of membrane phenomena can be traced to the 18^{th} century philosopher scientists. For example, Jean Antoine (Abbè) Nollet [1] coined the word *osmosis* to describe the permeation of water through a diaphragm in 1748. By the 19^{th} century, the simple form of the *solution-diffusion* model had been derived and checked [2,3], and by 20^{th} century, the time lag method to determine the diffusion coefficients had been developed [4,5]. Thomas Graham in 1829 [2] observed that a wet pig bladder inflated to the bursting point when placed in an atmosphere of carbon dioxide. In 1831, a systematic study of the permeation rates of ten different gases through natural rubber was reported by Mitchell [6,7]. A few papers regarding gas transport in rubber appeared in the interim, but the next major breakthrough was the publication of remarkable paper by Graham in 1863 [8], which truly laid the foundation for today's membrane science and technology. However, a major advancement in the field of gas and vapour transport in polymer membranes was achieved in the 20^{th} Century by Daynes [4,5] in 1920. He developed the so-called "*time lag*" method, which is the basis of most of the gas and some of the vapour transport studies made today.

Fundamental studies of gas transport in polymers other than rubbers began with the classical work of Meares [9] in 1954. He was the first to demonstrate the theories about the break in the Arrhenius plots at the glass transition temperature and to speculate approximately two modes of solution in glassy polymers. Later studies were initiated with many polymers by Barrer,

Mitchell and their co-workers together with important contribution by Brandt, Stern, and many others [10].

By 1960, the elements of modern membrane science had been developed. However, the membranes were used only in few laboratories and small specialized industrial applications. There was no significant membrane industry and total sales of membranes for all applications probably did not exceed $20 million per year. Membranes suffered from four problems that prohibited their widespread use: they were too unreliable, too slow, too unselective, and too expensive. Partial solutions to each of these problems have been developed during the last 30 years, and as a result there is a surge of interest in membrane-based separation techniques.

In the early 1960s, the seminal discovery that transformed the membrane separation from a laboratory to an industrial process was the development of the Loeb-Sourirajan process of making a defect-free, high-flux, ultrathin Reverse Osmosis (RO) membranes [11]. These membranes consist of an ultrathin, selective surface film supported on a microporous support that provides the mechanical strength. The first Loeb-Sourirajan membranes had fluxes 10 times higher than any membrane available during that period, which made reverse osmosis a practical technology. Using such processes, including interfacial polymerisation or multilayer composite casting and coating, it is now possible to prepare membranes as thin as 0.1 μm or less. Methods of packaging membranes into spiral wound, hollow fibre, capillary and plate and frame modules were also developed, and advances were made in improving membrane stability. As a result, by 1980 microfiltration, ultrafiltration, reverse osmosis and electrodialysis were all established processes with large plants installed around the world. During the past thirty years, membranes have become known to have the potential to separate important gas mixtures, but the technology to fabricate high performance membranes and modules economically was lacking. Today, the membrane gas separation technology has grown from a simple laboratory scale to an industrial scale with a significant technical and commercial impact, and a considerable amount of work is in progress in academic and industrial laboratories in order to improve the economics of the extant membrane processes for gas separations, as well as to extend the range of applications of this technology.

2. MOTIVATION AND OBJECTIVES

Within the last three decades, major developments in the membrane gas separation technology have been made by developing high-flux asymmetric membranes [11], and large surface area membrane modules [12,13]. Today in the present market, the sales of membrane gas separation equipments have grown to become a $150 million per year business, and substantial growth in the near future is likely [14].

Membrane based separation processes are proven to be energy efficient and technically attractive when compared to the traditional separation methods such as distillation, cryogenic, adsorption and absorption processes [15]. These traditional separation processes are based on differing physical or chemical properties of the stream's components, and do not allow separation of stream components having similar physical or chemical properties. The introduction of membrane technology to separate these components has provided a break-through to carry out these separations. Membrane based separation processes offer a number of significant advantages. First, energy requirements, and in some cases also capital investment costs, are lower than the conventional separation processes for a number of important industrial processes. Second, the necessary process equipment is simple, compact, and relatively easy to operate and control.

The immediate challenges faced by current membrane technology can essentially be summarised into a few key areas. Achieving higher permselectivity for the relevant application with at least equivalent productivity is the first of these challenges. Maintaining these properties in the presence of complex and aggressive feeds is the second challenge. A third challenge in certain applications is the need for recompression of the desired product.

Many polymeric materials are known that offer intrinsically attractive properties. That is, when the permeation performance of a film of the material is measured under laboratory conditions, using pure gas samples and operating conditions at modest temperature and pressure conditions, the film exhibits high permeability for some pure gases and low permeability for others, suggesting useful separation capability. Two-thirds of the total gas separation market has involved the separation of nitrogen or water from air and hydrogen from ammonia

purge gas or syngas. These gas streams are clean, and free from components that might foul or plasticise the membrane. However, growing application areas for membranes are in refineries, where the gas streams contain high levels of plasticising, condensable vapours that degrade membrane performance. Hydrogen/hydrocarbon and olefin/paraffin separation are some of the most important processes in the petrochemical industries. Ethylene and propylene are produced in larger quantities than any other organic substance in these industries. Due to very low relative volatility for olefin/paraffin gas mixtures, the separation is currently carried out by energy intensive cryogenic distillation processes [16]. These distillation columns are often up to 90 meters tall and typically contain over 200 trays with reflux ratios greater than 10, and require very high energy input to carry out the separation. According to a report by DOE, 1.27×10^{14} KJ (3.024×10^{6} tonne of fuel oil equivalent) of energy is used annually for olefin/paraffin distillation [17].

Membrane separation technology has been proposed to be a potential alternative approach to the conventional distillation process for olefin/paraffin separations [18-48]. Currently, only eight or nine polymer materials (see Table 1.1) have been used to make at least 90% of the total installed gas separation membrane base, and only a few of them are used for olefin/paraffin separations.

Table 1. 1 Principal gas separation markets and membrane systems (2000) [14].

Company	Principal Membrane Material Used	Module Type
Permea (Air Products)	Polysulfone	Hollow fibre
Medal (Air Liquide)	Polyimide/polyaramide	
IMS (Paraxair)	Polyimide	
Generon (MG)	Tetrabromo polycarbonate	
GMS (Kvaerner)	Cellulose acetate	Spiral-wound
Separex (UOP)		Hollow fibre
Cynara (Natco)		
Aquilo	Polyphenylene oxide	
Parker-Hannifin	Polyimide	
Ube	Silicone Rubber	Plate-and-frame
GKSS Licensees		Spiral-wound
MTR		

These materials remain susceptible to severe loss of performance through plasticisation and to catastrophic collapse if contacted by liquid hydrocarbons.

Several failures have been reported in refinery applications where these conditions occur. This low process reliability has caused a number of process operators to discontinue applications of membrane separation for hydrogen recovery from hydrocarbons and olefin/paraffin gas separations.

A great deal of research has been performed on improved membrane materials for hydrogen/hydrocarbon separations. During the past few years, several hundred new polymer materials have been reported, and many of them have substantially higher permeability and selectivities than those listed in Table 1.1. The permeabilities and olefin/paraffin selectivities of the conventional polymer membranes are generally too low for an economically viable process. In particular, the performance of polymeric membranes for ethylene/ethane separation is very poor. Currently, the best polymeric membrane exhibit ethylene/ethane selectivities of only 4 to 5 at room temperature, and propylene/propane selectivities of up to 16 [18-48].

Thus, the need remains to discover new membrane materials that will provide and maintain adequate performance under the conditions of exposure to hydrocarbons which are commonplace in refineries, chemical plants, and gas fields. The preferred membrane material for refinery gas separation applications should combine high selectivity (or separation efficiency) with high permeation flux (or productivity) along with durability and mechanical integrity at the operating conditions.

3. RAISON D'ETRE FOR THIS PROJECT

Refinery gas streams contain contaminants such as water vapour, acid gases, olefins, aromatics, and other hydrocarbons. At relatively low concentrations, these contaminants cause membrane plasticisation and loss of selectivity. At higher concentration they can condense on the membrane and cause irreversible damage to it. In the case of hydrogen/hydrocarbon separations, when a feed stream is introduced into a membrane system, the hydrogen permeates faster through the membrane and the gas remaining on the feed side becomes progressively enriched in hydrocarbons, raising the dew point [14]. For example, if the total hydrocarbon content increases from 60% in the feed gas to 85% in the residue gas, the dew point may increase by as much

as 25 C, or more, depending on the hydrocarbon mixture (see Figure 1.1). Maintaining this hydrocarbon rich mixture in a gas phase may require heating up this mixture at 60 C to 80 C or even more, which is costly and may itself eventually adversely affect the mechanical integrity of the membrane. Failure to do so means, the hydrocarbon stream may enter the liquid phase region of the phase diagram before it leaves the membrane module, and condense on the membrane surface, damaging it beyond recovery.

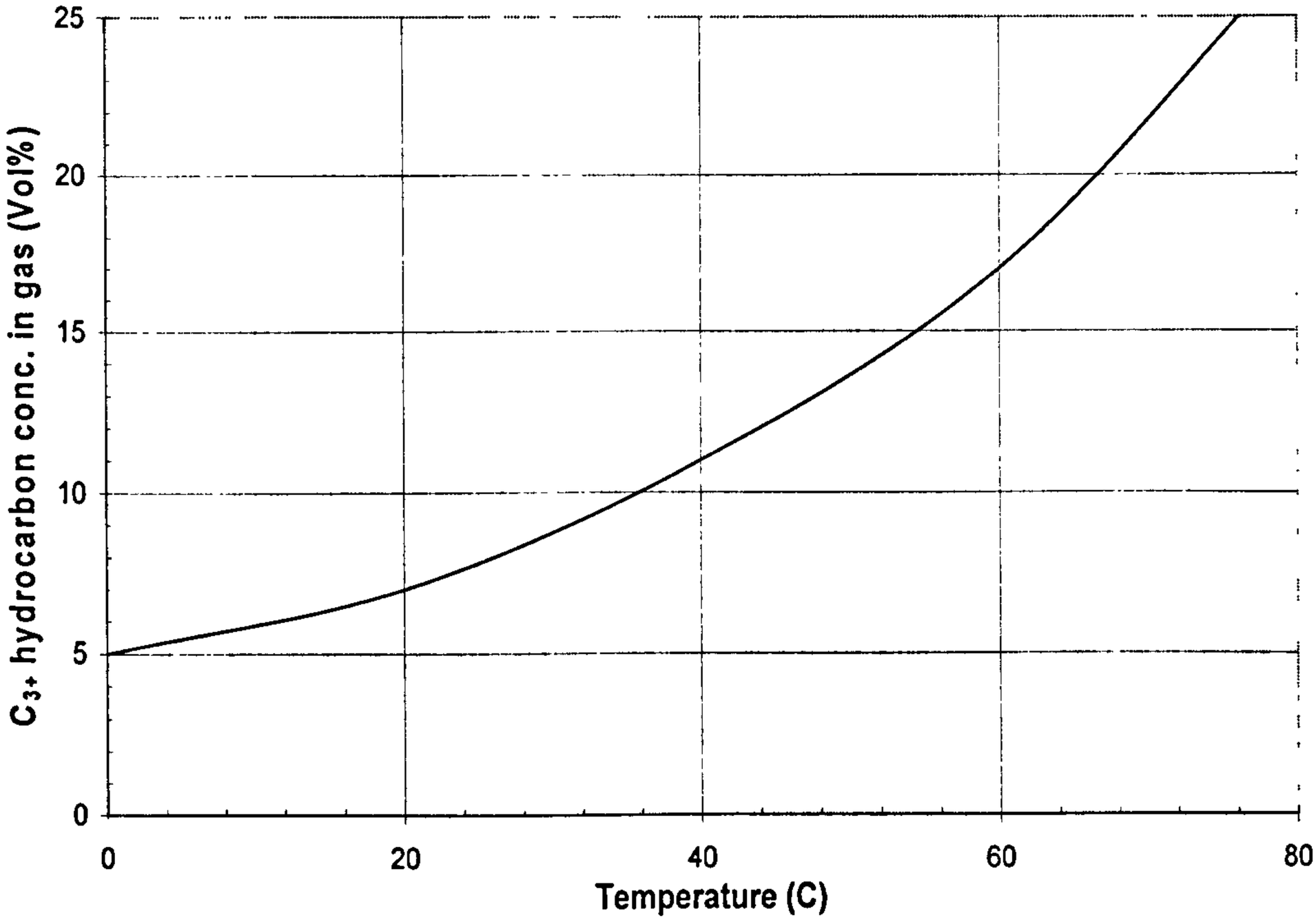

Figure 1. 1 Illustration of the hydrocarbon condensation problem on the residue side of a hydrogen-permeable membrane. As hydrogen is removed from the pressurised feed, the gas becomes enriched in condensable hydrocarbons, and its dew point increases [14].

Many refinery gas separation applications require the use of amorphous glassy polymeric materials for hydrogen/hydrocarbon gas separations. Recently, much of the attention has been directed to the application of conducting polymers for gas separation purposes [49-62]. The conducting polymers are unique types of polymers, which have π-conjugated electrons spread along the polymer backbone and have delocalised electron structure after doping. Polyaniline – refer to a very important class of electronic/conducting polymer – has the generalised composition (see Figure 1.2):

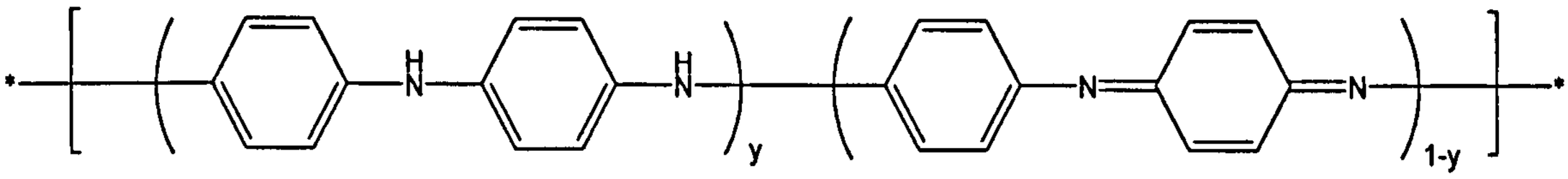

Figure 1. 2 The generalised composition of polyaniline [63].

which consists of alternating reduced (see Figure 1.3(i)), and oxidised (see Figure 1.3(ii)), repeat units [64,65].

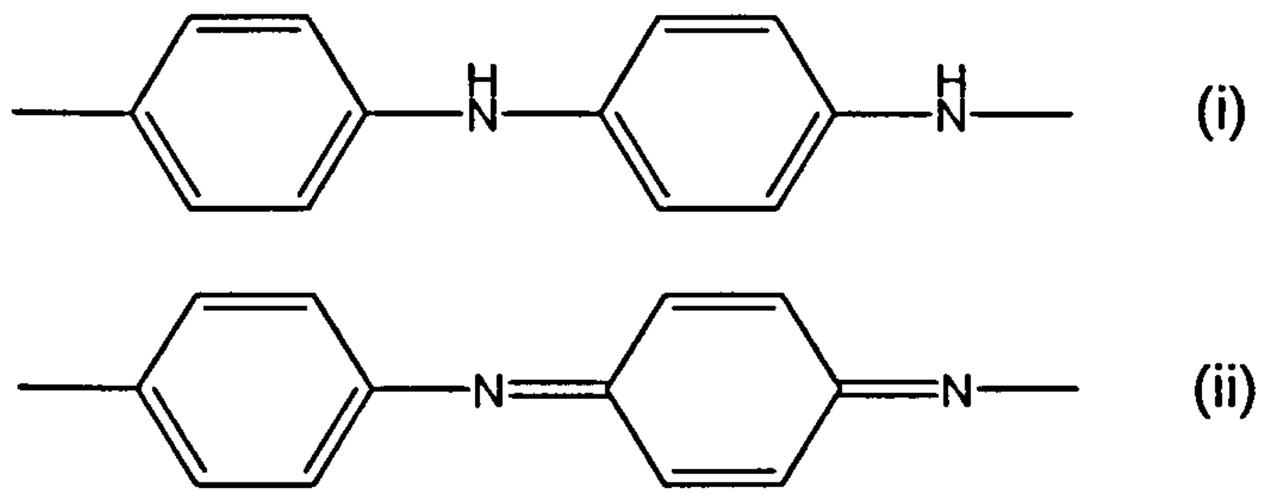

Figure 1. 3 (i) quinoid rings (reduced repeat units); (ii) benzenoid rings (oxidised repeat units).

The *average* oxidation state *(1-y)* can be varied continuously from zero to give the completely reduced polymer (leucoemeraldine) (see Figure 1.4(i)), to 0.5 to give the *"half oxidised"* polymer (emeraldine) (see Figure 1.4(ii)), to 1 to give the completely oxidised polymer (pernigraniline) (see Figure 1.4(iii)) [66,67]. The wide range of associated electrical, electrochemical and optical properties, coupled with good mechanical properties, makes polyaniline very attractive as a membrane material [51-53].

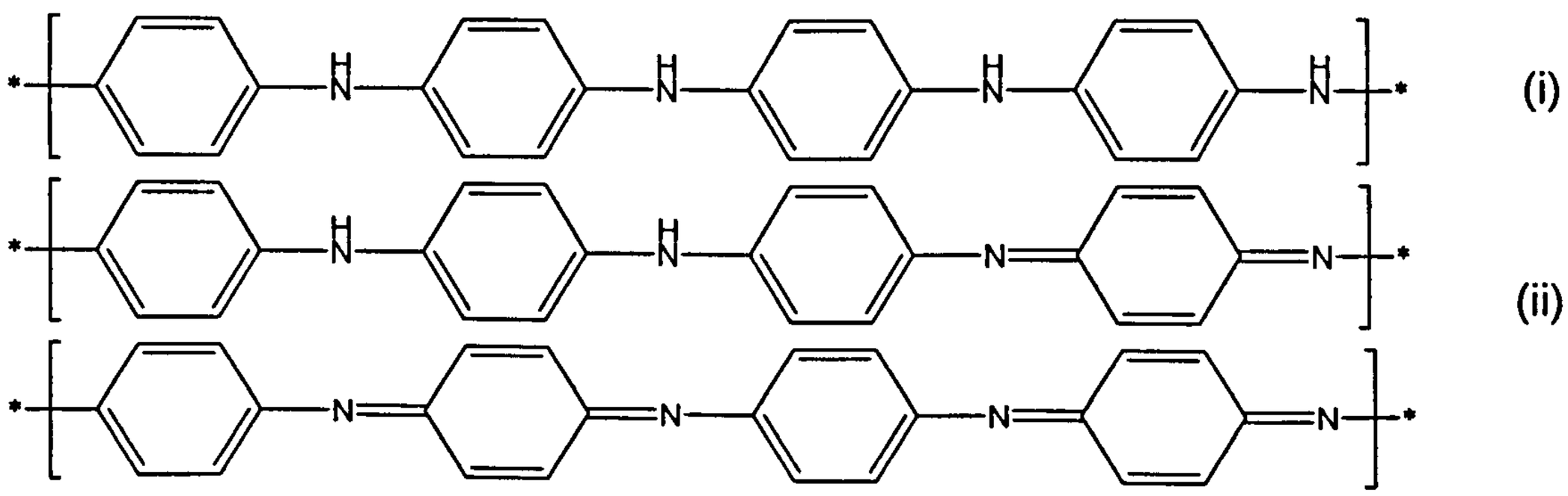

Figure 1. 4 (i) reduced leucoemeraldine form; (ii) half-oxidised emeraldine form; (iii) completely oxidised pernigraniline form.

Polyaniline can undergo a simple acid/base doping/dedoping chemistry enabling control over properties such as free volume [54], solubility [55], electric

conductivity [56], and optical activity [57,58]. Since the precise level of doping can be controlled simply by varying the pH of the doping acid solution, morphology of the polyaniline can be tuned even after the membrane has formed [64,65]. The reversible doping characteristic of polyaniline has been utilised in previous studies to investigate the effects of different dopants and their concentrations on gas permeability [50-62]. The nature of dopant and its concentration was found to have an effect on gas permeability and separation efficiency, as the doping of acids changes the ion selectivity of polyaniline [68], which enhances selectivities for various gas pairs through polyaniline membranes.

Polyaniline tends to be fairly impermeable compared with rubbery or elastomeric polymers, so the application potential for gas selective polyaniline membranes has been limited. The use of polyaniline membranes for gas separation applications requires the production of a thin dense selective layer of polyaniline supported on a porous substrate. The permselective polyaniline layer should be as thin as possible to achieve significant gas flux, and the substrate should have good mechanical and chemical strength with negligible gas transport resistance. The use of polyaniline membranes for gas separation applications has been limited, as there are no reports where sufficiently thin (<1 μm) selective layer has been has been generated to achieve commercially attractive gas transport rates. The gas separation process will be more efficient if the selectivity is high. Capital cost can be reduced by increasing gas transport rate (GTR) as less membrane area is required for the desired separation. In the absence of defects, the selectivity is a function of the membrane material properties at the operating conditions and the productivity is a function of the membrane material properties as well as the thickness of the barrier. The size of a membrane package is proportional to the membrane area. Since, the gas transfer is proportional to the membrane area; it remains unchanged for a reduction in both thickness and area by a common factor. This reduction, however, results in an equivalent reduction of the package size. Hence, for many applications, the minimum size of the package (and area of the membrane) will be limited by membrane thickness.

The aim of the present work is to develop a novel technique to produce defect-free self-supported polyaniline films and determine the application

potential of these membranes for hydrogen/hydrocarbon and olefin/paraffin gas separation applications, along with a model to interpret the transport and separation data. It is also proposed to find methods that will enhance the gas flux (productivity) and separation efficiency (performance) of polyaniline membranes, which involves extending the novel concept to produce polyaniline nano-membrane films on a porous substrate. The proposal also extends to doping polyaniline membranes with silver (Ag(I)) and test these membranes to evaluate permeability and selectivity values for ethylene/ethane and propylene/propane gas separations.

In particular, applicability of polyaniline membranes for hydrogen/hydrocarbon and olefin/paraffin (ethylene/ethane and propylene/propane) separations will be investigated, together with the effect of film/membrane thickness on gas transport rate and separation efficiency.

4. OUTLINE

The research presented in this thesis deals exclusively with gas separation through polymeric (polyaniline) membranes. The dissertation has been written as a collection of chapters which deal with the research objectives.

The first chapter (Introduction) provides a critical background about the state of art of membrane gas separation and points out the objectives of the research.

The second chapter (Literature Review) offers a general theoretical background concerning membranes for gas separation applications and the transport mechanisms involved. Various transport models to understand transport through polymeric membranes have been discussed. Trends and possible avenues for refinery gas separation applications (hydrogen purification and olefin/paraffin gas separations) with high performance membranes have been highlighted. At the end, the use of polyaniline as a potential alternative membrane material for these critical gas separation applications has been considered.

At the beginning of the third chapter (Experimental Techniques) the synthesis route to prepare polyaniline powder has been described, followed by the detailed descriptions regarding the techniques (such as FTIR spectroscopy,

UV-Vis spectroscopy, FEGSEM, density measurements, gel permeation chromatography) used to characterise the polyaniline powder. The detailed description of the novel technique developed to prepare self-supported polyaniline membranes and polyaniline nano-film membranes has been given later in the chapter. Finally, the experimental techniques (such as FEGSEM, AFM, mechanical properties, gas permeation measurements) used to characterise both, the self-supported polyaniline and the polyaniline/PVDF composite membranes have been described in details. The experimental tools (e.g. single gas and mixed gas permeation measurement set-ups), developed for the determination of the mass transport behaviours of polyaniline membranes, are also described in detail in this chapter.

In chapter four (Results and Discussion) the application potential of polyaniline membranes for gas separation purposes is emphasised. The gas transport properties of self-supported polyaniline and polyaniline/PVDF composite membranes are investigated and discussed. The effect of a selective polyaniline layer thickness on the productivity and separation effectiveness is investigated to explain the application potential of ultrathin polyaniline membranes for industrial gas separation applications. Finally, the correlation between selectivity and permeability (Robeson's plots) of polyaniline membranes for various gas pairs is discussed to place into context the potential to use ultrathin polyaniline membranes having higher permeability and gas flux with similar separation efficiency for various gas pairs for industrial gas separation applications.

Finally, the results obtained in this research are summarised in the last chapter and suggestions are given for future research work.

Chapter 2

LITERATURE REVIEW

Several books and reviews are available in the literature about gas transport through polymers and polymer membranes [69-105]. Membranes have been commercialised for liquid-liquid and liquid-solid separations long before being applied to gas separations. The knowledge gained during these years was then gradually transferred to gas separating membrane systems. Today, gas separation with polymer membranes is rapidly becoming a mainstream separation technology.

This chapter serves as a brief background concerning membranes for gas separation applications and the transport mechanisms involved. The substantial body of theoretical models on the sorption behaviour of polymers and polymeric membranes is reviewed. Trends and possible avenues for ongoing practical development for hydrogen/hydrocarbon and olefin/paraffin gas separations with high performance membranes are highlighted, with references given to more detailed analyses of these approaches. Finally, conducting polymers have been suggested to be the ideal candidates for critical refinery gas separation applications, and the application potential for polyaniline membranes is discussed within this context.

1. FUNDAMENTALS

Membranes have gained an important position in chemical technology and are used in a broad range of applications. Fundamental issues control the ability of the membrane materials and membrane structures to contribute to high productivity (permeance) and selectivity for important gas mixtures. To obtain a better understanding of the significance of membrane structures and their use in separation processes, a brief discussion of two aspects is essential:

- The basic properties and functions of synthetic membranes
- The driving forces and fluxes involved in separation processes.

1.1. Transport Parameters

The active layers of membranes used for gas separations are dense and do not separate species on the basis of an ordinary sieving mechanism. Separation using these dense membranes is achieved by the *solution-diffusion* mechanism [69,72,90,106-113]. Mass transport thorough a dense, selective polymeric membrane occurs according to a solution (sorption) step at the upstream side of the membrane, followed by diffusion through the membrane and a desorption step on the downstream side (see Figure 2.1).

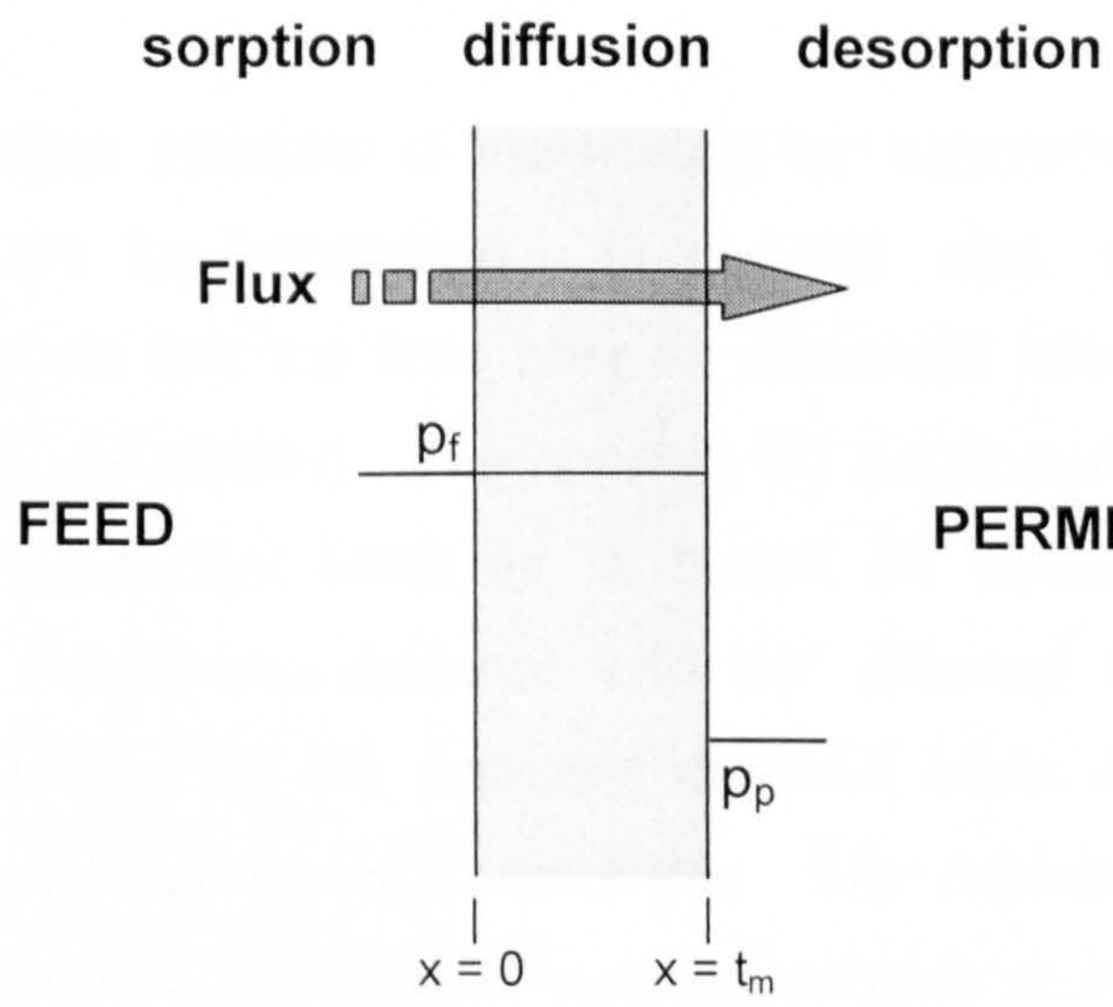

Figure 2. 1 Schematic representation of mass transport phenomena occurring in a *solution-diffusion* membrane.

The total amount of mass transported through a membrane is characterised by its permeability, *P*. The permeability indicates the rate at which permeate traverse through a membrane. It is a characteristic value for a specific polymer-penetrant system and quantifies the flux, *J*, which can be defined by:

$$J = P \cdot \frac{\Delta p}{dx} \qquad (2.1)$$

where $\Delta p / dx$, is the pressure gradient across the membrane with the film thickness, t_m. According to *solution-diffusion* mode, permeability is a product of diffusivity, *D*, and solubility, *S*;

$$P = D \times S \tag{2.2}$$

The solubility coefficient, *S*, is a measure of the amount of gas sorbed by the membrane when equilibrated with a given pressure of gas at given temperature. It is a thermodynamic parameter that is dependent on the amount of free volume, the condensability of the penetrant, and the degree to which the permeant interacts with the polymer matrix. The diffusion coefficient, *D*, indicates how fast a penetrant is transported through the membrane. It is a kinetic parameter, which is related to the polymer chain mobility or flexibility and permeating species.

Thermodynamics provides a framework for separation but it does not provide a mechanism for separation. In general, size, charge and affinity between the membrane and the feed play an important role in determining the selectivity (separation efficiency). The capacity of *solution-diffusion* membranes to separate multi-component mixtures is based on specific thermodynamic interactions of the membrane material with the different components in the mixture, and furthermore, on the selective diffusive mass transport through a dense homogeneous layer of the membrane. The selective diffusion of the penetrant molecules through a layer of a dense polymer is mainly influenced by the molecular structure of the polymer. Short range motions in the polymer chains, like chain bending, bond rotation and phenyl ring flips depend on the molecular structure, which allow penetrant molecules to proceed in the direction of the driving force [114,115]. The power to separate two constituents in a gas is given by the ratio, α, the separation factor, defined by:

$$\alpha_{i/j} = \frac{P_i}{P_j} = \frac{S_i \cdot D_i}{S_j \cdot D_j} \tag{2.3}$$

From which, it can be seen that the separation factor is a product of a thermodynamic factor (relative solubility) and a kinetic factor (relative diffusivity).

2. GENERAL THEORETICAL BACKGROUND

The gas stream to be separated is fed to a membrane device at an elevated pressure, where it passes across one side of the membrane (see Figure 2.2). The opposite (permeate) side of the membrane is held at a lower pressure. The pressure and/or concentration difference across the membrane provide the driving force for the gas to permeate through the membrane.

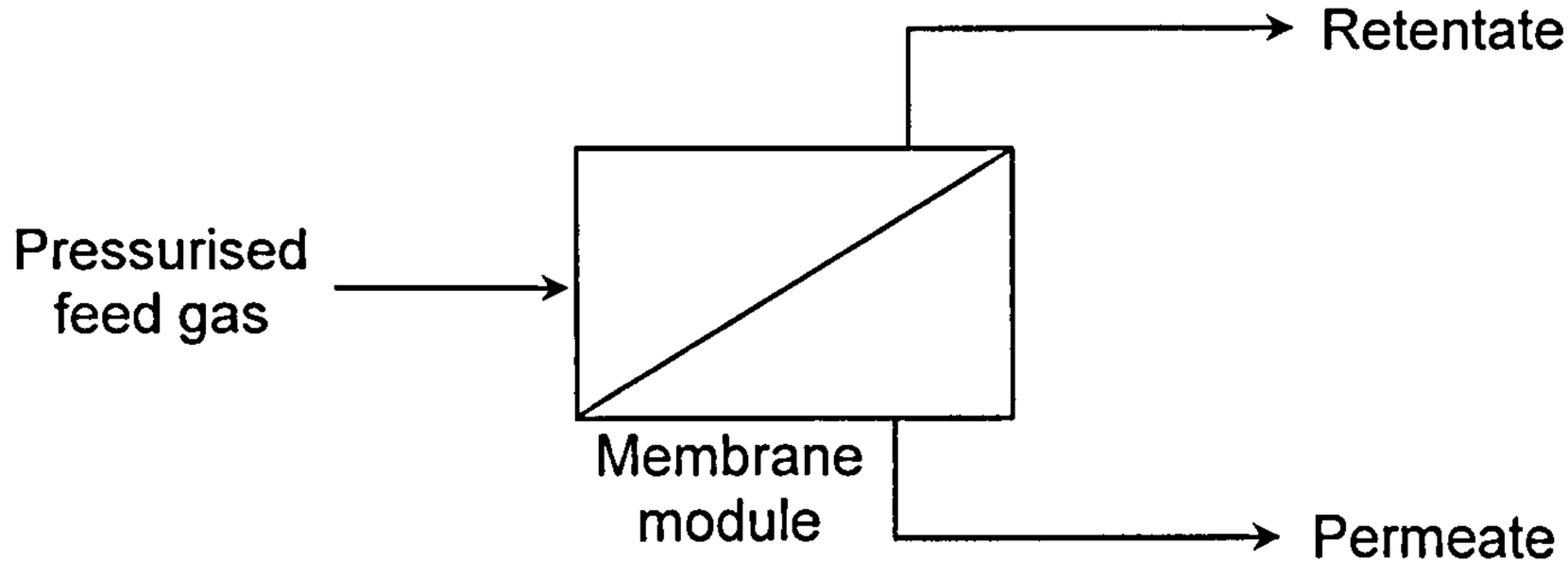

Figure 2. 2 Schematic of gas separation membrane module.

Separation is achieved because of the differences in the relative transport rates of the feed components. Components that diffuse more rapidly become enriched in the low-pressure *"permeate"* stream, while the slower components are concentrated in the *"retentate"* or *"residue"* stream. The degree to which components are separated is governed by the ability of the membrane to discriminate between those components, as well as by the relative driving force of each component. The ideal membrane material must have high permeability coupled with high permselectivity for a gas pair. If a membrane system were permitted to go to equilibrium, permeation would continue to occur until the pressure and composition of gas on both sides of membrane were equal, with no separation being achieved. Separation is achieved only if the system is maintained away from the equilibrium. The size of the permeant species can be significant factor in determining both permeability as well as permselectivity [107].

A membrane will separate gases only if some components pass through the membrane more rapidly than others. This requirement places constraints on the structure of the membrane's separating selective layer, as described in Figure 2.3.

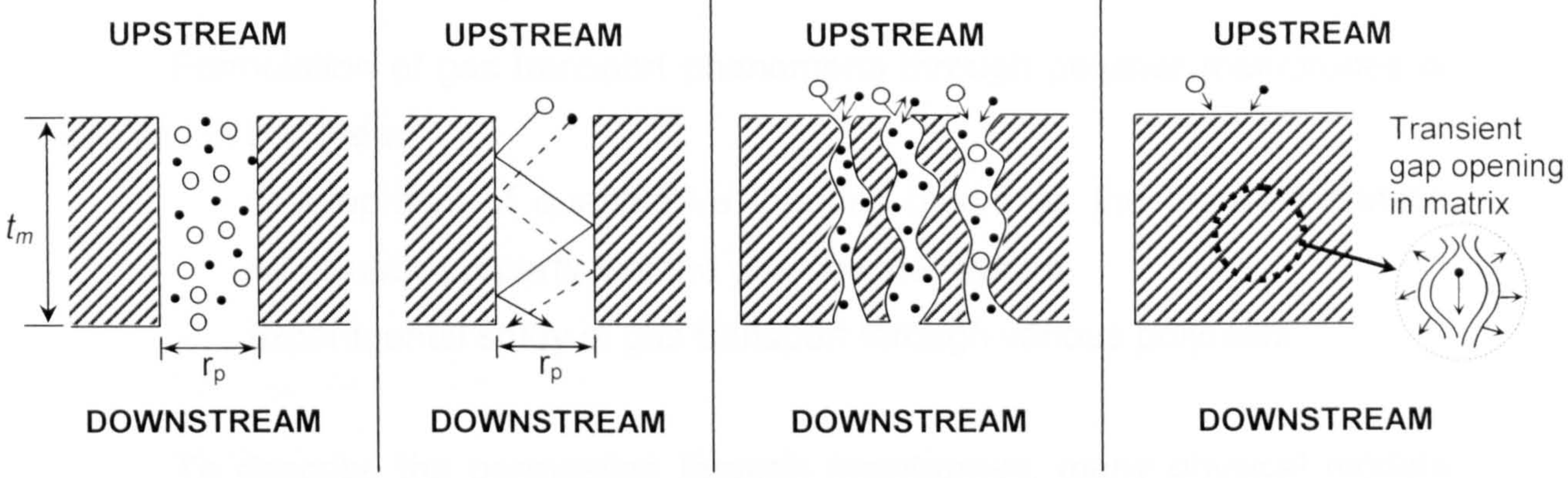

Figure 2. 3 Membrane Based Gas Transport and Separation Mechanisms [16].

If the membrane pores are relatively large, i.e. from 0.1 to 10 μm, gases permeate through membrane by convective flow, and no separation will occur. If the pores are smaller than 0.1 μm, then the pore diameter is the same size or smaller than mean free path of the gas molecules, and convective flow is replaced by *Knudsen diffusion*. For Knudsen diffusion, the transport rate of any gas is inversely proportional to the square root of its molecular weight. Finally, if the membrane pores are extremely small (of the order of 5 to 20 Å) then the gases are separated by molecular sieving. Transport through this type of membranes is complex and includes both diffusion in gas phase and diffusion of adsorbed species on the surface of the pores (surface diffusion). Commercial application of porous membranes for gas separation has not yet been realized. It is difficult to fabricate membranes with a narrow pore size distribution that is required for molecular sieving, and current materials are fragile. In addition, water and other vapours can condense within the fine pores and affect the transport rates across the membranes.

The membranes currently used in most commercial gas separation applications are non-porous or *solution-diffusion* membranes. In the next sub-section, the detailed phenomenon involved for the mass transfer in *solution-diffusion* membranes is discussed.

2.1. Membrane Transport Models

Formulation of gas transport phenomena through polymer membranes is directed in two areas:

- development of quantitative theories based on the thermodynamics and kinetic properties of the gas-polymer system
- experimental study of gas transport through various polymers.

To describe the permeation through membranes, many physical models have been proposed which are mainly based on thermodynamics and/or statistical mechanical principals, thus expressing permeation rates by parameters derived from bulk properties. Several authors [116,117] related the sorption and transport phenomena to molecular properties such as rigidity of polymer backbones, types of pendant group, molecular packing density, and interactions with polar groups, but this is still very qualitative. The later route represents the most fundamental scientific approach. In existing theories distinction is made between membrane separations of liquids and that of gases. In the literature usually one of the following three theories/models are used to describe the transport in dense membranes [89,118]:

- Irreversible thermodynamics
- Preferential sorption – capillary flow theory
- Solution – diffusion theory.

Since diffusion is the only possible transport mechanism in dense membranes, a diffusion coefficient appears, directly or indirectly, in all three models mentioned above.

2.1.1. Irreversible Thermodynamics

In models based on non-equilibrium or irreversible thermodynamics, the membrane is treated as a *"black box"* barrier separating two phases far from equilibrium. This procedure is useful, especially when the structure of the membrane is not known and the mechanism of transport within it is not fully understood. Less information is required to set up the model, but less

information can be obtained from it about the transport mechanism within the membrane.

For application of irreversible thermodynamics the basic assumption is made that the system can be divided into small subsystems in which *"local equilibria"* exist, so that they can be described by thermodynamic parameters [117]. Thus at least locally, the system is not too far from the equilibrium which might be correct for the slow transport processes observed in membranes.

Equations for transport rates (fluxes), retention and other membrane related parameters can be derived using general thermodynamic equations [119,120]. For example the flux for each component, J_i, is described by;

$$J_i = \sum_{k=1}^{n} L_{ik} \cdot F_k \qquad (2.4)$$

where the phenomenological coefficients, L_{ik}, are often complex functions of compositions and concentrations. The driving forces F_k, are chemical potential gradients, and described by;

$$F_k = \left(\bar{\upsilon} \cdot \frac{dp}{dx} + \frac{d\mu_k^c}{dx} \right) \qquad (2.5)$$

where, the first term indicates the pressure gradient and the second term expresses the concentration related gradients.

According to the friction model, the generalised force acting on solute *k* in the membrane is balanced by the frictional force between solute *k* and the membrane, and that between two solutes *k* and *j;*

$$F_k = \sum f_{kj} \cdot (u_k - u_j) + f_{km} \cdot u_k \qquad (2.6)$$

where u_k and u_j are the linear velocities of solute *k* and *j* in the membrane. In practice, the friction coefficients, f_{km}, are always larger than the free fraction coefficients, f_{kj}, which are related to diffusion coefficients, D_{kj}, by;

$$f_{kj} = \frac{RT}{N_{av} D_{kj}} \tag{2.7}$$

In a binary solution f_{kj} can be described as;

$$f_{kj} = 6\pi\eta R_s \tag{2.8}$$

in which, R_s is the Stoke's radius of the solute, which makes it difficult to get quantitative values for various friction coefficients, especially values of f_{km}. More information about the models based on irreversible thermodynamics is reviewed by Soltanieh and Gill [118].

2.1.2. Preferential Sorption – Capillary Flow Theory

Soltanieh and Gill [118] pointed out that, the concept of simple *"sieving filtration"* for separation on the basis of molecular size is ruled out in reverse osmosis. In late 1950s, Reid and Breton [121] proposed a model in which the membrane is preferentially wetted by water, forming an absorbed film that prevents solute ions from entering the membrane. Sourirajan [11,122] used the same principle and assumed that the mechanism of reverse osmosis is partly governed by surface phenomena and partly by fluid transport under pressure through capillary pores. The water layer thus formed is passed through the pores, as shown schematically in Figure 2.4.

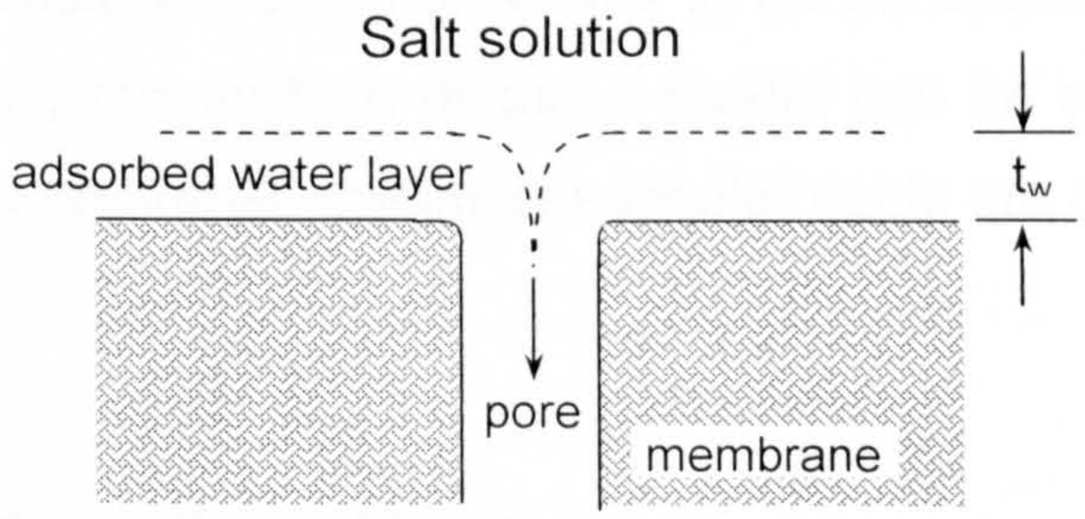

Figure 2. 4 Preferential sorption capillary flow – Sourirajan model [122].

According to this figure, there exists a critical pore size that yields optimum solute retention and fluid permeability, which should be twice the thickness of the sorbed water layer, t_w. Sourirajan also assumed that this pore size could be

several times larger than salt or water molecular diameters and still show reasonable separation.

This model is based on a capillary flow model with viscous flow of water and/or diffusion of the solute, while the "*film theory*" is applied for salt transport through the adsorbed water layer. If the pores in the dense membrane are small enough then the transport phenomenon takes place at the pore walls. Surface diffusion, or surface flow, can take place when the residence time of the molecule at the pore wall is larger than zero. Depending on the migration energy and the surface diffusivity, a molecule can move along a pore wall. Because of the differences in energies and diffusivities, some selectivity in transport rate can result. For component, i, the flux J_i, due to surface diffusion can be described as;

$$J_i = -C' \cdot D_i \left(\frac{dC_i}{dp} \right) \Delta p \qquad (2.9)$$

where C' is a geometrical parameter that depends on the pore system, and (dC_i/dp) can be determined from adsorption isotherm. The surface diffusion coefficient, D_i, is a function of the temperature;

$$D_i = D_{0i} \cdot exp(-E / RT) \qquad (2.10)$$

where D_{0i} depends on the main surface free path length, the jump frequency and the surface concentration.

Though the existence of pores seems to be contradictory to the tightness of dense membranes, this surface diffusion model can be used to describe the transport in dense membranes, the intermolecular voids are considered to be the *"pores"*.

2.1.3. The Solution-Diffusion Model

The *solution-diffusion* model [69,72,90,106-113] has emerged as the most widely accepted explanation of transport in dialysis, reverse osmosis, gas permeation and pervaporation. The model allows these membrane separation processes to be described by a series of simple interrelated equations.

In gas separations, gas dissolves in the *solution-diffusion* membrane material and diffuses through the membrane down a gradient of driving force (pressure, concentration, temperature). Gas transport across the dense (essentially pore free) polymers can be considered as a process comprising three successive steps:

- sorption of penetrant in the polymer membrane (feed–side)
- diffusion of penetrant through the polymer membrane matrix
- desorption from the polymeric film (permeate–side).

A number of assumptions must be made to define the *solution-diffusion* model of permeation. Usually, the first assumption governing transport through membranes is that the fluids on either side of the membrane are in equilibrium with the membrane material at the interface. The second assumption is the pressure within the membrane is uniform and that the chemical potential across the membrane is expressed only as a concentration gradient which is generated by a combination of pressure and concentration differences between the feed and permeate phases separated by the membrane. The third assumption is that the rates of absorption and desorption at the membrane interface are much higher than the rate of diffusion through the membrane.

The sorption/desorption and diffusion steps are dependent on the characteristics of the membrane material and the gases, and are studied separately with various sorption and diffusion models. The sorption models are based on the thermodynamics of the penetrant-membrane interaction, with the diffusion is primarily modelled with Fick's laws of diffusion [123], presented in different forms [124]. Ideally, the *solution-diffusion* model can only be applied to the polymers above their glass transition temperatures [69].

2.1.3.1. Macroscopic (Continuum) Models

The permeation of pure gases and gas mixtures through *nonporous* polymer membranes is a complex process, which is controlled by the diffusion of the penetrant gas molecules in the membrane matrix. Under the conditions that usually prevail in separation processes, the diffusion process generally satisfies Fick's two laws [123]. Figure 2.5 is a schematic of the transport mechanism of

solution-diffusion through a membrane, where the membrane and the permeants are one single membrane phase.

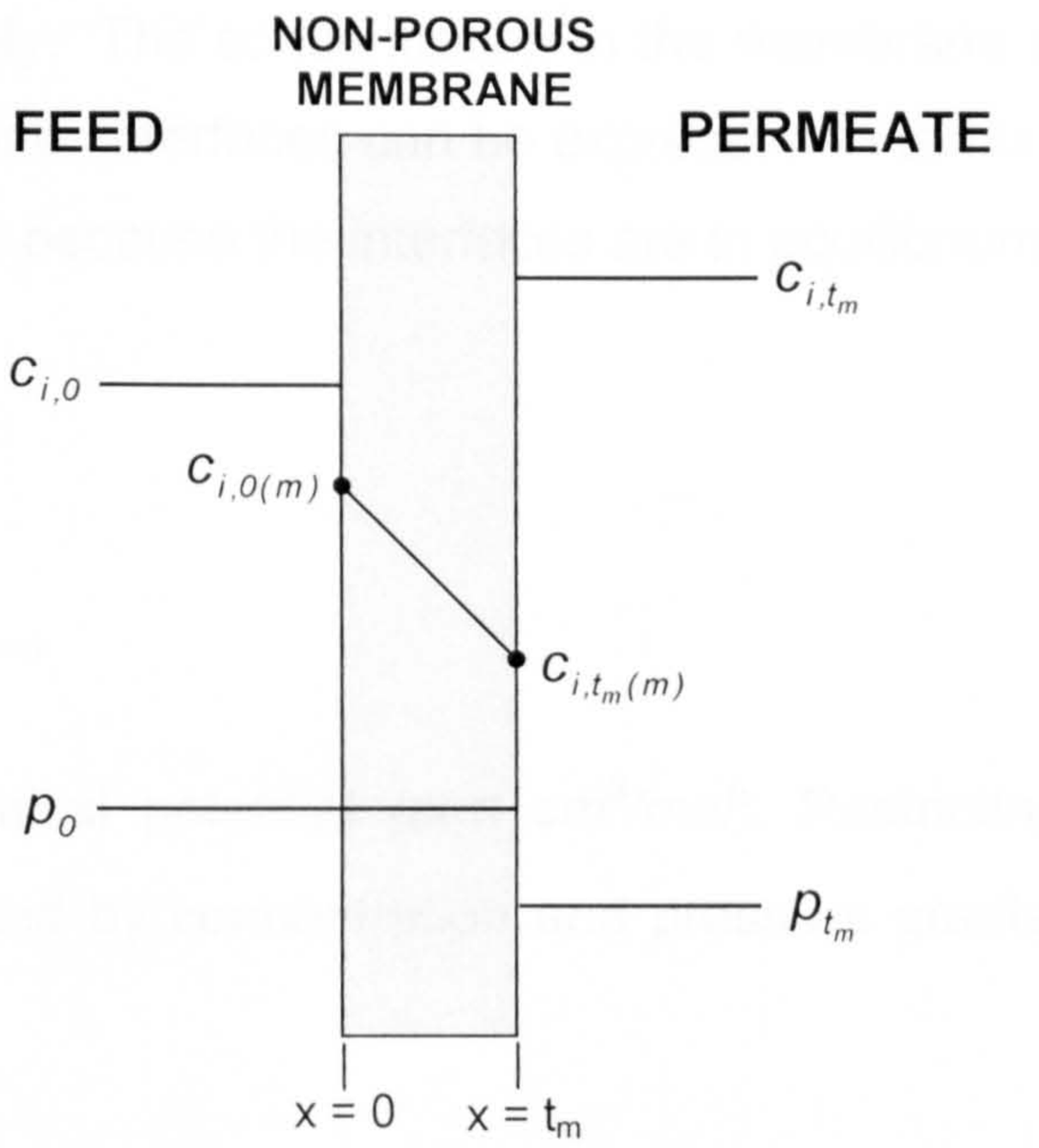

Figure 2. 5 Concentration (*c*) and pressure (p) profiles in *solution-diffusion* through nonporous membranes [125].

The entire feed side membrane phase is at feed pressure, and the pressure steps down from the feed pressure to the permeate pressure at the membrane/permeate interface. The rate of diffusive transport in the membrane is given by Fick's law of diffusion, which for molar fluxes is;

$$J_i = -\frac{D_i}{m_i} \cdot \frac{dc_{i(m)}}{dx} \tag{2.11}$$

where J_i is the molar rate of transfer of component *i* or molar flux *(mol/cm²s)*, D_i is the diffusion coefficient *(cm²/s)*, m_i is the molar weight of *i* *(g/mol)*, and the term $dc_{i(m)}/dx$ is concentration gradient of *i* in the membrane.

Integration of equation 2.11 over the thickness of the membrane, t_m, gives;

$$J_i = \rho_m D_i \cdot \frac{n_{i,o(m)} - n_{i,t_m(m)}}{t_m} \tag{2.12}$$

where ρ_m is the molar density of the membrane phase (mol/cm^3) and the subscripts *0(m)* and $t_m(m)$ denote the feed side and permeate side of the membrane, respectively. The concentration in the membrane at feed/membrane and membrane/permeate interfaces can be expressed in terms of concentrations outside the membrane because the interfaces are in equilibrium states;

$$\mu_{i,o} = \mu_{i,0(m)} \tag{2.13}$$

and;

$$\mu_{i,t_m} = \mu_{i,t_m(m)} \tag{2.14}$$

where μ is the chemical potential *(atm cm^3/mol)*. Restricting the analysis to driving forces generated by concentration and pressure gradients, the chemical potential is written as;

$$d\mu_i = R \cdot T \cdot d(ln(\gamma_i n_i)) + \upsilon_i \cdot dp \tag{2.15}$$

where R is the gas constant *(82 atm cm^3/mol K)*, T is the temperature *(K)*, n_i is the mole fraction *(mol/mol)* of component *i*, γ_i is the activity coefficient of the component *i* in the membrane, p is the pressure *(atm)*, and υ_i is the molar volume of component *i (cm^3/mol)*.

In compressible gases, the molar volume changes with pressure and using the ideal gas law to integrate the equation 2.15, gives;

$$\mu_i = \mu_i^o + R \cdot T \cdot ln(\gamma_i n_i) + R \cdot T \cdot ln\left(\frac{p}{p_i^{sat}}\right) \tag{2.16}$$

where μ_i^o is the reference chemical potential of pure *i* at the saturation vapour pressure of *i*, p_i^{sat} *(atm)*. The equilibrium equations 2.13 and 2.14 then take the following form for a gas phase in contact with membrane, and within the membrane (where it is suitable to assume that the gas is incompressible).

$$\mu_i^o + R \cdot T \cdot ln(\gamma_i n_i) + R \cdot T \cdot ln\left(\frac{p}{p_i^{sat}}\right)$$

$$= \mu_i^o + R \cdot T \cdot ln(\gamma_{i(m)} n_{i(m)}) + \upsilon_{i(m)}(p - p_i^{sat}) \tag{2.17}$$

In gas separation, the membrane is in contact with upstream and downstream gas phases, and the equilibrium equations for the two membrane interfaces are (assuming the activity coefficient is constant in upstream and downstream gas phases);

$$\mu_i^o + R \cdot T \cdot ln(\gamma_i n_{i,o}) + R \cdot T \cdot ln\left(\frac{p_o}{p_i^{sat}}\right)$$

$$= \mu_i^o + R \cdot T \cdot ln(\gamma_{i(m)} n_{i,o(m)}) + \upsilon_{i(m)}(p_o - p_i^{sat}) \qquad (2.18)$$

and;

$$\mu_i^o + R \cdot T \cdot ln(\gamma_i n_{i,t_m}) + R \cdot T \cdot ln\left(\frac{p_{t_m}}{p_i^{sat}}\right)$$

$$= \mu_i^o + R \cdot T \cdot ln(\gamma_{i(m)} n_{i,t_m(m)}) + \upsilon_{i(m)}(p_{t_m} - p_i^{sat}) \qquad (2.19)$$

which yield the following equations 2.20 and 2.21 for the mole fraction of the component *i* at the membrane feed and membrane permeate interfaces, respectively.

$$n_{i,o(m)} = \frac{\gamma_i}{\gamma_{i(m)}} \cdot \frac{p_o}{p_i^{sat}} n_{i,o} \cdot exp\left(\frac{-\upsilon_{i(m)}(p_o - p_i^{sat})}{R \cdot T}\right) \qquad (2.20)$$

and;

$$n_{i,t_m(m)} = \frac{\gamma_i}{\gamma_{i(m)}} \cdot \frac{p_{t_m}}{p_i^{sat}} n_{i,t_m} \cdot exp\left(\frac{-\upsilon_{i(m)}(p_o - p_i^{sat})}{R \cdot T}\right) \qquad (2.21)$$

By introducing a gas phase sorption coefficient K_i (atm^{-1});

$$K_i = \frac{\gamma_i}{\gamma_{i(m)} p_i^{sat}} \qquad (2.22)$$

Hence, equations 2.20 and 2.21 become;

$$n_{i,o(m)} = K_i \cdot p_o \cdot n_{i,o} \cdot exp\left(\frac{-\upsilon_{i(m)}(p_o - p_i^{sat})}{R \cdot T}\right) \qquad (2.23)$$

and;

$$n_{i,t_m(m)} = K_i \cdot p_{t_m} \cdot n_{i,t_m} \cdot exp\left(\frac{-\upsilon_{i(m)}(p_o - p_i^{sat})}{R \cdot T}\right) \quad (2.24)$$

which can be combined with the diffusion equation 2.12 to yield for the gas transport equation;

$$J_i = \rho_{(m)} \frac{D_i K_i}{t_m} \cdot exp\left(\frac{-\upsilon_{i(m)}(p_o - p_i^{sat})}{R \cdot T}\right) \cdot (n_{i,o} p_o - n_{i,t_m} p_{t_m}) \quad (2.25)$$

or,

$$J_i = \frac{P_i}{t_m} \cdot exp\left(\frac{-\upsilon_{i(m)}(p_o - p_i^{sat})}{R \cdot T}\right) \cdot (n_{i,o} p_o - n_{i,t_m} p_{t_m}) \quad (2.26)$$

The Poynting correction factor i.e. the exponential term in equation 2.26, is close to unity [126] in most gas separation applications because the molar volume of the permeants involved are relatively small (vapour separation being a potential exception). Hence, equation 2.26 can be reconfigured as;

$$J_i = \frac{P_i}{t_m} \cdot (n_{i,o} p_o - n_{i,t_m} p_{t_m}) = \frac{P_i}{t_m} \cdot (p_{i,o} - p_{i,t_m}) \quad (2.27)$$

Equation 2.27 is widely used to rationalise the properties of gas permeation membranes accurately and predictably.

A quantitative measure of the amount of mass transported through the polymeric membrane is characterised by the permeability coefficient, P_i *(mol cm/(cm^2 s atm))*, which is defined by;

$$P_i = \rho_{(m)} D_i K_i = \frac{\rho_{(m)} \gamma_i D_i}{\gamma_{i(m)} p_i^{sat}} \quad (2.28)$$

According to the *solution-diffusion* model, the permeability is a product of a thermodynamic factor called solubility coefficient, and a kinetic parameter called diffusion coefficient. Hence, a more common way of expressing the permeability coefficient is;

$$P_i = D_i \cdot S_i \tag{2.29}$$

where D_i and S_i are the diffusivity and solubility coefficients for component *i*.

Since the gas permeability is independent of the thickness of the membrane, it is a fundamental property of membrane materials, but it does not consider the detailed *solution-diffusion* nature of the process [16]. To achieve this description, the gas permeability is described as the product of a mobility (kinetic)-related term and a solubility (thermodynamic)-related term. According to the previous research [127], the diffusion coefficient is a measure of the amount of energy required for the penetrant to execute a diffusive jump through the polymer matrix and the intrinsic degree of segmental packing in the matrix. It is determined by packing and motion of the polymer segments and by size and shape of the penetrating molecules. On the other hand, the solubility coefficient depends on the condensability of the penetrant, the extent of the polymer-penetrant interactions, and the amount of excess volume existing in the glassy polymer. In general, the quantity, S_i, is thermodynamic in nature and is affected by polymer-penetrant interactions as well as excess inter-chain gaps in glassy polymers. The average diffusion coefficient, D_i, is kinetic in nature and largely determined by polymer-penetrant dynamics.

The ability of the membrane to separate gases is characterized by the separation factor. When the downstream pressure is negligible relative to the upstream pressure, then the selectivity or the separation factor, $\alpha_{i,j}$, of the polymeric membrane towards the different penetrant gases *i* and *j* is commonly expressed as;

$$\alpha_{i,j} = \frac{P_i}{P_j} = \frac{D_i \cdot S_i}{D_j \cdot S_j} \tag{2.30}$$

For the special case in which the absolute downstream pressure is close to zero, the above ratio of permeabilities is referred to as the *"ideal"* separation factor. In the absence of plasticising effects due to high levels of penetrant sorption, the separation factor for a mixed gas case, $\alpha_{i,j}$, can be closely approximated by the ratio of pure gas permeabilities for individual components *i* and *j* [128,129].

For the cases in which the downstream pressure cannot be ignored, the real separation factor can be defined by;

$$\alpha_{i,j} = \frac{y_i / y_j}{x_i / x_j} \tag{2.31}$$

where, y_i, x_i and y_j, x_j refer to the mole fraction of component *i* and *j* in the product and feed streams, respectively.

Clearly, in separation applications, the actual separation efficiency observed may be lower than the ideal selectivity, because the driving force term will not be equal to unity for non-zero downstream partial pressures. Nevertheless, this factor can be determined by the ideal selectivity and operating conditions are specified so it does not present serious complications.

2.1.3.2. Microscopic Models

Many theoretical models have been proposed in the literature to describe the mechanism of gas transport in polymers (by diffusion) and through polymer membranes (by permeation) on macroscopic level. Such models provide expressions for gas diffusion coefficients or permeability coefficients, or both, derived from free-volume, statistical mechanical, energy, structural, or other considerations. The formulation of these coefficients is complicated by the fact that the gas transport occurs by markedly different mechanisms in rubbery and glassy polymers, i.e., at the temperatures above and below the glass-transition temperature, T_g, of the polymers, respectively. Additional complications are due to polymer plasticisation (swelling) by penetrant gas, polymer crystallinity, pre-treatment (particularly in glassy polymers), etc.

As a result, the mechanisms of gas transport in polymers are incompletely understood, particularly below T_g, when considered on a microscopic level. The reader is encouraged to refer to the references [69,72,108,110-112,130-135] to understand the transport mechanism at microscopic level.

2.1.3.2.1. Transport in Rubbery Polymers

The transport models for gas transport in "rubbery" polymers are based on *free-volume* concepts. Such models commonly relate mutual diffusion coefficients for a gas/polymer system to the free volume of the system, and thereby to the concentration of the penetrant gas in the polymer. Reviews of various free-volume models have been published in [110-112,130-135].

One of the simplest free-volume models is that of Fujita [136], which describes the strong concentration dependence of organic vapours in some rubbery polymers. The sorption of low molecular weight penetrants in rubbery materials is typically described by the Henry's law for cases in which the sorbed concentrations are low [105];

$$c = k_D \cdot p \qquad (2.32)$$

where c is the gas concentration in the polymer $(cm^3_{STP}/cm^3_{polymer})$, k_D is the Henry's law coefficient $(cm^3_{STP}/cm^3_{polymer}atm)$, and p is the penetrant partial pressure.

For rubbery polymers and with low concentrations of penetrant, the diffusion coefficient is typically constant and the permeability is independent of the feed pressure as indicated in equation 2.33.

$$P = k_D D \qquad (2.33)$$

For rubbery polymers in the presence of high activity gases or vapours, deviations from the Henry's law sorption are observed. Sorption and permeation isotherms in such cases are typically strongly convex to the pressure axis. In the absence of strong polymer-penetrant interactions, the Flory-Huggins expression represented by equation 2.34 provides a satisfactory description of penetrant solubility for such behaviour [137].

$$ln(p/p_o) = ln(1-\phi_p)+\phi_p+\chi\phi_p^2 \qquad (2.34)$$

where, p is the penetrant partial pressure, p_o is the vapour pressure of the penetrant, ϕ_p, is the volume fraction of the polymer, and χ, is the so-called

Flory-Huggins parameter. For such cases the polymer is likely to be highly swollen, which may result in a concentration-dependent diffusion coefficient.

2.1.3.2.1.1. Free-Volume Theory

A number of free volume models of gas transport in and through polymers have been proposed, but some of these models have not been tested with a sufficient variety of experimental data or have not been tested at all. However, phenomenological transport models based on free-volume concepts are likely to become obsolete during the coming era due to the development of computational techniques of simulating polymer microstructures.

The free volume theory of transport postulates that movement of molecules depends on the free volume available as well as the availability of energy sufficient to overcome polymer-penetrant attractive forces [138]. The specific volume of the polymer is comprised of three components: the occupied volume, which is the volume of the equilibrium liquid at 0 K; the interstitial free volume, which is small and distributed uniformly throughout the material; and the hole free volume, which is large enough to facilitate molecular transport. Redistribution of interstitial free volume requires a large energy input. However, redistribution of hole free volume requires no additional energy, so this volume randomly migrates through the polymer matrix. Random mobility of the hole free volume may facilitate both a slow inter-diffusion of polymer chains as well as penetrant transport.

The flux of the penetrant can be written in terms of local volume fraction of penetrant in polymer, ϕ, and the mutual diffusion coefficient, D [139];

$$J = -\frac{D}{1-\phi}\cdot\frac{d\phi}{dx} \qquad (2.35)$$

If the partial molar volume of penetrant can be approximated by gaseous molar volume in organic liquids, the volume fraction of penetrant can be estimated from the penetrant sorption level. The relationship between the thermodynamic diffusion coefficient, D_T, and the mutual diffusion coefficient, D, is given by;

$$D_T = \left(\frac{D}{1-\phi}\right)\left[\frac{d\ln a}{d\ln\phi}\right]_T^{-1} \tag{2.36}$$

Because gases exhibit a relatively low solubility in polymers the term $\left[\frac{d\ln a}{d\ln\phi}\right]_T$ is ~ 1.0 [139]; hence, the flux can be expressed by;

$$J = -D_T \cdot \frac{d\phi}{dx} \tag{2.37}$$

The fractional free volume, V_f, in a polymer has been expressed as a linear function of temperature, pressure and concentration.

$$V_f = \phi_{fs}^{o} + \Delta\alpha(T - T_s) - \Delta\beta(p - p_s) + \gamma\phi \tag{2.38}$$

where ϕ_{fs}^{o} is the fractional free volume of the pure polymer at the reference temperature, T_s (or T_g), and pressure, p_s. Generally, the reference temperature T_s is chosen as the glass transition temperature T_g, and the reference pressure p_s is 1 atm. The terms $\Delta\alpha$ and $\Delta\beta$ are typically taken as the difference in the thermal expansion coefficients and compressibilities above and below T_g, respectively. The parameter γ is used to characterize the ability of the penetrant to plasticise the polymer. The dependence of self-diffusion coefficient on fractional free volume can be given as [136,140];

$$D_i = R \cdot T \cdot A_d \, exp\left(\frac{-B_d}{V_f}\right) = u_i R \cdot T \tag{2.39}$$

where A_d and B_d are related to the size and shape of the penetrant molecule and must be determined empirically, and V_f is the fractional free volume, which can be determined by equation 2.38. The term u_i is the so-called "*mobility*" of the penetrant, and is the inverse of the "*resistance coefficient*" of the medium.

2.1.3.2.2. Transport in Glassy Polymers

A glassy polymer is a polymeric material that is below its softening or glass transition temperature under the condition of use. Gas transport through glassy polymers has been the focus of intense research because of favourable separation properties observed with these polymers. However, full characterisation of the gas transport and separation properties of a glassy polymer is limited by the time dependent changes of the polymer's physical properties. These changes are important in evaluating the performance of the polymer during its anticipated service life. Attempts have been made to explain the observed time-dependent transport behaviour at a molecular level [141-152]. Models have been proposed to describe the observed transport behaviour based upon statistical, mechanical-structural, and thermodynamic considerations. The "hole" vacancy theory, the activated complex theory and the fluctuation theory are the three basic theories used to explain these models, which are originally derived from free volume molecular theory.

Due to more restricted segmental motions in glassy polymers, these materials offer enhanced "mobility selectivity" as compared to rubbery polymers. Because they are inherently more size and shape selective than rubbery materials, glassy polymers are more commonly used as the selective layer in gas separation membranes. Table 2.1 shows the diameter of several common gases [153]. Glassy polymers are able to discriminate effectively between extremely small differences in molecular dimensions of common gases. Solubility often dominates diffusional characteristics for transport in rubbery polymers.

The concept of free volume has been used qualitatively to describe the non-equilibrated nature of the polymer. However, the model is limited by its quantitative description of the nature of polymer chain mobility and free volume size distribution. The simplicity of the free volume theory, a single parameter model, has been the important reason for its wide application in gas transport studies through polymeric membrane [153].

Table 2. 1 Kinetic sieving dimensions of penetrants based on zeolite sorption cut-offs [153].

Molecule	Kinetic Diameter (Å)
He	2.60
H_2	2.89
NO	3.17
CO_2	3.30
Ar	3.40
O_2	3.46
N_2	3.64
CO	3.76
CH_4	3.80
C_2H_4	3.90
C_3H_8	3.96
n-C_4	4.30
CF_2CL_2	4.30
C_3H_6	4.40
CF_4	4.50
i-C_4	4.70

The physical characteristic of glassy polymers that is commonly linked to the complex sorption isotherm is the *"unrelaxed"* volume locked into the materials when they are quenched below the glass transition. As illustrated in Figure 2.6, there is a break in the volume *vs* temperature plot for a polymer as the temperature is lowered below the glass transition T_g, the excess or *"unrelaxed volume"* is $V_g - V_l$.

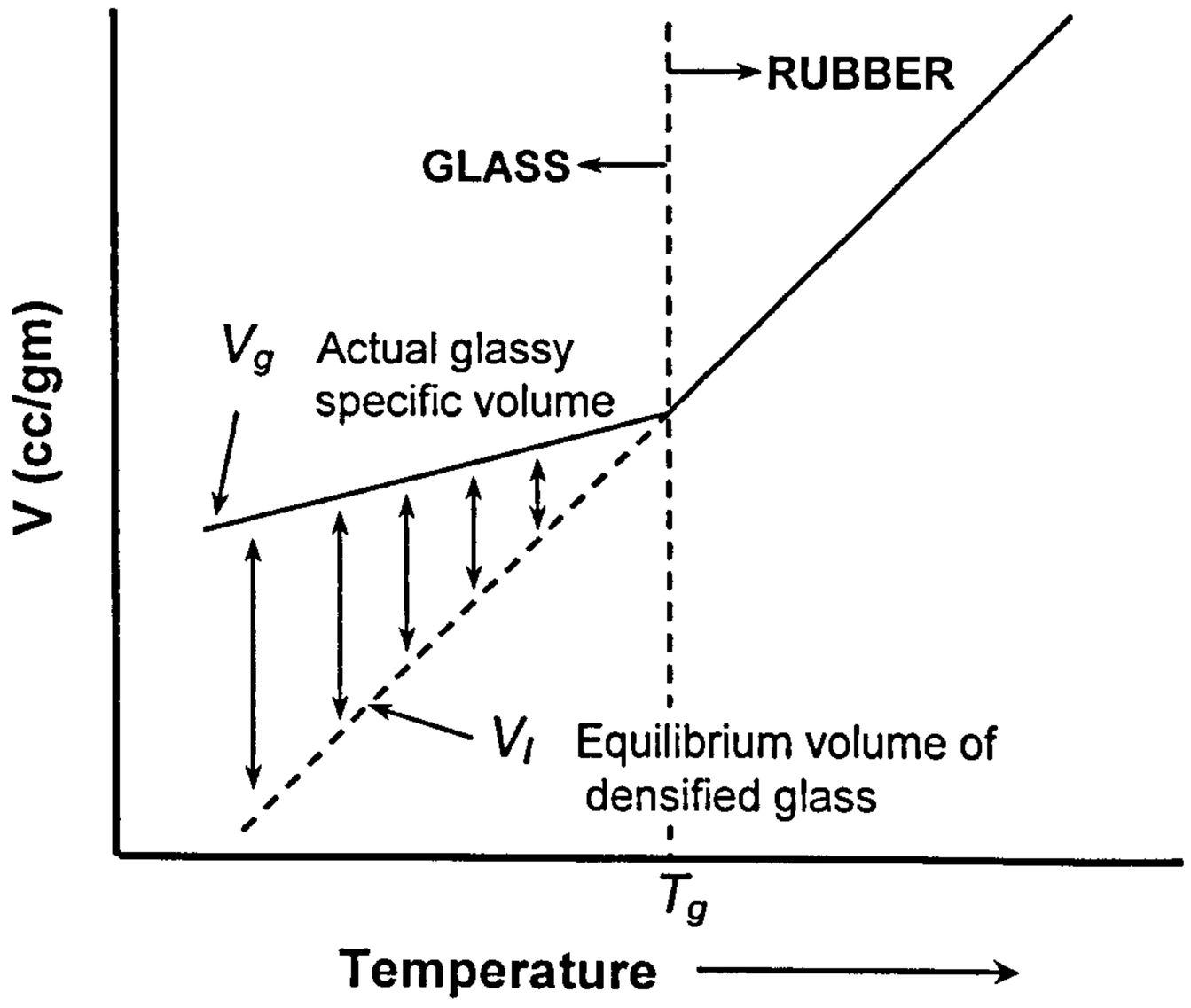

Figure 2. 6 Polymer specific volume as a function of temperature [107].

The excess volume is thought to be the result of trapped non-equilibrium chain conformations in quenched glasses, which results from the extraordinary long relaxation times for segmental motions in the glassy state. The excess volume present in glassy polymers allows for the accommodation of additional penetrant above that observed in low molecular weight liquids and rubbers [141]. The most useful phenomenological description of gas transport in glassy polymers is provided by the "*dual-mode sorption*" model, particularly by its partial immobilization version developed by Paul and Koros [142,143] and Petropoulos [144].

The dual-mode sorption model is strictly applicable in cases where the polymer is not significantly plasticised (swollen) by the penetrant gas.

2.1.3.2.2.1. Dual-Mode Sorption Model

The dual-mode sorption model has been extensively reviewed and discussed by a number of researchers [72,81,110-112,141-152]. The model represents the dependence of solubility, diffusion, and permeability coefficients on penetrant gas pressure, or concentration in the polymers, over a wide range of these variables. The validity of the model has been confirmed for a large number of gas/polymer systems by Paul and Koros [142,143], as well as contributions from many other investigators [72,81,110-112,141-152]. The model is also applicable to the permeation of gas mixtures [145].

The dual-mode sorption model is the concept of sorption into two idealized environments. One type of sorption is viewed as arising from uptake into a dissolved environment similar to sorption in low molecular weight liquids and rubbery polymers, and is described by a Henry's law relation. The second type of sorption is viewed as being due to uptake into the unrelaxed volume or *"microvoids"* present in glassy polymers, which is described as a Langmuir *"hole-filling"* process. The combination of these two modes of sorption leads to the commonly employed Dual-Mode sorption model.

The total sorption is the sum of these two types of sorption and can be represented by equation 2.40;

$$c = c_D + c_H \tag{2.40}$$

$$c = k_D p + c_H' \frac{bp}{1+bp} \tag{2.41}$$

where, k_D is the Henry's law solubility constant, p is the partial pressure of the penetrant, c_H' and b are the Langmuir capacity constant and hole affinity constant, respectively.

At low pressure $bp << 1$, hence equation 2.41 reduces to;

$$c = (k_D + c_H' b)p \tag{2.42}$$

At higher pressure $bp >> 1$, the modified Henry-like behaviour becomes;

$$c = k_D p + c_H' \tag{2.43}$$

Equations 2.42 and 2.43 represent c is a linear function of p at both low and high pressure with a nonlinear region in between. Hence, k_D and c_H' can be determined from the slope and intercept, respectively. From equations 2.40 and 2.41;

$$c_H = \frac{c_H' bp}{1+bp} \tag{2.44}$$

which can be rearranged to;

$$\frac{p}{c_H} = \frac{1}{b \cdot c_H'} + \frac{p}{c_H'} \tag{2.45}$$

The total solubility of gases in glassy polymers is higher than in rubbers, which is consistent with the apparent existence of an additional sorption site in such polymers.

The temperature dependence of the Henry's law constant can be represented by equation 2.46;

$$k_D = k_{D_o} exp\left(\frac{-\Delta H_D}{R} \times \left(\frac{1}{T} - \frac{1}{T_o}\right)\right) \quad (2.46)$$

and the temperature dependence of the Langmuir constant is;

$$b = b_o \cdot exp\left(\frac{-\Delta H_H}{R} \times \left(\frac{1}{T} - \frac{1}{T_o}\right)\right) \quad (2.47)$$

These equations enable the determination of the sorption enthalpies into the various sites. The Henry-type sorption enthalpy, ΔH_D, is of the same order as that in rubbers, whereas the enthalpy for sorption in Langmuir sites, ΔH_H, is appreciably higher. This accounts for the empirical finding that the gas sorption in glassy polymers is substantially more exothermic than in rubbers, and it is explained in dual sorption theory by the sorption of gas into pre-existing sites rather than sites that need to be formed by polymer molecular reorientations (as in rubbers).

While the permeability of most rubbery polymers to most gases is pressure independent, the permeability of glassy polymers is usually observed to decline with increasing pressure. This is accounted for by the dual sorption theory if one assumes that both the Henry and Langmuir type sites contribute to permeability [143].

Thus, the companion transport model to the dual-mode sorption model expresses the local flux '*J*' in terms of a two-part contribution [142,146,147].

$$J = -\left(D_D \frac{dc_D}{dx} + D_H \frac{dc_H}{dx}\right) \quad (2.48)$$

where D_D and D_H refer to the diffusivity of the Henry and Langmuir sorbed components, respectively. For the special case in which the downstream pressure is effectively zero, the appropriate expression derived from the dual-mode sorption and transport models for steady-state permeability of pure component in a glassy polymer is given by [148];

$$P_i = k_D D_D \left(1 + \frac{F \cdot Z}{1 + bp}\right) \tag{2.49}$$

where, $F = D_H / D_D$ and $Z = c_H^{\cdot} b / k_D$ are convenient dimensionless groups and p is the upstream driving pressure.

The above expression for dual-mode transport accounts for two types of diffusion jumps. The terms D_D and D_H represent diffusional jumps in the Henry's law and Langmuir environment, respectively. Barrer [149] extended the dual-mode transport model to account for the effect of neighbouring gas molecules on the transport, and it is assumed in this treatment that a gas molecule can execute four distinct diffusional jumps.

If the Henry's law and Langmuir environments are denoted as *'D'* and *'H'*, respectively, the four possible jumps are depicted by;

D to *D* : Dissolved to Dissolved

H to *H* : Hole to Hole

D to *H* : Dissolved to Hole

H to *D* : Hole to Dissolved.

where the four diffusion coefficients are represented by D_{DD}, D_{HH}, D_{DH} and D_{HD}. The resulting expression for dual-mode transport developed by Barrer [149] is;

$$P_i = k_D D_{DD} + \frac{c_H^{\cdot} b(D_{HH} + D_{HD}) - k_D D_{DH}}{1 + bp} + 2k_D D_{DH} \frac{ln(1 + bp)}{bp} \tag{2.50}$$

Attempts have been made to improve the dual-mode sorption model by formulating more detailed transport mechanisms [149,150]. However, this was achieved by the introduction of additional adjustable parameters which are difficult to evaluate and which decreases the usefulness of the model.

It is evident that some phenomenological models of gas transport in polymers (by solution and diffusion) and through polymer membranes (by permeation) have been useful for correlating and comparing the pertinent experimental data. The dual-mode sorption model has been particularly successful in this respect, and therefore has been widely applied to the study of structure/permeability relationships of polymers [72,81,110-112,141-152]. The main limitation of these phenomenological models is that they are not predictive

because the model parameters are not directly related to the chemical structure of the polymers.

2.1.3.3. Molecular Models

Efforts have also been made to formulate more detailed descriptions of the mechanisms of gas transport in polymers by means of "*molecular*" models. These models attempt to analyse specific motions of penetrant molecules and surrounding polymer chains relative to each other and take into consideration the pertinent intermolecular forces [78]. One of the most detailed of the earlier molecular models is that of Pace and Datyner [151,152], which incorporates the features of some previous models. Recent advances in the computer simulations of polymer microstructures and greatly increased capability of computers should make possible the formulation of much more realistic molecular models of gas transport in and through polymers. The first application of these computational techniques to estimate the fractional free volume in polypropylene and poly(vinyl chloride) appeared in 1989 [154].

Computer simulations of gas transport in polymeric membranes are still in an early stage of development. Most of these studies have involved rubbery polymers [155-160]. The transport of penetrant gas molecules in glassy polymers is more difficult to simulate realistically because such polymers are not in a state of true thermodynamic equilibrium. Moreover, gas diffusion coefficients are several orders of magnitude smaller in glassy polymers than in rubbery polymers. Therefore, the evaluation of diffusion coefficients in glassy polymers will require a very large amount of computer time.

Considerable work remains to be done before reliable predictions of diffusion coefficients, and solubility coefficients, for gases in rubbery and glassy polymers can be made by this technique. However, the computational technique has the potential of relating these coefficients, and also solubility and permeability coefficients, directly to the chemical structure of polymers.

2.2. Effect of Operating Conditions on Membrane Permeability

2.2.1. Effect of Concentration and Pressure on Diffusion Coefficient

Accurate engineering modelling of membrane-based gas permeation can be performed if the concentration and pressure dependence of the various component permeabilities are known at the temperature of interest.

For transport in both rubbery and glassy polymers, the flux can be written in terms of Fick's law with an effective diffusion coefficient, $D_{eff}\ (c)$, that is dependent on local concentration;

$$J = -D_{eff}(c)\cdot\frac{dc}{dx} \tag{2.51}$$

The concentration dependence of the diffusion coefficient for penetrant transport in polymers can be evaluated from steady-state permeability and equilibrium solubility data, without any reference to a particular model.

$$P\cdot p_o = -\int_{c_o}^{c_1} D_{eff}(c)dc \tag{2.52}$$

where c_1 is assumed to be zero for the case where the penetrant pressure is zero at the downstream face. Then by applying the Liebnitz rule,

$$D_{eff}(c_o) = p_o\left|\frac{dP}{dc}\right|_{c_o} + P\left|\frac{dp}{dc}\right|_{c_o} \tag{2.53}$$

which can be simplified to form [72,147];

$$D_{eff}(c_o) = \left|\frac{dp}{dc}\right|_{p_o}\left(p_o\left|\frac{dP}{dp}\right|_{p_o} + |P|_{p_o}\right) \tag{2.54}$$

Hence, the concentration dependence of the local diffusion coefficient, $D_{eff}\ (c_o)$, can be determined by the pressure dependence of both permeability and solubility isotherms.

For low sorbing gases in rubbery polymers, both *P* and *dc/dp* are essentially constant, leading the constant diffusion coefficient. On the other hand when the concentration dependence is observed, the form will generally take the shape of one of the curve shown in Figure 2.7. Transport of penetrants that have a strong affinity for rubbery polymers can be characterised by a linearly increasing diffusion coefficient, as shown in Figure 2.7(a). In cases for which the penetrant has a strong plasticising effect on rubbery polymer, an exponentially increasing diffusion coefficient is found, as illustrated in Figure 2.7(b) [108,110,138,140]. For the transport in glassy polymers, the diffusion coefficient is usually found to be concentration dependent even in the absence of a strong affinity of the penetrant for the material. As shown in Figure 2.7(c), the diffusion coefficient is usually convex to concentration at low sorption levels and is concave to concentration at higher sorption levels [147]. As shown in Figure 2.7(d), the clustering effect usually leads to a decreasing diffusion coefficient because the clustering becomes more severe at higher concentration [161].

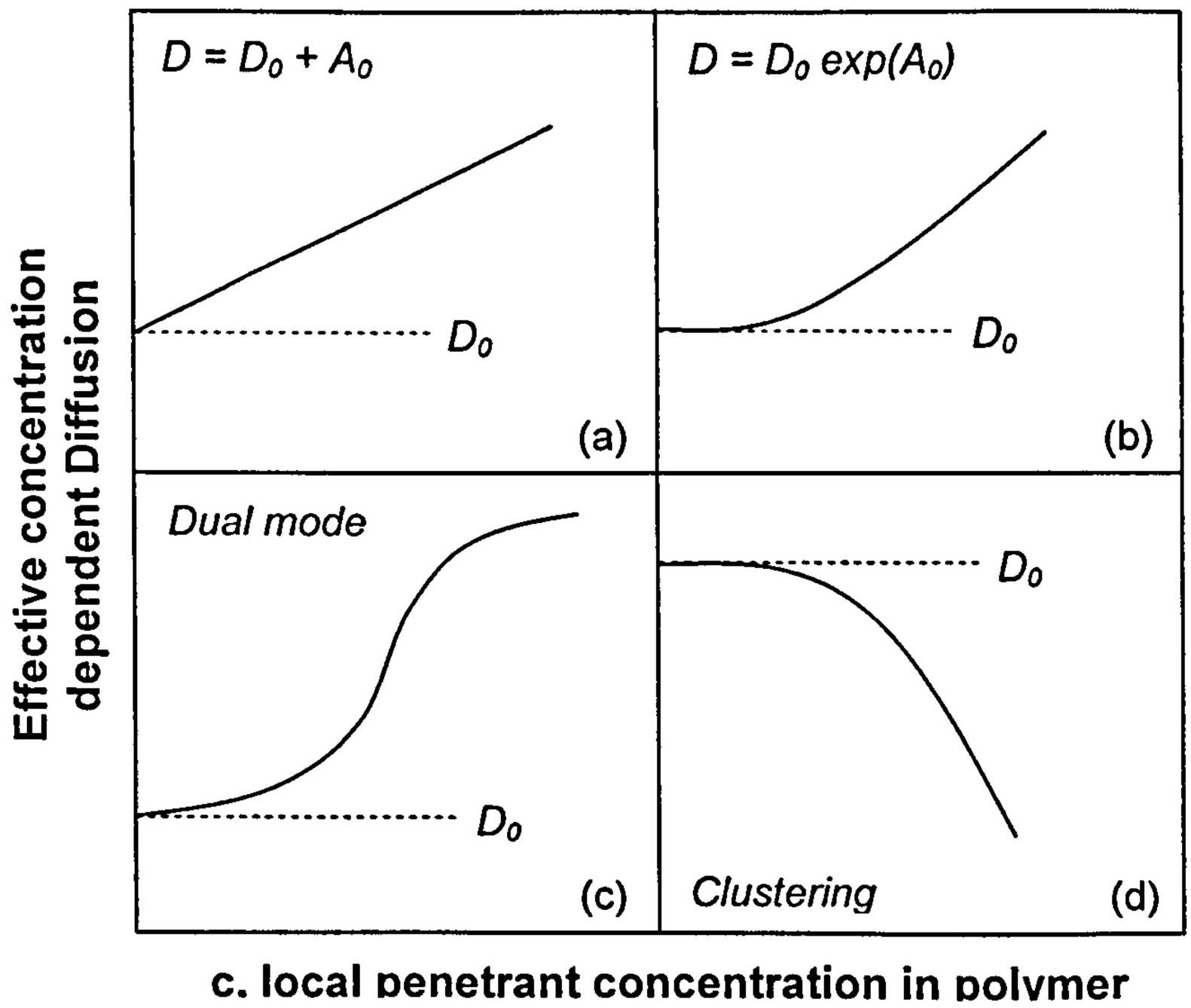

Figure 2. 7 Typical forms for concentration dependent diffusion coefficients in polymer media [72].

In some membrane applications, feed streams contain very high levels of strongly interacting gases, which plasticise the membranes. Exposure to high

levels of these gases results in a large depression of the effective glass transition temperature [162,163]. The pressure at which the plasticisation condition is reached roughly corresponds to the minimum in the permeability isotherms in Figure 2.8.

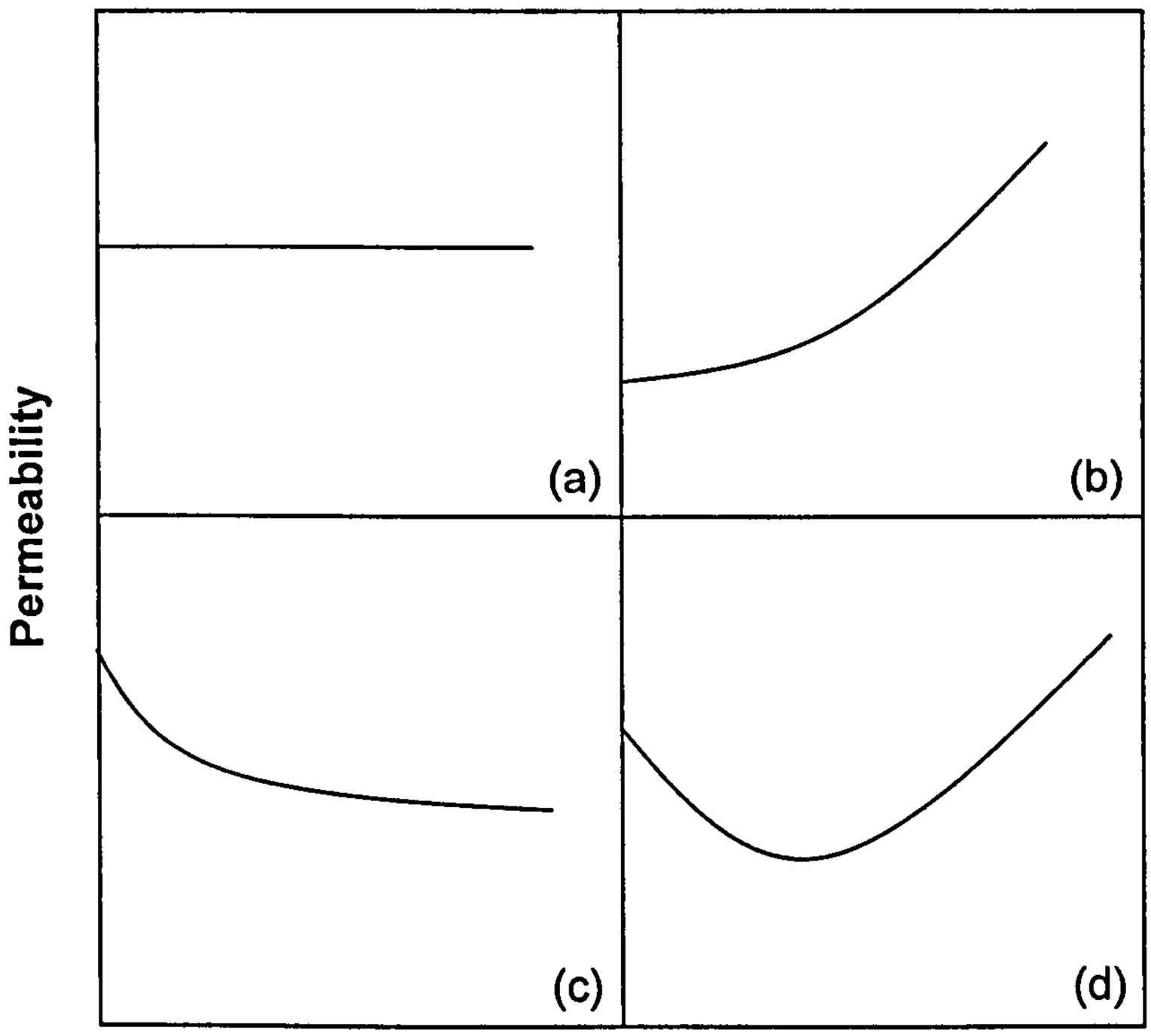

Figure 2. 8 Typical forms of permeability dependence on pressure during gas transport through polymeric membranes [107].

Figure 2.8(a), is for the ideal case as both diffusion and solubility are assumed independent of gas pressure. This type of behaviour is observed for the case of supercritical gas permeation in amorphous polymers. Figure 2.8(b) is characteristic of the gas plasticisation effect on the polymer and is observed during organic vapour permeation in rubbery polymers. Figure 2.8(c) corresponds to the case of highly soluble gases in glassy polymers, and Figure 2.8(d) is the combination of Figure 2.8(b) and Figure 2.8(c), which is observed in the case of permeation of organic vapours or plasticising gases in glassy polymers.

This shows that the useful operating range for various membrane materials is widely variable and dependent on a complex interrelation between the penetrant solubility and polymer chain rigidity.

2.2.2. Effect of Temperature on Permeability

Generally polymer permeability varies with concentration, temperature, chain mobility, crystallinity, cross-linking, polarity, gas-polymer interactions, etc. The effect of an increase in temperature may also be expressed in terms of an increase in free volume, which is related to the bulk expansion of the polymer that increases the permeability but decreases the selectivity. The thermal effects on solubility and diffusion show opposite trends. For gas adsorption, solubility decreases with increase in temperature as the condensability of the penetrant decreases with temperature. The solubility dependence with temperature is typically written in terms of the Van't Hoff relationship as follows;

$$S = S_0 exp\left[-\frac{\Delta H_s}{RT}\right] \tag{2.55}$$

where S_0 is constant and ΔH_s is the partial molar enthalpy of the sorption.

The solubility in thermodynamic terms is said to be a two step process [76]. The first step involves the condensation of the gas molecule in a polymer, followed by creation of a molecular scale gap for accommodating this gas molecule. These individual steps then contribute to the total enthalpy of sorption and are mathematically represented as;

$$\Delta H_s = \Delta H_{condensation} + \Delta H_{mixing} \tag{2.56}$$

Transport through dense films may be considered as an activated process which can usually be represented by an Arrhenius type of equation [164]. The temperature dependence equation for sorption, *S*, can be given as;

$$S = S_0 exp\left[\frac{-\Delta H_s}{R}\left(\frac{1}{T}-\frac{1}{T_0}\right)\right] \tag{2.57}$$

For low molecular weight super critical gases, low condensability causes the mixing step to control the sorption property of a polymer. For the case of weak interactions between the gas molecule and the polymer, the change in enthalpy of mixing is positive, which then leads to an increase in solubility with

increase in temperature. For the case of condensable gases and vapours, the enthalpy change for condensation is negative and dominant, thereby showing decreasing solubility with increasing temperature.

Temperature dependence on gas diffusion is well expressed in term of an Arrhenius type relationship, as the movement of gas molecules through a membrane is considered a thermally activated process [76]. Mathematically, the temperature dependence of diffusion is given as;

$$D = D_0 \exp\left[\frac{-\Delta E_D}{R}\left(\frac{1}{T}-\frac{1}{T_0}\right)\right] \tag{2.58}$$

where ΔH_s is solution enthalpy *(J/mol)* and ΔE_D is the energy for diffusion *(J/mol)*. Studies of the thermal effects during gas transport have shown that the activation energy term is dependent on the size of the penetrant, and not on its mass. Diffusion is the most temperature sensitive transport parameter, in comparison to solubility and permeability [72]. Combining the temperature dependence equations for the diffusion and sorption coefficients, the temperature effect on gas permeability is then given as:

$$P = P_0 \cdot exp\left[\frac{-\Delta E_p}{RT}\right] \tag{2.59}$$

where ΔE_p is activation energy for permeation *(J/mol)*, P_0 is permeability at STP $(cm^3_{STP} / cm^2 S \cdot Pa)$.

In general, permeability increases with increase in temperature. However, there are exceptions, especially near the glass transition temperature of the polymer, where opposite trends have been observed [126]. This observation was explained in terms of pressure effects on the polymer under isothermal operating conditions. The high stress caused by the applied gas pressure was said to cause a transition in the polymer from a rubbery state to a glassy state. In the case of the glassy polymers, all three gas transport parameters decrease with increasing temperature. Some exceptions are observed at high temperatures

where, due to low solubility, more errors are introduced in the fitting of the dual-mode sorption curve [76].

2.2.3. Effect of Concentration Polarisation

In membrane separation processes, a gaseous or liquid mixture is fed to the feed side of the membrane at higher pressure, and the permeate, enriched in one of the components of the mixture, is withdrawn from the downstream side of the membrane. Because the feed mixture components permeate at different rates, concentration gradients form in the fluids on both sides of the membrane. The phenomenon is called *concentration polarisation.* The layer of solution immediately adjacent to the membrane surface becomes depleted in permeating solute on the feed side of the membrane and enriched in this component on the permeate side. Concentration polarisation reduces the permeating component's concentration difference across the membrane, thereby lowering flux and the membrane selectivity.

Two approaches have been used to describe the effect of concentration polarisation. One has its origins in the dimensional analysis used to solve heat transfer problems. The second approach to concentration polarisation is to model the phenomenon by assuming that a thin layer of unmixed fluid, with thickness, δ, exists between the membrane surface and the well-mixed bulk solution. The concentration gradients that control concentration polarisation form in this layer. This boundary layer film model oversimplifies the fluid hydrodynamics occurring in membrane modules and still contains one adjustable parameter, the boundary layer thickness. Nonetheless, this simple model can explain most of the experimental data.

2.2.3.1. Concentration Polarisation in Gas Separation Processes

Concentration polarisation in gas separation processes has not been widely studied, and the effect is often assumed to be small because of the high diffusion coefficients of gases. However, the volume flux of gas through the membrane is also high, so concentration polarisation effects are important for several processes.

The simple mass balance for gas permeation can be written as;

$$J_{vf}c_i - D_i\frac{dc_i}{dx} = J_{vp}c_{ip} \quad (2.60)$$

where J_{vf} is the volume flux of gas on the feed side of the membrane and J_{vp} is the volume flux on the permeate side. The volume fluxes *($cm^3/(cm^2\ sec)$)* can be linked by correcting for the pressure on each side of the membrane using;

$$J_{vf}p_o = J_{vp}p_{t_m} \quad (2.61)$$

where p_o and p_{t_m} are the penetrant partial pressures on the feed and permeate sides of the membrane, respectively. Hence;

$$J_{vf}\frac{p_o}{p_{t_m}} = J_{vf}\phi = J_{vp} \quad (2.62)$$

where ϕ is the pressure ratio, p_o/p_{t_m} across the membrane. Substituting equation 2.62 into 2.60, and rearranging gives;

$$-D_i\frac{dc_i}{dx} = J_{vf}(\phi\cdot c_{ip} - c_i) \quad (2.63)$$

Integrating across the boundary later thickness, gives;

$$\frac{[c_{io}/(\phi - c_{ip})]}{[c_{ib}/(\phi - c_{ip})]} = exp\frac{J_{vf}\delta}{D_i} \quad (2.64)$$

For gases, the enrichment terms E and E_o are most conveniently expressed in volume fractions, so that;

$$E_o = \frac{c_{ip}}{p_{t_m}}\cdot\frac{p_o}{c_{io}} = \frac{c_{ip}}{c_{io}}\cdot\phi \quad (2.65)$$

and,

$$E = \frac{c_{ip}}{p_{t_m}}\cdot\frac{p_o}{c_{ib}} = \frac{c_{ip}}{c_{ib}}\cdot\phi \quad (2.66)$$

Equation 2.64 can then be written as;

$$exp\frac{J_{vf}\delta}{D_i} = \frac{1-1/E_o}{1-1/E} \tag{2.67}$$

which on rearranging gives;

$$\frac{E}{E_o} = \frac{c_{ip}}{c_{io}} = \frac{exp\left(\frac{J_{vf}\delta}{D_i}\right)}{1+E_o\left[exp\left(\frac{J_{vf}\delta}{D_i}\right)-1\right]} \tag{2.68}$$

Equation 2.68 can be used to calculate the expected concentration polarisation modulus for some of the better-known gas separation applications.

2.2.4. Effect of Plasticisation on Permeability

Plasticisation of the membrane polymer by a sorbed permeant can affect the permeability and selectivity properties significantly. For example, it is known that CO_2 acts as a plasticiser in CO_2/CH_4 separation using a membrane. Plasticisation occurs when the CO_2 concentration in the polymer is high enough to increase free volume and segmental mobility. Due to the swelling of the polymer matrix, the permeation of CH_4 is accelerated and as a consequence the polymer looses its selectivity. The study of CO_2 permeation in polycarbonate by Koros [147] shows minima in the sorption curve, and coincides with the decline in the selectivity of the material. The presence of hysteresis in many sorption/desorption experiments involving a CO_2 gas-polymer system confirms the plasticisation effects. A quantitative analysis for such behaviour was first given by Mauze and Stern [165], who assumed that the sorption due to the Henry's law is a much stronger function of concentration than the Langmuir mode sorption. Thus the gas concentration sorbed by the Henry's law mode is expressed as;

$$c_D = S(c)\cdot p = [k_D\, exp(\sigma\cdot c)]\cdot p \tag{2.69}$$

where σ is a characteristic parameter for the solubility dependence on concentration c. The dual-mode sorption equation is then represented as;

$$c = [k_D \, exp(\sigma \cdot c)]p + \frac{c_H' bp}{1 + bp} \tag{2.70}$$

A correlation for plasticisation effect on c_H' parameter was described by Kamiyu *et al.* [166,167]. Starting with the concentration effects on the glass transition temperature, an expression can be presented relating the excess free volume to the gas concentration and operating temperature;

$$v_H(c) = \Delta\alpha \cdot \left[\beta \cdot c_g \{T_g(O) - T_g(c)\}\right] \tag{2.71}$$

Considering the effects in terms of concentration only, the excess free volume can be modified and results in the following equation;

$$v_H(c) = \Delta\alpha \cdot \beta(c_g - c^*) \tag{2.72}$$

This equation can then be related to hole concentration coefficient using;

$$c_H' = \gamma \cdot v_H(c) = c_{HO}' \cdot \left(1 - \frac{c^*}{c_g}\right) \tag{2.73}$$

where, $v_H(c)$ is the excess free volume per unit volume of the penetrant polymer system, γ is the proportionality constant between the concentration and temperature at the glass transition point, c_g is the glass transition concentration at temperature T, and c^* is the same as the effective total concentration of sorbed penetrant. Substituting equation 2.73 into 2.70, the final expression for dual-mode sorption can be given as;

$$c = [k_D \, exp(\sigma \cdot c^*)]p + \frac{c_{HO}' bp}{1 + bp}\left(1 - \frac{c^*}{c_g}\right) \tag{2.74}$$

The validity of the equation 2.76, can be examined with a permeability study of CO_2 in poly(vinyl benzoate), poly(vinyl butyral) and poly(ethylene terephthalate) [166,167].

3. NEXT GENERATION MEMBRANES – *OPPORTUNITIES AND HURDLES*

This section seeks to define the current *scientific, technological* and *commercial* boundaries of the field of membrane-based gas separation and to project the position of these boundaries of the immediate future.

Scientific and engineering achievements over the past ten to fifteen years have promoted the current strong interest in membrane-based gas separations, and promise the steady progress towards removing remaining limitations and enabling long term growth as a technology. In 1991, Robeson [168] raised the important question whether an upper limit (*"upper bound"*) may exist to the gas selectivity of polymers with a given permeability. The *"upper bound"* will move upwards as new polymers with increased gas permeability and selectivity are synthesised. With suitable structural modifications it is possible to enhance both the permeability and selectivity. Availability of membranes that are simultaneously more robust and less expensive per unit separation area would make membranes a more attractive option in a broader array of applications.

The polymeric materials available currently can be visualised as having a broad free volume distribution, such as shown by the curve in Figure 2.9(a). The shaded area under the distribution curves marked *'A'* represents the free volume in a polymer available only to small penetrant molecule, whereas the cross hatched area marked *'B'* represents the free volume available to both small and large penetrants.

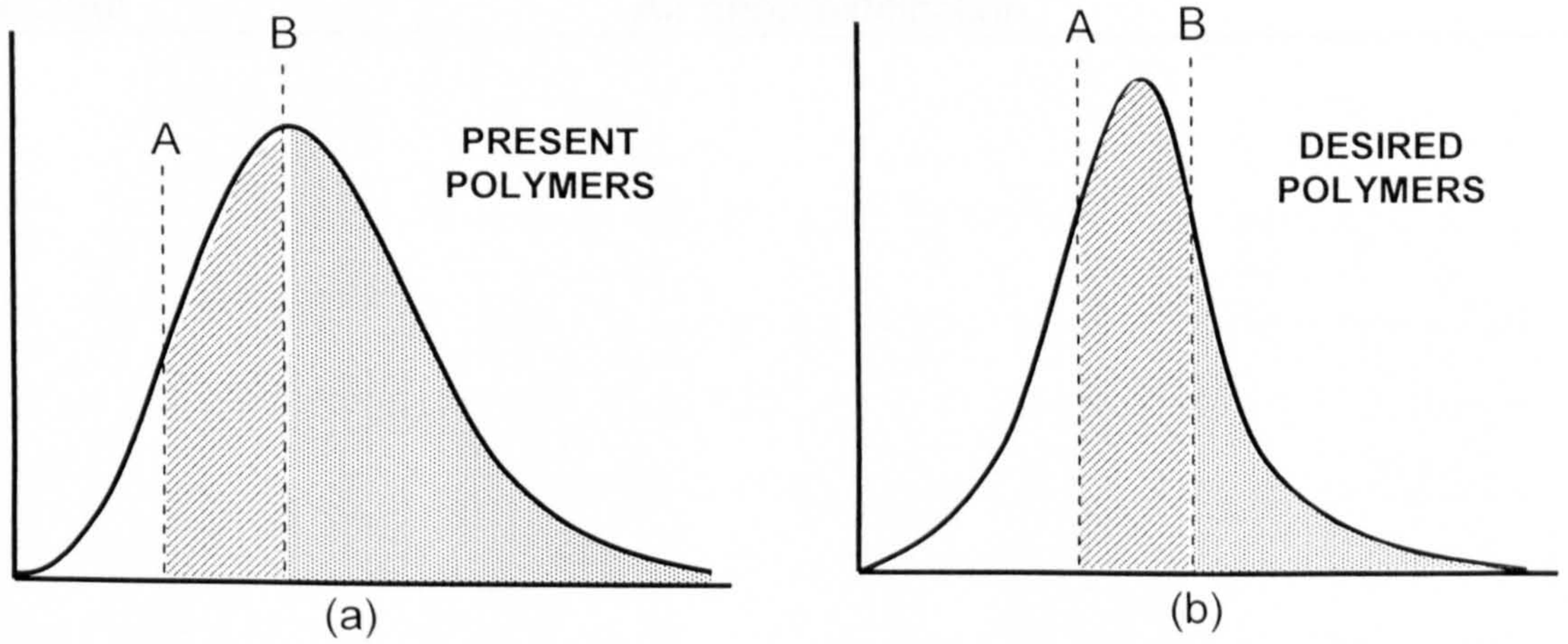

Figure 2. 9 Hypothetical present and desired free-volume distribution in polymers considered as membrane materials for gas separations [78].

Current, developing, and potential membrane processes for the separation for the gas mixture separation have been discussed by Koros and Fleming [16]. In the coming years, the economics of the membrane processes listed in Table 2.2 will be improved to various extents by the availability of more highly selective and high-flux polymeric materials. Such improvements are imperative for the membrane separation industry because the economics of competing separation techniques are also being continuously improved. Ultimate displacement of a older technology tends to occur if a new one offers:

- significantly better performance
- greater convenience
- lower cost.

State of the art membranes excel in the last category, primarily based on highly efficient processes adapted and tailored to producing asymmetric and composite asymmetric fibres.

Table 2. 2 Current membrane processes for gas separations [90].

Common gas separation	**Application**
O_2/N_2	Oxygen enrichment, inert gas generation
H_2/Hydrocarbons	*Refinery hydrogen recovery*
H_2/N_2	Ammonia purge gas
H_2/CO	Syngas ratio adjustment
CO_2/Hydrocarbons	Acid gas treatment, landfill gas upgrading
H_2O/Hydrocarbons	Natural gas dehydration
H_2S/Hydrocarbons	Sour gas treatment
He/Hydrocarbons	Helium separation
He/N_2	Helium recovery
Hydrocarbons/Air	Hydrocarbons recovery, pollution control
H_2O/Air	Air dehumidification

Some developing and potential membrane processes for separation of gas mixtures are listed in Table 2.3.

Table 2. 3 Developing and potential membrane processes for gas separations [76].

Removal of organic vapours from air
Dehydration of air
Dehydration of Natural Gas
Upgrading of low-quality Natural Gas
Upgrading of biomass and landfill gases
O_2 enrichment of air
Olefin/Paraffin separations (e.g., ethylene/ethane, propylene/propane)
Flue gas desulphurisation
CO_2 removal from diving atmospheres
High temperature separations

These applications would benefit from more intrinsically selective and robust membranes. On the other hand, while some new membrane materials often satisfy the first two criteria, high module production cost is currently a serious hurdle to the widespread adoption of higher performance materials with the potential to capture large new markets for membranes.

Another key factor in the development of membrane separation processes is the fabrication of high flux asymmetric or "composite" membranes from a given polymer, either in the hollow fibre or in a flat sheet form [72,98,107,169,170]. Polymer properties required for high gas permeability and selectivity can be very different from those necessary for membrane fabrication. An additional hurdle for these high flux membranes is the chemical and mechanical stability of the polymer membranes under actual operating conditions, especially when the membranes are exposed to a high pressure gas mixture that plasticises (swells) the polymer membrane.

3.1. A Practical Path Forward to the Next Generation Membranes

Evolutionary advancement, based on successive improvements in existing technology, has many attractive aspects as a strategy to introduce advanced materials. In this case, progression from the current state of the art to continually more advanced materials occurs in a series of more or less incremental steps. In this case, each evolutionary step reflects a response to a market pull for higher performance. Alternatively one can seek to jump directly from the current limited

technology to a much higher performance and cost goal. To move beyond the current generation to higher performance, to enable capturing these markets, the evolutionary path appears advisable and is the focus of the current applications.

In some applications, the intrinsic selectivity of current membrane materials may be adequate, but this selectivity cannot be maintained even under moderately aggressive feed conditions. Current focus is on the commercial availability of physically or chemically stabilised materials, and economical pure molecular sieving modules, which would unquestionably expand the markets and application options significantly. The combinations of technical and economic advantages make membranes an exciting new area with a potential to expand to a significant range of applications. All applications listed in Table 2.3 are important emerging membrane processes. In the following sections a detailed review on the opportunities, hurdles, and a possible practical approach forward for hydrogen purification and olefin/paraffin separations is described.

4. HYDROGEN PURIFICATION

The first large scale commercial applications of membranes to gas separations were the separation of hydrogen from nitrogen, methane and argon in ammonia purge gas streams [14]. Another even larger and more important application of hydrogen permeable membranes exists for hydrogen recovery in refineries. The demand for hydrogen recovery in refineries is increasing because of environmental regulations and heavier crudes. To reduce the economic penalty of environmental compliance, low-cost hydrocarbon separation technologies are required. The need to reduce hydrocarbon losses is especially critical, and facilities can no longer afford to dispose of waste hydrocarbon streams in their flare systems.

The gas separation applications in refineries are seldom simple. The gas mixtures to which the separation membranes are exposed may be hot, contaminated with solid or liquid particles, or at high pressure, may fluctuate in composition or flow rate or, more likely, may exhibit several of these features. Even in a most straightforward situation where the gas stream to be separated is a two component mixture and uncontaminated by other components, at ambient temperature and pressure, one component may interact with the membrane in

such a way as to change the permeation characteristics of the other component, so that the separation factor or selectivity suggested by the pure gas measurements cannot be achieved.

In refineries, ethylene, propylene and other higher olefins may be produced by heating saturated hydrocarbons such as ethane, propane or butane to elevated temperatures. The cracking effluent contains hydrogen, carbon dioxide, steam, olefins, light saturated hydrocarbons, heavy hydrocarbons, and other components. This effluent is sent to a product recovery system. The problem that inhibits the application of membranes in refineries is poor reliability. The condensable component, which is readily sorbed into the polymer matrix, swells or plasticises the membrane, thereby reducing its selective capabilities. Fouling, plasticisation, and condensation of hydrocarbon vapours on the membrane surface are all serious issues.

In principle, recovering hydrogen from the inert purge gas is an easy application for membranes. However, in the case of refinery applications, as hydrogen is removed through the membrane the remaining gas becomes enriched in hydrocarbons raising the dew point. For example, if the total hydrocarbon content increases from 60% in the feed gas to 85% in the residue gas, the dew point may increase by as much as 25 C or more, depending on the hydrocarbon mixture (see Chapter 1, Figure 1.1). In practice, to provide a safety margin and to minimise plasticisation of the membrane, the gas must be heated to 15-20 C above the expected residue gas dew point, at which the membrane and module performance can be adversely affected. Failure to do so means, the hydrocarbon stream may enter into the liquid phase region of the phase diagram before it leaves the membrane module, and condense on the membrane surface to damage it beyond recovery.

Even heating the gas does not provide absolute membrane protection. Variations in gas composition are common in refinery applications, for example, when the gas source is a catalytic process from which off-gas content changes as the catalyst activity changes. More sudden changes occur when the feedstock to the upstream unit changes. The hydrocracker typically handles multiple streams from diverse sources; feed quality changes can be rapid and substantial as one or more streams are added or subtracted. Process parameters, such as pressure and temperature, deviate from the normal

operating range as a result of plant upsets or deliberate plant operator action to optimise the particular product. Any of these changes can bring the gas close to its dew point and cause membrane failure.

The principal technologies available to recover hydrogen from the refinery off-gases are cryogenic separation, pressure swing adsorption (PSA), and membrane separation [16]. Many membrane materials are much more permeable to hydrogen than to other gases and vapours. As many as 100 membrane plants have been installed in refineries, but the market is far from saturated. There are approximately 450-550 large refineries around the world, as well as many smaller ones [14]. Opportunities to place multiple hydrogen recovery units exist in all of these refineries, particularly if the operating margins and capital equipment budgets of refineries continue to increase from the very low levels of the past decade. However, the application of membranes to refinery gas separation operations has been much less successful. Refinery gas streams contain contaminants such as water vapour, acid gases, olefins, aromatics, and other organics. The experience of operators with the membrane plants installed in refineries to date has not been uniformly good, and the problems described above have led to discontinuation of a number of plants. This has inhibited widespread adoption of membrane technology, but nevertheless the opportunity is real. A great deal of research has been performed on improved membrane materials for hydrogen separation. A number of these materials appear to have significantly better properties than the original cellulose acetate or polysulfone membranes [171,172]. Hydrogen selective membranes have their own operating ranges, in terms of temperatures and flow compositions. The properties of the flow to be separated are therefore a starting point to select a suitable membrane. Developing new hydrogen permeable membrane materials able to operate at high hydrocarbon partial pressure and at high temperatures is one approach. The following Table 2.4 shows the properties of the relevant hydrogen selective membranes.

Table 2. 4 Properties of relevant hydrogen selective membranes [173].

	Dense polymer	Micro porous ceramic	Dense metallic	Porous carbon	Dense ceramic
Temperature range	< 100 C	200-600 C	300-600 C	500-900 C	600-900 C
H_2 selectivity	5-350	5-139	> 1000	4-20	> 1000
H_2 flux *	Low	60-300	60-300	10-200	6-800
Stability	Swelling, compaction, mechanical strength	Stable in H_2O	Phase transition	Brittle oxidising	Stable in CO_2
Poisoning	HCl, SO_x, CO_2	H_2S	H_2S, HCl, CO	Organic vapours	H_2S
Development status	Commercially available	Prototype tubular silica membranes available up to 90cm.	Commercially available	Small membrane modules at commercial level	Small modules at commercial level

* flux in 10^{-3} mol/m^2sec, calculated at 1 bar TMP

Once the membrane type is selected, the membrane module can be chosen or designed taking into account consideration such as manufacturability, maintainability, operability, efficiency, membrane deterioration and costs. Another approach is to use better feed gas pre-treatment to reduce the dew point of the feed gas to the hydrogen permeable membrane. As these problems are solved, this type of refinery application is likely to expand significantly.

The use of hydrogen separation membranes in large scale applications such as ethylene cracker, in which mixtures of hydrogen, methane, ethane, propylene, and other hydrocarbons are separated by low temperature condensation followed by fractional distillation. Hence, a number of opportunities exist for membrane separation units in these plants. A number of companies have worked on different approaches, and some pilot plants have been installed. Table 2.5 gives a brief overview on the present technologies available for hydrogen separations, and compares the membrane technology with them.

Table 2. 5 Technology selection criteria [173].

Features	Pressure Swing Adsorption	Membranes	Cryogenics
H_2 purity	99.9% +	90 – 98 %	90 – 96%
H_2 recovery	50 – 92%	85 – 95%	90 – 99%
Feed pressure	150 – 600 psig	300 – 2300 psig	> 75 – 1100 psig
Feed H_2 content	> 40%	> 25 – 50%	> 10%
H_2 product pressure	Feed	< 1/3 feed pressure	Feed / low pressure
H_2 capacity	1 – 200 MMSCFD	1 – 50 MMSCFD	10 – 75 MMSCFD
Pre-treatment requirements	None	Minimum	CO_2, H_2O removal
Multiple products	No	No	Liquid HC's
Power requirements	None / fuel	H_2 / fuel	None / H_2 / refrigeration
Turndown	Good	Good	Very good
Reliability	Good	Very good	Less
Ease of future expansion	Suitable	Very suitable	Suitable
By product recovery	Not economical	Economical	Very economical
Capital cost	Medium	Low	Higher
Scale economics	Moderate	Modular	Good

5. OLEFIN / PARAFFIN SEPARATION

Light olefins and paraffins are valuable raw materials in a wide range of petrochemical applications [174,175]. A significant amount of the light olefins produced during the refining of crude oil is used as refinery fuel. Low molecular weight olefins (C_2-C_5) are widely used for production of plastics and chemicals in the petrochemical industry, or of octane boosters and alkylated hydrocarbons by refineries; the corresponding iso-alkanes are also significant raw materials in alkylation processes for the production of high octane branched paraffins. Large quantities of ethylene and propylene are used as feedstock in the production of a very important industrial polymer such as polyethylene or polypropylene. The most widely used production process for olefins is the cracking of C_4-hydrocarbon fractions, followed by dehydrogenation reaction. The obtained olefin/paraffin mixture is difficult to separate, because the boiling points

and the kinetic diameters of olefins and their saturated counterparts are very close, as shown in Table 2.6.

Table 2. 6 Physical properties of olefins and paraffins [176,177].

	Ethylene	Ethane	Propylene	Propane
Boiling Point (C)	-103.9	-88.6	-48	-42.2
σ_{LJ} (Å)	3.90	4.0	4.4	3.96

The separation of olefins from paraffins has been ranked at a high level in evaluation of the potential impact of membrane separations in petroleum refining [178-180]. A large corpus of patent and literature data on membranes for refinery gas separation applications has been accumulated so far that requires generalisation (about 2000 documents over recent 20 years) [181]. The flow of patent and periodic information on the problem of membrane separation of volatile hydrocarbons is steadily growing. The flow is dominated by articles in journals whereas the share of patents is only about one-third. This indicates that for the time being researchers are mainly taking a scientific, rather than commercial, interest in the problem.

Separation of olefin and paraffin gases is currently carried out by energy intensive low temperature distillation. These distillation columns are often up to 300 ft tall and typically contain over 200 trays with reflux ratios greater than 10, which require very high energy input to carry out separation. According to a report by DOE, 1.27×10^{14} kJ (3.024×10^{6} tonne of fuel oil equivalent) of energy is used annually for olefin/paraffin distillation [17]. This large energy and capital investment requirement provides the incentive for research in developing new techniques for olefin/paraffin separations.

Membrane separation technology has been proposed as a potential alternative approach to the conventional distillation process for olefin/paraffin separation, and various membrane types have been examined for separation of gaseous olefin/alkanes (e.g., ethylene/ethane, propylene/propane) [18-48]. Membrane separations are based on one of the three mechanisms; size difference, charge difference, and solubility difference. In membrane separation of the olefin/paraffin mixture, the predominant selective separation of olefin is evident. Firstly, the olefin molecule is smaller in size as compared to the respective paraffin. It is known that the C-C distance in paraffin is 0.1534 nm,

where the C=C distance in olefins is 0.1337 nm [181]. Atoms of carbon in paraffins are characterised by sp^3 hybridisation (and free rotation around C-C bonds), and atoms of olefins are characterised by sp^2 hybridisation. The rigid C=C bond impedes internal rotation in the olefin molecule and makes it flat. It is, therefore, clear why the olefin molecule is smaller in size compared to paraffin and why the diffusion coefficient of olefins in polymers would be higher than those of paraffins. Secondly, the presence of unsaturated bonds in olefin molecules makes them capable of specific interactions with the membrane matrix. The attempt of implementing these capabilities resulted in development of an important field of research: facilitated transport. The membrane process using the concept of facilitated transport has been considered to be an energy-saving process to separate olefins from paraffins. In facilitated transport membranes carrier-mediated transport occurs, in addition to a normal Fickian transport, due to the reversible reaction of carrier with a specific solute, and separation efficiency can be improved remarkably. The basis for the separation is the formation of a reversible π-bond complexation reaction between metal ions such as Ag^+ which are incorporated into the membrane polymer matrix, and olefin, when the gas mixture is contacted with a second phase (membrane) containing complexing agent (see Figure 2.10) [19,182].

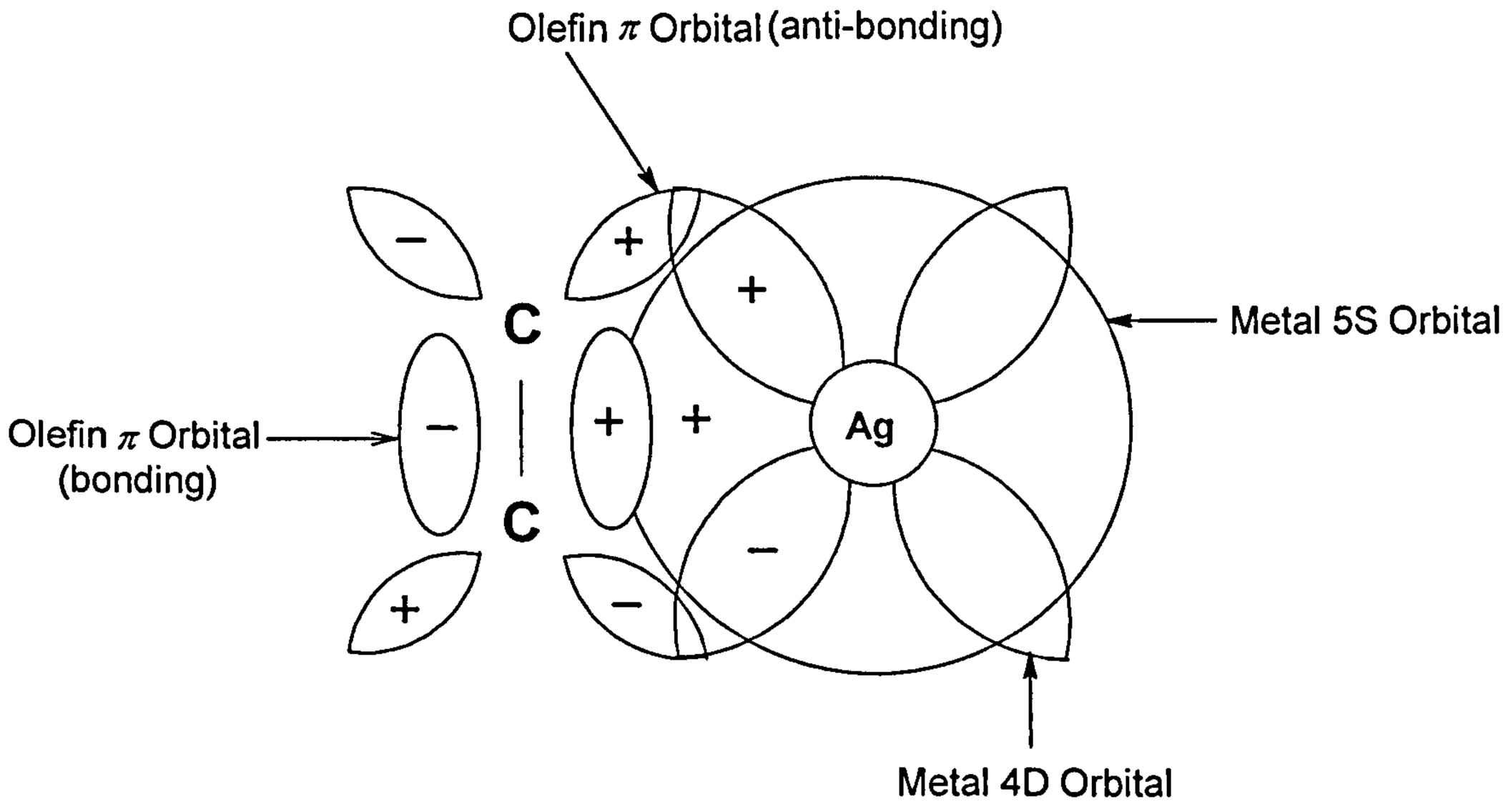

Figure 2. 10 Schematic representation of chemisorption of olefin by a metal complex (Dewar-Chatt Model) [182].

The un-bonded and filled π-orbitals of the olefin molecules overlap with the vacant hybridised *d*-orbitals of the metal and donate electrons forming a σ- bond. More important is the back donation of electrons from the filled *d*-orbitals of the metal to the π*-orbitals of the olefins which determines the stability of the olefin-metal complex. It follows that an electron withdrawing group present close to the olefin double bonds in such a complex has a strong stabilising effect on the complex. Also, a more nucleophilic transition metal ion usually forms a more stable complex.

Two possible different types of facilitated transport are schematically shown in Figure 2.11; the olefin transport with mobile carriers and the transport with fixed-site carriers. In the first case (see Figure 2.11(a)), the olefin/silver complexes formed at the feed-side boundary of the membrane permeate due to their concentration gradient and after decomplexation at the permeate side the silver ions permeate back and the circle starts again. In the second case (see Figure 2.11(b)), silver ions are fixed in the polymer and olefin molecules permeate the membrane by "hopping" from one fixed silver ion to another. The complex diffuses owing to its concentration differences across the membrane from the high-pressure side to the low-pressure side, where decomplexation takes place. This completes a facilitated transport cycle, and the complexing agent repeats the cycle. Because of the complexation, the concentration of the olefin in the membrane increases, and the transport of olefin is thus facilitated.

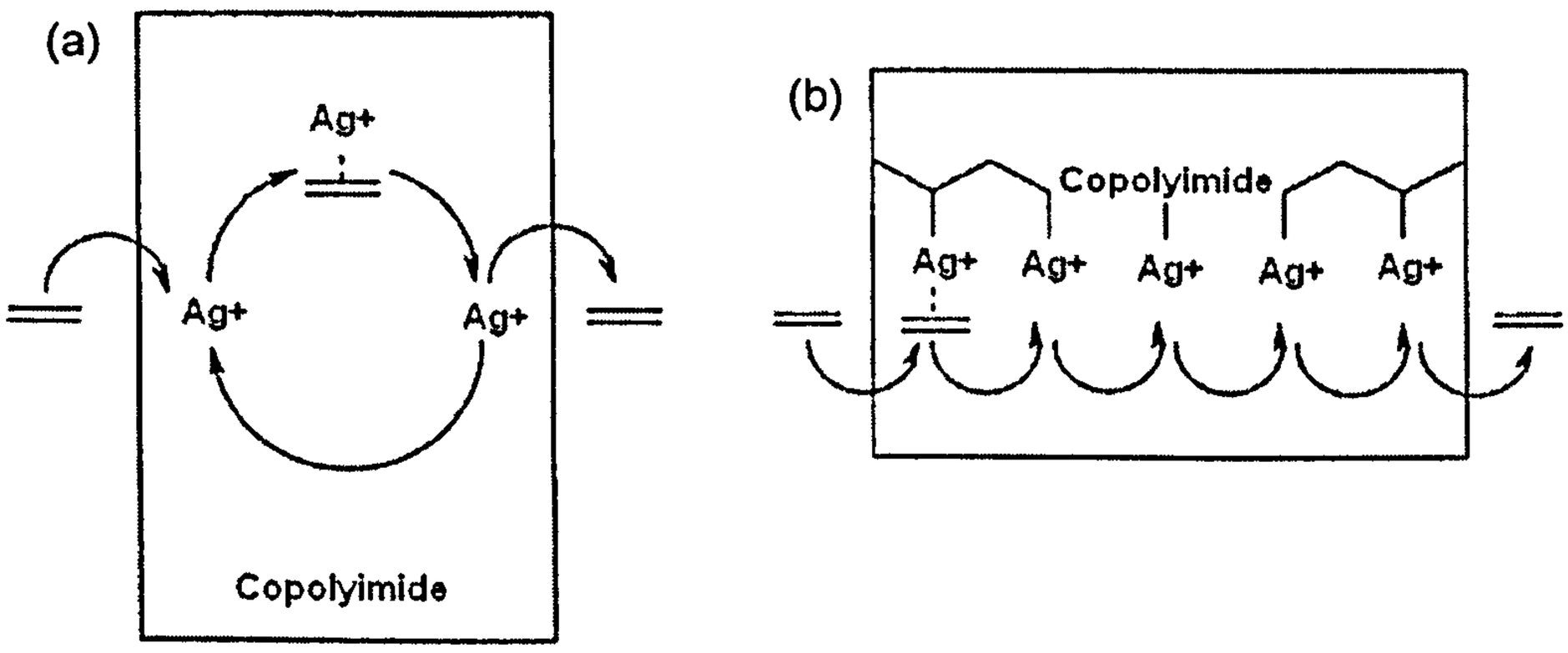

Figure 2. 11 Mechanism of facilitated transport: a) mobile Ag^+-carriers; b) fixed-site Ag^+-carriers [183].

On the other hand, paraffin can not form a complex with silver and the majority of the paraffin is thus rejected. Therefore, the facilitated transport membrane can give high olefin/paraffin selectivity and high olefin purity. However, currently four problems limit the use of facilitated transport membranes for industrial applications:

- poor mechanical stability
- difficulty in preparing thin, high-flux composite membranes
- requirement of a water-vapour-saturated feed to provide mobility for the olefin-selective carrier
- poor chemical stability due to carrier poisoning.

Further research in developing ideal polymer and polymeric membranes which are viable and acceptable in all respect is, therefore, required and emphasised in this work.

6. SELECTION OF THE POLYMERIC MATERIAL

As discussed earlier, hydrogen/hydrocarbon and olefin/paraffin separation processes are energy intensive, and consequently polymer membrane based separations have been considered as an attractive alternative. Most of the commercially available membrane polymers show plasticisation effects when exposed to hydrocarbon mixtures resulting in loss of separation efficiency. Plasticisation is caused by the high solubility of such components in the polymer, and as a consequence an increase in permeability is usually observed with decrease in selectivity. Two important classes of material that may offer the potential for capturing new high volume opportunities in the harsh and demanding operating environment of a petroleum refinery are: cross-linked polymers and blends of molecular sieving domains in polymers (mixed matrix membranes).

Remarkable separation performance of olefin/paraffin mixtures was previously reported by facilitated olefin transport through silver based polymer membranes using the concept of facilitated transport in liquid [21-29], solid membranes [30-47], as well as copper cation membranes [48]. Since, the evaporation of liquid media in liquid membranes is a serious drawback in

practical applications, the development of solid facilitated transport membranes is demanded. Hughes *et al.* [18,26] described supported liquid membranes of aqueous $AgNO_3$ solutions in a porous cellulose acetate reverse osmosis membrane for ethylene/ethane and propylene/propane separations. Shukla and Pienemann [30] were one of the first who recognized the importance of incorporation of silver ions into a polymer matrix as a method to enhance olefin transport and to obtain high olefin/paraffin separation factors. Sungpet *et al.* [38] described incorporation of silver salt into grafted polymers prepared by pre-irradiation graft methods. Kawakami *et al.* [22] reported supported liquid membranes of $Rh(NO_3)_3$,-poly(ethylene glycol) in a glass microfiber filter for selective permeation of ethylene and propylene. Tsou *et al.* [24] investigated the silver facilitated transport of ethylene in liquid membrane contactor system. They applied a supported liquid membrane in the absorption part of the contactor, whereas desorption was established using a flash pot swept with helium. On silver sulfonate membranes, LeBlanc *et al.* [25] described a silver-containing cation-exchange sulfonated poly (dimethylphenylene oxide) membrane saturated with water. This membrane showed a very high permeability ratio for ethylene versus ethane, and generated considerable research interest in the facilitated transport of olefins using silver sulfonate membranes [27,29,31,33]. Cation-exchange membranes are able to exchange H^+ for Ag^+ like sulfonated poly (ether ether ketone) (SPEEK) [38], sulfonated polysulfone [39,42], and Nafion® [34], which are more stable since Ag^+ is not only physically but also ionically bond to the sulfonated membranes due to the exchange of H^+ with Ag^+. Kraus [27] reported on a water-free ion-exchange Nafion® 415 (Du Pont) perfluorosulfonate ionomer membrane containing silver ions and a poly(hydric alcohol) solution for the separation of ethylene from ethane. Koval and Spontarelli [28] described a water-saturated Nafion® 111 membrane with Ag^+ for the liquid phase facilitated transport of 1-hexane and 1,5 hexadiene between feed and permeate water-saturated decane solutions. They also used the same membrane and a Nafion® 117 membrane with Ag^+, both saturated with water, for the separation of styrene from ethylbenzene [154]. Employing these membranes, Koval *et al.* [31] further investigated this separation with respect to membrane thickness, membrane solvent and feed concentration. Koval *et al.* [33] reported that heat treatment of Nafion® membranes with glycerin

at elevated temperatures caused a permanent expansion of the membrane structure, i.e. swelling, which increased the diffusion coefficients by one order of magnitude for the styrene/ethylbenzene separation.

Only limited work has been done to develop new membranes which combine increased selectivities with higher permeation rates towards ethylene/ethane and propylene/propane separations for solid membranes. In the separation of propylene and propane, cellulose and polysulfone membranes were reported to show a selectivity of 3.78 and 1.42, respectively [189]. Membranes of PPO based co-polymers have exhibited higher selectivities of 17.8, and higher propylene permeabilities at 50 C [32]. Polyimide membranes showed extremely high permeabilities of 30-37 Barrers with ideal selectivities of 8.6-11 at 50 C, however, their room temperature values were relatively low [36].

However, recent success [190-204] in achieving excellent separation performance of propylene/propane and ethylene/ethane mixtures has encouraged researchers to continue. For many gas separations, to obtain good selectivity requires the use of amorphous glassy polymer materials. These materials, however, tend to be fairly impermeable compared with rubbery or elastomeric polymers, so very thin selective layers need to be produced to provide adequate *trans-membrane* flux of the permeating gases. If the polymer exhibits very high values of permeability and selectivity with dense films then it may be a good candidate for development of a practical membrane.

7. POLYANILINE – *A POSSIBLE SOLUTION ???...*

The 2000 Nobel Prize in Chemistry recognised the discovery of conducting polymers and over 25 years of progress in this field [205]. Conducting polymers are unique type polymers, which have π-conjugated electrons spread along the polymer backbone and have delocalised electron structure after doping. The science of the conducting polymer is rather young. Following the successful synthesis of conducting polyacetylene in 1970 by Shirakawa *et al.* [206,207], electrically conducting polymers have generated tremendous interest. Chiang *et al.* [208] discovered that chemical doping of polyacetylene $(CH)_x$, with iodine increases the electric conductivity by several order of magnitude. Many of these properties result from the nature of the polymer backbone, which consists

of the alternating C_6 rings and nitrogen hetero-atoms in either the amine (N-H) or imine (N only) form. Conducting or conjugated polymers are representative of a low dimensional solid with strong covalent bonds along the molecular backbone and very much weaker inter-chain interactions in the two orthogonal directions. Conductive polymeric materials with π-conjugated bonds are now finding growing applications in optoelectronic and microelectronic components [209-213].

a) trans - polyacetylene

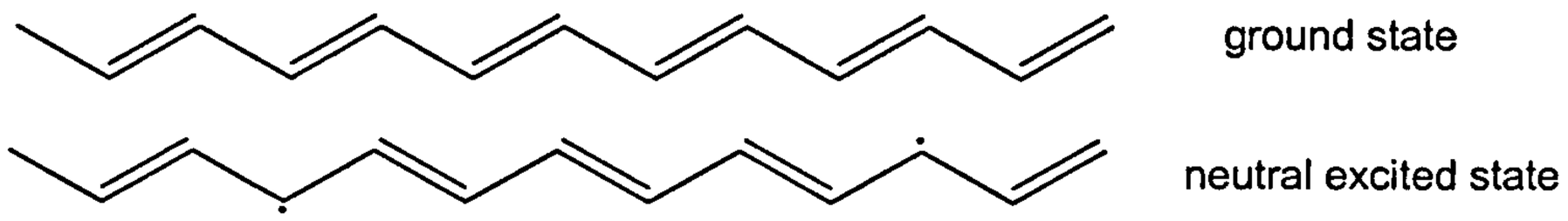

b) poly(p-phenylene)

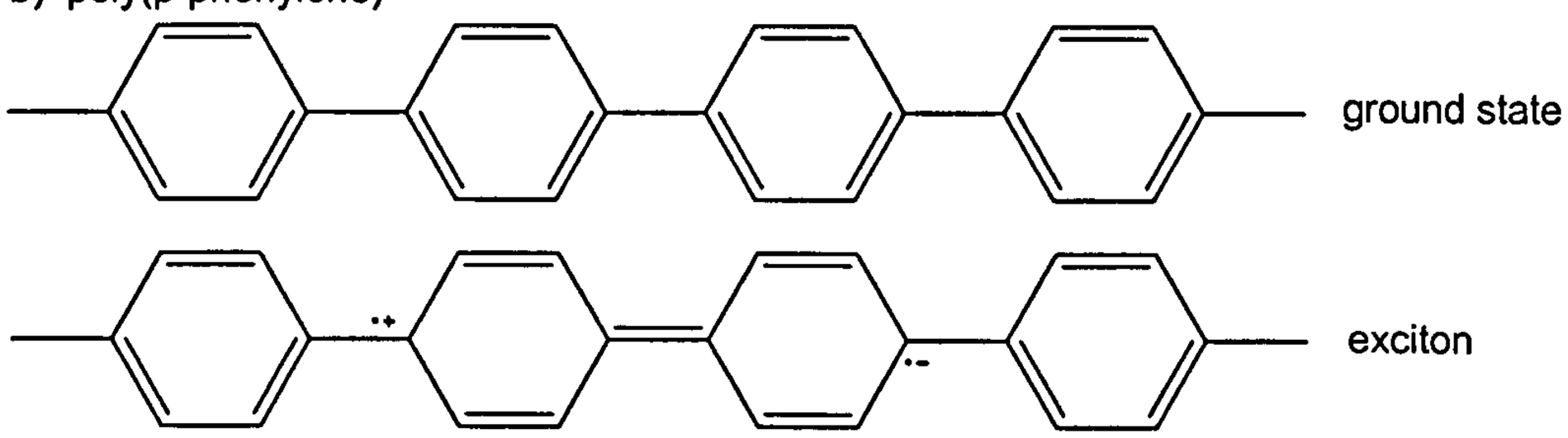

c) poly(p-phenylene vinylene)

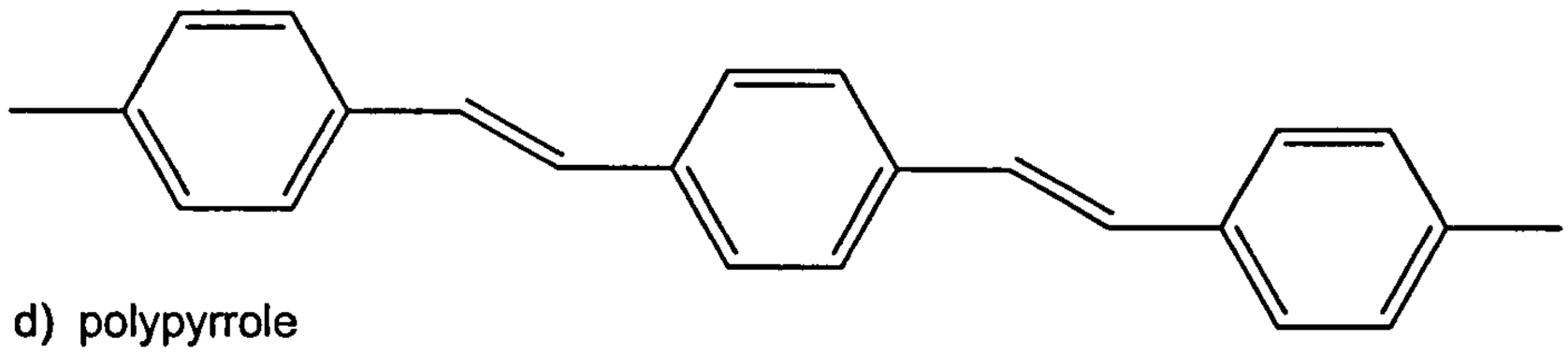

d) polypyrrole

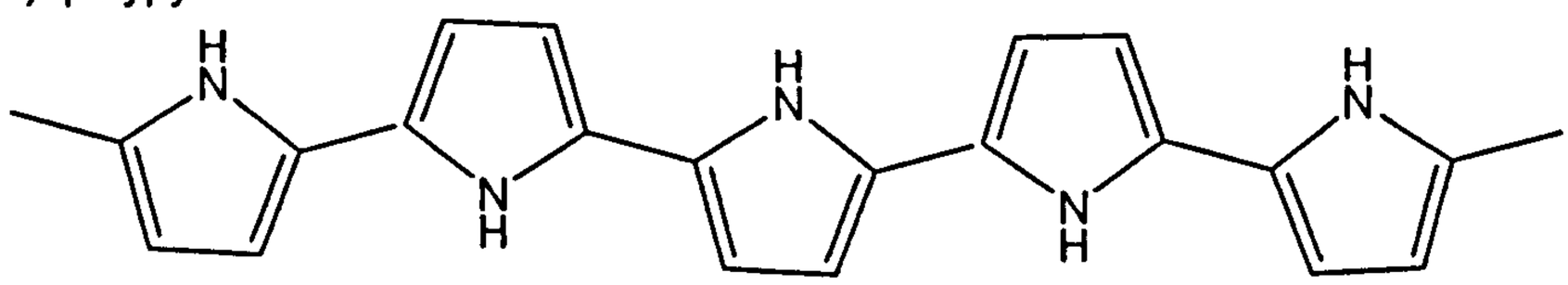

e) polythiophene

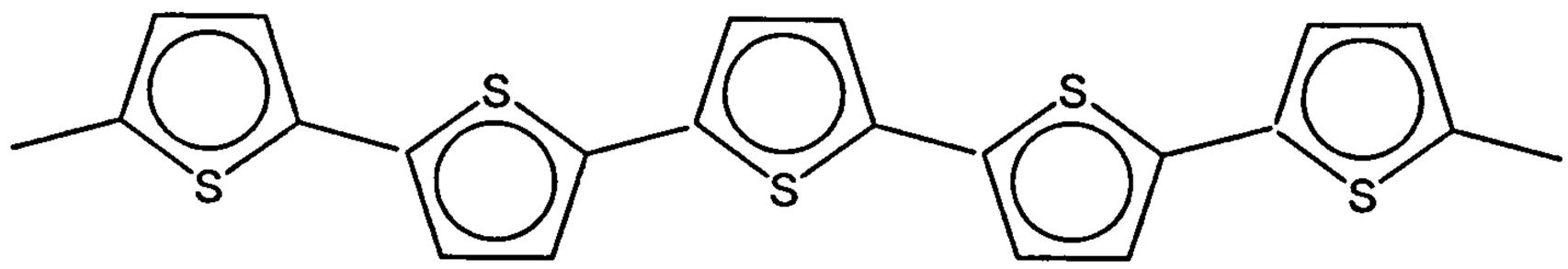

f) polyaniline

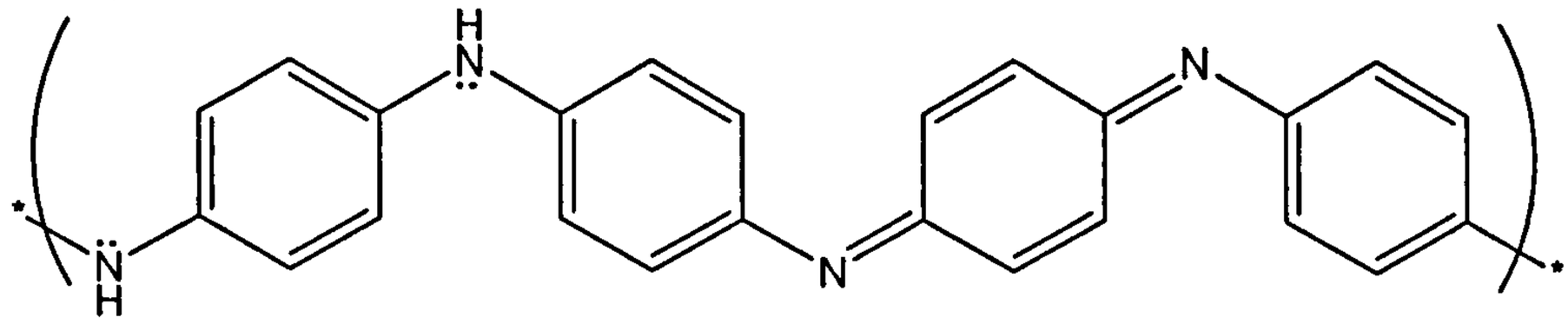

Figure 2. 12 Repeat unit of several pertinent conducting polymers [214].

The "*simple*" electronic polymers (see Figure 2.12) were synthesised and studied well over 2 decades, with a strong focus on polyaniline [49-62]. More complex homopolymers were developed and major parallel efforts were made in the study of π-conjugated polymers with non-degenerate ground states including polythiophene, *polyaniline*, polypyrrole, and poly(*p*-phenylene).

Polyaniline was first studied in 1910 by Green and Woodhead [215]. Since then, there have been numerous articles and reviews covering this polymer [216-220]. It has been of particular interest because of its environmental stability [221-222], controllable electrical conductivity [223,224], and interesting redox properties associated with the chain nitrogens. The structure of the oxidised insulating form of polyaniline prepared via oxidative polymerisation consists of a mixture of four species, as shown in Figure 2.13.

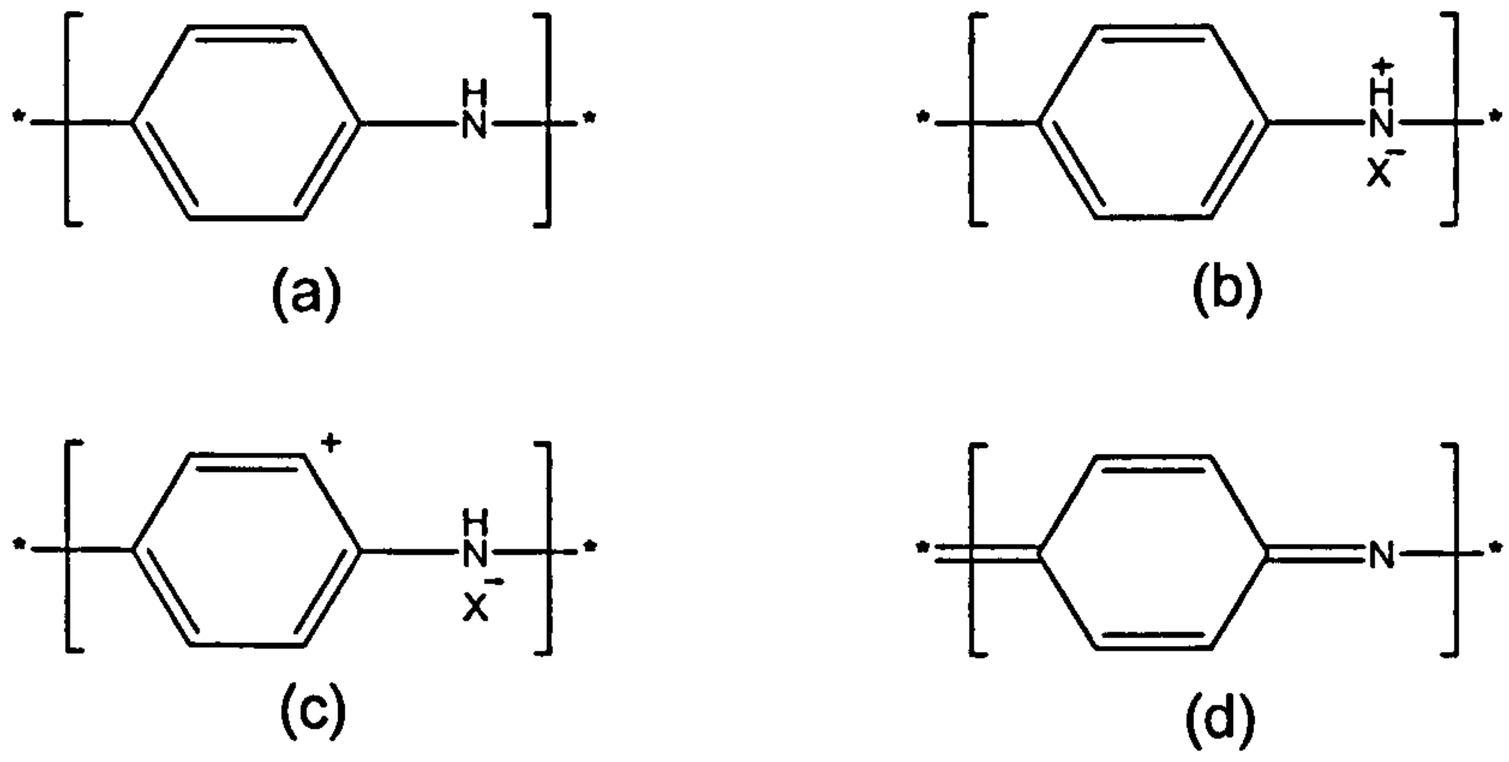

Figure 2. 13 Polyaniline represented with its four basic species; (a) benzenoid-amine state, (b) benzenoid-ammonium salt state, (c) dope-semiquinone radical state, (d) quinoid-diimine state.

Polyaniline is a mixture of a benzenoid-amine state (a), a benzenoid-ammonium salt state (b), a dope-semiquinone radical state (c), and a quinoid-diimine state (d). According to previously prevailing belief [225], polyaniline shows electrochemical behaviour between the benzenoid-amine state or benzenoid-ammonium salt state and the quinoid-diimine state, but Nakajima *et al.* [226], discovered that polyaniline shows electrochemical or charging/discharging behaviour between the benzenoid-amine state or benzenoid-ammonium salt state and the dope-semiquinone radical state, and that the less the quinoid-diimine state the more the discharge capacity is.

Polyaniline and its derivatives have the peculiarity to present the electrical conductivity that can be controlled either by redox chemistry (i.e. charge transfer doping) [227] or by Brønsted acid-base chemistry (i.e. protonation) [64,228]. The Pauli susceptibility, also known as charge paramagnetism, is essentially linearly proportional to the percentage of protonation [65], in agreement with the proposal that protonation ("proton doping") leads to phase segregation of unprotonated and fully protonated domains. A model based upon a two-step transition from isolated, doubly charged, spin-less bipolarons to a polaronic metal has therefore been suggested (see Figure 2.14). In the bipolaron-lattice case, the benzene ring between the two proton carrying nitrogens has a strongly quinoid geometry with double C=C bonds of 1.362 Å and single C–C bonds of 1.474 Å; the C–N bonds around the charged nitrogen posses very different lengths. In the polaron-lattice case, those latter C–N bonds are equal (1.411 Å), and only slightly shorter than those around the other nitrogen (1.414 Å); the benzene rings mostly adopt an aromatic geometry, the C–C bond lengths, as one goes away from the charged nitrogen, being equal to 1.440, 1.400, and 1.417 Å. Only the 1.440 Å bonds are reminiscent of some residual quinoid character [229].

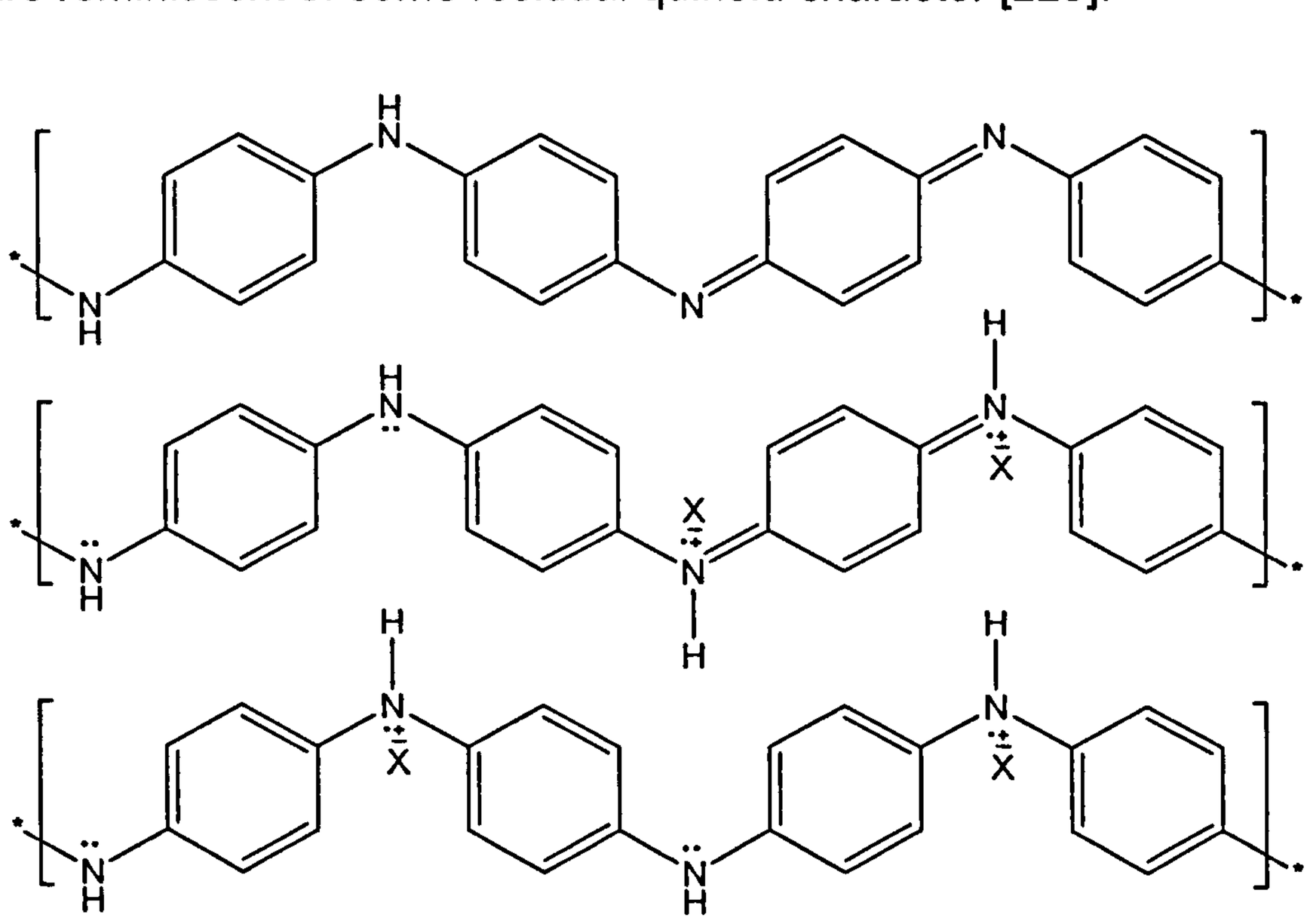

Figure 2. 14 Chemical structure of polyaniline; protonation-induced spin un-pairing in polyaniline, conversion from insulator to metal with no change in the number of electrons [228].

The physical and chemical properties of polyaniline are influenced by the synthesis route [230-232], chemical constitution [232], morphology [233-235], doping [236-240], and oxidation state [216-220]. The organic metal polyaniline has some curious properties [241]: it is an organic polymer, but totally un-mouldable and insoluble. Polyaniline is considered as a metal, i.e. it has free electrons in a metallic "conduction band", but the conduction band is "only" extending over about 10 nm, which is the reason why this metal is referred to as a "mesoscopic metal" and behaves as other mesoscopic metals (see Figure 2.15). Polyaniline is a redox active material and can exist in at least three oxidation states (see Figure 2.14), of which only one is metallic, but does not change its macroscopic form during reversible oxidation or reduction, hence, it can act as a "redox catalyst".

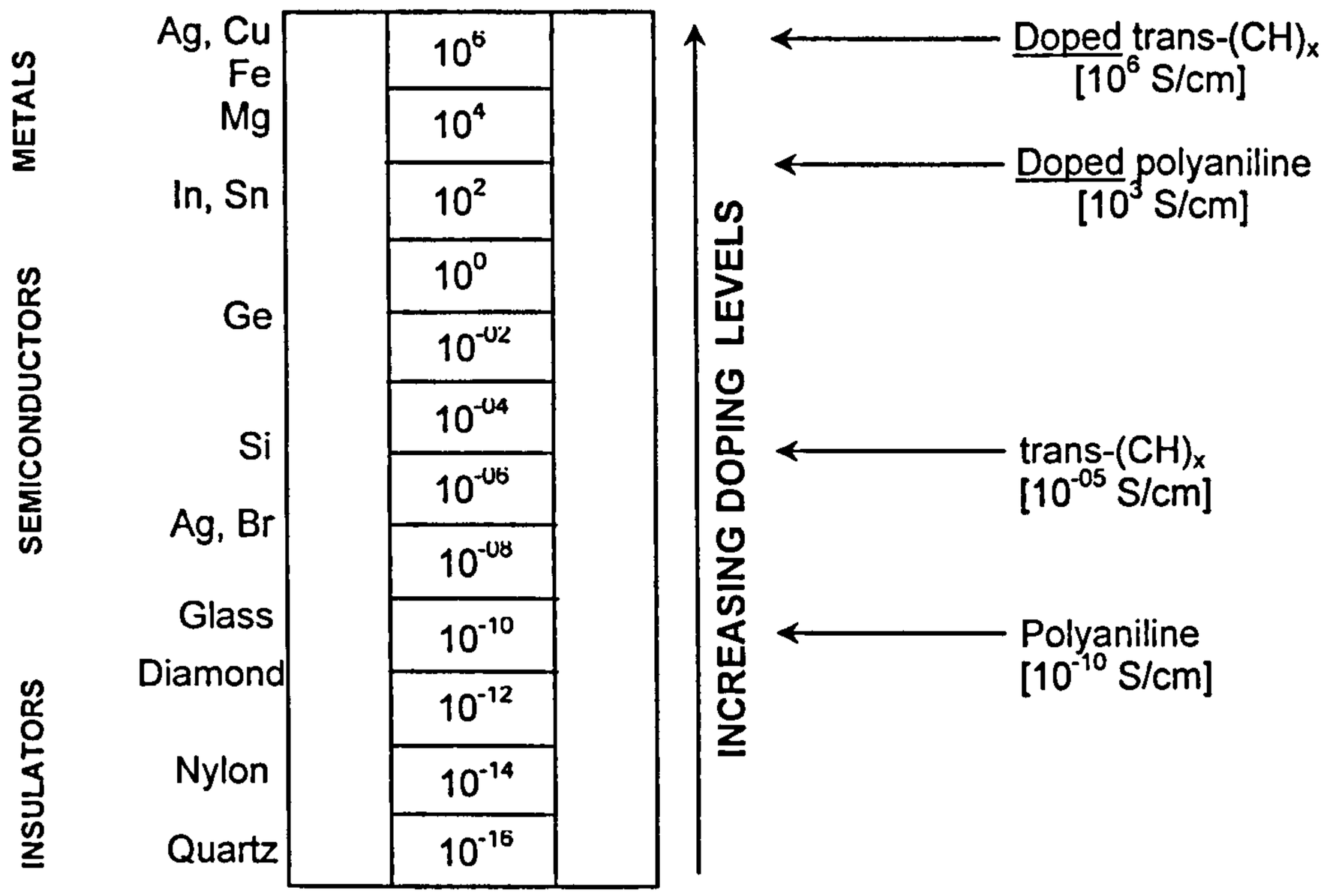

Figure 2. 15 Conductivity of electronically conducting polymer [242].

Polyaniline is "electro- and chemo-chromic", i.e. it changes its transparent colour upon oxidation or reduction. It is green in the stable metal state, blue in the stable oxidised or neutralised form and transparent in the reduced form which is readily reoxidised to the green or blue. In polyaniline a single broad polaron band appears deep in the gap instead of two, and a second very narrow band appears near the conduction band edge, and the band structure for the polaron lattice fully accounts for the optical transition [243]. The plasma frequency of

polyaniline is in the infrared, so it looks shiny and reflective in the infrared but in the visible spectrum it is basically transparent [242].

Great advancements have been made in our understanding of the chemistry, electrochemistry, structure, electrical and optical phenomena, processing and applications of polyaniline since the mid 1980s. The inspiration for using polyaniline for separation stems from the ability to control morphology of a polymer on the molecular level via the doping process either during or after its synthesis. An ability to reproducibly synthesise the pure polymers in a known oxidation state, with a known molecular weight and degree of doping has permitted meaningful physical studies involving structure, conductivity, magnetic and optical phenomena which have resulted in a better understanding of factors controlling conductivity and transport phenomena in general. The molecular conformation of doped polyaniline, i.e. "tight coil" or "expanded" coil, has been shown to have a very large effect on conductivity and transport mechanisms of films of the polymer [244]. An important step in polyaniline research is the solution processing of polyaniline, which has been brought about by the ability to synthesise the doped polyaniline soluble in a variety of solvents by using organic sulfonic acids, containing large organic groups as the dopant acids [245]. Polyaniline in the emeraldine base form is soluble in several solvents including N-methyl pyrrolidinone (NMP) [246,247], sulphuric acid [54], 80% aqueous acetic acid [48], chloroform and m-cresol [249,250].

The wealth of the chemical and physical properties of polyaniline makes it a good candidate for a wide range of technological applications [251-253]. In recent years, there is an increasing interest in the idea of using intrinsically conductive polyaniline membranes for industrial gas separation applications [49-62]. The gas transport selectivity data obtained by Anderson *et al.* [51] were remarkable. Indeed, if these data are correct, polyaniline is one of the most exciting materials for potential applications in industrial gas separations to be discovered in many years. When polyaniline membranes are exposed to different gases, the measured permeabilities are found to be dependent on the size of the penetrant gas [51]. The values range from 20 Barrers for the relatively small gas helium (2.6 Å) to 0.03 Barrers for the much larger gas methane (3.8 Å). The kinetic diameters of the gases are known from sorption experiments in

zeolites [153]. As cast polyaniline membranes permeate oxygen over nitrogen by a selectivity factor, 'α', of up to 9 [51-53].

8. CONCLUSION

Because of the exceptional gas-transport data obtained in the previous investigation, this project set out to explore the gas transport properties of polyaniline. The approach, however, is different from that used by Anderson *et al.* [51] who used thick (≈ 0.1mm) free-standing polyaniline films to conduct transport studies. Dense film tests are generally with film samples that are many microns in thickness and therefore actual gas flux through the film is low. To further expand the polyaniline membranes for industrial applications, one must find ways to enhance the gas permeation flux (productivity) and separation efficiency by combining the synthesis of high performance polymeric materials with the innovation of membrane fabrication technology. In this project the concept of supported ultrathin polyaniline films for membrane based separation will be explored. The diffusion through the polymeric layer is a rate-controlling step, and the gas flux through the membrane is inversely proportional to the membrane thickness. The membrane must be made extremely thin to achieve high fluxes, but must also be strong enough to withstand the operating pressures. The approach will be to produce thin film composite membranes consisting of a thin film of selective polymer (polyaniline) coated onto the surface of microporous support material. It is hoped that the advantage of this approach will be to obtain a higher net flux across the composite membrane, noting that the highly permeable support layer do not offer any resistance relative to the selective polymeric layer. Therefore, the gas flux and selectivity characteristics of the composite membrane should be determined solely by the chemically selective polyaniline layer.

It has been shown that electroactive polyaniline based membranes can undergo sharp changes as a result of doping by acids [51,64,250,254-256]. Polyaniline has a simple acid/base doping/dedoping chemistry enabling control over properties such as free volume [51], solubility [250], electric conductivity [64], and optical activity [254-256]. The dopant induced bipolaron to polaron transition is attributed to Coulombic repulsion that leads to enhanced resonance

energy stabilization; hence interaction between polaron and different gases increases solubility. In 1995, Rebattet *et al.* [58] showed the increase in sorption of various gases in polaron form of polyaniline was the result of interaction between polaron nitrogen atoms to oxygen. Since, polyaniline is dopable material, it can be doped with Group I-B metal ions, such as Ag(I) to facilitate transport of olefins through polyaniline membranes. The effect of doping, dedoping and controlled redoping of silver (Ag(I)) on permeation rate and separation efficiency of ethylene and propylene through ultrathin polyaniline-based composite membranes will be investigated. Permeability and separation efficiency of free standing undoped polyaniline will also be investigated in the present project.

This research will be therefore to develop a technique to synthesise polyaniline and produce polyaniline membranes for separating a gas from a gas mixture containing organic vapour or vapours. The gas transport properties of free standing undoped polyaniline films as well as polyaniline based nano-membranes for various gas pairs will be investigated. The gas mixture comprises the gas that is required to be separated and other vapour component or components, of which at least one is usually a C_{2+} hydrocarbon (i.e. ethane, ethylene, propane, propylene). The separation will be carried out by running a stream of gas mixture across a polyaniline membrane that is selective for the desired gas to be separated over another component or components. Polyaniline membranes have been selected for this work since they:

- are able to maintain useful separation properties in the presence of organic vapours, particularly C_{2+} hydrocarbon vapours, even at high levels in the gas mixtures.
- can recover from accidental exposure to liquid organic components.

In particular, this research will focus on determining various important transport parameters (e.g., permeability, ideal and separation factors), stability, and mechanical properties of polyaniline membranes for hydrogen/hydrocarbon and olefin/paraffin separations.

Chapter 3

EXPERIMENTAL TECHNIQUES

This chapter describes the synthesis route to prepare polyaniline powder followed by the techniques used to characterise as-synthesised polyaniline powder. The detailed description of the novel technique developed to prepare self-supported polyaniline and polyaniline/PVDF composite membranes has been given later in the chapter followed by the experimental techniques to characterise the polyaniline membranes (self-supported polyaniline films and polyaniline nano-film membranes supported on porous PVDF substrate). Finally, the experimental tools (e.g. single and mixed gas permeation measurement set-ups), developed to determine the transport properties of the polyaniline membranes, are discussed in detail at the end of the chapter.

1. MATERIALS AND INSTRUMENTATION

Polyaniline Synthesis : Analytical grade aniline, ammonium peroxodisulfate and *p*-toluene sulfonic acid (*p*-TSA) were obtained from Sigma-Aldrich, UK. Aniline was distilled in a nitrogen environment before it was used. All the other reactants were used without further purification. Analytical grade methanol was obtained from Fisher Scientific, UK, to wash the as-synthesised polyaniline salt.

Solvents : Analytical grade 1-methyl 2-pyrrolidone (NMP) was obtained from Acros Organics, UK, and analytical grade dimethyl sulfoxide (DMSO) was purchased from Sigma-Aldrich, UK.

Support Polymers : Laboratory grade cellulose acetate and ethyl cellulose were obtained from Fisher Scientific, UK. Analytical grade poly(vinylidene fluoride) (PVDF) was purchased from Sigma-Aldrich, UK.

Test Gases : Hydrogen, carbon dioxide, oxygen, nitrogen, methane, propylene, propane, ethylene, and ethane were purchased from BOC and were used in the pure permeation experiments. From these gases a gas mixtures with desired gas compositions were prepared.

Instrumentation : As-synthesised polyaniline batches were characterised using FT-IR spectrometry (Mattson-3000, UNICAM), UV-Vis spectrometry (Lambda 12, PERKIN ELMER), field emission scanning electron microscopy (Leo-1530 VP), Multivolume Helium pycnometry (Pycnometer-1305, MICROMERITIES), and gel permeation chromatography (Alliance GPC Systems, WATERS). FTIR grade potassium bromide was purchased from Sigma-Aldrich, UK to prepare translucent pellets to obtain FTIR absorption (or transmission) spectra.

Self-supported polyaniline and polyaniline/PVDF composite membranes were characterised using atomic force microscopy (Dimension 3100, VEECO), and field emission scanning electron microscopy (Leo-1530 VP). The experimental tools (e.g. single gas and mixed gas permeation measurement set-ups) were developed for the determination of the transport properties of both the self-supported polyaniline and the polyaniline/PVDF composite membranes.

2. SYNTHESIS OF POLYANILINE

During the past two decades, the chemical and physical properties of polyaniline have been studied extensively under different conditions, and a complete review on the tremendous advances made to understand the chemistry, electrochemistry, physics, and processing of polyaniline has been given by MacDiarmid [233].

Polyaniline is typically synthesised by oxidizing aniline monomer either electrochemically [257,258] or chemically [259-266]. The physical properties of the polymer are significantly affected by a number of reaction parameters such as oxidant type, solution pH, oxidant/aniline molar ratio, dopant type, dopant size and synthesis temperature [267-274]. In this work, aniline was chemically oxidised with ammonium peroxodisulfate in the presence of *p*-toluene sulfonic acid. In this work, the effect of reaction parameters such as the starting reaction mixture pH (3.0 to 0.5), oxidant/aniline molar ratio (0.5 to 1.3), oxidant addition

time (0 to 4 hours), total reaction time (0.5 to 4 hours) and polymerisation reaction temperature (+24 C to -20 C) on yield (polymer/monomer weight ratio), molecular weight and physical, chemical as well as transport properties of polyaniline is investigated.

The polymerisation reactions were performed in a reactor which allowed continuous stirring of the reaction mixture and also *in situ* measurement of the media temperature. The anchor stirrer was designed and used to scrape off polymer as it built up on the inner wall of the reactor. An anchor stirrer is useful because its outer diameter is designed only 4 mm less than the inner diameter of the reactor, hence it does not allow the produced polymer to stick on the inner surface of the reactor. It was possible (see description of the procedure below) to reduce the temperature of the reaction mixture to sub-ambient temperatures (temperature range: 30 C to -60 C) using an external ethylene glycol circulating chilling unit.

2.1. A General Chemical Route to Produce Polyaniline

Aniline was distilled under a nitrogen atmosphere in a distillation apparatus at 120 C before it was used. 9.313 g (0.1 mol) of distilled aniline was taken into the glass jacketed reactor. 100 g of 1M *p*-toluene sulfonic acid (*p*-TSA) solution was then gradually added (addition time: 2 hours) into the reactor containing distilled aniline with constant stirring. 26.243 g (0.115 mol) of ammonium peroxodisulfate was dissolved in 100 ml deionised water. The oxidant (0.115 mol ammonium peroxodisulfate) solution was dropped gradually into the reactor containing aniline and 1 M *p*-TSA with stirring speed of 150 to 160 rpm. The progress of polymerisation reaction can be confirmed by change in colour of the solution from white to green, increase in temperature, and precipitation of polymer.

All the reactions were carried out at starting pH ~ 1.0, except that the starting pH was adjusted to 3.0, 2.0, 1.0 and 0.5 by the addition of a small amount of ammonium hydroxide or *p*-toluene sulfonic acid, at a reaction temperature 0 C, oxidant/aniline molar ratio 1.15, oxidation addition time 2 hours, and total reaction time 48 hours.

The oxidant to aniline molar ratio was varied from 0.5 to 1.3 to observe its effect on polymer yield and molecular weight of polyaniline, and the oxidant addition time was varied between instantaneous addition and 4 hours and the total reaction time was varied from 0.5 to 48 hours, at a reaction temperature of 0 C, and starting pH ~ 1.0.

Figure 3.1 represents the steps involved in the general chemical synthesis of polyaniline. For polymerisation above 0 C (e.g. for the polyaniline batches produced at 24, 20, 15, and 10 C), Solution 1 and Solution 2 (see Figure 3.1) were kept at the same temperature (i.e. at reaction temperature) before being mixed. Below this temperature the reaction mixture freezes and polymerisation then proceeds in the solid state. The dielectric constant of water increases as the temperature is lowered; a salt or co-solvent must be added to Solution 1 if the temperature is to be lower than 0 C.

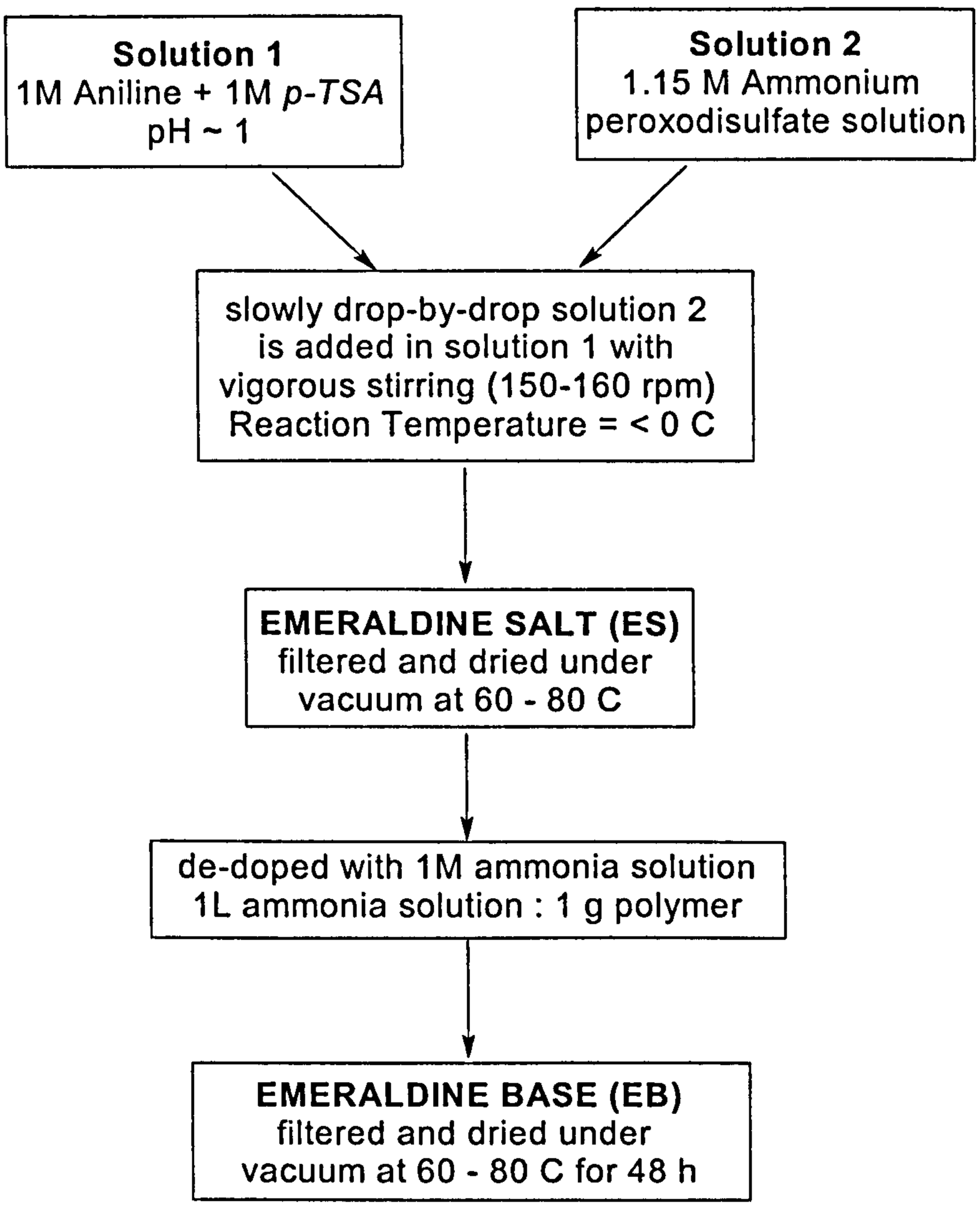

Figure 3. 1 Steps involved in chemical synthesis of polyaniline.

For polymerisations below 0 C, the best salt to use is lithium chloride due to its low molecular mass and high depression of the freezing point of water. Addition of lithium chloride to the reaction mixture enables it to remain mobile at sub-ambient temperatures and increases the dielectric constant of the medium. So, an aqueous solution of lithium chloride would appear to be the best reaction medium for aniline polymerisation at sub-ambient temperatures.

The freezing of the reaction mixture (Solution 1) does not hinder the polymerisation of aniline. The polymerisation also proceeds well in the frozen (solid) state. This was an additional feature which stimulated our interest in producing polyaniline at various temperatures (24 C to -20 C). An external ethylene glycol chilling unit was used to maintain the reaction temperature at 0, -10 and -20 C to synthesise polyaniline at low temperatures.

After 48 hours of complete addition of oxidant solution, the produced polymer (emeraldine salt) was filtered using an "ash-less" cellulose filter paper to separate by-products and oligomers from polyaniline. The remaining residue is washed with 2 x 500 ml of demineralised water followed by 1 x 500 ml methanol and again with 2 x 500 ml of demineralised water to remove oligomers. The washing steps were repeated up to six times. The colour of as-synthesised polyaniline salt is emeraldine-green. The polymer was then dried in a vacuum oven at 60 C for 48 hours and then kept in a desiccator at room temperature.

The dried polyaniline salt (emeraldine salt) was de-protonated to obtain an undoped emeraldine base (EB). The polyaniline salt was dedoped in an excess amount of ammonia water (about 500 ml 1 M NH_4OH for 0.5 g of polyaniline salt) for 24 hours. This step was repeated 2 to 3 times to obtain a fully dedoped form of polyaniline, having better solution properties of emeraldine base into 1-methyl, 2-pyrrolidone (NMP). When the ion-exchange was complete, the emeraldine base was washed with demineralised water several times. The dedoped emeraldine base was then dried in a vacuum oven at 60 C for about 48 hours. The colour of the dedoped polyaniline base is emeraldine blue.

3. POLYANILINE CHARACTERISATION

The synthesis of a polymer is, quite clearly, the *sine qua non* for polymer characterisation, but without the latter the former becomes an exercise of dubious value no matter how sophisticated the synthesis technique is. There is no definite sequence of characterisation methods that can be applied to a polymer. In this work, various characterisation methods were used to measure molecular structure and physical as well as chemical properties of the polyaniline powder.

3.1. Fourier Transform Infrared (FT–IR) Spectroscopy

Fourier transform infrared spectroscopy is a powerful tool to identify the types of chemical bonds in a polymer molecule by producing an infrared absorption (or transmission) spectrum that is like a molecular "fingerprint" [275]. The wavelength of light absorbed is a characteristic of the chemical bond. Molecular bonds vibrate at various frequencies depending on the elements and the type of bonds. For any given bond, there are several specific frequencies at which it can vibrate. According to quantum mechanics, these frequencies correspond to the ground state (lowest frequency) and several excited states (higher frequencies). One way to cause the frequency of a molecular vibration to increase is to excite the bond by having it absorb light energy. The energy corresponding to these transitions between molecular vibrational states generally corresponds to the infrared portion of the electromagnetic spectrum.

Infrared spectroscopy can be conveniently used to study the various intrinsic oxidation states of polyaniline [233,276-280]. In this work, FTIR spectra of polyaniline were recorded in the range 400 to 4000 cm^{-1} on a Mattson-3000 (UNICAM) instrument with a resolution of 2 cm^{-1}.

3.1.1. Sample Preparation

Since FTIR is an absorption process, there is often a high probability that samples will absorb some bands so intensely that light will not penetrate through the samples. Thus, the sample must be carefully prepared for FTIR

measurements. The samples need to be appropriately thinned or diluted by mixing with potassium bromide (KBr) crystals to obtain transmission spectra.

0.03 to 0.05% by weight dried polyaniline EB powder was mixed with FTIR grade potassium bromide (KBr) and pressed in a mechanical die press to form a translucent pellet. The diameter and thickness of the pellet were 13 mm and 1.3 to 1.5 mm, respectively. The analysis was carried out at ambient temperature (20 C). Both, absorption and transmission spectra were obtained for the all polyaniline batches produced at various polymerisation reaction temperatures (24 to 0 C). It is important to note that spectra obtained from different sample preparation methods looked slightly different from each other due to the different physical and oxidation states of the sample.

3.2. UV / Vis Spectrometry

Ultraviolet (UV) and visible (Vis) absorption spectroscopy is the measurement of the attenuation of a beam of light after it passes through a sample or after reflection from a sample surface. It corresponds to electronic excitations between the energy levels that correspond to the molecular orbitals of the system. Absorption of UV and visible radiation in organic molecules is restricted to certain functional groups (chromophores) that contain valence electrons of low excitation energy. The spectrum of a molecule containing these chromophores is complex. This is because superposition of rotational and vibrational transitions on the electronic transitions gives a combination of overlapping lines. This appears as a continuous absorption band.

UV-Vis spectroscopy has been widely used to characterise polyaniline composites [233,279-284]. In this work, a dual-beam UV-Vis spectrometer (Lambda 12 (PERKIN ELMER)) was used to determine different concentration and compositions of polyaniline solutions prepared in 1-methyl, 2-pyrrolildone (NMP). The dual-beam design greatly simplifies the measurement process by obtaining transmittance of the sample and solvent simultaneously. The detection electronics then manipulate the measurements to give absorbance. The use of UV-Vis spectra allow identification of various doping states of polyaniline since the transmission in UV-Vis range (wavelength: 190 to 900 nm) is directly related to the doping state and the degree of doping.

3.2.1. Sample Preparation

0.001% by weight clean, dried polyaniline powder was dissolved in NMP to prepare the sample solutions. Quartz cells were used for the analysis. The spectrometer was calibrated with pure NMP before the UV-Vis spectra for each polyaniline batches was obtained.

3.3. Polymer Morphology

Molecular shape and the way molecules are arranged in a polymer matrix are important factors in determining properties of polymers. The morphology of most polymers is semi-crystalline. That is, if the molecular weight of the polymer is large, it generally packs together in a non-uniform fashion, with ordered or crystalline like regions mixed together with disordered or amorphous domains. The observed morphology is a strong function of the level of magnification at which a material is observed. Polymer morphology can be observed using structural characterisation techniques such as, scanning electron microscopy (SEM), atomic mass spectroscopy (AFM), and scanning tunnelling microscopy (STM).

Scanning electron microscopy (SEM) is a useful tool to determine the morphology of polyaniline. This structural characterisation technique was used to observe the effect of the polymerisation reaction temperature on the morphology of polyaniline powder. Electron micrographs of polyaniline powder produced at various reaction temperatures were taken using a Leo-1530 VP field emission scanning electron microscope (FEGSEM).

3.3.1. Sample Preparation

A small quantity of clean, dried polyaniline powder was glued to a holder using an adhesive tape. Since, EB form of polyaniline is non-conducting, the polymer sample was sputtered with gold for the imaging analysis. As the morphology is a function of the level of magnification at which a material is observed, all SEM images were taken with the accelerating voltage 5 kV.

3.4. Polymer Density Measurements (Pycnometry)

Density is a basic physical property of the polymer, which is calculated by taking the ratio of polymer mass to volume. Determining the mass of the polymer is straightforward; it is the determination of volume which is more difficult. The volume of a solid object, whether a single piece of a mass of finely divided powder, is one of those concepts that cannot be bundled up into a single, neat definition.

A number of manual and automated methods are used to determine the volume and density of a polymer. The laboratory automated methods are often used in research and quality control applications. A multivolume pycnometer was used to measure the density of the polyaniline produced in our laboratory. It operates by detecting the pressure change resulting from displacement of gas by the polymer. The multivolume pycnometer is designed to measure rapidly the skeletal volume of the powders, granules, or any other solid objects having low vapour pressures and to permit computation of absolute density when weight information is supplied. The skeletal volume is the sum of volumes of the solid material and closed (or blind) pores within the pieces. The multivolume pycnometer measures with diminishing effectiveness the volumes of polyaniline which have appreciable vapour pressures. It differs from similar products in that three different size sample chamber configurations are provided and each has an associated expansion volume sized to provide the maximum accuracy and resolution for that range.

The accuracy and precision of the gas pycnometer in the determination of skeletal volume and density is quite high, but relies greatly on the sample material analysis gas being free of moisture. The sample must also be free from any volatile substances that can contribute their partial pressures and cause error and instability. The polyaniline sample was dried in a vacuum oven at 60 C for 48 hours before it was analysed. Helium was used as a displacement gas as it readily diffuses into small pores, and the volume obtained permits computation of the ultimate theoretical density of the polyaniline comprising the sample if there are no closed pores. 35 cm^3 sample chamber was used to analyse all polyaniline samples.

3.4.1. Sample Preparation

Polyaniline sample batches were dried in a vacuum oven at 60 C for 48 hours to remove any volatile substances. The clean, dried polyaniline was taken into the 35 cm^3 sample chamber and weighed accurately. During the analysis, the helium gas inlet pressure was limited to 19.5 ± 0.2 psi (134 ± 1.4 kPa) to avoid possible damage to the instrument.

3.5. Molecular Weight Measurements

The chain length is an important parameter in determining the properties of a polymer. Polymers generally consist of a large number of chains and these do not necessarily have the same chain length. Hence, there is a distribution in molecular weight. The length of the chain can often be expressed quite adequately by means of the molecular weight. The consequence of the existence of different chain lengths in a polymer is that a uniform molecular weight does not exist but rather a molecular weight average. Figure 3.2 shows a histogram of a polymer exhibiting a particular molecular weight distribution. This figure illustrates the number of fractions of molecules, n_i, with a particular molecular weight, M_i. The molecular weight distribution is an important property relative to membrane preparation and particularly to membrane characterisation.

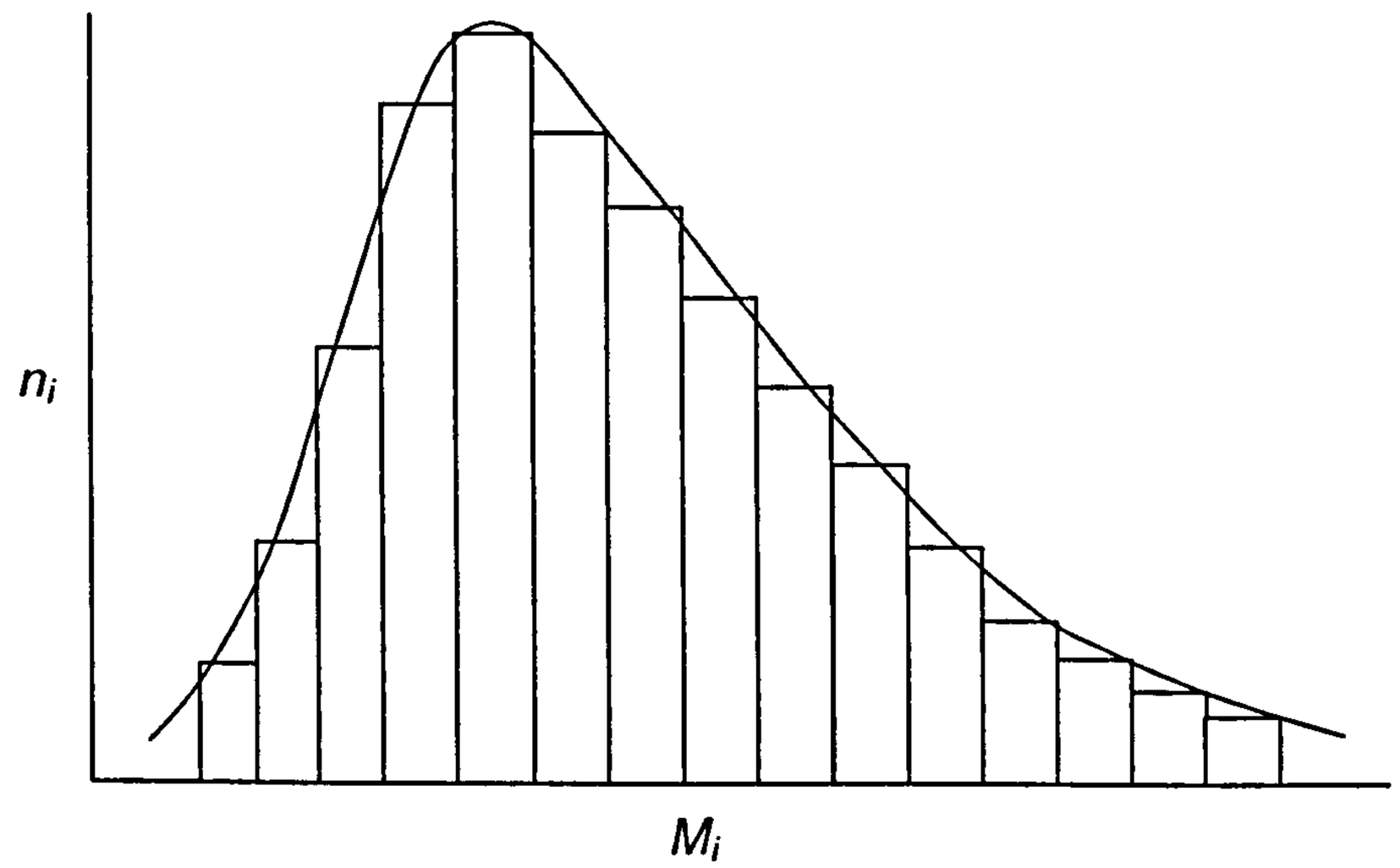

Figure 3. 2 Histogram demonstrating a possible molecular weight distribution in a polymer.

There is some difference of opinion as to what constitutes a polymer in terms of molecular weight. There are various definitions of the molecular weight of polymer [100]. The methods of molecular weight measurement are distinguished by whether the contribution of each molecule to a measured property is proportional to the number of molecules or to a power of the weight of the molecules present. The first category leads to a number average molecular weight, M_n which can be calculated by multiplying the number of chains of a certain length with their weight and adding this to the number of a second class of chain multiplied by their molecular weight, and so on, and then dividing by the total number of chains (see equation 3.1).

$$M_n = \frac{\sum_i n_i \cdot M_i}{\sum_i n_i} \tag{3.1}$$

In order to calculate the weight average molecular weight, M_w, the weight of the fraction, w_i, is used instead of number of molecules, n_i with a molecular weight, M_i.

$$M_w = \frac{\sum_i w_i \cdot M_i}{\sum_i w_i} \tag{3.2}$$

When a relatively small amount of very long chains is present in the polymer, M_w may differ quite considerably from M_n. This broad distribution can be expressed in terms of the polydispersity, which is the ratio of the weight average molecular weight, M_w to number average molecular weight M_n.

The analytical techniques used for the determination of molecular weight can be categorised into absolute and relative techniques. The main applicable technologies used to measure molecular weight of a polymer are:

- Mass spectrometry coupled with time-of-flight (MALDI–TOF MS)
- Gel permeation chromatography (GPC)
- Multiple angle laser light scattering (MALLS)
- Viscometry.

Amongst these, gel permeation chromatography was used to measure the molecular weight of polyaniline which was produced at various polymerisation reaction temperatures.

3.5.1. Gel Permeation Chromatography (GPC)

Since the introduction of gel permeation chromatography (GPC) by Moore [288], this physicochemical method of polymer characterisation has progressed at an extraordinary rate [289]. The primary purpose and use of the GPC is to provide molecular weight (MW) and molecular weight distribution (MWD) information about a particular polymeric material. The graphical data display typically depicts a linear detector response on the ordinate *vs* either chromatographic elution volume or, if processed, the logarithm of molecular weight on the abscissa. A typical GPC system is essentially a specialised isocratic high performance liquid chromatography. It is commonly purged with helium in order to degas it and prevent air bubbles from entering the detector downstream. A high pressure pump capable of operating at pressures up to 6000 psi (41.4 MPa) forces the mobile phase through line filters and pulse dampeners to the sample injector where an aliquot of dilute polymer solution is introduced. The polymer solution sample, which initially exists as a narrow band in the system, is then carried through the pre-column and the analytical column set where molecular size discrimination occurs. The discriminated sample elutes from the column set and passes through a detector, which generates an electrical signal proportional to the instantaneous sample concentration. The sample and mobile phase then exit the detector and are carried to a waste container while the electrical signal is transmitted to an integrator, recorder, or computer for display and/or further processing.

3.5.1.1. Primary Calibration

The purpose of calibration in GPC is to define the relationship between molecular weight and retention volume in the selective permeation range of the column set used and to calculate the molecular weight average of the polymer sample. In modern high performance GPC, there are four commonly employed

calibration methods. Three of these can be utilised in conjunction with a single (i.e. concentration) detector GPC system. The fourth type of GPC calibration requires the use of a second, molecular weight sensitive detector connected in series with the concentration detector.

A primary calibration curve (i.e. molecular weight *vs* retention volume) of standard monodispersed polystyrenes was used for the calibrations. Polystyrene molecular weight standards were made to 0.05% by weight solutions in NMP and detected at 264 nm. The calibration curve for monodispersed polystyrene for the molecular weight range 8,500 to 316,500 was obtained, and is only valid for GPC analysis of linear polystyrene samples.

3.5.1.2. Sample Preparation for GPC Analysis

Polyaniline sample batches were dried in a vacuum oven at 60 C for 48 hours. The clean, dried polyaniline samples (0.002 g of each) were dissolved in HPLC grade NMP (4 gm) to give 0.05% by weight solutions. The solution was placed in an ultrasonic bath for 15 minutes and then left to stand for 2 hours before passing through a 0.45 µm syringe filter to remove undissolved polyaniline particles. The GPC Styragel® HT4 column (300 x 7.8 mm), consisting 10 µm spherical particles with polymer substrate was obtained from Waters Corporation together with the molecular weight standards (molecular weight range: 5K to 600K). A column oven was set to 100 C for the sample flow rate of 0.5 µl at a pressure between 300 to 325 psi (2 to 2.24 MPa). The carrier solvent was HPLC grade NMP which was degassed by dynamic vacuum while immersed in an ultrasonic bath. The degassing of carrier solvent reduces the noise in the GPC chromatograms. The GPC system consisted of a Waters low pressure gradient pump (600E Multisolvent delivery system), a 717plus Autosampler and a 2996 Photodiode Array UV Detector. The UV detector was set to 350 nm to monitor the polyaniline elution, and the size of the sample injection coil was 20 µl.

4. PREPARATION OF POLYANILINE FILMS

4.1. Un-doped Self-supported Polyaniline Films

Currently, there are no commercial membrane technology products that use π-conjugated polymers (conducting polymers) [290]. Nonetheless, during the past 10-15 years there have been considerable research studies that have explored the potential of the conducting polymers for gas separations [49-62]. Interest in polyaniline membranes for gas separation stems from the work by Anderson *et al.* [51-53,55-57] who reported some of the highest ideal separation factors ever achieved for polymer films. However, processing polyaniline into useful forms for membranes with common organic solvents has been a key problem due to insolubility and unmouldability for basic research and industrial applications.

Based on experimental and thermodynamical considerations, it is reasonable to state that polyaniline cannot be truly soluble, but processable in colloidal dispersion [291]. This creates more doubts about whether the solvent approach – which in reality is only a different form of colloidal dispersion – is appropriate for improving the metallic properties and for making industrially useful, reproducible properties and products. Most other scientists [49,51-54,60,291-296] claimed that the true solutions of polyaniline exist, and the solvents have positive effects on crystallinity and metallic properties. However, according to Wessling [291], basic thermodynamic properties which prevent polyaniline from becoming completely soluble are:

- Unmouldability: solvent has to overcome the melt enthalpy before it can solvate; unmouldable polymers cannot be solvated.
- If a hypothetical melting point is assumed, and a hypothetical melting enthalpy, then the dissolution enthalpy prevents any solubility, as calculated using Flory-Huggins equation.
- The extremely high lattice energy which was calculated to be *ca.* 1.100 KJ/mol; the hydration energy of the anion and the cation is much smaller, resulting in insolubility in water, or organic solvents cannot invest a higher solvation energy

- the extremely high surface tension, as measured by inverse gas chromatography, around 150 MN/m, and expected to be even up to 1,500 MN/m; no solvent can overcome these surface energies.

The substances that dissolve polyaniline can be divided into two groups. The first group comprises substances with strong hydrogen-bonding groups, such as 1-methyl, 2-pyrrolidone (NMP), dimethyl sulfoxide (DMSO), *m*-cresol, dimethylformamide (DMF) [233,246,248,291-295], formic acid and other strong acids. These substances are capable of readily dissolving polyaniline at room temperature. A second class of organic solvents are those species without hydrogen bonding ability or with only very weak hydrogen bonding ability, such as toluene, *p*-xylene, decain and chlorobenzenes [291,295]. In general, the solvents used to dissolve polyaniline have carbonyl functional groups which form strong hydrogen bonds between the carbonyl group of the solvent and the secondary amine group of the emeraldine base.

4.1.1. Method to Prepare Self-supported Polyaniline Membranes

In this work, NMP was used as a suitable solvent to prepare polyaniline (EB) solutions. Such solutions were cast into dry dense films after the wet film was thermally treated to evaporate the solvent. Before the polymer could be dissolved into NMP, it has to be essentially water free as the residual water in the polymer matrix greatly reduces its solubility in NMP. The polyaniline powder was dried in a vacuum oven at 50 C for 48 hours before it was processed.

5 g of clean and dry polyaniline polymer was dissolved in 500 g of NMP. About 0.5 gm of polymer was added at an interval of half an hour with constant stirring. After addition of all 5 g of polymer, the temperature of the NMP was raised to at 50 C for 30 minutes. The polymer was stirred for 24 hours with a magnetic stirrer and then homogenised with an ultra-turrax homogeniser for 30 minutes. This solution was then filtered by glass wool followed by ash less filter papers of different grade and pore size down to 0.45 µm. The final filtered solution was analysed by Zetasizer (MALVERN Instruments) to measure the particle size of undissolved polyaniline particles. It was observed that the final filtered polyaniline solution did not contain particles larger than 300 nm.

In this work, ground glass petri dishes (20 cm diameter) were obtained from Glasgerätebau Ochs GmbH, Germany, and used to produce uniform layers of emeraldine base self-supported films. In order to get defect-free and stable membrane films, the glass petri dish used to produce the membranes had to be extremely flat, clean and without any scratches. The petri dish was washed with soap, rinsed with demineralised water and methanol and dried for approximately 2 to 3 hours, before being used. Defect-free polyaniline films of desired thicknesses were prepared by pouring a known amount of the final filtered polyaniline (EB) solution onto glass plate (petri dish) followed by evaporation of solvent. Approximately 0.16 ml/cm^2 of 1% by weight of polyaniline emeraldine base solution in NMP was required to produce a 1 µm thick film. The emeraldine base solution prepared in NMP was spread onto a glass petri dish and the solvent was evaporated at 70 C for 12 hours followed by annealing at 120 C for 2 hours in an oven fitted with NMP recovery system. The NMP recovery system was designed and mounted onto the oven, which allowed the recovery of approximately 40 to 50% of NMP which was purified by distillation and recycled for membrane preparation. The copper coloured polyaniline film was cooled down for 1 hour, and separated from the petri dish by scratching along the outer edge using a spatula and rinsing with the mixture of *iso*-propanol and water (1:1 by volume) underneath of the membrane. When the membrane was totally separated from the petri dish, it was taken out carefully and placed between 2 to 4 paper towels. With the weight of a 15 kg press, the membrane was pressed for 2 to 3 days between these paper towels.

In this way it was possible to produce reproducible defect-free, self-supported, polyaniline membranes with thicknesses of 2 to 6 µm.

4.2. Polyaniline based Nano-Membranes

Reducing the polyaniline membrane thickness will increase the gas transport rate, and supporting them with a suitable porous support layer will increase their mechanical properties. A selective separation layer can be supported by the same type of polymers (asymmetric gas separation membranes), or a porous support layer of a different polymeric material (composite gas separation membranes). Polysulfone, polyamide, polyimide,

polyetherimide, poly(vinylidene) fluoride (PVDF), etc... can be used as a support polymer to increase the mechanical strength of an ultrathin selective polyaniline layer. Illing *et al.* [296] discovered that PVDF, cellulose acetate, ethyl cellulose and PEI served best as a support material as they have maximum mechanical stability together with excellent support porosity.

In this work, the gas mixtures, to which the polyaniline membranes are exposed, are condensable (i.e. ethylene, ethane, propylene, propane) and have potential to degrade the performance of a selective polyaniline layer through plasticisation. The polymer material used to support the selective polyaniline layer would also suffer from such severe conditions and should be chemically stable to withstand these conditions. The preferred support materials to withstand these severe conditions are the co-polymers of the fluorinated or per-fluorinated polymers [297]. PVDF is chosen for this work as it does not fuse with polyaniline, and makes a stable entity with it. It is comparatively flexible after having been dried, and has negligible resistance to the permeating gas; the permeation properties only governed by the polyaniline layer. Hence, due to its excellent support porosity and mechanical as well as chemical stability, PVDF was used as a support polymer in this work.

4.2.1. Method to Prepare Polyaniline/PVDF Composite Membranes

A process to prepare polyaniline nano-film membranes can be divided into two steps. In the first step a dense, defect-free, ultrathin layer of polyaniline was produced on a glass petri dish. A known amount of 1% by weight of polyaniline solution in NMP was spread onto a clean glass petri dish to produce polyaniline film having thickness between 0.4 and 0.8 μm. The solvent was evaporated in a clean oven as per the method described earlier (see Section 4.1.1) except the film was annealed for 1 hour at 120 C. In the second step, the copper coloured ultrathin, dense polyaniline film was supported by poly(vinylidene) fluoride (PVDF). 3% by weight PVDF was dissolved in 3:1 mixture of NMP and dimethyl sulfoxide (DMSO). A known amount of PVDF solution was poured onto the ultrathin polyaniline film onto the petri dish. The ultrathin film of emeraldine base does not redissolve entirely when PVDF solution is poured onto it, because the initial solvent evaporation process at 120 C transforms amorphous glassy

polyaniline films into crystalline polyaniline films, which decreases the solubility of the polymer [298]. Approximately 25 ml of 3% by weight PVDF solution was required to support 100 cm^2 of the ultrathin polyaniline film. The solvent mixture was evaporated at 60 C for 6 to 7 hours in a clean oven. After complete evaporation, a porous support structure of PVDF that is combined with the ultrathin polyaniline emeraldine layer forms. The ultrathin polyaniline membrane supported on PVDF was separated from the petri dish by immersing it into 1:1 mixture of *iso*-propanol and distilled water. The prepared composite membrane was taken off the petri dish and pressed for 2 to 3 days between the paper towels with the weight of a 15 kg press.

This novel technique allows production of reproducible defect-free, ultrathin polyaniline membranes with thicknesses of 0.4 to 0.8 μm.

5. CHARACTERISATION OF POLYANILINE MEMBRANES

5.1. Membrane Morphology Analysis

5.1.1. Field Emission Gun Scanning Electron Microscopy (FEGSEM)

FEGSEM is an ultra-high resolution field emission scanning electron microscope and is ideal to study materials on the nanometer scale. A field emission cathode in the electron gun of a scanning electron microscope provides narrower probing beams at low as well as high electron energy, resulting in both improved spatial resolution and minimised sample charging and damage. FEGSEM produces clearer, less electrostatically distorted images with spatial resolution down to 1.5 nm, which is 3 to 6 times better than conventional SEM.

The Leo-1530 VP FEGSEM is a high-resolution field emission scanning electron microscope, and used for imaging and analysis of self-supported polyaniline films as well as ultrathin polyaniline films supported on PVDF. The membrane thicknesses for self-supported polyaniline membranes were measured using a micrometer with the accuracy of ± 1 μm and the data were verified by electron micrographs obtained by FEGSEM facility. The use of the FEGSEM facility was a suitable approach to measure the thickness of the selective polyaniline layer supported on PVDF. The thicknesses measured by

FEGSEM imaging were used to calculate permeability of various gases through polyaniline films.

5.1.1.1. Sample Preparation and Handling

Polyaniline films were freeze fractured using liquid nitrogen and glued to the holder. Similar to the polyaniline EB powder, polyaniline EB films were sputtered with gold for the imaging analysis. The samples were placed in a sample chamber through a large front door. The FEGSEM was equipped with a TV-camera which was mounted parallel to the sample stage tilt axis to facilitate operations at short working distances. The eccentric specimen stage was capable of an 80 mm x 80 mm x 30 mm range of travel, 360 degrees of rotation, and 15 to 80 degrees of tilt. The thickness of a film was calculated by averaging the measured thicknesses at various points from a graduation scale in the lens.

5.1.2. Atomic Force Microscopy (AFM)

The atomic force microscope (AFM) is a very high resolution type of scanning probe microscope, with demonstrated resolution of fractions of an Angstrom, more than a 1000 times better than the optical diffraction limit. The AFM consists of a micro-scale cantilever with a sharp "tip" (probe) at its end that is used to scan the specimen surface. The cantilever is typically silicon or silicon nitride with a tip radius of curvature on the order of nanometers. When the tip is brought into the proximity of a sample surface, forces between the tip and the sample lead to a deflection of the cantilever. This deflection is measured using a laser spot reflected from the top of the cantilever into an array of photodiodes.

An AFM image contrast can be obtained in many ways. The primary imaging modes of operation are static (contact) and dynamic (tapping) mode. In the static (contact) mode of operation, the static tip deflection is used as a feedback signal. It operates by measuring attractive or repulsive forces between a tip and the sample. In the case of the dynamic (tapping) mode, the cantilever is externally oscillated at or close to its resonance frequency (often hundreds of kHz) and positioned above the surface so that it only taps the surface for a very small fraction of its oscillation period. In the case of polymer films, if the film

were scanned with the contact mode method, there would be a risk that the tip would collide with the surface, causing damage. Hence, the tapping mode of operation is the more appropriate way to obtain AFM images for polymeric films.

AFM images of ultrathin polyaniline membranes supported on PVDF were obtained using a Dimension 3100 (VEECO) atomic force microscope with tapping mode of operation. The images were analysed by NanoScope™ 3D, and a 1 μm x 1 μm area of surface was scanned using an etched Silicon probe ("tip"). Height image data obtained by the AFM was three dimensional. The usual method of colour mapping for height was used to display the data.

5.1.2.1. Sample Preparation

An adhesive tape was used to glue 0.5 cm x 0.5 cm sample of PVDF supported polyaniline membrane to a magnetic sample holder. For tapping mode AFM, an etched silicon probe was installed in the AFM tip holder. The membrane was placed on the sample holder in a way that a selective polyaniline layer was facing the cantilever and the tip. The magnet of the sample holder holds the sample mounting disk securely in place. The cantilever was placed above the polyaniline membrane surface and oscillated at 300 kHz. The laser deflection method was used to detect the root-mean-square amplitude of the cantilever oscillation. A feedback loop maintained the constant oscillation amplitude by moving the scanner vertically at every x, y data point. Recording this movement formed the topographical image of polyaniline layer, which was analysed by the NanoScope™ 3D controller.

5.2. Mechanical Properties

The mechanical behaviour involves the deformation of a polyaniline film under the influence of an applied force. Generally, mechanical properties are not very important in membrane processes because the membrane is held by supporting material. However, it becomes important for high pressure gas separation processes used to separate various gas mixtures.

The tensile testing of self-supported polyaniline films were performed by elongating a polyaniline film and measuring the load carried by the film. The load

and deflection data were translated into a stress-strain curve from the knowledge of the film dimensions. The shape of the test polyaniline film sample is described in ISO 527-2 [299], with an overall length of 150 mm, and effective test length 50 mm and a width of 10 mm. The thicknesses of the self-supported polyaniline sample membranes were between 95 and 100 μm.

5.2.1. Sample Preparation

Prior to the analysis, the polyaniline test samples were dried in a vacuum oven at 60 C for 24 hours and then exposed to the atmospheric conditions for 3 hours. The polyaniline membranes were cut into the shape as described in ISO 527-2 [299]. The elongation rate of 0.2 mm per minute was kept for all polyaniline samples. The linear interpolation in the appropriate part of the stress *vs* strain graph was used to calculate the Young's Modulus.

5.3. Experimental Determination of Gas Transport Properties

The permeation rate of a penetrant through a membrane can be obtained by either the steady state diffusion or time-lag techniques. Both of these techniques require well defined conditions of membrane surface concentration. In this work, an integral permeation method [80,300] was used to estimate gas transport properties through polyaniline membranes. This method is usually performed by allowing the penetrant to permeate through an initially degassed polymeric membrane, and accumulate in an evacuated chamber. The rise in pressure at constant volume or the increase in the volume at constant pressure is then monitored with respect to time. The barometric technique was used to monitor the pressure rise in a known downstream volume and is the most commonly used technique to measure the permeability of pure gases.

The permeability for pure penetrating gas was calculated independently using the following equation 3.3;

$$P_i = \frac{1}{p_{i,o}} \times \frac{V_d \cdot t_m}{R \cdot T \cdot A_m} \times \left[\left(\frac{dp_i}{dt} \right)_{steady-state} - \left(\frac{dp_i}{dt} \right)_{leak} \right] \qquad (3.3)$$

where V_d is the down stream volume of the permeation cell (cm^3), t_m is membrane thickness (cm), $p_{i,o}$ is the feed side penetrant pressure maintained in the permeation cell, R is the gas constant (0.278 $cm^3 \cdot cmHg / cm^3_{STP} \cdot K$), and T represents the absolute temperature (K). A_m is the membrane surface area (cm^2), and $(dp/dt)_{steady\text{-}state}$ and $(dp/dt)_{leak}$ are the steady-state rates of pressure rise $(cmHg/s)$ in the downstream (permeate) volume at a fixed pressure and under vacuum , respectively. The permeability coefficient, P_i, is often expressed with the unit Barrer,

$$1 \text{ Barrer} = 1 \times 10^{-10} \left(\frac{cm^3_{STP} \cdot cm_{polymer}}{cm^2_{polymer} \cdot s \cdot cmHg} \right) \quad (3.4)$$

The schematic of the experimental technique is shown in Figure 3.3. The set-up is best described by categorising it into five broad sections. Every section is interconnected and performs different functions at various stages of an experimental run. Besides allowing pure gas permeation experiments, the set-up can be used to carry out mixed gas permeation experiments, with minor modifications during the data collection. With prior knowledge of the volume of the downstream chamber and the applied feed gas pressure, the measured accumulation rate is then related to the membrane's gas permeability. For mixed gas permeation experiments, besides monitoring the accumulation rate, the concentration of the permeate gas mixture is also measured at regular time intervals. The set-up is designed and constructed with 316 stainless steel case (operating pressure up to 50 bar (5 MPa)), tubing and fittings for high pressure permeation studies (0 to 150 psi; 0 to 1.03 MPa).

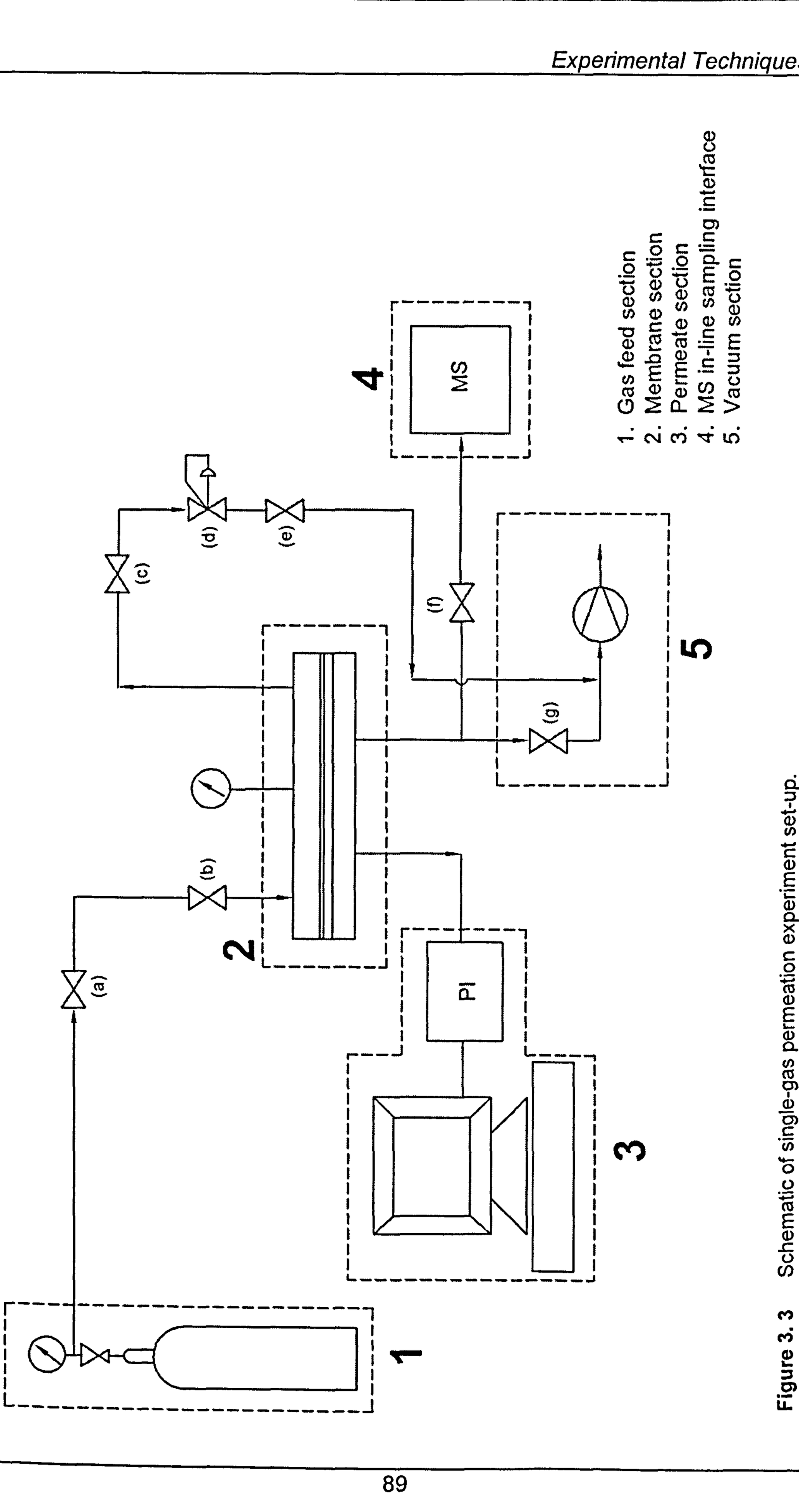

Figure 3. 3 Schematic of single-gas permeation experiment set-up.

5.3.1. Construction of Gas Permeation Experimental Set-up

5.3.1.1. Feed Gas Supply and Regulatory System

The feed section supplies the test gases to the feed side of the membrane in the permeation test cell. The feed section is connected to the membrane cell through valve (a), and to the vacuum system through valve (g). The feed pressure is regulated by a two stage pressure regulator and valve (a), and measured by a pressure gauge having a range 0 to 150 psi (0 to 1.03 MPa). The pressure in the upstream section of the permeation cell is maintained by back pressure regulator (valve (d)). Valve (c) and back pressure regulator (valve (d)) can be used to depressurise the system if and when needed.

5.3.1.2. Membrane Permeation Cell

The permeation cell was designed and made in the laboratory. The detailed design of the permeation cell is discussed in Appendix 2. The cell is made of stainless steel (SS 316) and consists of two halves which are bolted together. The upstream section is connected to the gas supply section and the bottom part to the permeate section. The cell houses a circular membrane with the diameter 90 mm, with the effective diameter for diffusion being 80 mm. A flat rubber gasket was used to provide the vacuum seal between the upstream and downstream sections. The membrane is supported against pressure stress by a fritted stainless steel disc. The sintered steel disc, with a porosity of over 100 microns, acts as a highly porous ineffective filter for the permeating gases.

5.3.1.3. Permeate (Downstream) Section

The permeate section constitutes the calibrated constant volume downstream chamber used for accumulating the permeating gases during the experiments. The gas permeation rate was calculated by measuring the rise in pressure in downstream section by a MKS Baratron pressure transducer having a range of 0 to 1000 torr. Valve (g) can act as a safeguard against overpressurisation in the downstream section due to membrane breakdown. The design of this section has a provision for changing the total volume of the

chamber by connecting the gas sample cylinders of a known volume. This permits the transport study of high flux polyaniline nano-membranes with optimised transducer response. The data collected by the MKS Baratron pressure transducer were analysed by PicoLog® 16 which was installed in a computer connected to it.

5.3.1.4. Mass Spectrometer In-line Sample Interface

The sampling interface (mass spectrometer) is used only for mixed gas permeation experiments. The mass spectrometer separates the gas molecules by mass. The major usage of such an instrument is in identification of elements and hence it is more popular in the study of reactive systems where species are being generated or lost. The instrumentation of mass spectrometer involves performing following steps.

- Sample ionisation : Here the sample, injected as a low pressure gas into the chamber, is ionised by either bombarding it with electrons generated from a filament (electron-impact ionisation) or from an ion-molecule reaction in the gas phase (chemical ionisation).
- Acceleration of ions by applied electric field : This helps in speeding up the charged molecules to produce their own magnetic field.
- Dispersion of the ions : The accelerated ions are passed through a magnetic field where the interaction between applied and generated magnetic field occurs which then tends to change the path of ions.
- Detection of ions : The deflection of the ions is recorded on a detector plate to produce a corresponding electrical signal. This is then used for quantitative and qualitative analysis of the gas molecule.

5.3.1.5. Vacuum Supply Section

The vacuum pump used to evacuate the entire set-up is a two stage vacuum pump obtained from Edwards, and can generate vacuum up to 0.2 torr.

5.3.2. Operational Procedure

5.3.2.1. Inherent Leak Testing

The inherent leak rate of the feed (upstream) and permeate (downstream) sections was measured by using an aluminium foil as a membrane. The entire gas permeation set-up was degassed for 48 hours. The pressure increase in both sections was monitored for 8 hours. Necessary adjustments were made with the tube fittings to minimise the leak rate. The experiment was repeated with another sample of aluminium foil to confirm the leak rate and the sealing of the permeation cell.

5.3.2.2. Permeate Volume Calibration

The volume of the downstream section must be measured accurately, in order to obtain the correct permeability values of various permeating gases through polyaniline membranes. The volume calibration involved measurement of the internal volume of the tube segments and fittings which constitutes the permeate section volume. The downstream volume was determined with high accuracy by using a Manometric method, and the measured value was confirmed by conducting single permeation test with standard membrane with known permeability, under similar operating conditions.

5.3.2.2.1. Manometric Method

A circular (90 mm) sample of aluminium foil is used as a membrane to isolate the downstream section from the upstream section. A sample of aluminium foil was placed on a sintered metal disk in the permeation cell. A flat rubber gasket was used to provide the vacuum seal between upstream and downstream section. The downstream section was evacuated using a vacuum pump for 48 hours. Once steady state is reached, valve (g) (see Figure 3.3) which connects the downstream section to the vacuum pump was closed. The pressure change with time in the downstream section was monitored for 8 hours using a MKS Baratron pressure transducer. The data were analysed on a computer using PicoLog® 16. This experiment was run for 8 hours, and the

pressure change monitored over 8 hours was 0.008 cmHg, which could reasonably be neglected.

Once the leak test was performed, the downstream section was evacuated using a vacuum pump for 12 hours. When steady state was reached, the valve (g) was closed. The vacuum pump was replaced by a gas sample cylinder of known gas volume at atmospheric pressure. The valve (g) was then opened briefly (for 2 to 3 s). The rise in pressure in the downstream section is measured using a MKS Baratron pressure transducer. Several sets of calibration runs were performed for one gas sample cylinder to calculate the downstream volume, V_d, in order to reduce the manual error. The experiment was performed with three gas sample cylinders (10, 15 and 25 cm^3). The following equation was used to calculate downstream volume:

$$V_d \times p_0 + V_1 \times p_1 = p_2(V_d + V_1) \qquad (3.5)$$

where, V_d is the downstream volume of the permeation cell (cm^3), V_1 is volume of gas sample cylinder (cm^3), p_0 is the pressure in the downstream section before opening the valve (g) (cmHg), p_1 is atmospheric pressure (cmHg) and p_2 is pressure in the downstream section after opening the valve (g) (cmHg).

5.3.2.2.2. Gas Permeation Method

To confirm the value obtained for the downstream volume using a manometric method, a single gas permeation test was conducted using a PDMS membrane having selective layer thickness 2 µm. The aluminium foil seal used in the Manometric method (see Section 5.3.2.2.1) in the permeation cell was replaced by the PDMS membrane. The permeation cell was degassed under vacuum for 24 hours to eliminate the effect of adsorbed volatile chemicals in the PDMS membrane. The upstream section was pressurised and gas permeation through the PDMS membrane was monitored by measuring the rise in pressure in the downstream section using a MKS Baratron transducer. The detailed operational steps, to carry out the experiment, are discussed in Section 5.3.2.4 of this chapter.

The approach was to calculate the downstream volume by rearranging equation 3.3 to the following equation 3.6;

$$V_d = \frac{P_i \cdot p_{i,o} \cdot R \cdot T \cdot A_m}{t_m\left[\left(\frac{dp_i}{dt}\right)_{steady-state} - \left(\frac{dp_i}{dt}\right)_{leak}\right]} \qquad (3.6)$$

where, V_d is the down stream volume of the permeation cell (cm^3), t_m is the selective PDMS layer thickness (cm), $p_{i,o}$ is the feed side penetrant pressure maintained in the permeation cell, R is the gas constant ($0.278\ cm^3 \cdot cmHg / cm^3_{STP} \cdot K$), and T represents the absolute temperature *(K)*. A_m is the membrane surface area *(cm^2)*, and $(dp_i/dt)_{steady\text{-}state}$ and $(dp_i/dt)_{leak}$ are the steady-state rates of pressure rise *(cmHg/s)* in the downstream (permeate) volume at a fixed pressure and under vacuum, respectively; and P_i is the permeability coefficient (Barrer) of a penetrant gas.

5.3.2.3. Membrane Installation and Membrane Defect Test

The proper placement of the membrane in the cell is important in preventing membrane damage and in accurately defining the effective surface area of the membrane available for permeation. Precaution has to be taken, especially in the case of curled polyaniline membranes (films with thickness less than 5 μm), where it is difficult to place the membrane flat on top of the sintered metal disc and tighten the membrane cell blocks together. Also, stress from uneven contact between the membrane and flat rubber gasket, during tightening two blocks together, could damage the polyaniline film. The procedure employed for membrane placement in the cell was to tighten the blocks slowly while allowing some gas from the feed section to press the membrane against the metal sintered disc. With the gas escaping radially from the membrane top surface, the two blocks were tightened to lock the membrane flat with the flat rubber gasket in the permeation cell.

After the membrane installation, tests were conducted to check for any membrane defects, such as stress fracture and pin-holes. The presence of defects can be detected by performing single gas permeation experiments using

nitrogen and oxygen. The presence of stress fracture is evident when no resistance is observed by the membrane to the applied feed pressure. The membrane is regarded as pin-hole free by matching the calculated permeability and the selectivity of the oxygen and nitrogen gases (α_{O_2/N_2}) with data available in literature.

5.3.2.4. Single (Pure) Gas Permeation Experiment

Single gas permeation experimental set-up is given schematically in Figure 3.3. Once the membrane (i.e. polyaniline self-supported membrane or polyaniline nano-membrane) was properly mounted and checked for defects, the feed and permeate section along with the membrane section were degassed for at least 24 hours. The complete degassing of the membrane was checked by closing valve (b), valve (c), and valve (g) (see Figure 3.3) and monitoring the pressure increase in the upstream and downstream sections. An observed leak rate in the permeation section, close to the inherent leak rate of the system, confirmed the degassing of the membrane.

The experiment was then started by running the PicoLog 16 program on the computer, which records the downstream pressure of the permeation cell. The test gas was introduced by opening valve (a) and valve (b). This was simultaneously accompanied by a measurement of the feed pressure and the permeate pressure with respect to time. The feed pressure was maintained at the test pressure using back pressure regulator (valve (d)). The time difference between the opening of valve (b) and attainment of constant feed pressure at the surface of the membrane was assumed negligible. The total time of the experiment was set to 4 hours, that is the time at which the change in permeate pressure rate was observed to be constant for at least 1000 sampling periods.

As the gas starts permeating through the membrane the rise in pressure in the downstream section with time is measured and plotted by PicoLog®. The gradient of pressure *vs* time graph can be calculated and utilised to calculate permeability, *P*, using equation 3.3. The whole procedure was repeated twice (with two different polyaniline membrane samples) before changing any operating conditions such as, feed gas, or feed pressure.

5.3.2.5. *Mixed Gas Permeation Experiment*

Pure gas permeation measurements have often been used to estimate the intrinsic separation properties of polymeric membranes. Understanding the transport behaviour of the target gases through membranes is the foundation of realising effective separation of mixed gases and selecting the appropriate feed conditions. Considerable amounts of data are available on the permeation of pure gases through polyaniline membrane [49-62], but less or none on the permeation of gas mixtures.

Pure and mixed gas permeation experiments differ in two ways:

- In a mixed gas experiment, the feed flows along the film and the permeate flows perpendicular to the film (cross flow configuration).
- It is necessary to measure the gas composition of the permeate as well as the feed gas in mixed gas experiments. This is done using a mass spectrometer which can be brought online by opening valve (f) (see Figure 3.3).

The permeation behaviour of a pure gas through a polyaniline membrane depends mainly on the properties of the gas and membrane as well as feed conditions. However, some differences between pure gas and mixed-gas permeation results may exist because of:

- the competition in sorption amongst the penetrants
- the possible plasticisation induced by CO_2 and hydrocarbon gases when this exist in the feed
- concentration polarisation
- non-ideal gas behaviour.

Therefore, in actual membrane separation applications, it is very important to measure the permeation data of the mixed-gas for a polymeric membrane to optimise the separation design and determine the true membrane performance in industrial applications. It is also necessary to establish a mathematical model based on the available experimental data. The model can be used as a powerful tool to evaluate or predict the performance of the separation system at various feed conditions for a specific gas pair-membrane system.

The permeate flow, J_p, is calculated using the following equation;

$$J_p = \frac{P_{total}}{t_m} \cdot p_f \cdot A_m \qquad (3.7)$$

The separation factor is calculated with the ratio of the mole fractions in the permeate divided by the ratio of the mole fractions in the feed (see equation 2.31; Chapter 2). Since the permeate pressure is kept close to zero, the separation factor will further be referred to as the selectivity. Furthermore, equation 2.31 is only valid if the feed composition is kept constant during the permeation experiment.

The mixed gas permeation experiment involved similar start-up as the single gas permeation experiment, except some modifications in the gas feed section are required to prepare the gas mixture to the desired composition (see Figure 3.4).

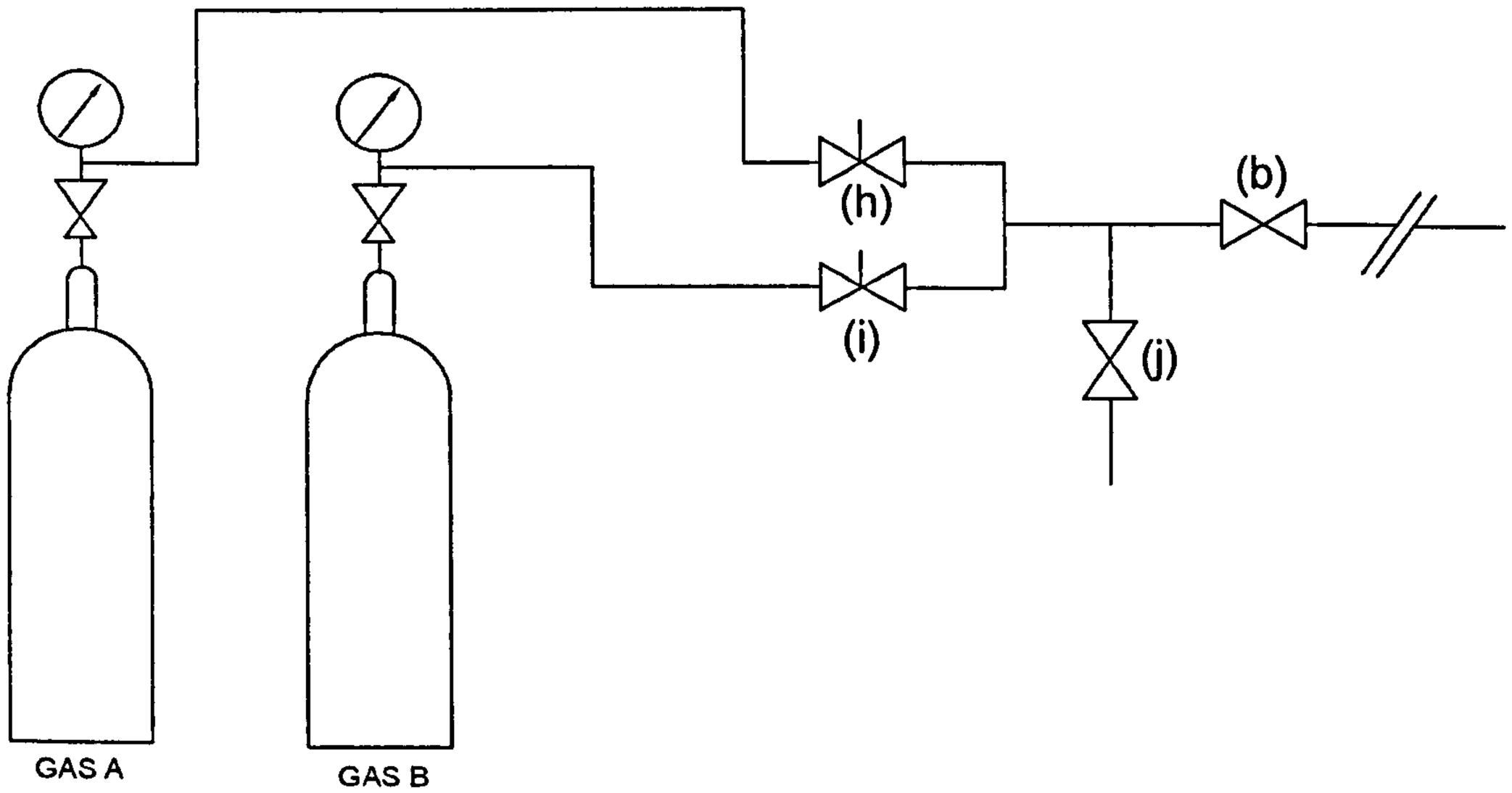

Figure 3. 4 Modification in gas feed section to perform mixed gas permeation experiments.

Before any mixed gas permeation experiments were performed, a calibration curve was plotted between the intensity and the injected standard gas samples of known concentration, under fixed operating conditions. The same operating conditions were then maintained during the mixed gas permeation experiments. The permeate concentration at the start of any permeation experiment for self-supported polyaniline films is very low, so it is difficult to

measure the gas concentration in the first 15 to 20 minutes. Several attempts to detect this low mixed gas concentration by changing permeate volume did not result in any reliable results.

The mixed gas permeation experiment was performed in two consecutive steps. In the first stage, the permeation cell along with polyaniline membrane was degassed using a vacuum pump for 24 hours. After the complete degassing of the membrane, valves (b), (c), and (g) were closed. In the second stage valves (h) and (i) were used to control the flow of gas A and gas B, respectively. Gas A and gas B were mixed in the desired proportion to feed the upstream section of the permeation cell. The feed mixed gas was allowed to escape through valve (j) till the steady gas composition was monitored on the mass spectrometer. Once the steady gas composition rate was monitored on the mass spectrometer, the valve (j) was closed and valve (b) was opened to feed the gas mixture to the permeation cell (see Figure 3.3). The experiment was then started by running the PicoLog 16 program to record the downstream pressure of the permeation cell. The feed pressure was maintained at the test pressure using a back pressure regulator (valve (d)). The total time of the experiment was set to 4 hours, that is the time at which the change in permeate pressure rate was observed to be constant for at least 1000 sampling periods. As the gas starts permeating through the membrane the rise in pressure in the downstream section with time is measured by a pressure transducer and plotted by PicoLog. After the permeate rate had reached steady state condition, the in-line sampling interface was used to transfer the permeate mixed gas sample to the mass spectrometer. In order to accomplish this, valve (f), shown in Figure 3.3, was opened to inject the permeate gas mixture to the mass spectrometer. The intensity response for the permeate gas mixture was measured and plotted against time. Once the steady state was reached, equation 2.31 was used to measure the selectivity of the permeating gas mixture.

The whole procedure was repeated twice (with two different polyaniline membrane samples) before changing any operating conditions such as, feed gas, or feed pressure.

Chapter 4

RESULTS & DISCUSSION

1. MECHANISM OF OXIDATIVE POLYMERISATION OF ANILINE

Polyaniline can be chemically synthesised by the polymerisation of aniline in acidic aqueous solution using $(NH_4)_2S_2O_8$ [263-264], KIO_3 [266], or H_2O_2 [269] as an oxidant. The protonic acid used in oxidative polymerisation of aniline is not especially limited as long as the acid dissociation constant, pK_a, value is less than 3.0 [268]. For example, inorganic acids such as hydrochloric acid, sulphuric acid, nitric acid, perchloric acid, hydrofluoroboric acid, hydrofluorophosphoric acid, hydrofluoric acid, hydro-iodic acid, etc., aromatic sulfonic acids such as benzene sulfonic acid, *p*-toluene sulfonic acid, etc., alkane sulfonic acids such as methanesulfonic acid, ethanesulfonic acid, etc., phenols such as picric acid, etc., aromatic carboxylic acids such as m-nitrobenzoic acid, etc., aliphatic carboxylic acids such as dichloroacetic acid, malonic acid, etc., and polymer acids such as, polystyrene sulfonic acid, polyvinyl sulphuric acid, etc., can be used as a protonic acid. In order to improve the solubility of polyaniline in common solvents, the use of functionalised protonic acids (e.g. *p*- toluene sulfonic acid, octyl-benzene-sulfonic acid, camphor sulfonic acid, etc.) as dopants was proposed [245,250]. The amount of protonic acid used depends on the reaction mode of the oxidising agent used. However, Tzou and Gregory [272] observed that increasing the acid concentration (between 0.1M and 1M) increases the polymerisation rate.

In this work, ammonium peroxodisulfate ($(NH_4)_2S_2O_8$) was used as an oxidant and *p*-toluene sulfonic acid (*p*-TSA) was chosen as a functionalised protonic acid. During the polyaniline synthesis, the effect of the starting reaction solution pH, polymerisation reaction temperature and oxidant to aniline molar ratio on the molecular weight and percentage yield of polyaniline was investigated in this study.

According to most authors [216-220,301-308], the first step in polyaniline polymerisation involves the oxidation of aniline to form a radical cation. This

initial step is pH independent, and is the governing criterion for the polymerisation reaction. However, the subsequent coupling step is strongly dependent on pH of the reaction medium. Ohaska *et al.* [309] compared the oxidation products of aniline prepared in a sulphuric acid medium (pH = 1), in a neutral phosphoric medium (pH = 7), and in an acetonitrile/pyridine (0.3 M) solution. They noticed that the N–N characteristics arising from the *"head-to-head"* coupling was observed only in the spectra of products produced under neutral or alkaline conditions. On the other hand, the aniline oxidation products obtained in acid media had a predominantly *"head-to-tail"* arrangement. These results were consistent with the work published by Mohilner *et al.* [305].

Figure 4.1 shows the effect of initial polymerisation reaction pH on the yield (product/monomer weight ratio) of the polyaniline. The highest yield was obtained for the reactions at the starting solution pH of +1.0, at 0 C. Polyaniline yield dropped only slightly for the starting reaction solution pH below +1.0 and sharply for the solution pH above +1.5. Hence, the optimum starting reaction pH found to be was +1.0, and used to produce further polyaniline batches at various reaction temperatures.

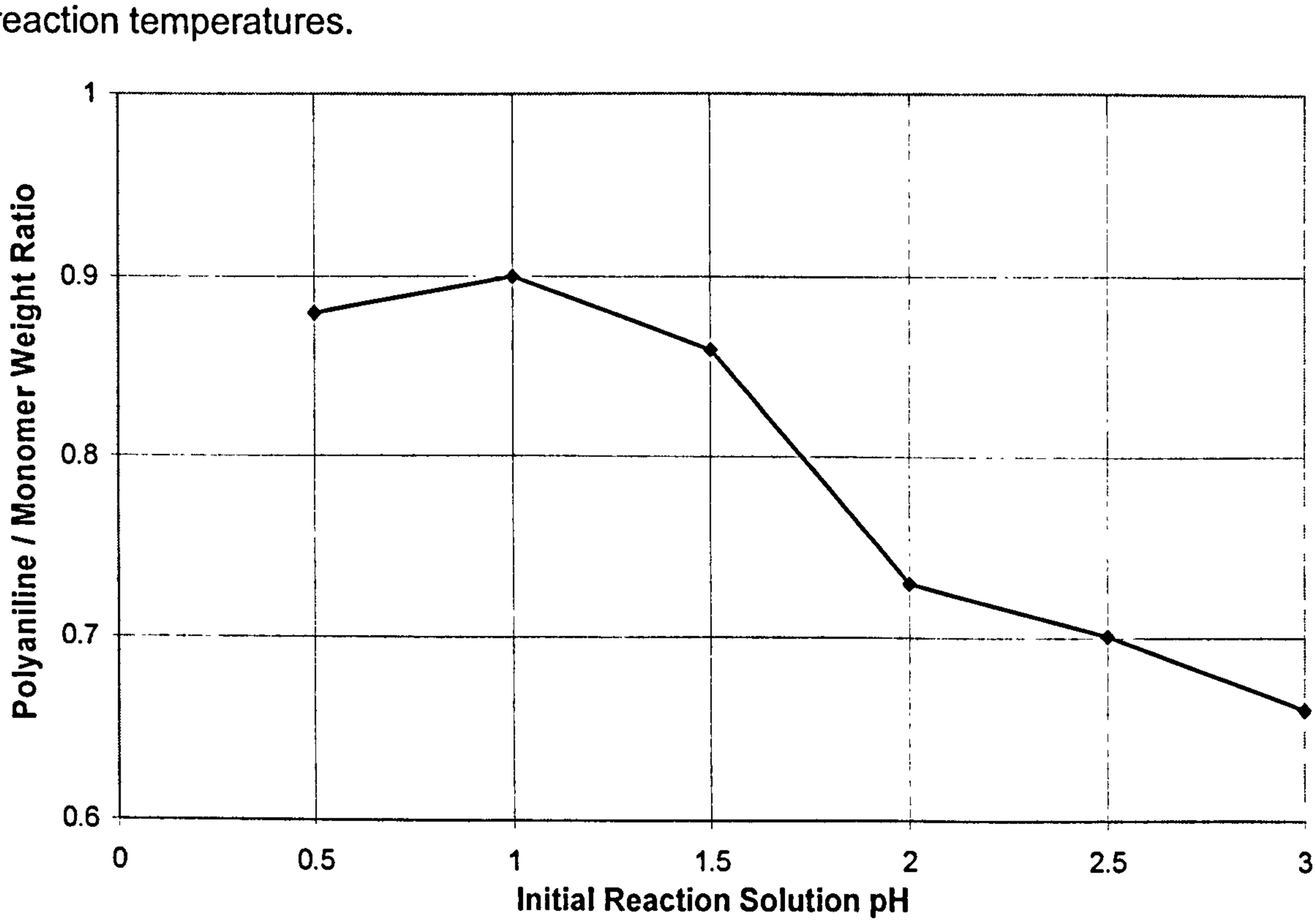

Figure 4. 1 Effect of initial reaction solution pH on polyaniline yield.

The progress of the polymerisation reaction can be monitored by measuring the change in the colour of the reaction solution from white to emeraldine green, the increase in reaction temperature, and the reduction in pH. Figure 4.2 shows that as the polymerisation progressed the temperature of the reaction mixture increased (where the reaction temperature wasn't maintained externally), and the pH of the solution dropped from the initial value +1.0 to +0.75.

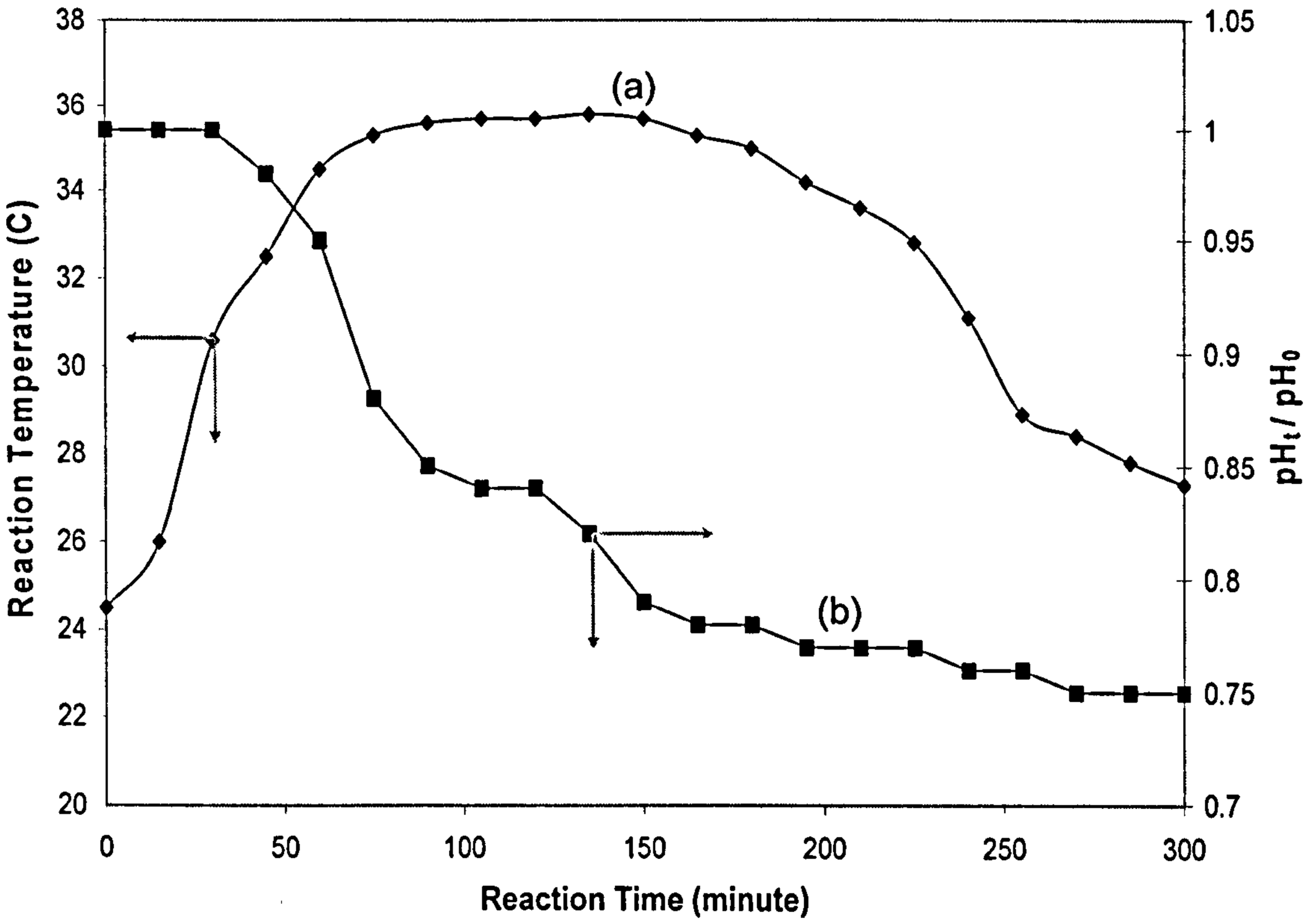

Figure 4. 2 (a) Reaction solution temperature profile during the oxidative polymerisation of aniline in 1M *p*-TSA; (b) Ratio of pH of reaction medium at any time (pH_t) to the initial solution pH (pH_0), for polymerisation of aniline in 1M *p*-TSA, at 0 C.

Figure 4.3 shows the reaction stoichiometry for the polymerisation of aniline in 1M *p*-TSA using ammonium peroxodisulfate as an oxidant. According to reaction stoichiometry, 1.25 mols of ammonium peroxodisulfate are needed for the polymerisation of 1 mol of aniline into the emeraldine form of polyaniline. The oxidation proceeds with stoichiometric yield in aqueous media at ambient or lowered temperature.

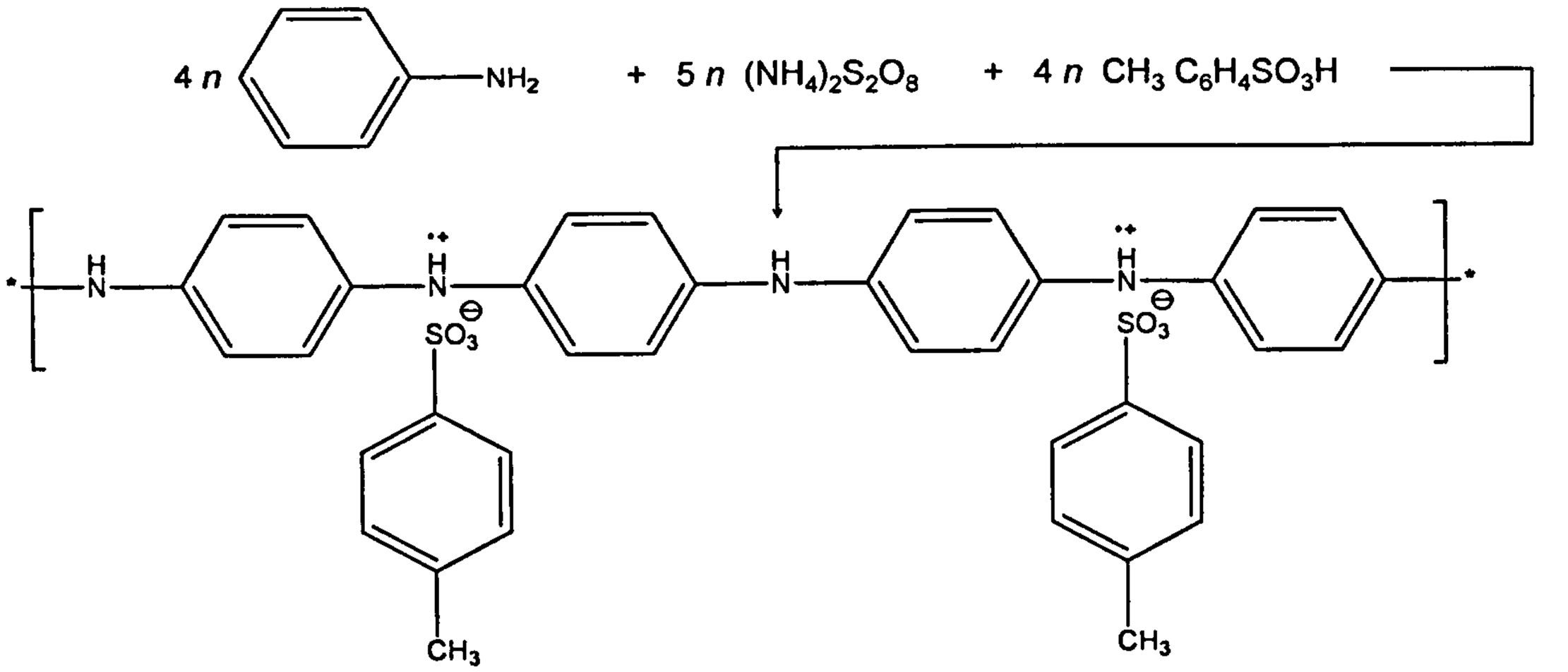

Figure 4. 3 Polyaniline polymerisation reaction stoichiometry.

Figure 4.4 shows the effect of oxidant/aniline molar ratio on percentage yield of polyaniline. The starting pH of the reaction solution was 1.0, and polymerisation was carried out at 0 C. The oxidant addition time and the total reaction time were kept to 2 hours and 48 hours, respectively. The values for percent yield and the mole ratio of oxidant to aniline at 0 C show that the yield is only just below 90% for the oxidant to aniline mole ratio of 1.15.

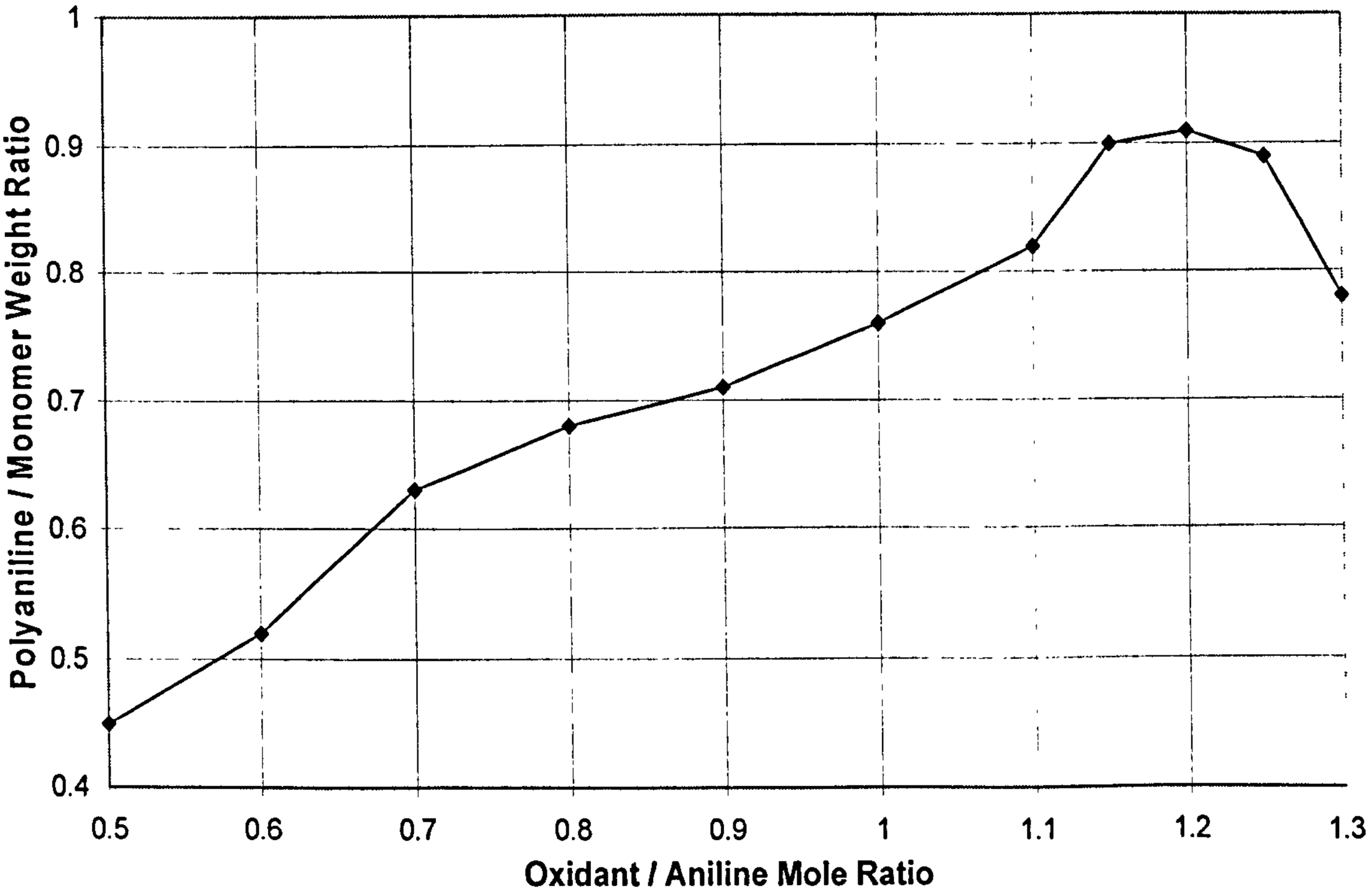

Figure 4. 4 Variation of polyaniline yield, as a function of oxidant/aniline mole ratio.

The polymer yield increases with the use of larger amount of oxidant. The concentration of radical cation increases with increasing the amount of oxidant, however the excess oxidising agent decomposes the polyaniline to colourless low-molecular-weight products of the quinone type and the yield of emeraldine reduces. Hence, the yield drops when the oxidant to aniline mole ratio is higher than 1.25. The percent yield rises only slightly with increasing oxidant addition times from instantaneous addition to 8 hours. The minimum reaction time of about 15 hours was necessary for the polymerisation reactions below 0 C, whereas about 4 to 6 hours was sufficient at 0 C. The polyaniline percent yield rise is only slight for the polymerisation reactions with oxidant addition time more than 4 hours and total reaction time more than 24 hours.

The results on Figure 4.5 show that the polyaniline yield increased when the polymerisation reaction temperature was reduced. The percentage yields calculated were subject to an estimated 2% by weight error due to sulphur (and oxygen) contaminants. The weight of the polymer obtained was reproducible to the variation of ± 1% by weight in identical reaction conditions.

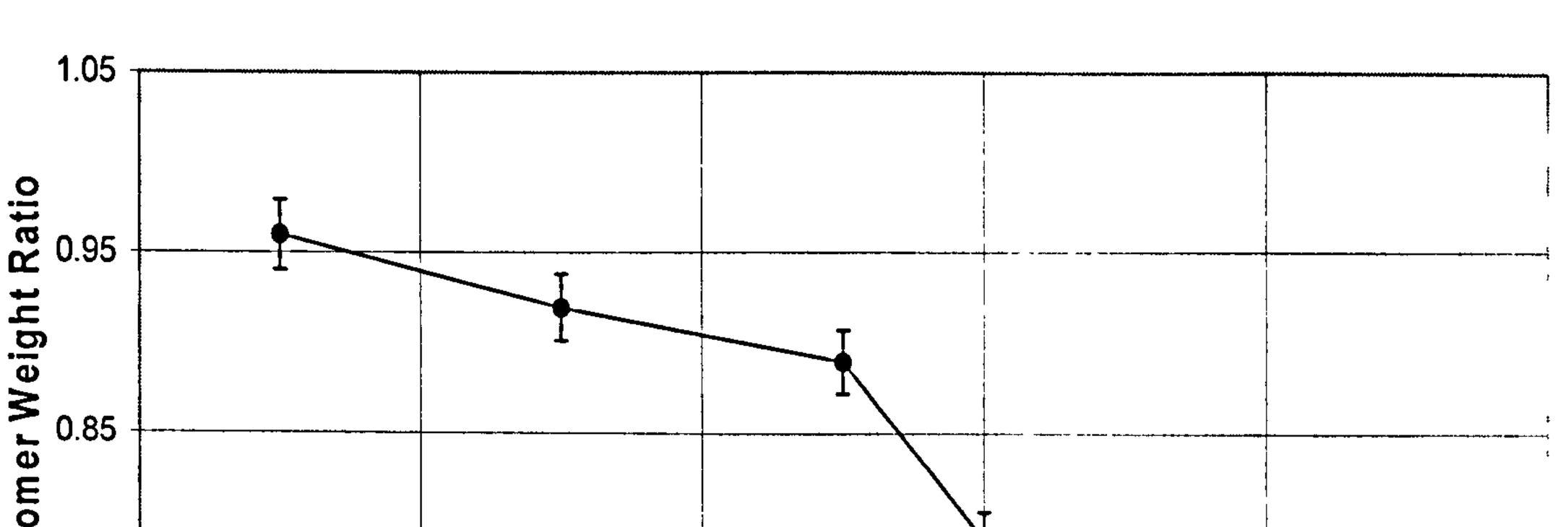

Figure 4. 5 Effect of polymerisation reaction temperature on polyaniline yield.

The mechanism of oxidative polymerisation of aniline is still debatable. However, it is likely that the radical cation species are produced as a result of oxidative attack on the aniline monomers; these then condense with the loss of protons to give the protonated, semi-oxidised emeraldine salt form of polyaniline as a reaction product [267]. If aniline polymerisation does indeed follow the proposed theory, it is a difficult reaction to classify as it shows characteristics of both cationic chain polymerisation and condensation polymerisation reactions. Cationic chain polymerisations are usually carried out at low polymerisation temperatures, which favour propagation over competing side reactions, and use solvents with a high dielectric constant, which favours both initiation and propagation leading to high molecular weight polymers. One of the characteristics of condensation polymerisation is that the molecular weight of the polymer rises steadily through the reaction, and therefore long reaction times are essential to obtain high molecular weights.

The consideration of the mechanism of oxidative polymerisation of aniline as a redox process, however, has been limited basically to the initial stage of the process, while at further stages a kinetic approach, which is characteristic of polymerisation studies, has been used [301-303]. The most generalised mechanism of aniline polymerisation, suggested by Wei *et al.* [301,303], is based on kinetic studies of the electrochemical polymerisation of aniline. The slowest step in the polymerisation is the oxidation of aniline monomers to form dimeric species, because the oxidation potential of aniline is higher than those of dimers, subsequently formed oligomers and polymers [218]. Upon formation, the dimers are immediately oxidised and then react with an aniline monomer via an electrophilic aromatic substitution, followed by further oxidation and deprotonation to form the trimers; this process is repeated, leading eventually to the formation of polyaniline [301]. However, Genies *et al.* [304] suggested that the oxidation of aniline up to the dimer occurred by formation of the nitrenium cation and it was not the slowest step in the polymerisation, but appeared to be the step requiring the highest electrochemical potential of the system.

The mechanism proposed by Wei *et al.* [303], which is illustrated in Figure 4.6, is consistent and widely accepted [216-220,302] mechanism. In this mechanism, the first step involves the oxidation of the neutral aniline monomers to radical cations, which leads to formation of the dimeric species.

Mohilner *et al.* [305] suggested that these dimeric species result from radical coupling of the radical cations. Because these dimeric species have lower oxidation potentials than aniline, oxidation will occur immediately after their formation, to yield their corresponding quinoidal diiminium ions.

Initiation

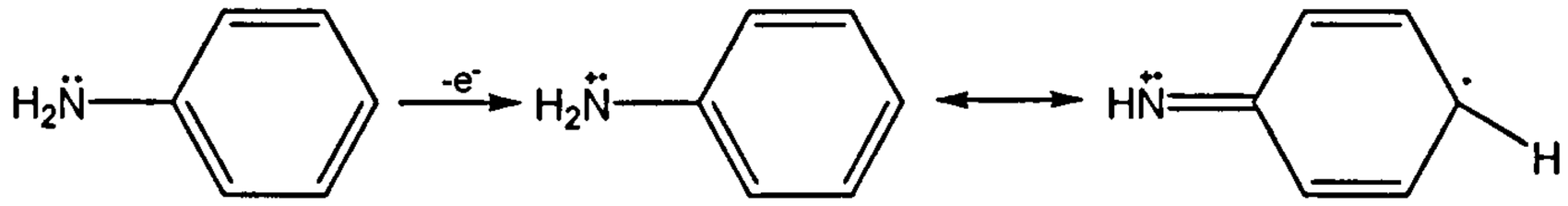

Propogation

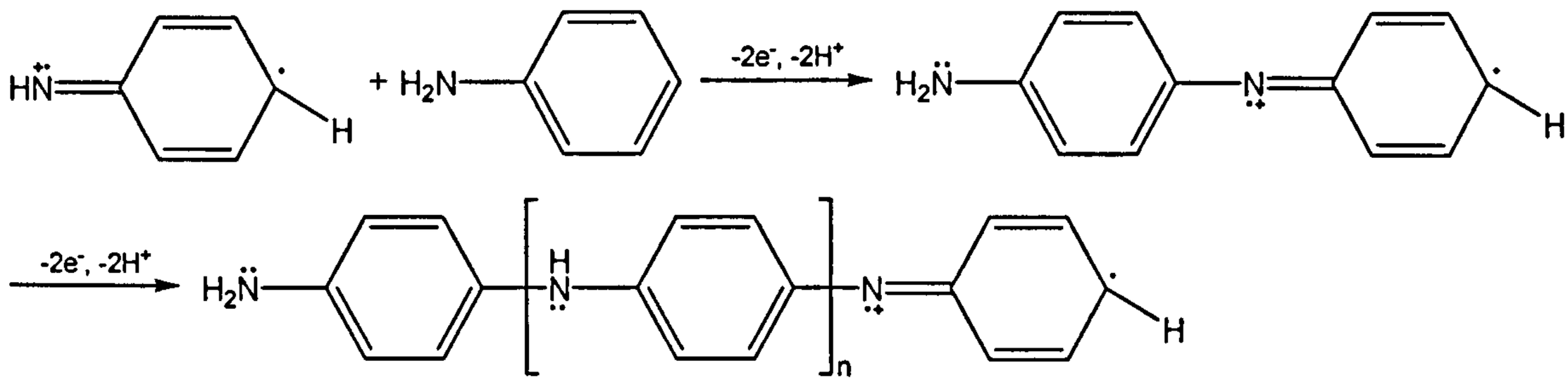

Termination

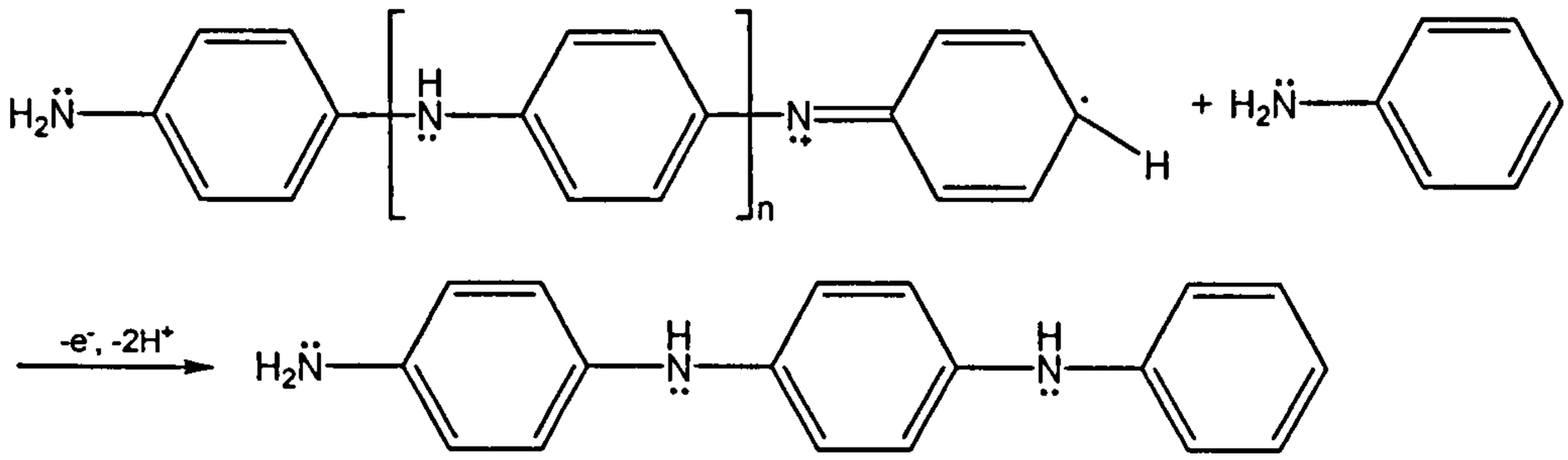

Figure 4. 6 Proposed polymerisation mechanism of aniline [303].

An electrophilic attack of aniline monomer either by the diiminium ion [303] or by the nitrenium ion [306,307], which could be readily generated from a deprotonation of diiminium ions, would accomplish a polymer growth step. The propagation of polymer chains proceeds by a redox process between the growing chain (as an oxidant) and aniline (as a reducer) with addition of monomer to the chain end. The high concentration of a strong oxidant, $(NH_4)_2S_2O_8$, at the initial stage of the polymerisation enables the fast oxidation of oligo- and poly-aniline, as well as their existence (and consequently their registration) in the oxidised

form. This explains the presence of oxidised oligomers and pernigraniline at the initial stage of polymerisation. The high degree of oxidation (and consequently a high concentration of the imine bonds) of the growing chains at the initial stage of the polymerisation, favours the hydrolysis of imine bonds. The subsequent oligomers also have lower oxidation potentials then aniline [305,308] and the reactions proceed leading eventually to the emeraldine salt form of polyaniline. The oxidation potential of oligo- and poly-aniline chains depends not only on the degree of oxidation, but also on the degree of protonation of the chains. Thus, a decreasing degree of protonation of the medium brings about a lowering of the oxidation potential of the chains. This results not only in retardation or even impossibility of chain growth, but also in their easy oxidation by traces of oxidant, or even by atmospheric oxygen.

Therefore, the oxidative polymerisation of aniline can be regarded as a new area in cationic polymerisation, since during the polymerisation the chain propagation all the chains are thermodynamically equivalent with respect both to the monomer addition (since they have the same oxidation potential) and the termination. The termination is a result of the establishment of thermodynamic equilibrium in the redox process corresponding to the chain propagation.

2. POLYANILINE CHARACTERISATION

2.1. Fourier Transform Infrared (FTIR) Spectroscopy

The FTIR spectrum is one of the most informative fingerprints of a compound, and is frequently used to obtain specific information about emeraldine base (EB) molecular conformations and oxidation states [311-314]. The infrared transmittance spectra for polyaniline powder produced at different reaction temperature are shown in Figure 4.7. Since, all polyaniline batches were washed with demineralised water, the hydrolysed product was present in all FTIR spectra. The absorption due to the deformation vibrations outside the C–H plane of mono-substituted benzene is clearly recognised by the peaks between 650 and 850 cm^{-1}. However, these peaks might be also indicative of some sort of branching on the individual molecules. A blue shift of the bands at 1580 and

1508 cm^{-1} indicate quinoid ring C=C stretch and benzenoid ring C=C stretch, respectively. The polyaniline EB FTIR spectra obtained here were similar to the spectra reported by other researchers [278,279,283,284,311-314].

The emeraldine base form of the polymer should contain the equal numbers of benzenoid and quinoid units [66,67]. From the ratio of the intensity of the peaks at 1580 and 1508cm^{-1}, a *Q/B* (quinoid/benzenoid) ratio between 0.50 and 0.53 can be determined. Based on this, it can be attributed that some of the polyaniline batches contain more benzenoid rings than quinoid rings.

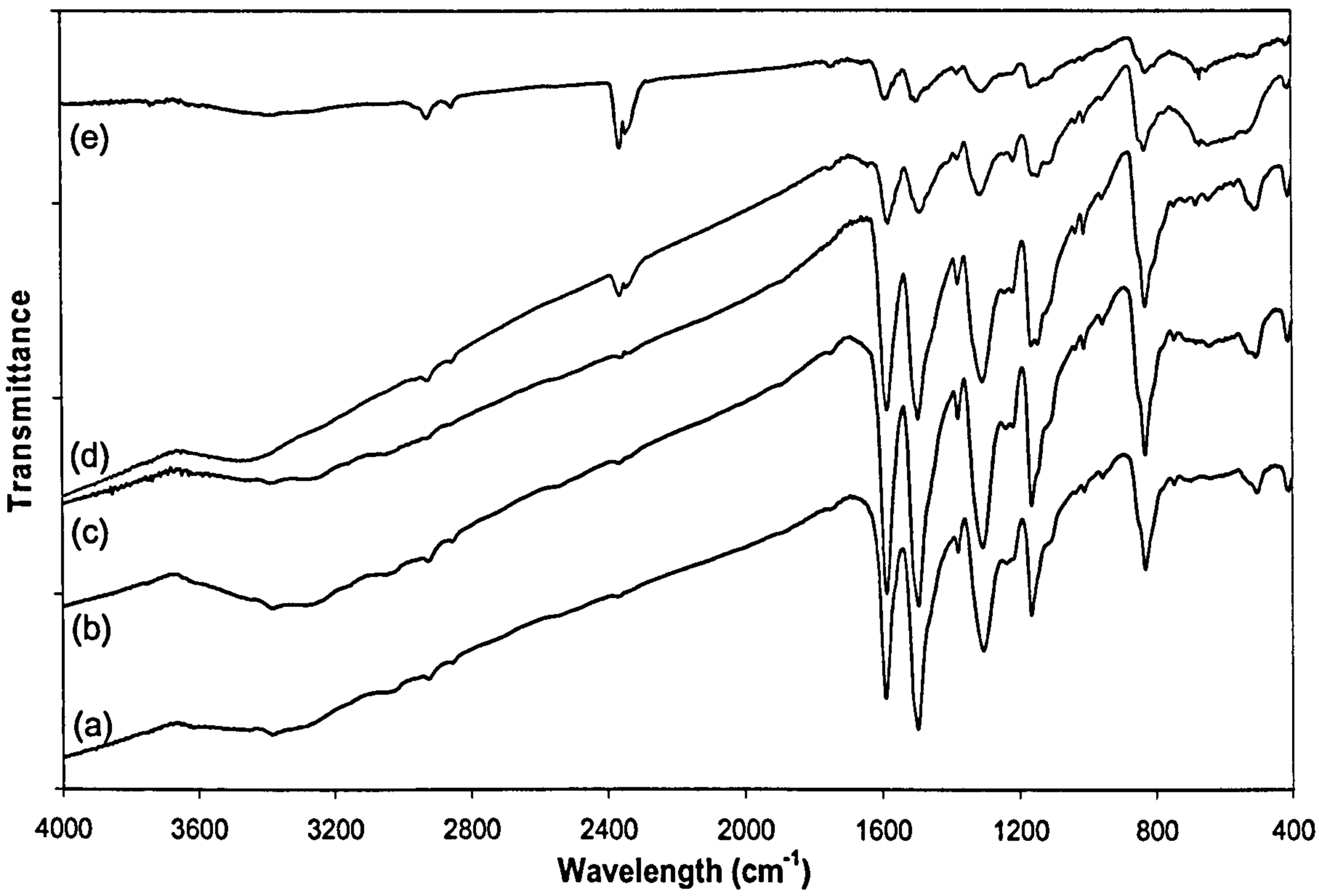

Figure 4. 7 FTIR spectra of polyaniline powder: (a) reaction temperature 23.8 C; (b) reaction temperature 15 C; (c) reaction temperature 10 C; (d) reaction temperature 5 C; (e) reaction temperature 0 C.

The peaks at 1245 and 1100 cm^{-1} represent, C–N stretch and C–O stretch in the aromatic ring, respectively. The peaks at 2360 cm^{-1} represent C=O pollution from air (CO_2). The amount of CO_2 present in different branches of polyaniline produced at 23.8, 15, 10, 5 and 0 C was 14.06, 14.58, 16.58, 33.92, and 50.18, respectively. Earlier, it was the general notion that the CO_2 solubility in the polymer is a function of pressure and temperature only [310]. In fact, the amount of dissolved CO_2 varies from one polymer to another even at the

same conditions. The specific intermolecular interaction between CO_2 and polymer is responsible for the difference in solubility. The nature of interaction present between CO_2 and the polymer is mostly of a Lewis acid-base kind. In CO_2, a Lewis acidity results from the electro-positivity of the carbon atom due to a deficiency of the electron density compared to the oxygen atom. Thus, an electron acceptor-donor interaction is present when CO_2 is contacted with the polymer containing Lewis base sites. Higher interaction between CO_2 and polyaniline was observed when polymer was produced at sub-ambient reaction temperature due to fewer defect sites on the polymer chain, which accounts for the higher transport rates for CO_2 observed in gas permeation experiments. Table 4.1 summarises the assignments of IR absorption bands for polyaniline powder.

Table 4. 1 Assignments for IR absorption bends for polyaniline [313].

Frequency (cm^{-1})	Assignment
3460	NH_2 asymmetric stretching
3380	NH_2 asymmetric stretching, N–H stretching
3310	H-bonded N–H stretching
3170	=N–H stretching
2930	Impurity or sum frequency
2850	Impurity or sum frequency
1580	Stretching of N=*Q*=N
1508	Stretching of N–*B*–N
1450	Stretching of benzene ring
1380	C–N stretching in $Q–B_{trans}–Q$
1315	C–N stretching in $Q–B_{cis}–Q$, *Q–B–B, B–B–Q*
1240	C–N stretching in *B–B–B*
1160	A mode of N=*Q*=N
1140	A mode of $Q=N^{+}H–B$ or *B*–NH–*B*
1220	C–H in-plane bending of 1,4-ring
1105	
1010	
1115	C–H out-of-plane bending of 1,2,4-ring
1060	
960	
910	C–H out-of-plane bending of 1,2,4-ring
895	
850	
830	C–H out-of-plane bending of 1,4-ring
740	C–H out-of-plane bending of 1,2-ring
690	
645	Aromatic ring deformation
530	

Abbreviations: *Q*, Quinoid unit, *B*, benzenoid unit

2.2. UV – Vis Spectrometry

The degree of aggregation in the as-synthesised polyaniline EB powder impacts the solubility and solution characteristics of the polymer. The more aggregated the structure, the less soluble is the EB. In the solution, depending on the nature of the solvent polyaniline dissolves to different extents. As the polymer is dissolved, some of the internal H-bonding disrupts. The better the solvent, the less aggregated will be the polymer. As the polymer is deaggregated, the solvent can better dissolve the individual chains and thus, a conformational change occurs in which the chains become more expanded. The solution characteristics in turn determine the morphology of emeraldine base films [233]. EB films will have different levels of deaggregation and chain expansion depending on the solvent, and therefore exhibit different properties. The optical absorption, and in particular the exciton absorption, of EB films is found to depend on the solvent and the concentration of the solution used to process the films and on the amount of residual solvent in the film.

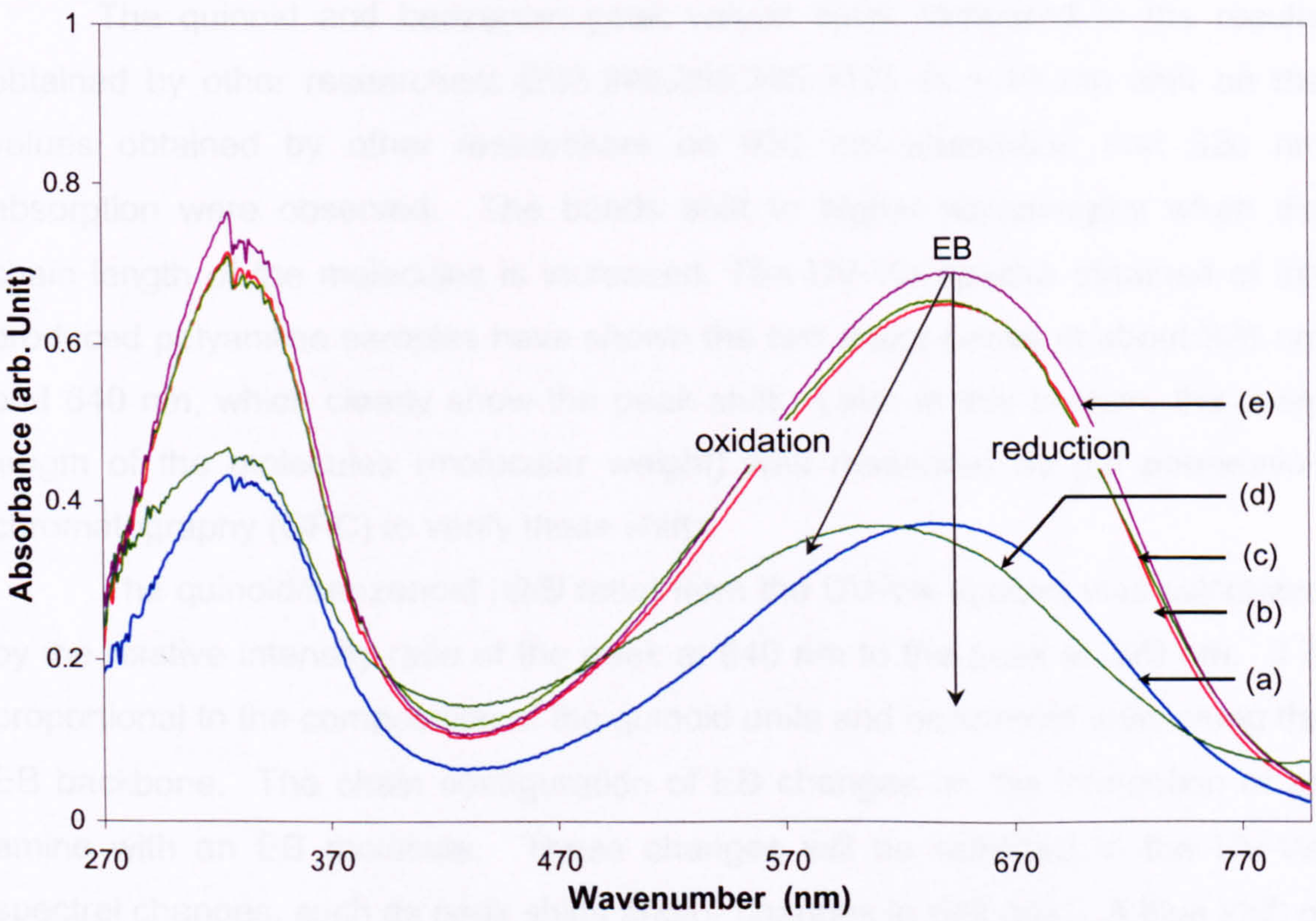

Figure 4. 8 UV-Vis spectra of polyaniline solutions in NMP: (a) reaction temperature 23.8 C; (b) reaction temperature 15 C; (c) reaction temperature 10 C; (d) reaction temperature 5 C; (e) reaction temperature 0 C.

A red shift was observed in the λ_{max} of the exciton absorption when the expanded coil structure of polyaniline is attained. The UV-Vis spectra of polyaniline in NMP, shown in Figure 4.8, show that at least two major absorption peaks exist in all spectra for polyaniline batches produced at different polymerisation reaction temperatures. The first band at ~ 640 nm is indicative of a charge-transfer exciton-like transition from the highest occupied levels on benzenoid rings to the lowest occupied energy levels on quinoid rings. This peak results from either intra- or inter-chain absorption; therefore, its intensity changes with the EB inter-chain configuration [233,315,316], which is affected by the solution's concentration, solvent and doping level. The second band at ~ 320 nm can be attributed to the π–π^* transition associated with the π electrons of the benzene ring, and it is contributed to mainly by intra-chain absorption [316-318]. Albuquerque *et al.* [282] observed that, the benzenoid peak (~ 640 nm) tends to disappear as the EB samples were more and more reduced. In the oxidised samples, this peak is replaced by other absorption whose maximum from 600 nm, reaching to 570 nm, was observed in the oxidised samples.

The quinoid and benzenoid peak values were compared to the results obtained by other researchers [233,246,282,315-317]. A ~ 10 nm shift on the values obtained by other researchers on 630 nm absorption and 320 nm absorption were observed. The bands shift to higher wavelengths when the chain length of the molecules is increased. The UV-Vis-spectra obtained of the produced polyaniline samples have shown the two major peaks at about 326 nm and 640 nm, which clearly show the peak shift. Later in this section, the chain length of the molecules (molecular weight) was measured by gel permeation chromatography (GPC) to verify these shifts.

The quinoid/benzenoid (*Q/B* ratio) from the UV-Vis spectra was calculated by the relative intensity ratio of the peak at 640 nm to the peak at 320 nm. It is proportional to the composition of the quinoid units and benzenoid units along the EB backbone. The chain configuration of EB changes on the interaction of an amine with an EB molecule. These changes will be reflected in the UV-Vis spectral changes, such as peak shifts and/or changes in *Q/B* ratio. A blue shift of the Q peak is caused by an increased energy gap between of the highest occupied molecular orbit of benzenoid rings and the lowest unoccupied molecular orbit of the localised quinoid rings. When the quinoid rings are reduced to

benzenoid rings, a decrease in the *Q/B* ratio and a blue shift on the *B* peak are observed [315]. The red shifts on both *Q* and *B* peaks indicate that their absorptions have shifted to a lower energy. This red energy shift has been observed when polymer chains take on a more expanded configuration [233,315,316]. Table 4.2 shows absorptions and *Q/B* ratios in UV-Vis spectra of polyaniline batches produced at various polymerisation reaction temperatures. The *Q/B* ratio for polyaniline batches produced at various polymerisation reaction temperatures was calculated. The *Q/B* values obtained through UV-Vis spectra corresponded to the values obtained through FTIR analysis. The effect of EB solution ageing on *Q/B* ratio was examined and found to change negligibly up to 72 hours.

Table 4. 2 Absorptions and *Q/B* ratios in UV-Vis spectra of EB in liquid states.

Label	Wavelength (nm)		*Q/B* ratio
	Benzenoid peak (*B*)	Quinoid peak (*Q*)	
EB (a)	637	326	0.51
EB (b)	639	326	0.51
EB (c)	633	326	0.52
EB (d)	611	326	0.53
EB (e)	640	326	0.50

Polyaniline sample batches: EB (a): produced at 23.8 C; EB (b): produced at 15 C; EB (c): produced at 10 C; EB (d): produced at 5 C; EB (e): produced at 0 C.

2.3. Polymer Morphology

The properties of polyaniline such as conductivity, mechanical properties, transport properties, etc. have been shown to be dependent on the morphology of the polymer [228,233,245,250,259]. The morphology (i.e. the molecular chain conformation with twisting and bending of the chain backbone, and the intermolecular chain to chain configuration) is at the heart of their complex phenomenology, and generally determined by the polymerisation reaction conditions in which the polymer is produced. Therefore, there is a strong interdependence between the properties of polyaniline, its processing parameters, and its morphology. It has been shown that the polymer synthesised at room temperature was of fairly low molecular weight [273] and contained defect sites [274]. In this work, it was hoped that a sub-ambient polymerisation reaction temperature would result polyaniline having higher crystallinity and

higher molecular weight, which may lead to the improvements in its mechanical and transport properties.

Morphology is a generic term encompassing various levels of structure in the solid state including the molecular chain conformation, intermolecular chain to chain configuration, degree of order, and crystallinity. The granular morphology produced by the polymerisation in liquid mixture changes to the continuous structure, when the polymerisation proceeds in the frozen state (see Figure 4.9 and Figure 4.10).

Polyaniline prepared at higher temperatures was obtained as a fluffy emeraldine blue powder, while that produced at sub-ambient temperatures was a macro-porous material. The distinction in morphology was well seen when polyaniline was washed with acetone after preparation. Direct drying from aqueous medium results in more compact products; the interfacial tension between polyaniline and water is higher compared with acetone and it forces polyaniline entities close to each other during drying process. As can be seen from Figures 4.9 and 4.10, the crystallinity of polyaniline powder increased when the polymer was produced at reduced polymerisation reaction temperature. This increased crystallinity results in higher free volume and this higher free volume then leads to higher permeability for various gases, which was observed during the permeation experiments (discussed later in the chapter).

Figure 4. 9 Scanning electron micrographs of polyaniline powder prepared in a liquid reaction mixture: polymerisation reaction temperature: (a) 21 C; (b) 10 C; (c) 5 C; (d) 0 C.

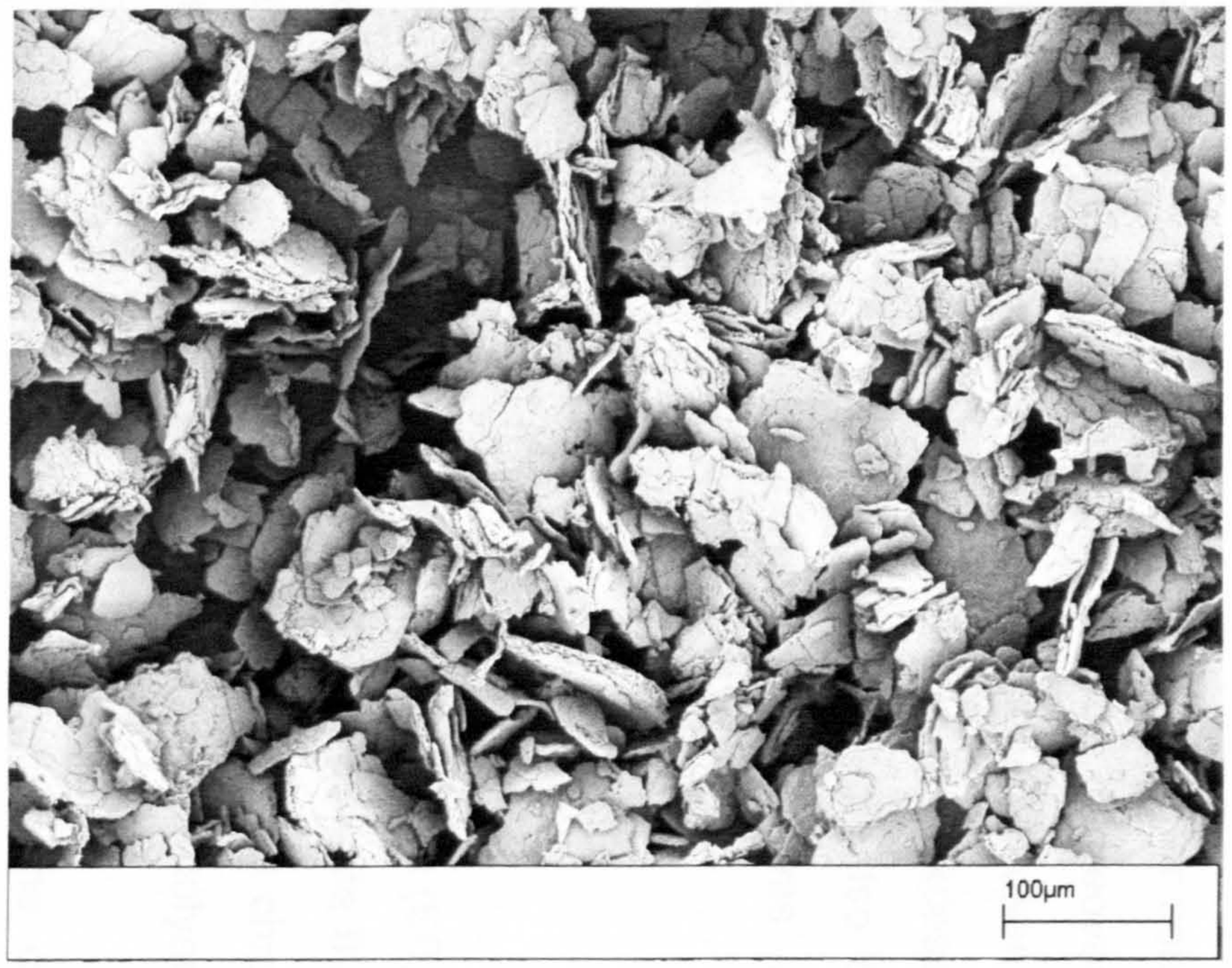

(a)

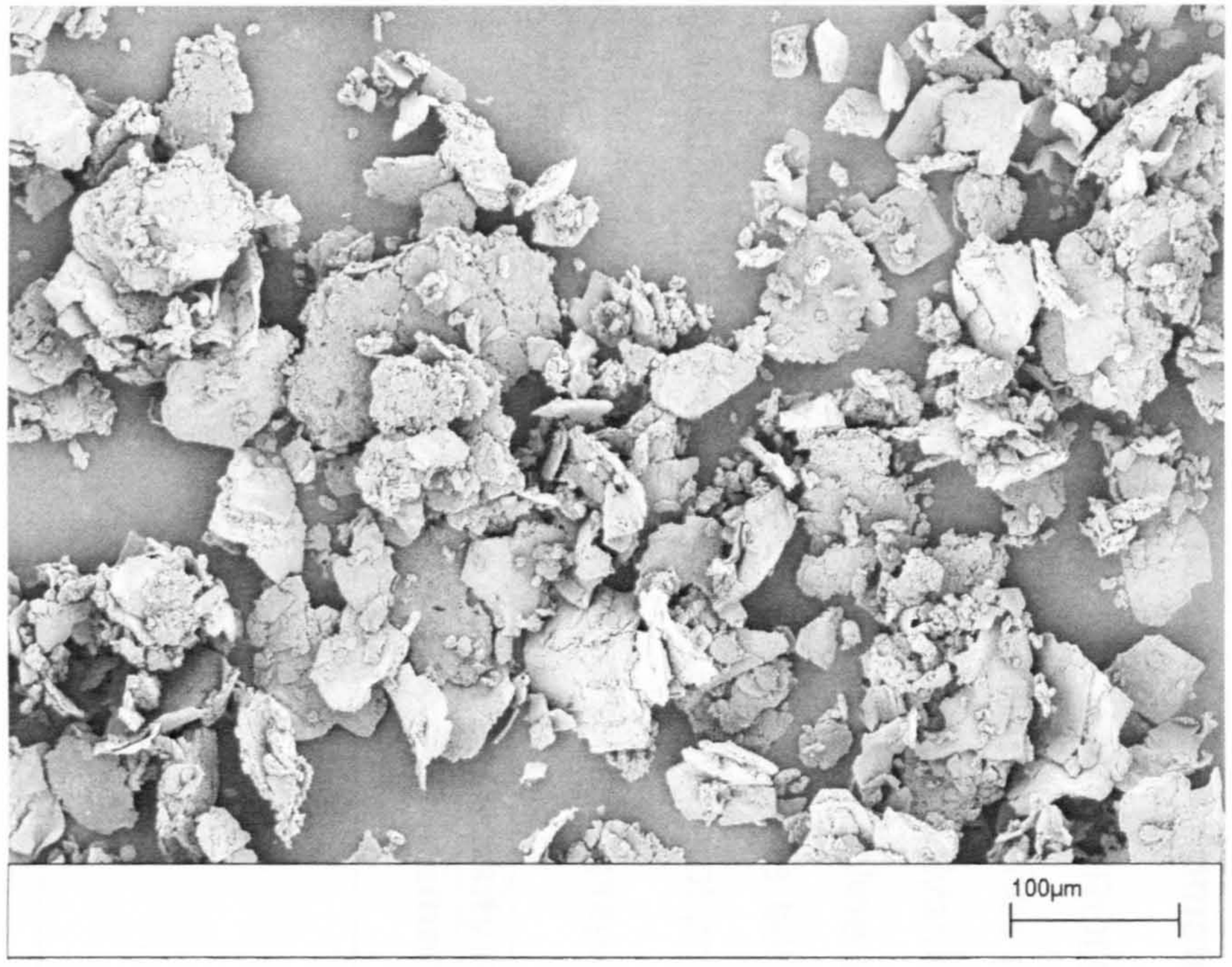

(b)

Figure 4. 10 Scanning electron micrographs of polyaniline powder prepared in a frozen reaction mixture: polymerisation reaction temperature: (a) -10 C; (b) -20 C.

2.4. Polymer Density Measurements (Pycnometer)

A multivolume pycnometer 1305 (MICROMERITICS) was used to measure the densities of various polyaniline batches prepared at our laboratory. Table 4.3 represents the densities of various polyaniline samples. The density values of the emeraldine salt (ES) form of polyaniline samples were measured to be between 1.34 and 1.44 g/cm^3, whereas values between 1.25 and 1.31 g/cm^3 were obtained for the emeraldine base (EB) form of polyaniline.

Table 4. 3 Skeletal density of polyaniline samples prepared at various polymerisation reaction temperature.

Reaction Temperature (C)	Polymer Density (g/cm^3)	
	Emeraldine Salt (ES)	Emeraldine Base (EB)
21	1.342	1.248
10	1.385	1.255
5	1.394	1.270
0	1.408	1.281
-10	1.431	1.295
-20	1.438	1.307

The density values obtained for doped samples (ES) were higher than un-doped ones. This is because of the polymer contains small amount of the *p*-toluenesulfonate atom on C_6 rings. Moreover, lowering the reaction temperature (and therefore the amount of LiCl present) increases the amount of ring chlorination (although the amount is not excessive), which increases the polymer density. The results obtained here also correspond to Figure 4.5, showing that the higher polyaniline yield was obtained at sub-ambient polymerisation reaction temperatures.

2.5. Molecular Weight Measurements

In this study, several batches of polyaniline (EB) were produced at various polymerisation reaction temperatures to investigate their effect on the molecular weight of polyaniline. The Waters gel permeation chromatography (GPC) facility was used to evaluate the molecular weights of polyaniline samples prepared in our laboratory.

The molecular weight of the polyaniline can be controlled by the polymerisation reaction conditions. Zheng *et al.* [319] reported that the molecular

weight of polyaniline can be increased by decreasing the polymerisation reaction temperature. Ohtani *et al.* [320] observed that weight-average molecular weight, M_w, of polyaniline, increased from 120,000 to 160,000 when polymerisation was carried out below -3 C. Oh *et al.* [321] polymerised aniline at 0 and -30 C; molecular weight was 6.8 times higher at lower temperature. Mattoso *et al.* [322] similarly found that molecular weight of polyaniline increased 7.3 times when the polymerisation reaction proceeded at -40 C instead at 0 C. Adams *et al.* [263-265] showed that the molecular weight of polyaniline prepared by oxidation of aniline with ammonium peroxodisulfate was M_w = 29,700 at 18 C and 122,000 at 0 C while it increased to 166,000 at -35 C. In all cases, at sub-ambient temperatures, the polymerisation reactions were carried out in presence of added inorganic salts, e.g. lithium chloride.

GPC, also known as specialised isocratic high performance liquid chromatography, is widely used to provide molecular weight (MW) and molecular weight distribution (MWD) information about polyaniline [231,263-265,319-325]. However, the determination of molecular weight of polyaniline by GPC is questionable due to the presence of aggregates in NMP, formed by hydrogen bonds between the amine and imine segments when the polyaniline solutions are left for a prolonged period. To overcome this, the polyaniline samples were prepared 30 minutes prior to GPC analysis.

Firstly, the calibration plot with a straight-line fit for log (peak molecular weight) *vs* retention time was obtained for polystyrene molecular weight standards (see Figure 4.11). The primary calibration curve of the monodispersed polystyrene is analysed using the peak position method; the retention volume of the chromatographic peak is precisely measured and the molecular weight is deduced from the calibration curve:

$$y = 8.197 - 0.241x \qquad (4.1)$$

where y = log (molecular weight) and x = retention time, fitting this straight line.

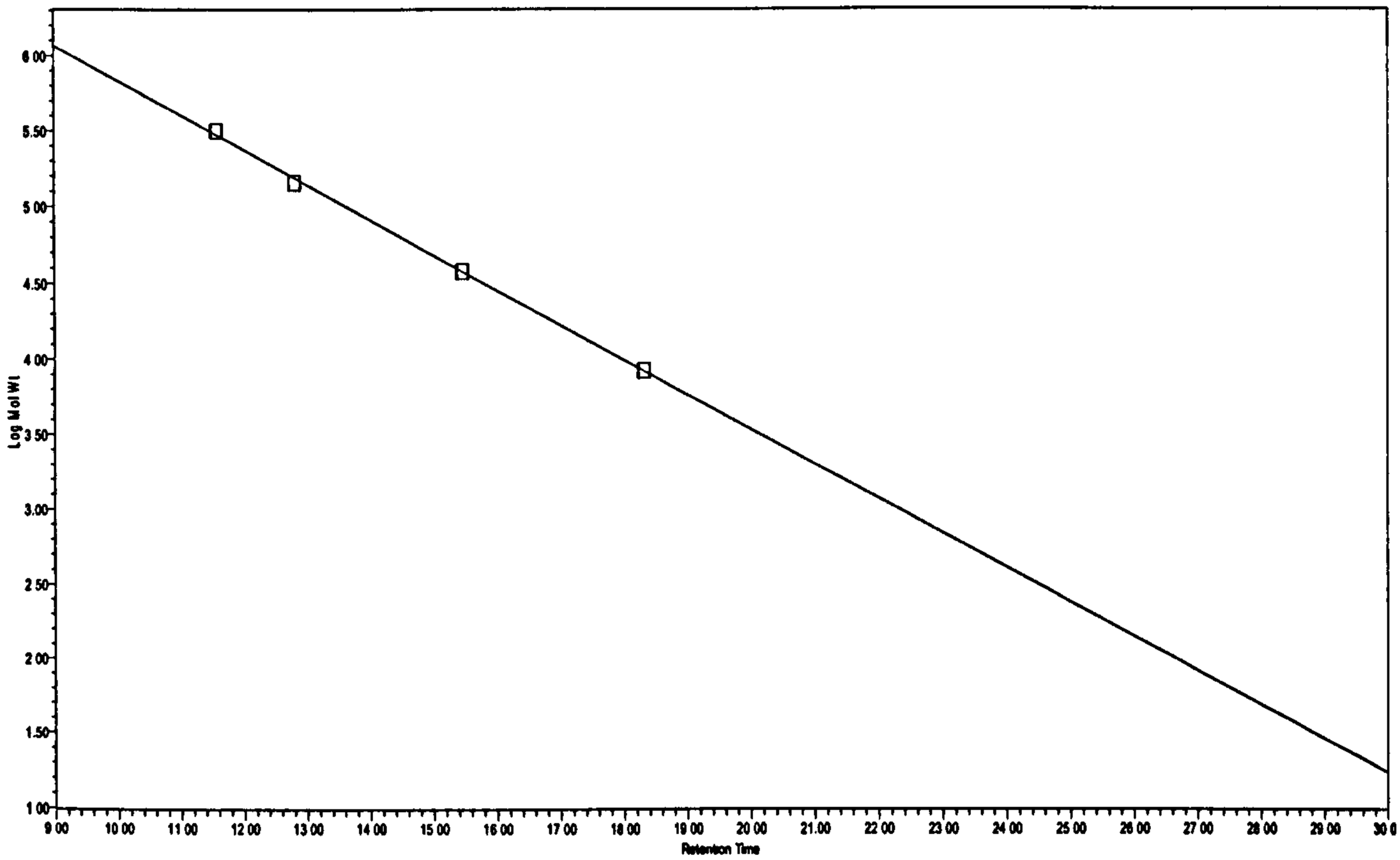

Figure 4. 11 Straight line plot of log (molecular weight) *vs* GPC retention time for monodispersed polystyrene molecular weight standards at column temperature of 100 C.

The weight-average and number-average molecular weights, M_w and M_n, were calculated from the GPC chromatographs (see Figures 4.12, 4.13 and 4.14) by the usual method of dividing the space under the chromatogram into equal segments, measuring the heights from the baseline to the curve and calculating the corresponding molecular weight for each line (see equations 3.1 and 3.2; Chapter 3). An estimate of the errors for these points was made by calculating the molecular weight with the longer of the two retention times, followed by the shorter of the two retention times. All the retention times were within 0.04 minutes of each sample, which represents 10% error in the experimental results.

Figures 4.12, 4.13 and 4.14 show the gel permeation chromatographs of polyaniline samples produced at 21 C, 0 C and -20 C, respectively. A comparison between these three graphs (Figures 4.12, 4.13 and 4.14) clearly indicates that the sample prepared at ambient temperature has longer exit times and thus shorter polymer chain length. Polyaniline prepared at ambient temperature was poorly soluble in any solvents due to large amount of by-products which was produced due to side reactions at ambient temperature. The mechanical properties of polyaniline prepared at lower temperature were

likely to improve compared with those of obtained at higher polymerisation temperatures, because of the higher molecular weight of the products.

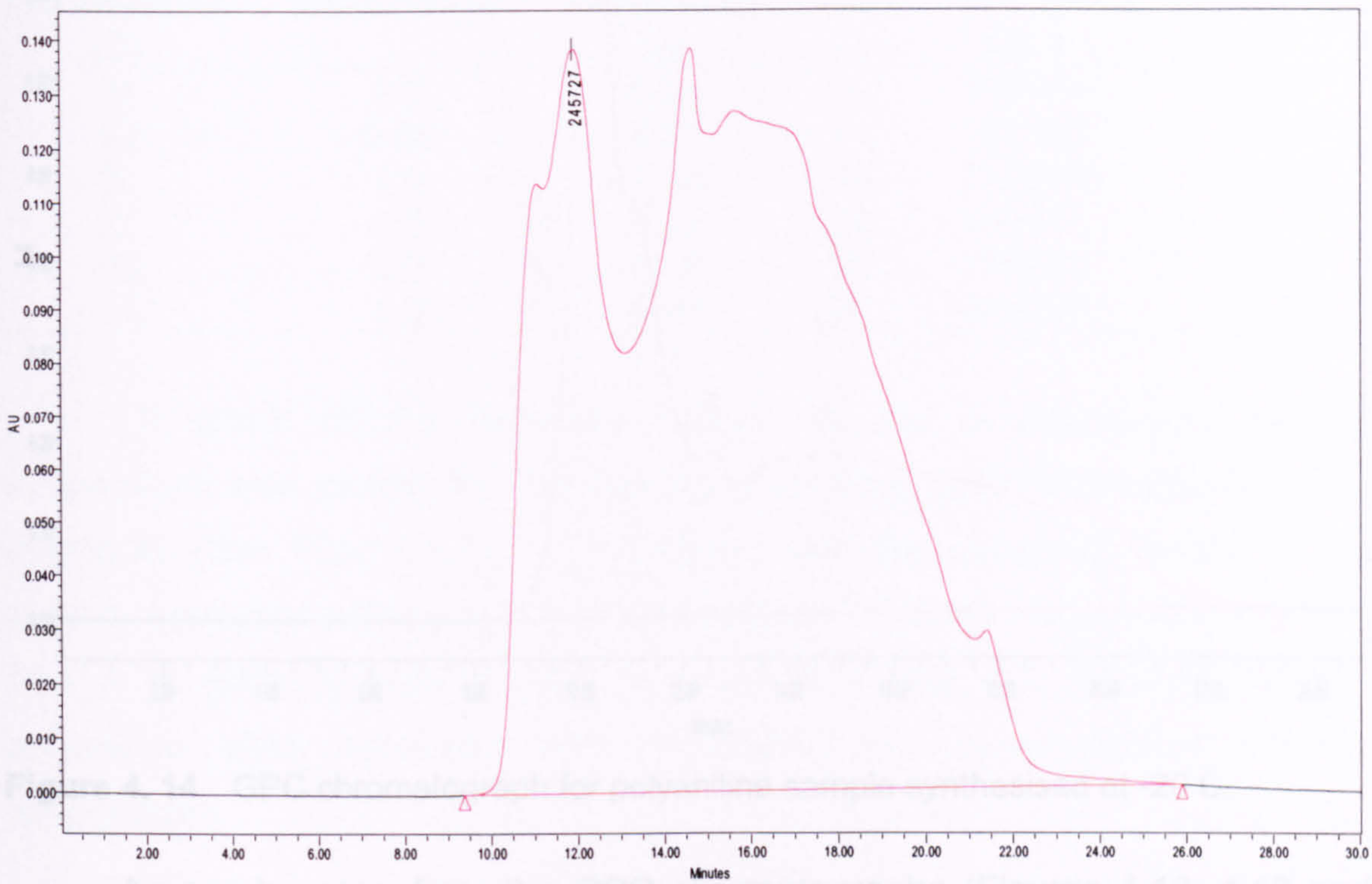

Figure 4. 12 GPC chromatograph for polyaniline sample synthesised at 21 C.

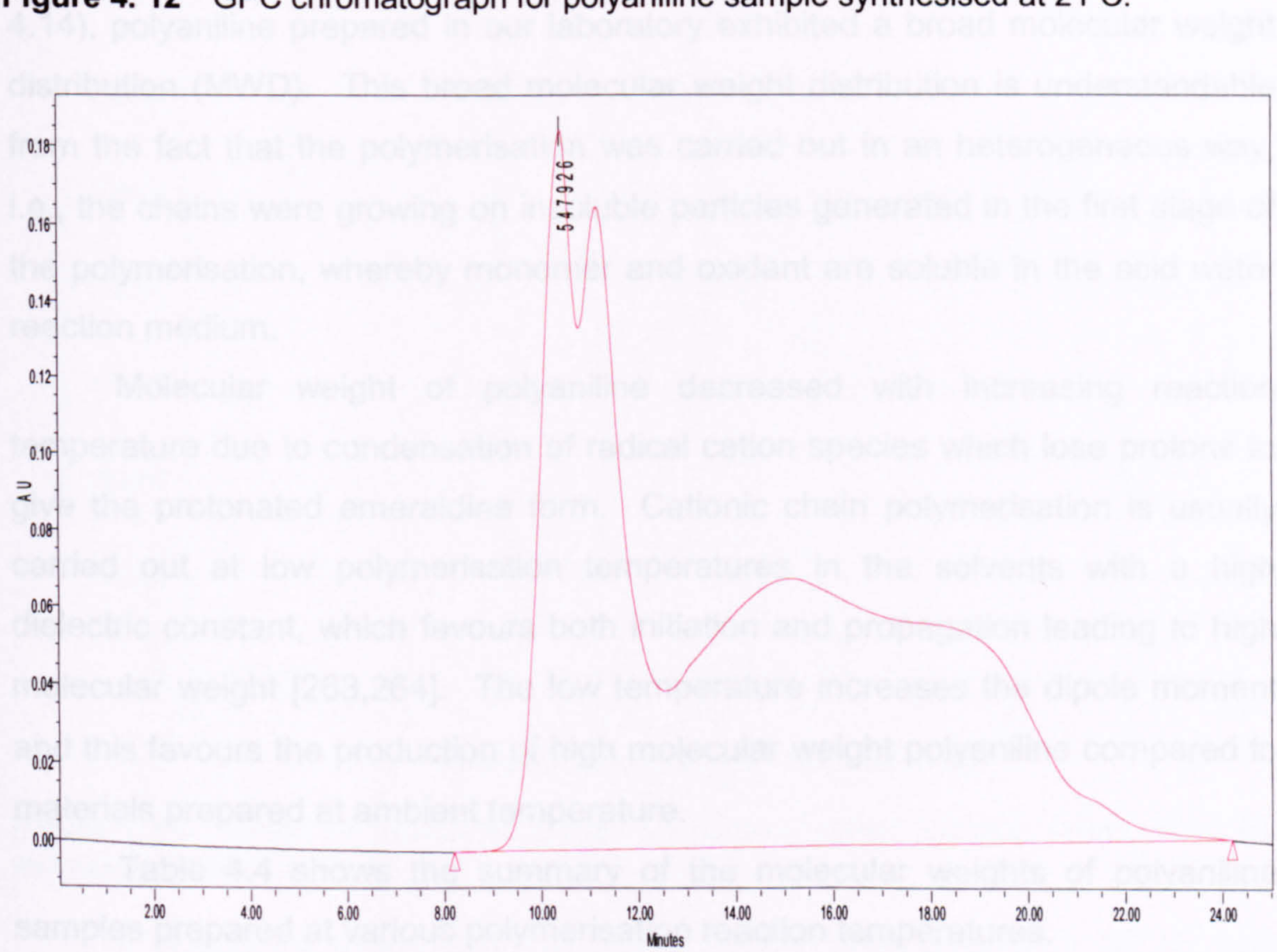

Figure 4. 13 GPC chromatograph for polyaniline sample synthesised at 0 C.

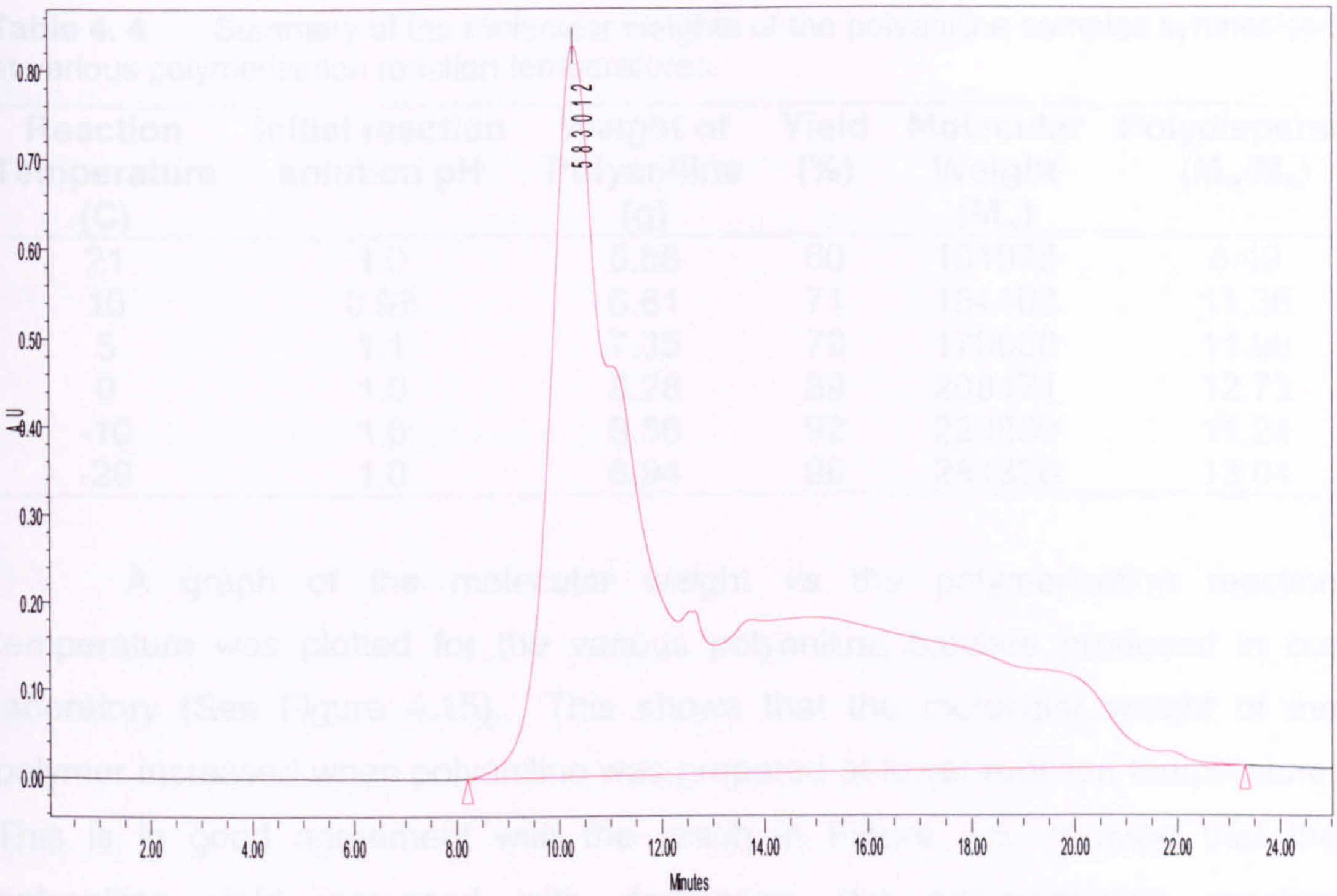

Figure 4. 14 GPC chromatograph for polyaniline sample synthesised at -20 C.

As can be seen from the GPC chromatographs (Figures 4.12, 4.13 and 4.14), polyaniline prepared in our laboratory exhibited a broad molecular weight distribution (MWD). This broad molecular weight distribution is understandable from the fact that the polymerisation was carried out in an heterogeneous way, i.e., the chains were growing on insoluble particles generated in the first stage of the polymerisation, whereby monomer and oxidant are soluble in the acid water reaction medium.

Molecular weight of polyaniline decreased with increasing reaction temperature due to condensation of radical cation species which lose protons to give the protonated emeraldine form. Cationic chain polymerisation is usually carried out at low polymerisation temperatures in the solvents with a high dielectric constant, which favours both initiation and propagation leading to high molecular weight [263,264]. The low temperature increases the dipole moment and this favours the production of high molecular weight polyaniline compared to materials prepared at ambient temperature.

Table 4.4 shows the summary of the molecular weights of polyaniline samples prepared at various polymerisation reaction temperatures.

Table 4. 4 Summary of the molecular weights of the polyaniline samples synthesised at various polymerisation reaction temperatures.

Reaction Temperature (C)	Initial reaction solution pH	Weight of Polyaniline (g)	Yield (%)	Molecular Weight (M_w)	Polydispersity (M_w/M_n)
21	1.0	5.58	60	101078	8.49
10	0.98	6.61	71	154103	11.36
5	1.1	7.35	79	170650	11.90
0	1.0	8.28	89	208471	12.73
-10	1.0	8.56	92	229860	11.24
-20	1.0	8.94	96	281338	13.04

A graph of the molecular weight *vs* the polymerisation reaction temperature was plotted for the various polyaniline batches produced in our laboratory (See Figure 4.15). This shows that the molecular weight of the polymer increased when polyaniline was prepared at lower reaction temperature. This is in good agreement with the graph in Figure 4.5, showing that the polyaniline yield increased with decreasing the polymerisation reaction temperature.

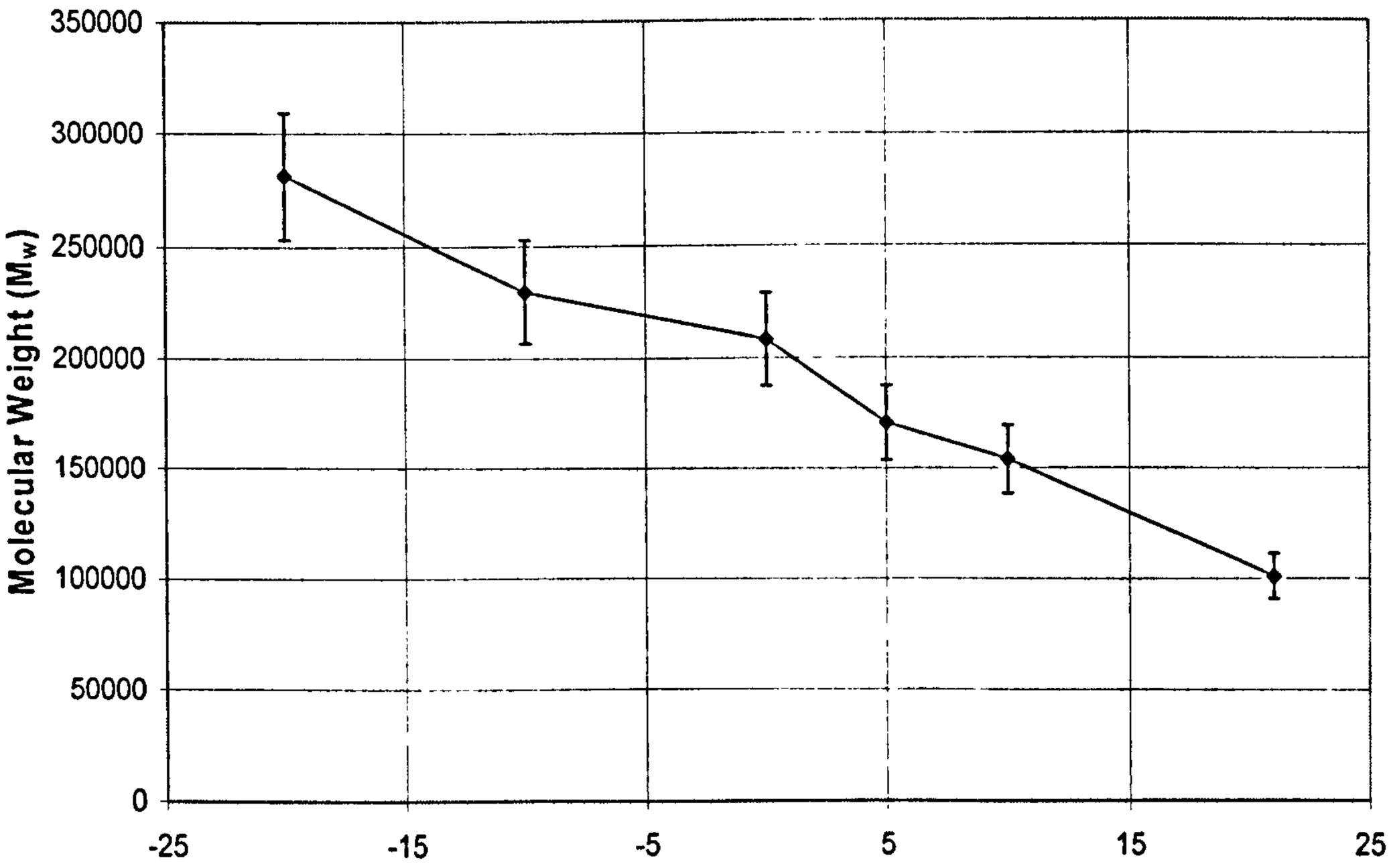

Figure 4. 15 Graph of molecular weight *vs* polymerisation reaction temperature for various polyaniline batches.

It should be noted that the higher column temperature (> 80 C) was required for the GPC analysis, because the polystyrene standards do not

dissolve well in NMP. Also, the absorption peak at ~ 264 nm for polystyrene is at the cut-off point of the NMP carrier solvent. Clearly, for this reason, polyvinylpyridine standards, which are more soluble and give a better straight line fit for a graph of log (molecular weight) *vs* retention time, are recommended in the future work.

3. POLYANILINE MEMBRNAES

3.1. Self-supported Polyaniline EB Films

Many researchers have published permeabilities for various gases permeating through polyaniline membranes with thicknesses between 10 and 100 μm [49-62], and it was claimed that it would be impossible to produce defect-free self supported polyaniline films with thickness less than 10 μm. This is because defects in the polyaniline layer can result from a number of causes: for example, solvent evaporation, or un-dissolved polyaniline particles, or micro-agglomeration of the polyaniline in the solution, can result in micro scale defects.

In this study, the defect-free self-supported polyaniline EB films with film thicknesses between 2 and 7 μm were prepared by the novel method reported earlier (Section 4.1.1; Chapter 3). It was necessary to examine the structure and thickness of polyaniline EB films to evaluate the permeation coefficient for various gases. Field emission gun scanning electron micrographs were used for imaging and analysis of self-supported polyaniline films.

Figures 4.16(a) and (b) represent scanning electron micrographs of the dense, defect-free self supported polyaniline films having film thicknesses of 6.9 and 4.0 μm, respectively. The thickness of the polyaniline film was controlled by the amount of 1% by weight polyaniline solution in NMP used to prepare the membranes. The membrane thickness for a self-supported polyaniline film was measured by a micrometer and verified by the electron micrographs. For the better accuracy in evaluating permeability for various gases through polyaniline membranes, the film thickness values measured by SEM images were used. The thicknesses of the self-supported membranes were observed to be between 2 and 7 μm for various samples. These self-supported membranes were

essentially pore-free and did not show any microporous structures even at higher magnifications.

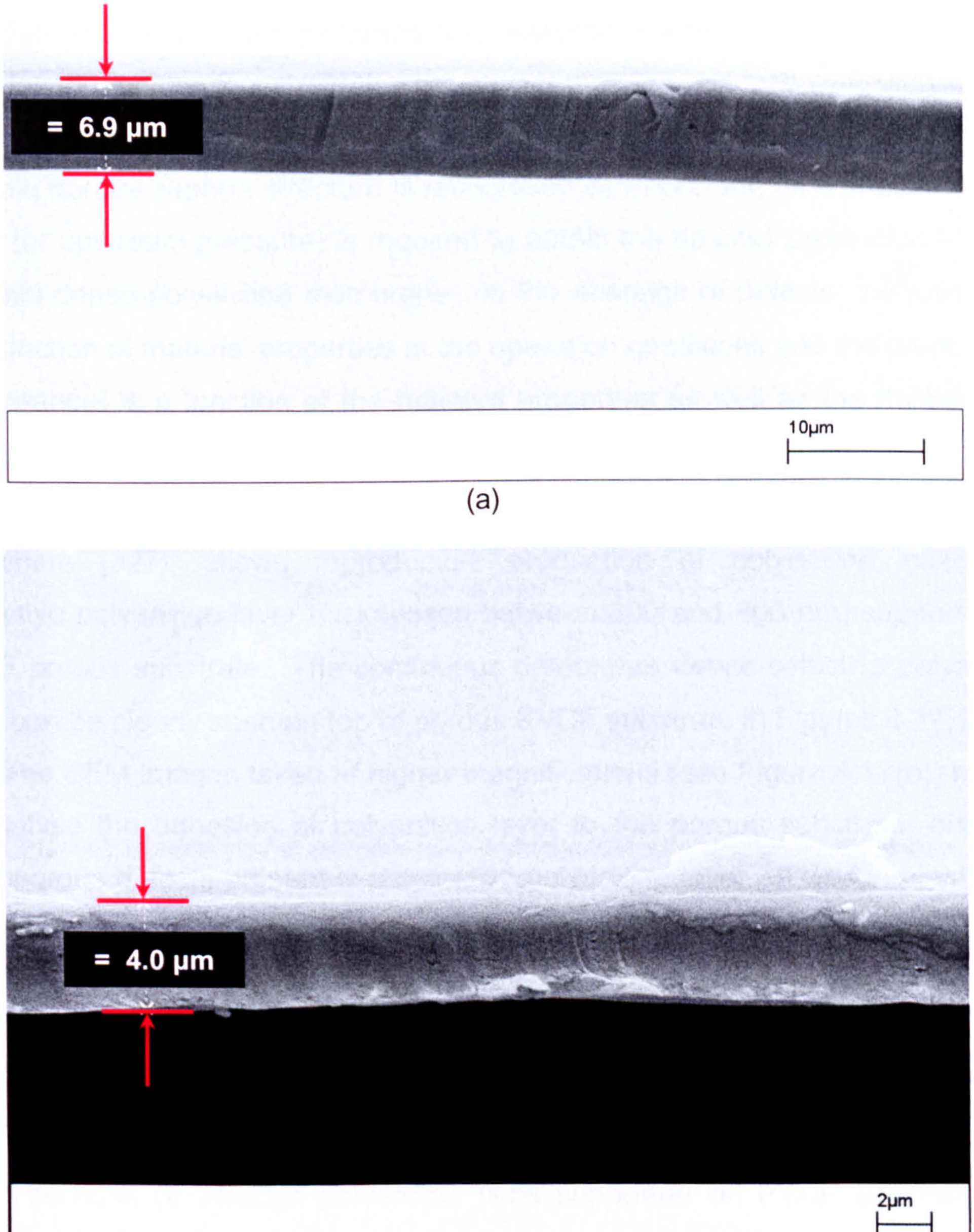

Figure 4. 16 Scanning electron micrographs of a cross section of self-supported dense polyaniline films: polyaniline film thickness (a) 6.9 µm; (b) 4.0 µm.

3.2. Polyaniline Nano-Membranes

To be of commercial interest, the active separation later of a composite membrane should probably have an equivalent dense polymeric film thickness of the order of 100 nm [326]; if thin coherent films of the polymer cannot be prepared then useful membrane devices will not result. Asymmetric membranes, having an ultrathin dense selective layer made from glassy polymers supported on a porous substrate are widely used in industrial gas separations [72,76]. A selective polymeric layer performs the separation and the suitable substrate provides the mechanical strength.

Production of the thinnest possible selective polyaniline layer on a suitable porous support structure is recognised as important, as a smaller driving force (or upstream pressure) is required to obtain the desired separation through ultrathin dense polyaniline membrane. In the absence of defects, the selectivity is a function of material properties at the operation conditions and the productivity (permeance) is a function of the material properties as well as the thickness of the barrier; and the smaller the thickness, the higher the productivity.

The novel technique developed in this research, also published elsewhere [327], allows reproducible production of polyaniline nano-films (selective polyaniline layer thicknesses between 300 and 800 nm) supported on PVDF porous substrate. The continuous defect-free dense selective polyaniline layer can be clearly seen on top of porous PVDF substrate in Figures 4.17(a) and (b). The SEM images taken at higher magnifications (see Figure 4.17(b)) helped to analyse the adhesion of polyaniline layer to the porous substrate, and any microporous defects present in a selective polyaniline layer. It was interesting to see (in Figure 4.17(b)) that the ultrathin polyaniline layer on top of PVDF substrate is anisotropic. The ultrathin polyaniline film structure appeared to be denser for approximately 50 to 70 nm (from the top) than rest of the polyaniline film.

Figures 4.18(a), (b) and (c) represent scanning electron micrographs of cross sections of ultrathin polyaniline films supported on PVDF substrate; the selective polyaniline layer thickness were 1.9 μm, 501 nm and 325 nm, respectively. These micrographs were also useful to get an insight into the morphology of the composite materials.

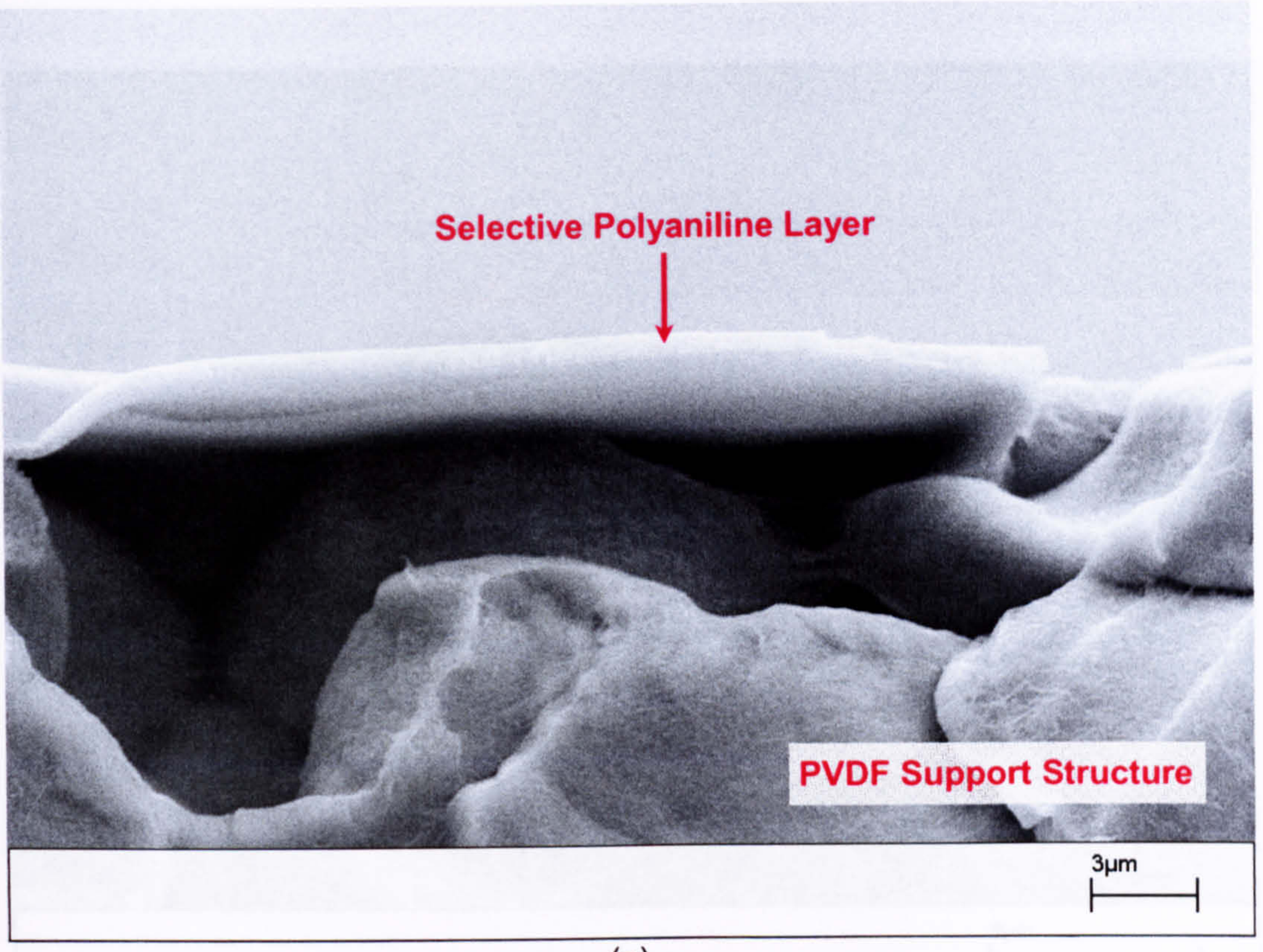

Figure 4. 17 SEM images of polyaniline/PVDF composite membranes.

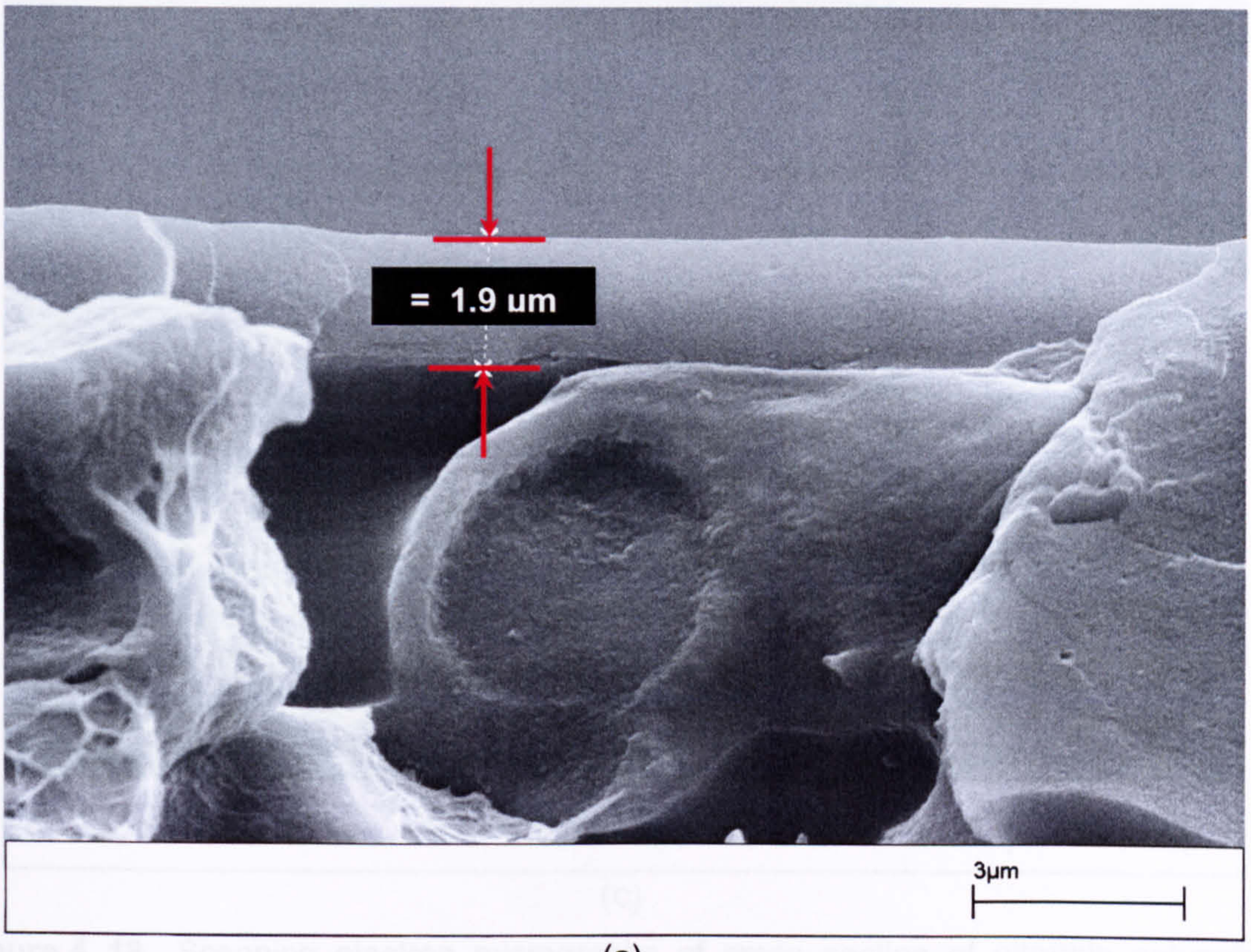

(a)

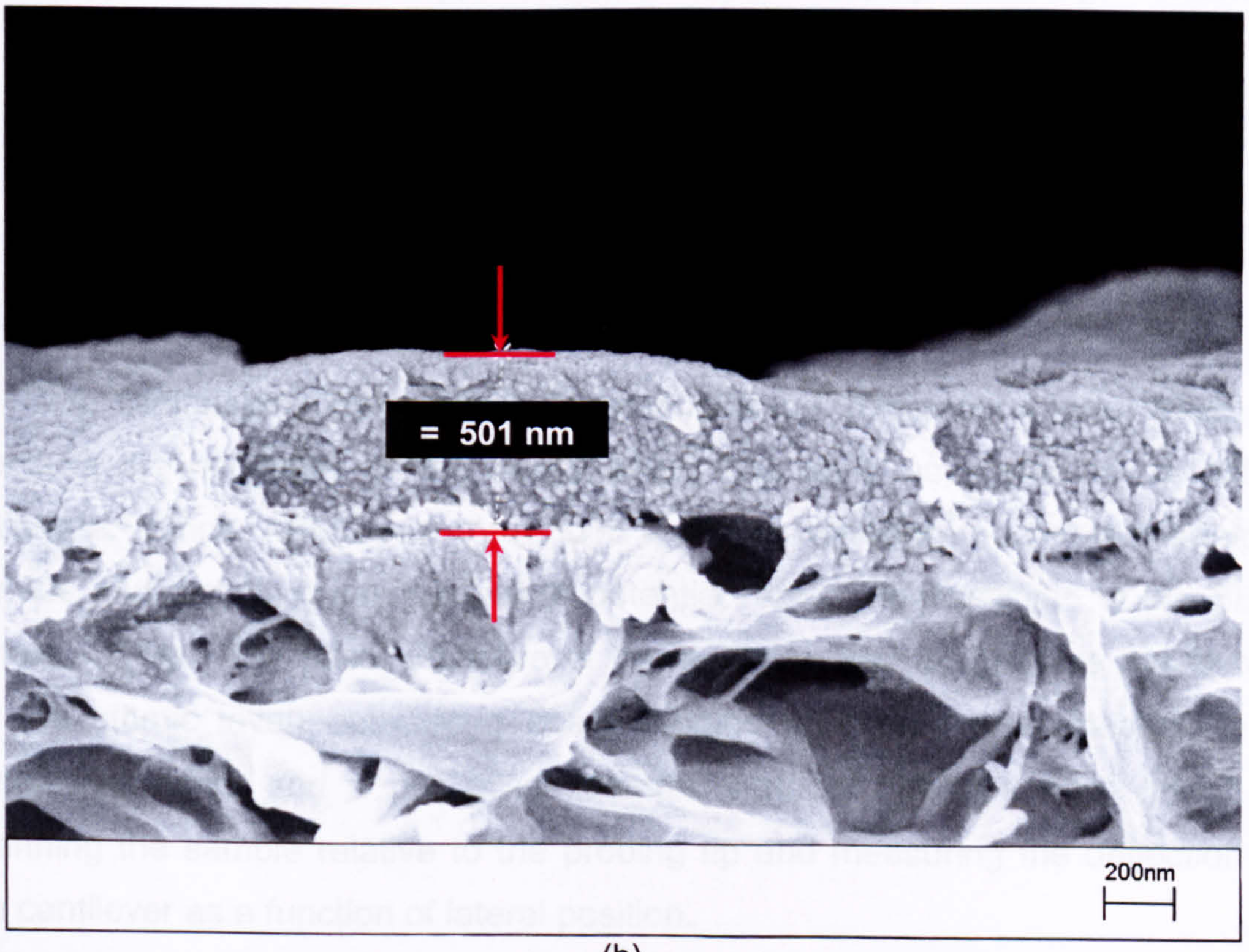

(b)

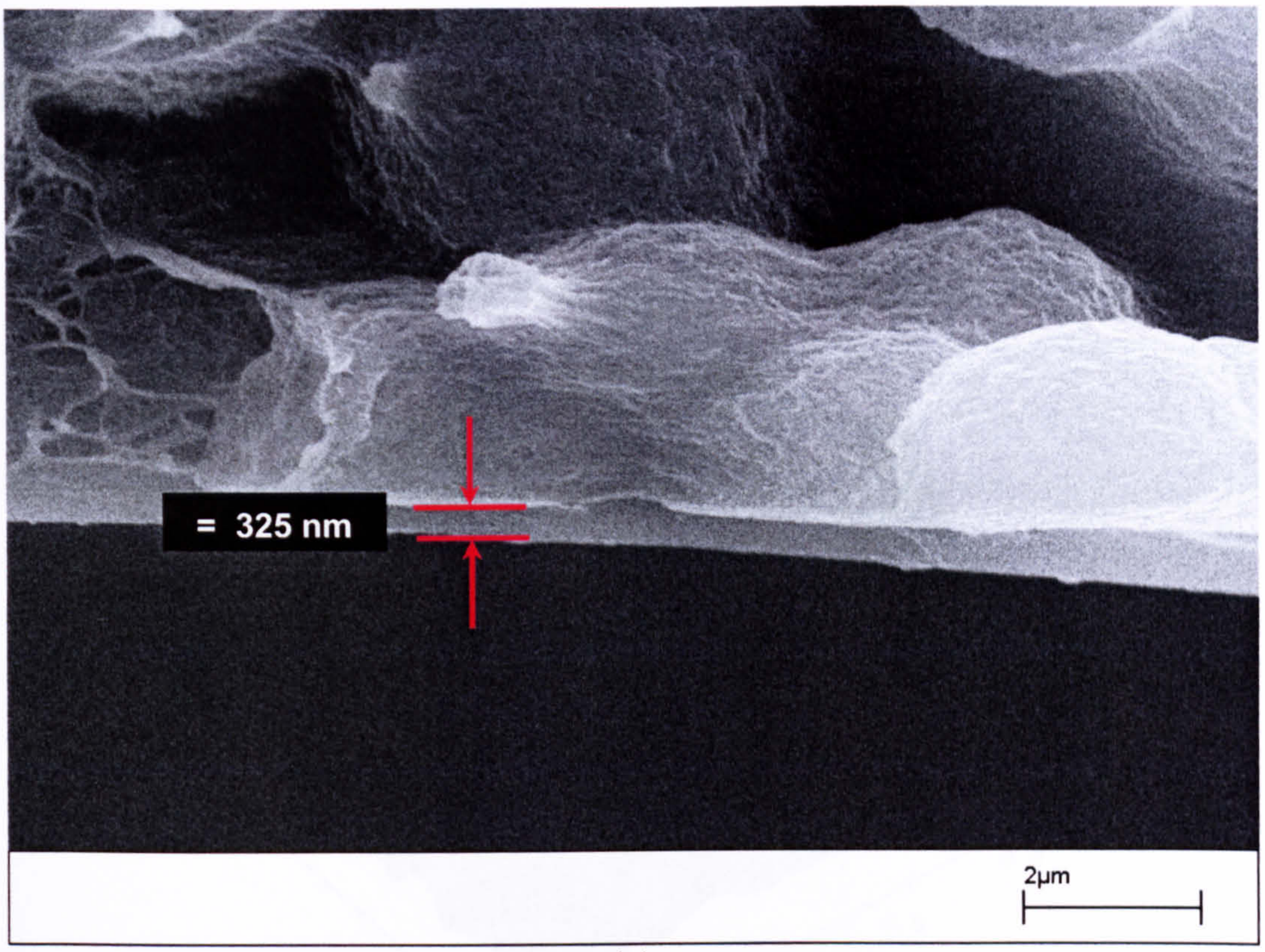

(c)

Figure 4. 18 Scanning electron micrographs of cross section of ultrathin polyaniline films supported on PVDF support structure: selective polyaniline layer thickness (a) 1.9 μm; (b) 501 nm; (c) 325 nm.

4. CHARACTERISATION OF POLYANILINE FILMS

4.1. Morphology Analysis

A Dimension 3100 (VEECO) atomic force microscope was used to measure the continuity of the dense polyaniline layer supported on a PVDF substrate. Since, AFM does not require a current between the polymer sample surface and the tip, it can move into potential regions inaccessible to the SEM (and/or STM). The basic objective of the analysis was to measure the forces (at the atomic level) between a sharp probing tip (which was attached to a cantilever spring) and a polyaniline sample surface. Images were taken by scanning the sample relative to the probing tip and measuring the deflection of the cantilever as a function of lateral position.

AFM images of ultrathin polyaniline films supported on PVDF substrate were obtained using the tapping mode of operation, which was used as the soft

polymeric surfaces could be damaged by a direct contact with the tip. The following Figures 4.19(a) and (b) show the sectional analysis for the selected scanning area of the ultrathin polyaniline layer.

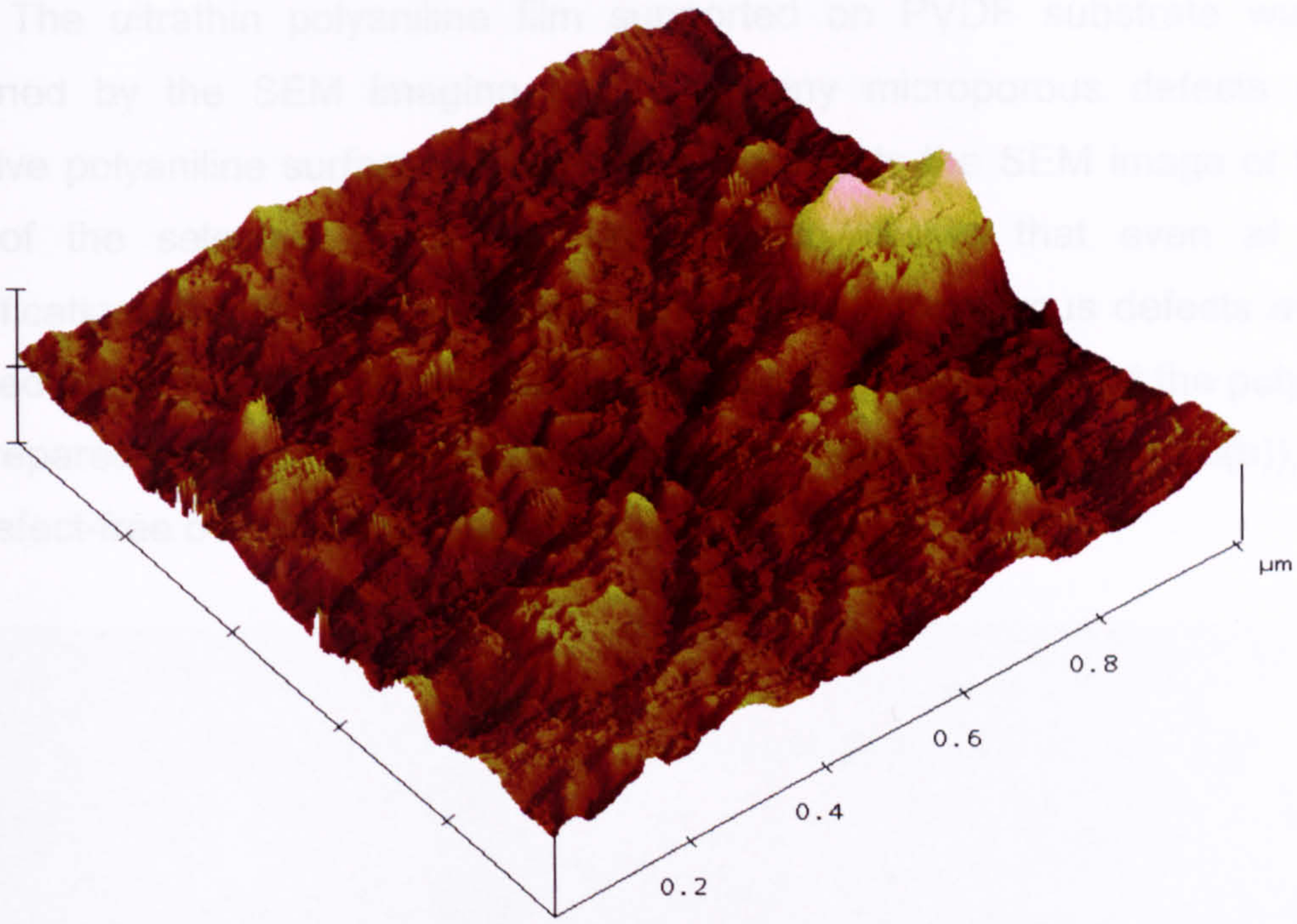

(a)

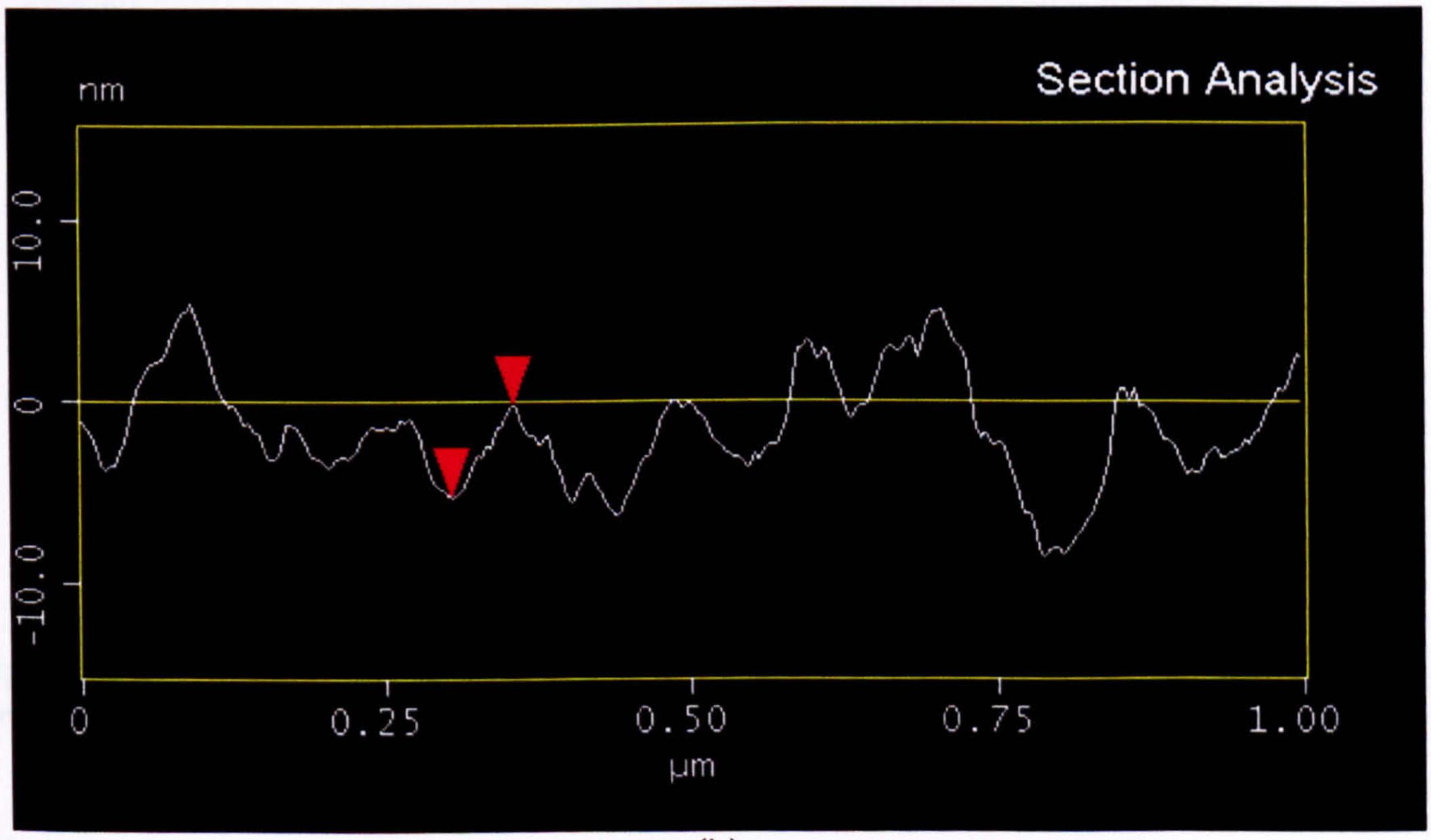

(b)

Figure 4. 19 Sectional analysis of ultrathin polyaniline layer: (a) AFM image of ultrathin polyaniline film supported on PVDF; (b) the sectional height analysis of the film.

The sectional analysis of a polyaniline nano-film over the scanned area revealed that the layer has structural dips up to 8 nm and peaks up to 6 nm, which are orders of magnitude smaller than the total selective polyaniline layer thickness (total selective polyaniline layer thickness = 501 nm).

The ultrathin polyaniline film supported on PVDF substrate was also examined by the SEM imaging facility for any microporous defects on the selective polyaniline surface. Figure 4.20 represents the SEM image of the top view of the selective polyaniline layer, which shows that even at higher magnifications the film did not contain any visible microporous defects over the scanned area. Figure 4.20 also provides supporting evidence that the polyaniline film prepared on the PVDF substrate was anisotropic (see Figure 4.18(b)), dense and defect-free over the scanned area.

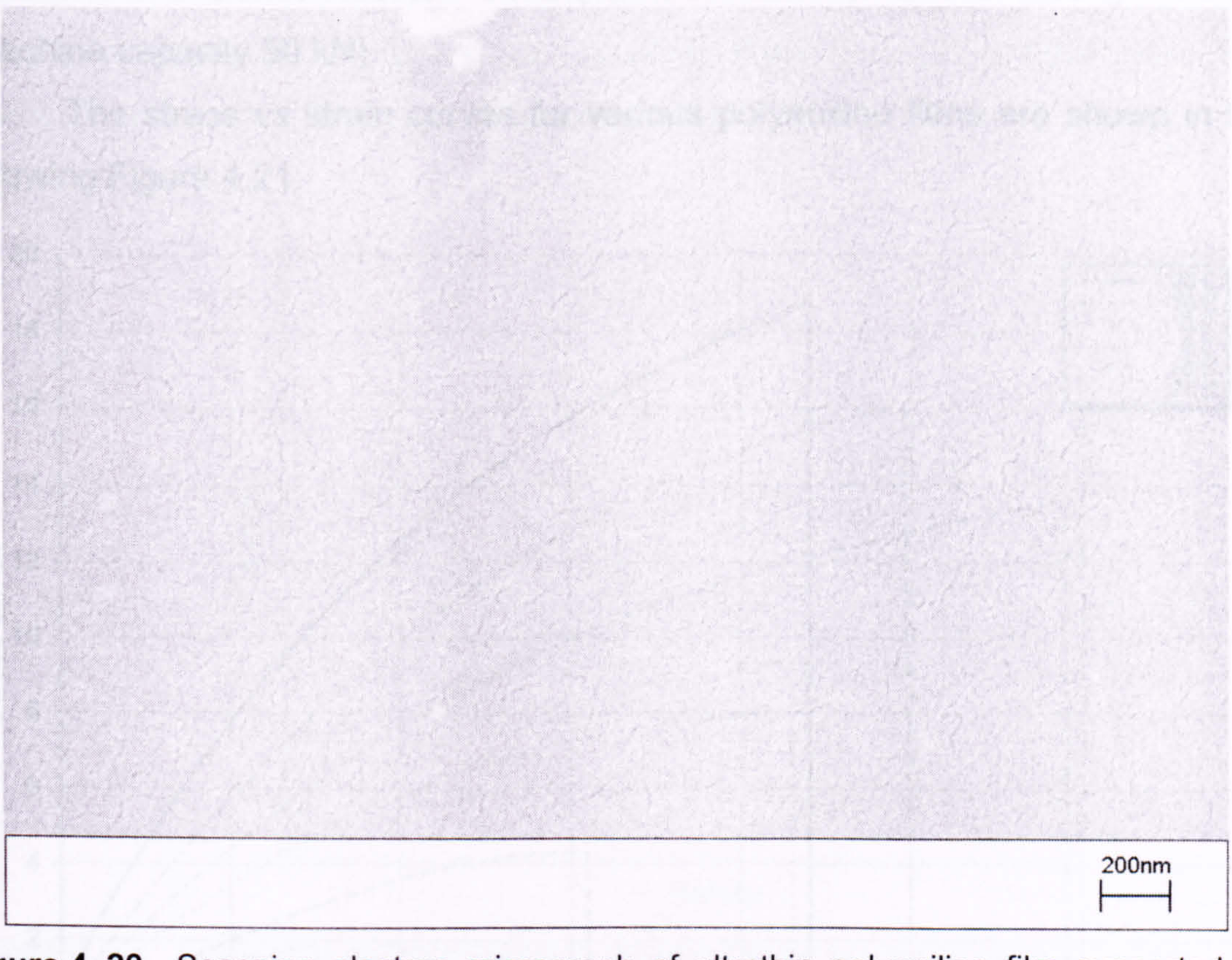

Figure 4. 20 Scanning electron micrograph of ultrathin polyaniline film supported on PVDF substrate.

4.2. Mechanical Properties of Polyaniline Membranes

The mechanical properties of a polymer are the facets of behaviour that are evident when the polymer is subjected to some form of a mechanical stress.

One of the goals of this research has been to produce polyaniline with increased crystallinity and higher molecular weight to improve its mechanical and transport properties. The increased molecular weight and crystallinity (among samples of the same polymer) tend generally to give a higher modulus, lower elongation, higher tensile strength, and greater resistance to creep [275].

The precise determination of mechanical properties requires that samples used are free of defects, such as voids, cracks, nicks and other abnormalities that could act as stress concentrators. Defect-free self-supported polyaniline films, with the film thicknesses between 95 and 100 μm, were prepared using the method described in Section 4.1.1 (see Chapter 3). The mechanical properties of the self-supported polyaniline (EB) films cast from different polyaniline samples (produced at various polymerisation reaction temperatures) were studied using a dual column S Series H50KS - 0476 (TINIUS OLSEN) material testing machine (machine capacity 50 kN).

The stress *vs* strain curves for various polyaniline films are shown in the following Figure 4.21.

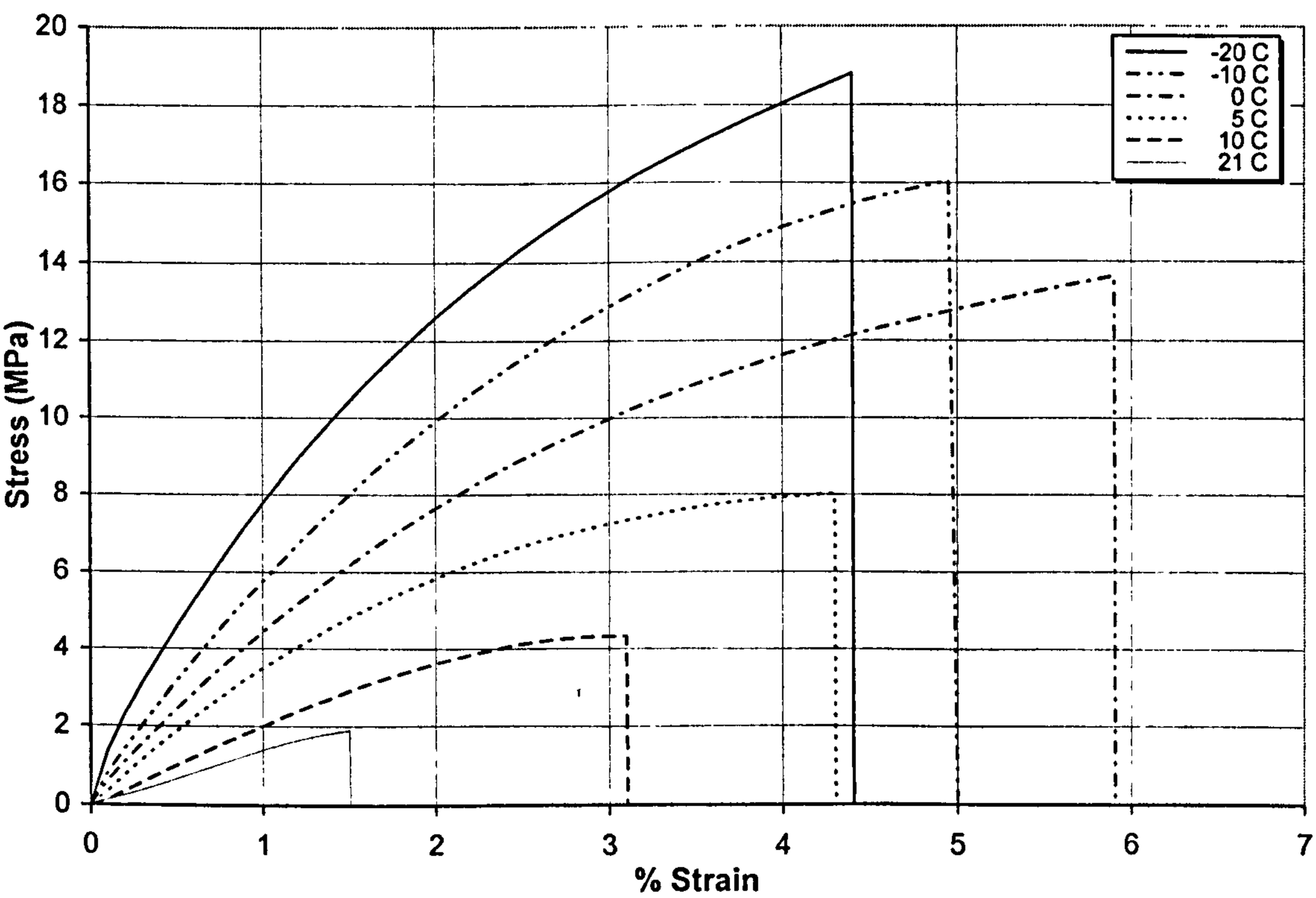

Figure 4. 21 Mechanical properties of polyaniline membranes with approximately 100 μm film thickness cast from different polyaniline samples (produced at various polymerisation reaction temperatures).

The area under the stress-strain curve, also known as the toughness, is a valuable piece of information that can be calculated. Toughness is a measure of the energy that a sample can absorb before it breaks. It is important to know that a strong material is not necessarily going to be tough. Figure 4.22 shows a schematic explanation of the toughness of the material using stress-strain curves. Plot 'A' is the stress-strain curve for a sample that is strong, but not tough. It takes a lot of force to break the sample, but not much energy, as the area under the curve is small. Likewise, this sample cannot be stretched very far before it breaks. A material like this is strong, but cannot deform very much before it breaks. On the other hand, plot 'B' is a stress-strain curve for a sample that is both strong and tough. This material is not as strong as the sample in plot 'A', but the area under this curve is a lot larger than the area under the plot 'A'. So, this material can absorb more energy than the plot 'A' sample. The plot 'B' sample elongate lot more before breaking than plot 'A' sample, and this deformation allows a sample to dissipate energy.

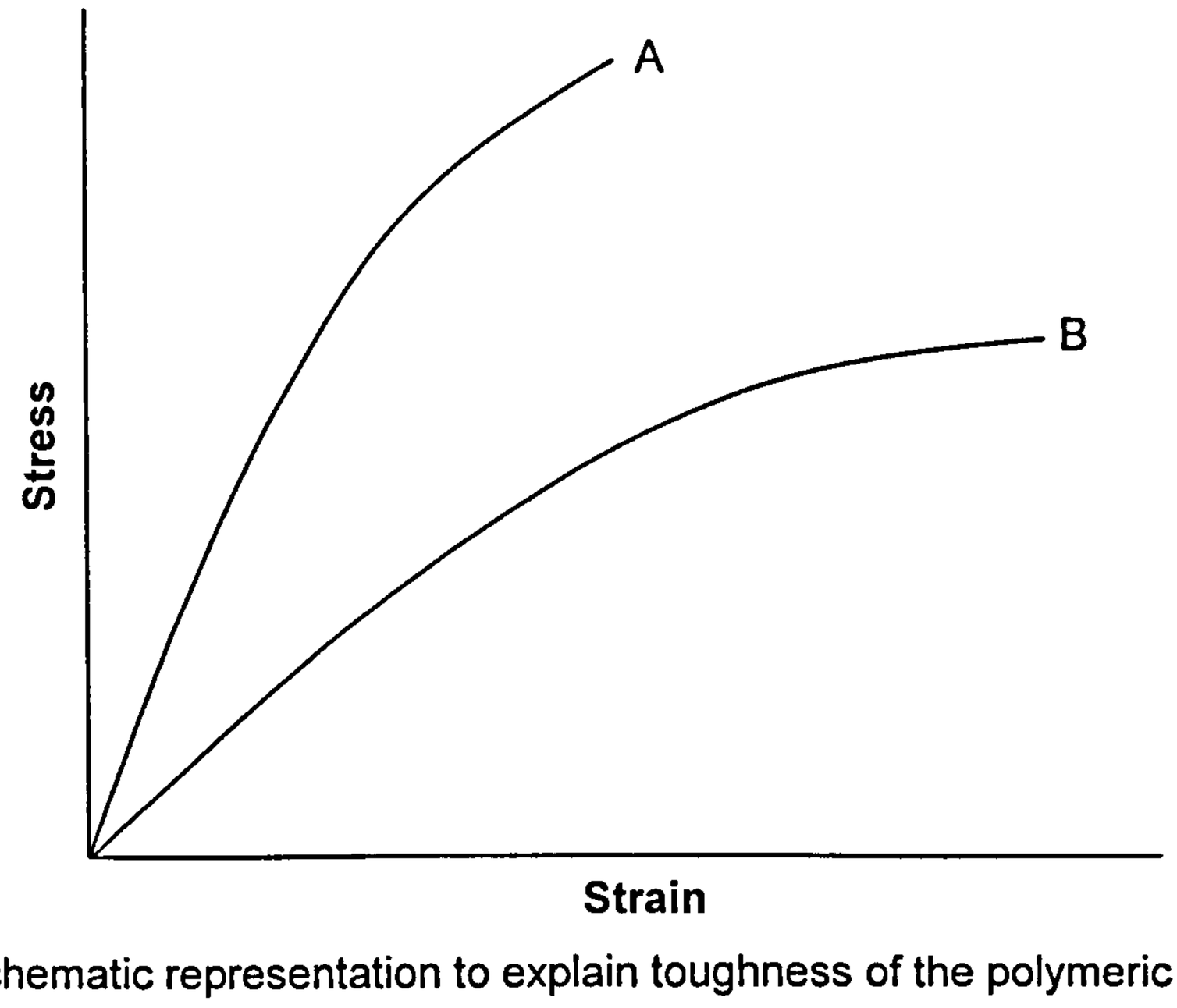

Figure 4. 22 Schematic representation to explain toughness of the polymeric films.

Young's Modulus (the initial slope of the stress-strain curve), also known as *initial linear modulus*, tensile strength (fracture stress) and toughness values for the polyaniline membranes prepared from different polyaniline samples (produced at various polymerisation reaction temperature) are summarised in Table 4.5.

Table 4. 5 Young's Modulus and fracture stress values for polyaniline film samples prepared from the different polyaniline samples (produced at various polymerisation reaction temperatures).

Polyaniline Membrane Sample	Molecular Weight (M_w)	Young's Modulus (MPa)	Tensile Strength (MPa)	Toughness (MPa)
21 C	101078	1.384	1.906	1.508
10 C	154103	1.892	4.335	8.357
5 C	170650	3.046	8.029	23.229
0 C	208471	3.662	13.633	52.382
-10 C	229860	4.951	16.064	51.208
-20 C	281338	6.389	18.861	50.967

It was clear from the stress-strain curves plotted for polyaniline (produced at -10 and -20 C) film samples that these membranes were strong but not tough. On the other hand films produced from polyaniline produced at 0 C were not as strong as the films produced at -10 and -20 C. However, the toughness values of these films were in a close proximity to the films produced at -10 and -20 C. Figure 4.23 shows the relationship between Young's Modulus, tensile strength and polyaniline polymerisation reaction temperature.

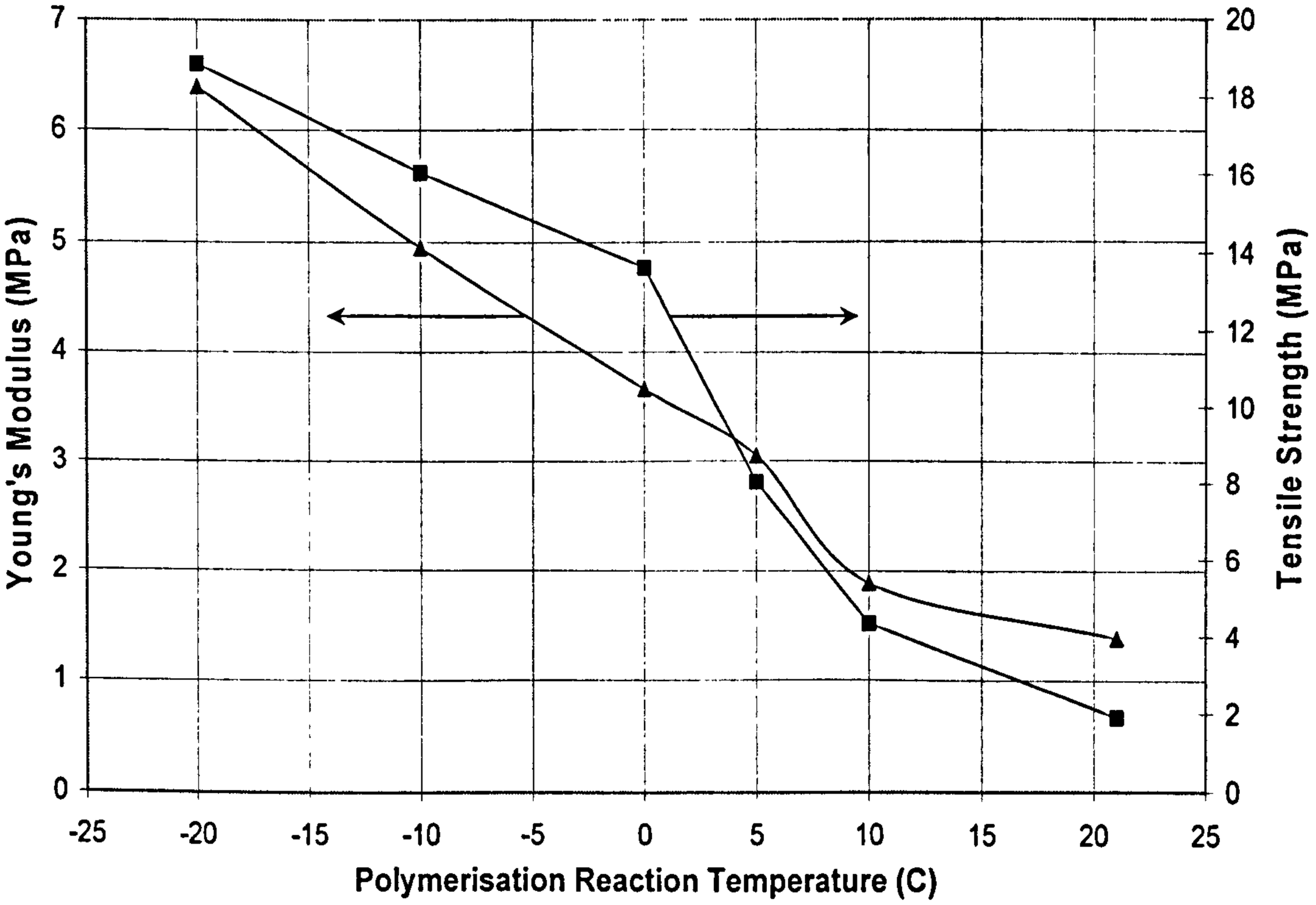

Figure 4. 23 Graph of Young's Modulus and Break Stress *versus* polyaniline polymerisation reaction temperature.

The gel permeation chromatography results showed that higher molecular weight polyaniline was obtained when the polymerisation was carried out at sub-ambient temperatures. The physical properties are strongly affected by the molecular weight and crystallinity of the polymers. It is apparent from Table 4.5 and Figure 4.23 that the strength and toughness as measured by tensile strength and elongation at breakage for polyaniline film samples increased with the molecular weight and crystallinity of the polymer.

Hence, the higher molecular weight polyaniline samples resulted in higher tenacity and higher Young's Modulus polyaniline EB films due to the structure and chain length of the polymer.

4.3. Membrane Permeation Cell

4.3.1. Construction of a Membrane Permeation Cell

The permeation rates of various penetrant gases through a polyaniline membrane were measured by an integral permeation method. The permeation cell was designed (see Appendix 2) and constructed from stainless steel (SS 316) in our laboratory to investigate the gas transport properties of polyaniline membranes (free standing self-supported polyaniline membranes and ultrathin polyaniline/PVDF composite membranes). The operating pressure of the permeation cell was designed to be up to 60 bar (6 MPa) with the tubing and fittings for high pressure gas permeation experiments. Figures 4.24(a) and (b) show the plan and elevation drawings of the permeation cell used to conduct gas permeation experiments.

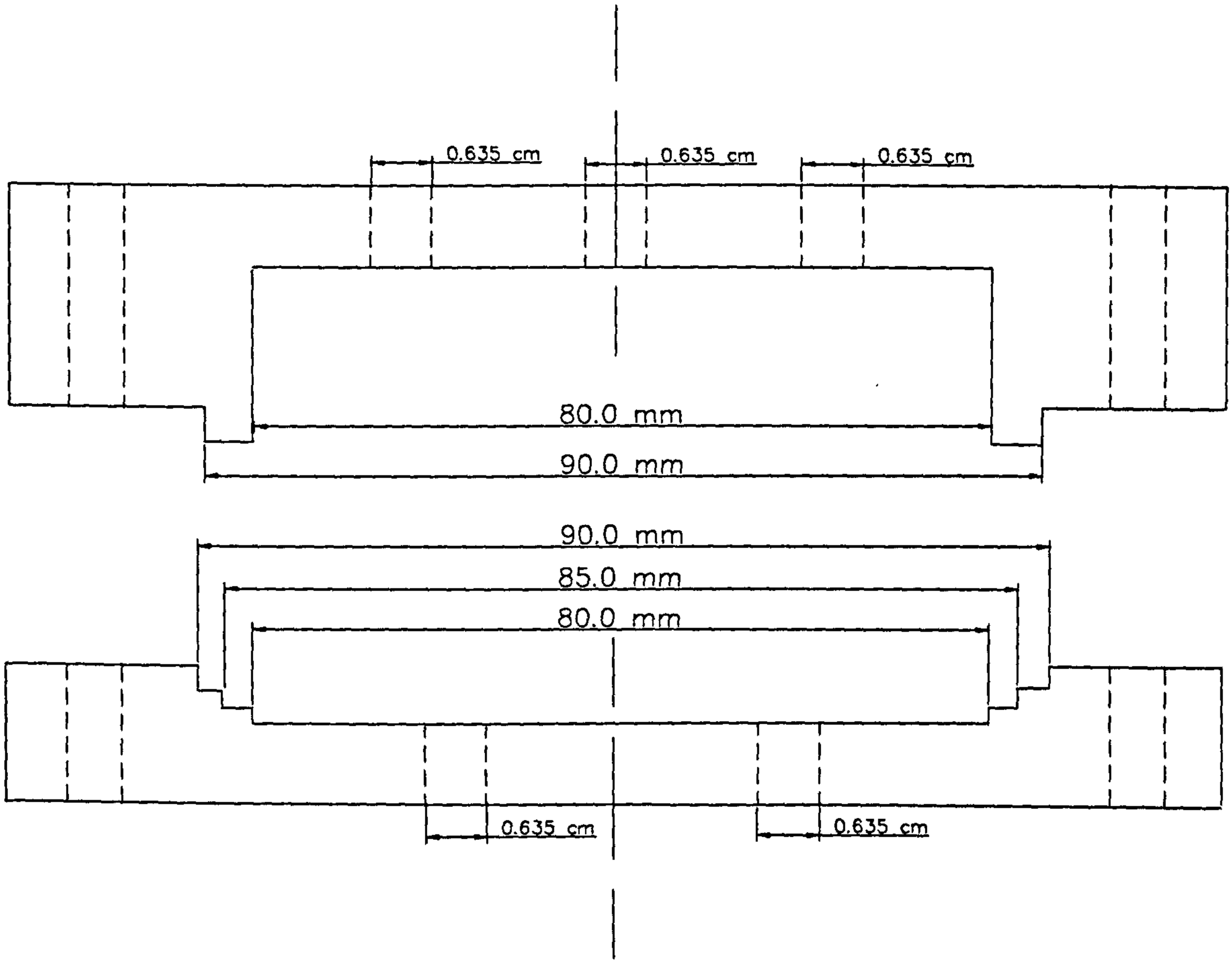
0.635 cm
0.635 cm
0.635 cm
80.0 mm
90.0 mm
90.0 mm
85.0 mm
80.0 mm
0.635 cm
0.635 cm

(a)

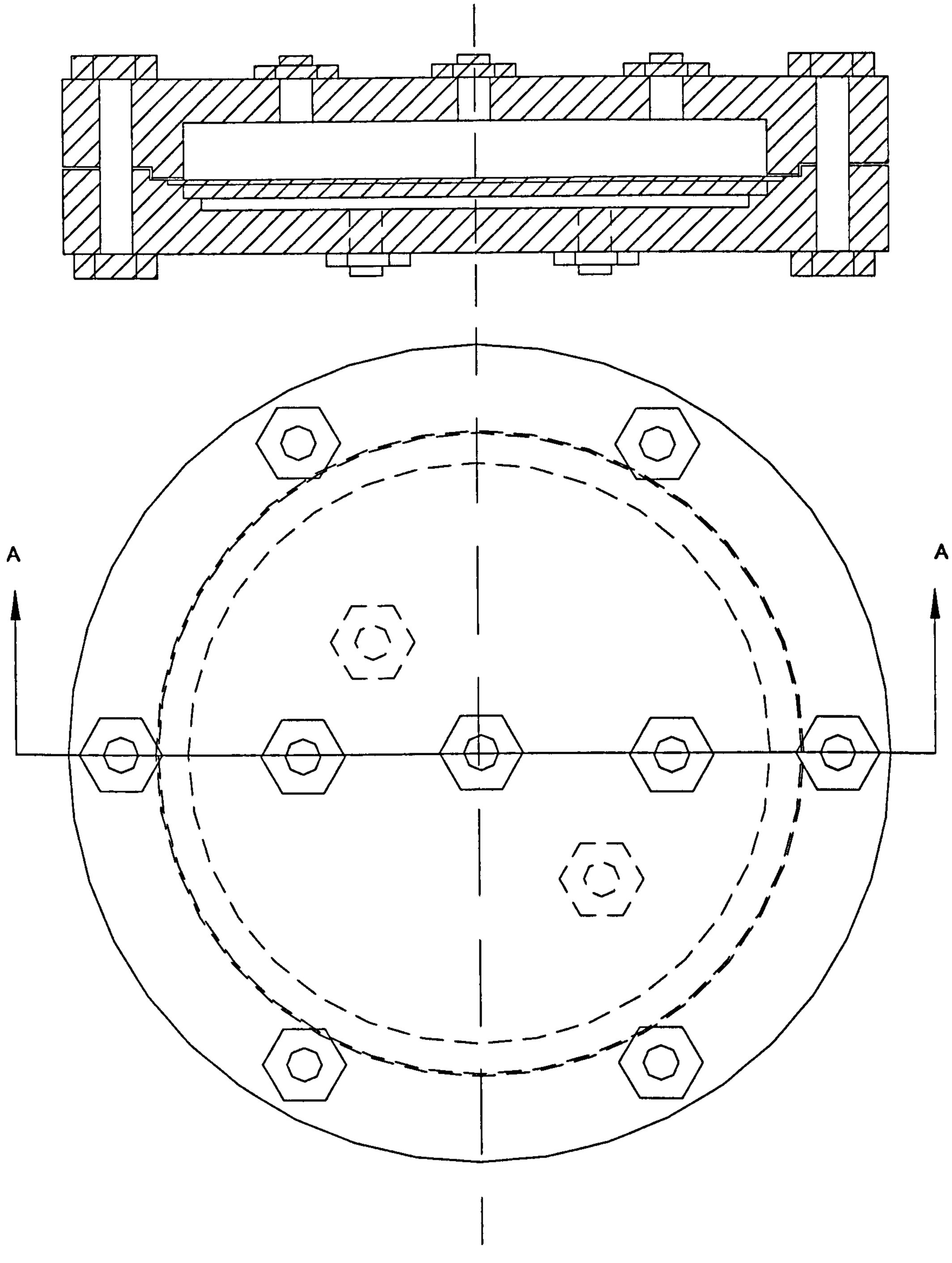

(b)

Figure 4. 24 Plan and elevation drawings of membrane permeation cell.

4.3.2. Permeation Cell Downstream Section Volume Calibration

The volume of the permeate (downstream) section was calibrated to calculate the permeation coefficients of various permeating gases through polyaniline membranes precisely. The downstream volume was evaluated with high accuracy by using a Manometric method, and the obtained value was verified by using a gas permeation method with PDMS membrane (selective PDMS layer thickness = 2 μm) under similar operating conditions.

The Manometric method was repeated for several times with different gas sample cylinders of known gas volumes (10, 15 and 25 cm^3), and the downstream section volume was calculated using equation 3.3 (see Chapter 3), and the calculated downstream volume data were averaged to obtain the accurate permeate section volume. The downstream section volume calculated from the Manometric method (from equation 3.3) was 30.0829 cm^3, which corresponds to the geometrical value (29.8815 cm^3) of the downstream section volume of the permeation cell.

A single gas permeation experiment was conducted using a circular sample of flat sheet PDMS membrane having a selective layer thickness of 2 μm with nitrogen as a permeating gas, as per the method described in Section 5.3.2.4 (see Chapter 3). The downstream volume of the permeation cell was calculated using equation 3.4. The permeate section volume obtained by using the gas permeation method (calculated using equation 3.4) was 31.1628 cm^3, which is in a close proximity of the value obtained by Manometric method. Since the permeation data for PDMS membrane vary with the operating conditions, the downstream volume value of the permeation cell obtained by Manometric method was considered appropriate to calculate permeability coefficients of various permeating gases through polyaniline membrane.

The procedure and calculation steps involved to calibrate permeate section volume is explained in detain in Appendix 3.

4.4. Gas Transport Properties of Polyaniline Membranes

4.4.1. Membrane Defects Test

The proper placement of the polyaniline membrane in the permeation cell is important, as the stress from uneven contact between the membrane and flat rubber gasket during bolting together of the upstream and downstream sections could damage the polyaniline film. On the other hand, the sudden overpressurisation of the upstream section of the permeation cell can also damage the polymer film. The bursting pressure values of the test polyaniline films (self-supported polyaniline films and polyaniline/PVDF composite films) were calculated from the stress-strain curve (see Figure 4.21). The upstream pressure in the permeation study was maintained always below the bursting pressure value of the test polyaniline sample. The bursting pressure value for the ultrathin polyaniline film (selective polyaniline film thickness = 500 nm) was calculated to be 0.6 bar (0.06 MPa), assuming the linear relationship between calculated bursting pressure and polyaniline film thickness. However, gas permeation tests, with ultrathin polyaniline films, were conducted at the maximum upstream pressure of 1.5 bar (0.15 MPa), which shows the contribution of the PVDF support layer to the mechanical strength of the composite film.

A test was conducted to check for any microporous defects (including stress fracture) on the polyaniline membrane surface. The feed (upstream) side of the permeation section was pressurised to test the stress fracture. The absence of any membrane fracture was evident since the membrane showed a resistance to the applied feed pressure. Single gas permeation experiments were conducted to monitor any microporous (or macroporous) defects in the polyaniline membrane, using oxygen and nitrogen as a permeating gas and the procedure discussed in Section 5.3.2.4 (see Chapter 3). The rise in the pressure in the downstream section of the permeation cell was monitored by a pressure transducer. Figure 4.25 shows typical test results of the increase in permeation section pressure with time for oxygen and nitrogen.

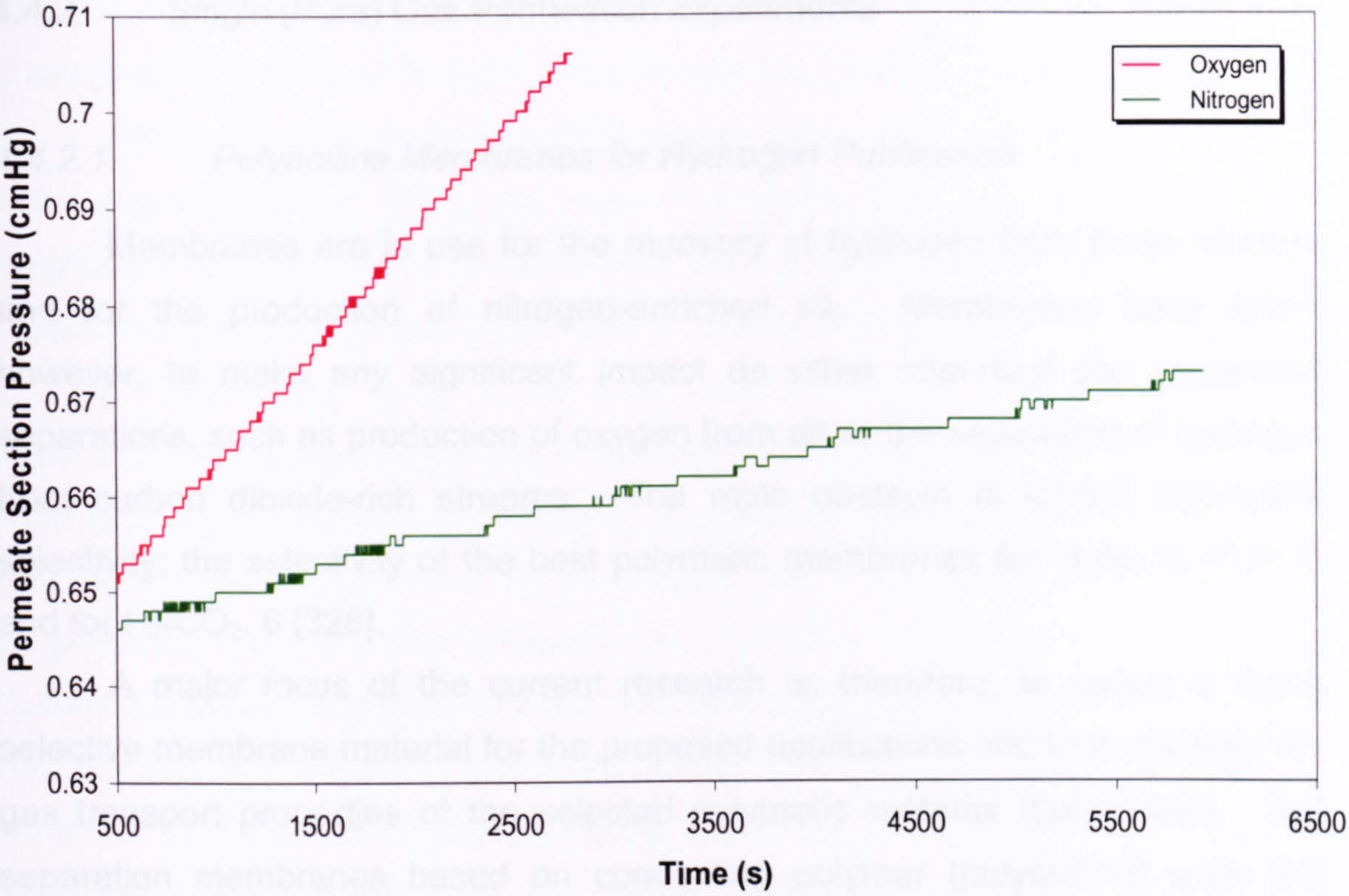

Figure 4. 25 Graph of rise in the permeate section pressure *vs* time to test the defects on polyaniline membrane with oxygen and nitrogen as permeating test gases.

The permeability and selectivity values were calculated by equations 3.3 (see Chapter 3) and 2.30 (see Chapter 2), respectively. The experiment was repeated at least three times to verify the ideal separation efficiency value for oxygen and nitrogen (α_{O_2/N_2}). The calculated ideal separation efficiency for oxygen and nitrogen (using equation 2.32) was compared with the values obtained by the other researchers [50-56]. The ideal separation (α_{O_2/N_2}) obtained was 5.3 ± 0.2, which corresponds to the values obtained by other researchers.

It was evident from the results obtained by gas permeation experiments that the polyaniline membrane was a dense and defect-free continuous layer.

4.4.2. Single (Pure) Gas Permeation Experiments

4.4.2.1. Polyaniline Membranes for Hydrogen Purification

Membranes are in use for the recovery of hydrogen from purge streams and for the production of nitrogen-enriched air. Membranes have failed, however, to make any significant impact on other important gas separation separations, such as production of oxygen from air or the separation of hydrogen from carbon dioxide-rich streams. The main obstacle is limited membrane selectivity; the selectivity of the best polymeric membranes for O_2/N_2 is ~6 to 8, and for H_2/CO_2, 6 [328].

A major focus of the current research is, therefore, to assign a highly selective membrane material for the proposed applications and to investigate the gas transport properties of the selected polymeric material (polyaniline). Gas separation membranes based on conducting polymer (polyaniline) were first reported in the early 1990s [51-53], in which permeability and selectivity of gas pairs were modified by altering the morphology and oxidation states of polymer through doping, dedoping and redoping. The exceptional gas transport data obtained in previous investigations [50-57] have encouraged us to explore the gas transport properties of polyaniline membranes and investigate the effect of film thickness on the separation efficiency and gas transport rate of various gases through polyaniline membranes.

In the following sub-sections, the gas transport properties of self-supported polyaniline films (film thickness = 2 to 6 μm) as well as ultrathin polyaniline films supported on PVDF substrate (selective polyaniline layer thickness = 0.4 to 0.8 μm), in respect to hydrogen purifications, are presented and discussed.

4.4.2.1.1. Self-supported Polyaniline Films for Hydrogen Purification

The gas permeation measurements were conducted for self-supported polyaniline membranes using the pure (single) gas permeation method at a feed pressure of 1 to 4 bar (0.1 to 0.4 MPa) at room temperature (21 ± 2 C). The single gas permeation apparatus used in this study is shown in Figure 3.3 (see

Chapter 3). The operational procedure to conduct a single gas permeation experiment is discussed in detail in Section 5.3.2.4 (see Chapter 3).

Self-supported polyaniline (EB) membranes were prepared reproducibly using a novel method [327], and used to evaluate their potential for hydrogen purification applications. The polyaniline films having selective polyaniline layer thicknesses between 2 and 6 μm were tested for various pure gases – H_2, CO_2, O_2, N_2, CH_4, C_2H_4, C_2H_6, C_3H_6 and C_3H_8. Prior to the gas permeation measurements, these polyaniline membranes were dried overnight in a vacuum oven at 60 C. A free standing undoped polyaniline membrane was mounted on a porous sintered metal plate in the permeation cell. A flat rubber gasket was used to provide a vacuum seal between the upstream and downstream sections. Before the permeation experiments, both upstream and downstream sections of the permeation cell were degassed under vacuum ($<10^{-9}$ bar) overnight to eliminate the effect of adsorbed volatile chemicals in the polyaniline film. The gas permeation experiments were conducted using a standard manometric method (also known as constant volume method). The upstream section was pressurised and permeation through the polyaniline membrane was measured using the integral permeation method (also known as manometric time-lag method) of analysis. The rise in pressure against time in the permeate section was monitored by a MKS Baratron pressure transducer, and equation 3.3 (in Chapter 3) was used to calculate the permeability of a permeating gas through undoped free standing polyaniline membranes.

It was hoped that the polyaniline membranes will maintain useful separation properties in the presence of organic vapours, particularly C_{2+} hydrocarbon vapours. To quantify this, single (pure) gas permeation experiments were conducted using various gases (H_2, CO_2, O_2, N_2, CH_4, C_2H_4, C_2H_6, C_3H_6 and C_3H_8) with respect to upstream (feed gas) pressure (between 1 and 4 bar) to observe the effect of the plasticising gases on the performance of the polyaniline membranes. A single gas permeation test was performed three times at the same operating (feed gas) pressure to check the reproducibility of the permeability data. Since the tests were conducted at ambient temperature (without an external oven), a slight variation in room temperature and manual errors have resulted ± 10% experimental error in the permeation data.

In Table 4.6, the permeability values of various gases through undoped self-supported polyaniline membranes (polyaniline film thickness ~ 2 to 4 μm) are summarised against operating (feed gas) pressure.

Table 4. 6 Pure gas permeability values of various gases through undoped self-supported polyaniline membranes.

Upstream Pressure (bar)	Permeability (Barrers*)								
	H_2	CO_2	O_2	N_2	CH_4	C_2H_4	C_2H_6	C_3H_6	C_3H_8
4.01 μm									
1	1.407	0.573	0.082	0.015	0.0034	0.058	0.015	0.014	0.0015
2	1.438	0.571	0.081	0.016	0.0034	0.058	0.015	0.014	0.0016
3	1.426	0.579	0.086	0.015	0.0034	0.067	0.018	0.015	0.0016
4	1.460	0.583	0.087	0.015	0.0036	0.072	0.017	0.015	0.0018
2.89 μm									
1	1.446	0.583	0.088	0.016	0.0034	0.083	0.016	0.009	0.0019
2	1.429	0.588	0.088	0.016	0.0037	0.092	0.016	0.012	0.0019
3	1.486	0.587	0.093	0.016	0.0037	0.093	0.019	0.014	0.0023
4	1.481	0.594	0.098	0.017	0.0038	0.108	0.021	0.015	0.0023
2.52 μm									
1	1.433	0.589	0.095	0.016	0.0035	0.068	0.011	0.014	0.0031
2	1.459	0.592	0.097	0.015	0.0036	0.073	0.013	0.015	0.0035
3	1.410	0.592	0.097	0.017	0.0036	0.081	0.016	0.017	0.0035
4	1.488	0.595	0.107	0.016	0.0038	0.076	0.016	0.018	0.0037

* 1 Barrer = 1 x 10^{-10} $cm^3_{(STP)} \cdot cm/cm^2 \cdot s \cdot cmHg$

It was apparent from the permeability data (see Table 4.6) that the permeability values of most gases through self-supported polyaniline membranes varied only slightly within the operating pressure range (1 to 4 bar), hence the solution-diffusion model is supported by the lack of influence of pressure on the permeability. Furthermore, the effect of polar gases (CH_4, C_2H_4, C_2H_6, C_3H_6 and C_3H_8) on the separation properties of polyaniline membranes was very little, within the operating pressure range, i.e. 1 to 4 bar.

Henceforth, the single gas permeation experiments, for self-supported polyaniline membranes, were conducted within the feed gas pressure range of 1 to 4 bar to avoid any plasticisation of the polyaniline films.

The permeability values, calculated at room temperature, i.e. 21 ± 2 C and upstream pressure of 4 bar (0.4 MPa), of various gases through self-supported polyaniline membranes are plotted in the following Figure 4.26.

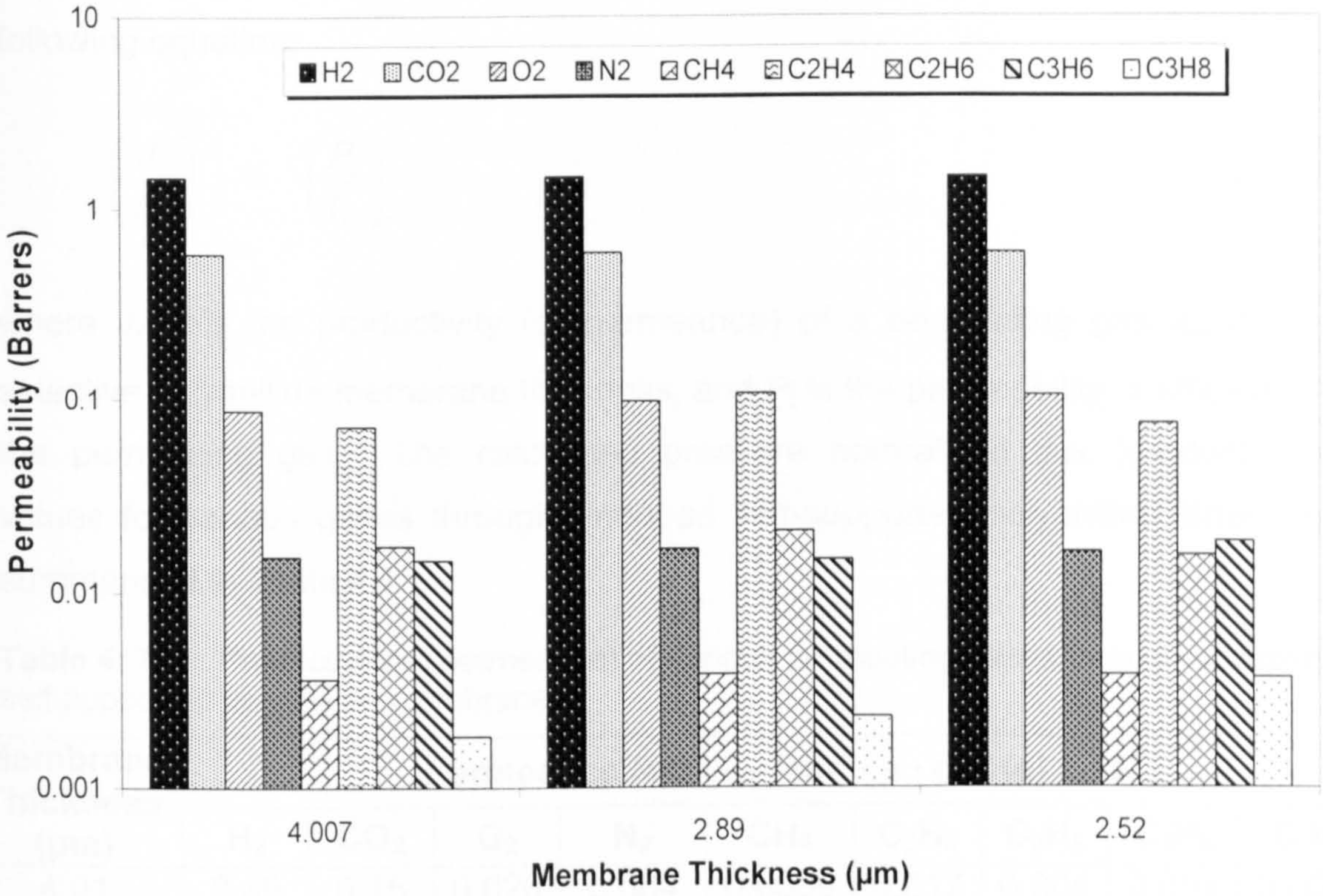

Figure 4. 26 Permeability, in Barrers (1 Barrer = 10^{-10} $cm^3_{(STP)} \cdot cm/cm^2 \cdot s \cdot cmHg$), for various gases permeating through freestanding undoped polyaniline membranes.

Currently, permeability is widely used to characterise the performance of a polymeric gas separation membrane. For example, Robeson [168] proposed the upper limit of the separation performance of polymeric gas separation membranes, and Singh *et al.* [330] identified the commercially attractive membrane performance area for separation of oxygen and nitrogen. In those two papers, the performance of a gas separation membrane was characterised with the permeability. The permeability, or more precisely permeability coefficient, is a thickness-normalised productivity of a polymeric gas separation membrane. Though permeability is calculated from the product of the productivity of a membrane and its thickness, permeability and productivity are two different concepts. The permeability is a material characteristic, which is not a membrane characteristic. The permeability of a membrane material is independent of the thickness of a membrane while the productivity of a membrane is always related

to its thickness. Hence, from the concept point of view, it is not correct to use permeability to characterise the performance of a gas separation membrane. The productivity (permeance, or the pressure normalised gas flux) of self-supported polyaniline films for various permeating gases as calculated using the following equation;

$$\left(\frac{J_i}{\Delta p}\right) = \left(\frac{P_i}{t_m}\right) \qquad (4.2)$$

where $J_i/\Delta p$ is the productivity (or permeance) of a permeating gas, t_m is the selective polyaniline membrane thickness, and P_i is the permeability coefficient of the permeating gas. The calculated pressure normalised flux (productivity) values for various gases through undoped self-supported polyaniline films are summarised in Table 4.7.

Table 4. 7 Productivities (permeance) of various permeating gases through undoped self-supported polyaniline membranes.

Membrane Thickness (μm)	Permeance ($cm^3_{(STP)}/cm^2 \cdot s \cdot cmHg$) x 10^6								
	H_2	CO_2	O_2	N_2	CH_4	C_2H_4	C_2H_6	C_3H_6	C_3H_8
4.01	0.36	0.15	0.026	0.004	0.0009	0.017	0.004	0.004	0.0004
2.89	0.52	0.20	0.033	0.006	0.001	0.037	0.007	0.005	0.0008
2.52	0.56	0.23	0.042	0.006	0.001	0.030	0.006	0.007	0.0009

In the Figure 4.27, the productivity (permeance) of various permeating gases through various polyaniline membranes are plotted (polyaniline film thickness = 2 to 4 μm).

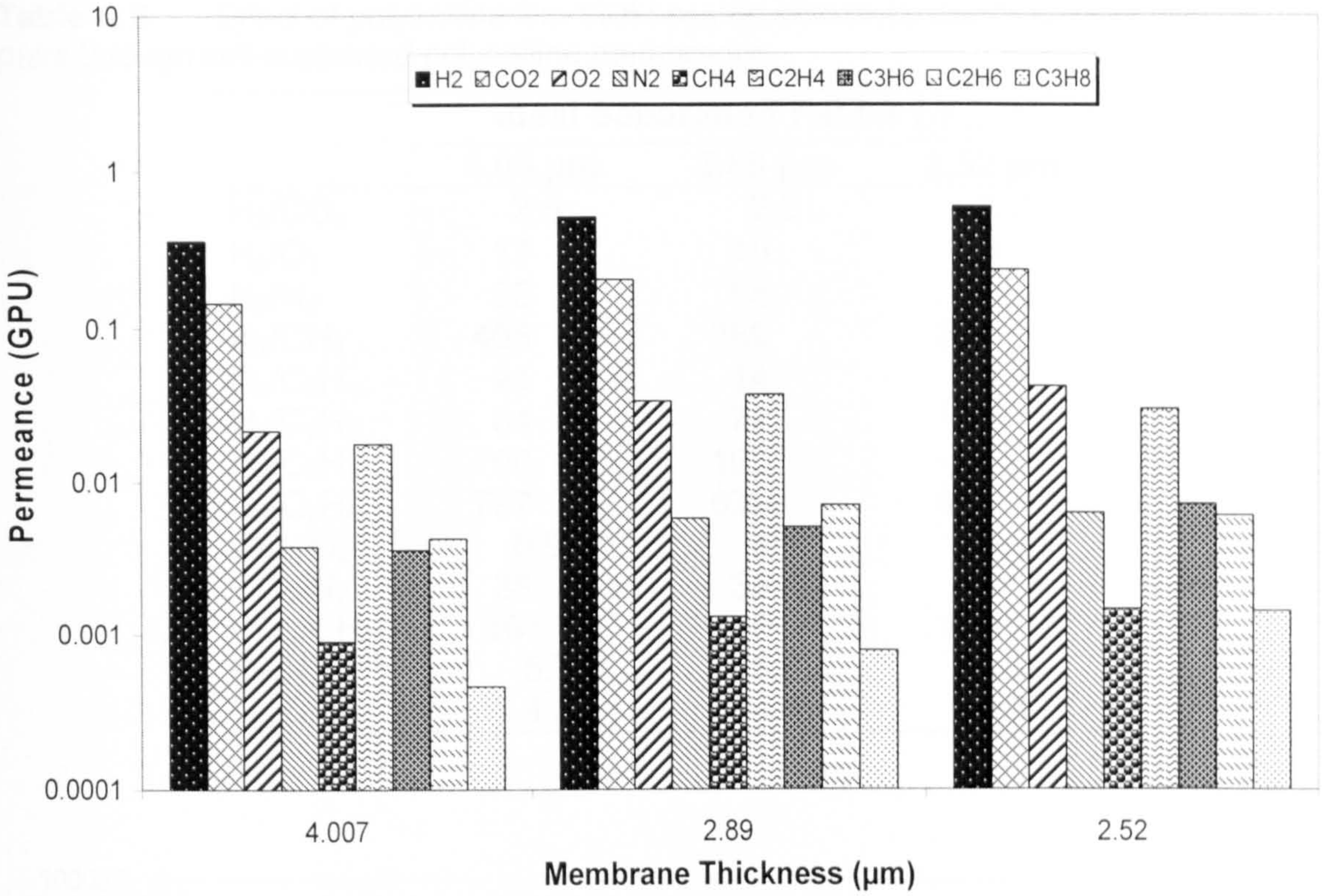

Figure 4. 27 The performance of undoped self-supported polyaniline membranes characterised with productivity (permeance) in Gas Permeation Unit.

1 Gas Permeation Unit (GPU) = 1 x 10^6 $cm^3_{(STP)}$ /cm^2 · s · cmHg.

It is possible to use the permeability of a membrane material to represent the relative productivity of membranes if all membranes have the same thickness. However, in this work, self-supported polyaniline membranes with the selective polyaniline layer thicknesses between 2 and 4 µm were produced and tested with various pure gases. Henceforth, the productivity (or permeance) of a permeating gas through polyaniline membranes is used to characterise the performance of the self-supported polyaniline membranes.

Ideal separation factors ($\alpha_{A/B}$), also known as the ratio of the rates at which two gases traverse through the membrane, were calculated using equation 2.30 (which is the ratio of the permeability of gas 'A' to gas 'B'). The calculated ideal (pure gas) separation efficiencies for various gas pairs through various undoped polyaniline membranes (polyaniline film thickness = 2 to 4 µm) are summarised in Table 4.8), and plotted in Figures 4.28 (a) and (b)).

Table 4. 8 Effect of polyaniline film thickness on selectivity coefficients of various gas pairs through self-supported polyaniline membranes.

	Ideal Separation Factor ($\alpha_{A/B}$)		
	4.00 μm	**2.89 μm**	**2.52 μm**
H_2/CO_2	2.5	2.5	2.7
H_2/O_2	17	15	15
H_2/N_2	95	85	89
H_2/CH_4	405	389	391
H_2/C_2H_4	21	14	20
H_2/C_2H_6	84	72	96
H_2/C_3H_6	100	100	81
H_2/C_3H_8	797	639	401
CO_2/O_2	6.9	6.1	5.6
CO_2/N_2	38	36	37
CO_2/CH_4	161	156	156
O_2/N_2	5.7	5.8	6.7
N_2/CH_4	4.3	4.4	4.3

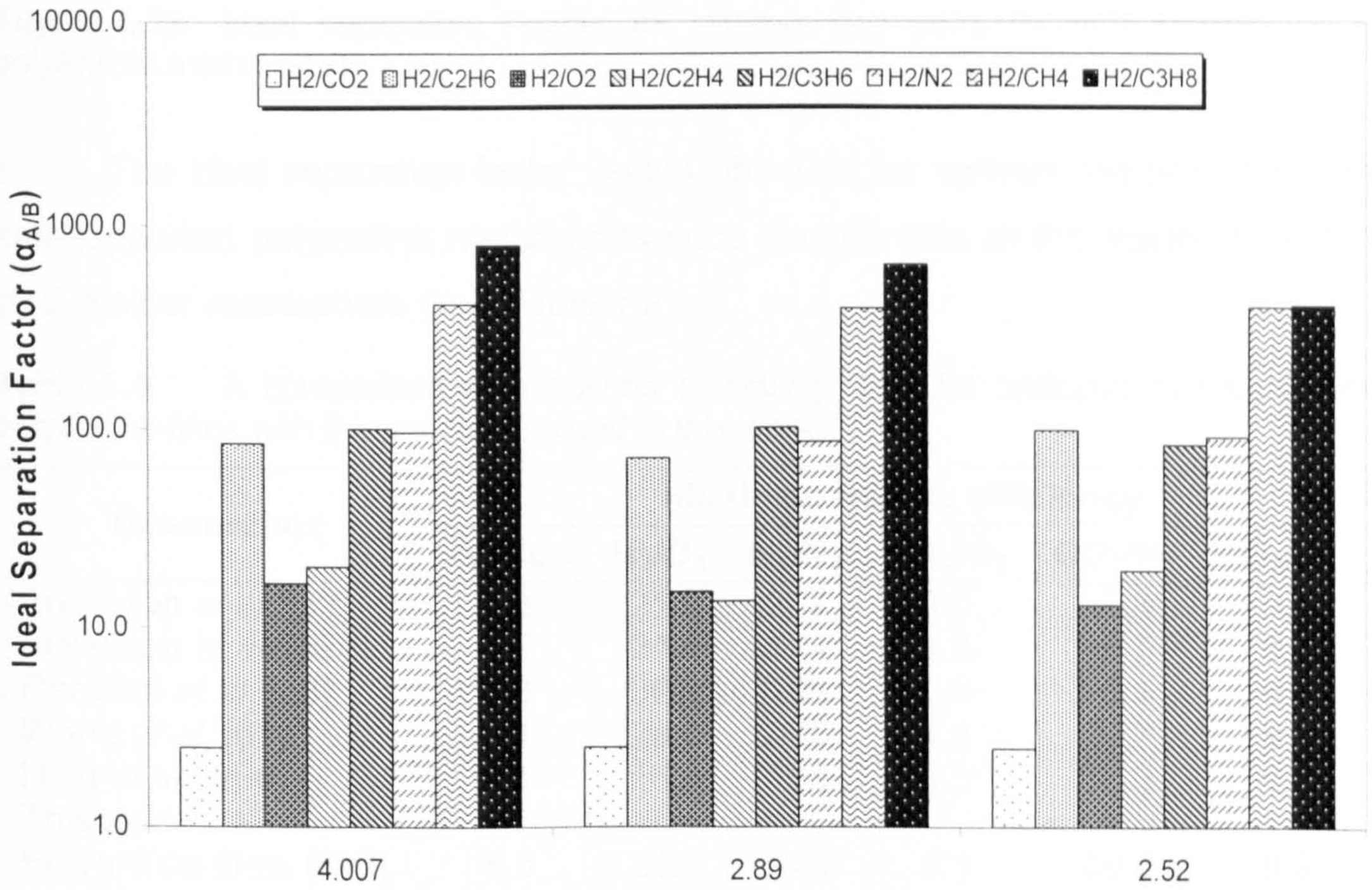

(a)

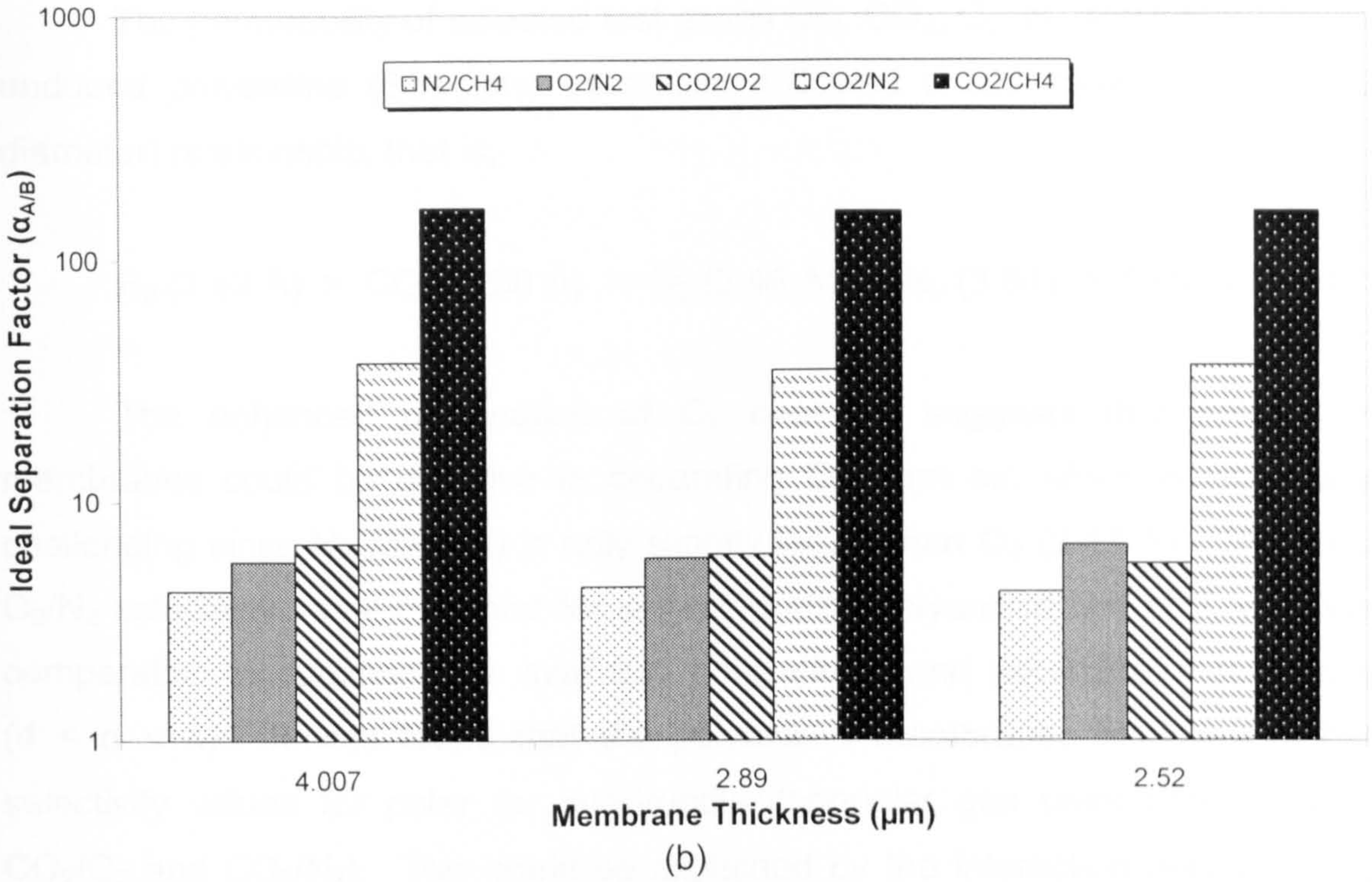

(b)

Figure 4. 28 Ideal separation factors for various gas pairs through self-supported polyaniline membranes.

The ideal separation factor values obtained for various gas pairs through self-supported polyaniline membranes were comparable to the values reported by the other researchers (see Table 4.9).

Table 4. 9 A comparison of published selectivity data for undoped self-supported polyaniline films with the results obtained in this work.

Researcher	Ideal separation efficiency					
	H_2/CO_2	H_2/O_2	H_2/N_2	CO_2/O_2	CO_2/N_2	O_2/N_2
Anderson *et al.* [51]	7.3	21.8	207	3.0	28.3	9.5
Anderson *et al.* [57]	5.0	24.6	164	4.9	32.7	6.7
Rebattet *et al.* [58]	7.8	30.7	195	3.9	25.1	6.4
Wang *et al.* [61]	6.1	29.0	265	4.8	38.7	9.1
Illing *et al.* [296]	5.1	16.8	164	3.3	32.3	9.8
This work: Polyaniline films [327] (film thickness: 6.9 μm)	*8.6*	*69.5*	*348*	*8.1*	*40.4*	*6.8*

The ideal (pure gas) selectivity ($\alpha_{A/B}$) values obtained for some of the gas pairs (i.e. H_2/N_2 (348), H_2/O_2 (69.5), H_2/CO_2 (8.6), CO_2/O_2 (8.1), CO_2/N_2 (40.4), H_2/C_3H_8 (757), CO_2/C_3H_8 (256)), in the case of undoped self supported polyaniline films, surpassed the selectivities of the majority of the conventional polymeric materials.

The permeability of selected test gases (H_2, CO_2, O_2, N_2 and CH_4) through undoped polyaniline (EB) films essentially followed a size dependent (kinetic diameter) relationship, that is;

H_2 (2.89 Å) > CO_2 (3.30 Å) > O_2 (3.46 Å) > N_2 (3.64) > CH_4 (3.80 Å)

The enhanced permeation of O_2 over N_2 suggests that polyaniline membranes could be effective in separating O_2 from air, which is especially challenging since N_2 (3.64 Å) is only slightly larger than O_2 (3.47 Å). The ideal O_2/N_2 selectivity value obtained for self-supported polyaniline film of 7, which is comparable to commercially available polysulfone and polyimide membranes ($4 < \alpha < 8$). It was found that the polyaniline membranes exhibited higher selectivity values for polar (or quadrupolar)/nonpolar gas pairs (e.g. H_2/CO_2, CO_2/O_2 and CO_2/N_2). This could be explained by the interaction between CO_2 (polar gas) and the polymeric matrix. In the FTIR spectra (see Figure 4.7) of various polyaniline batches prepared at various polymerisation reaction temperatures, it can be seen that the interaction between CO_2 and polyaniline polymer matrix increases with the polymerisation reaction temperature.

The results obtained during this work were reproducible for both self-supported polyaniline films and ultrathin polyaniline films supported on porous PVDF substrate.

4.4.2.1.2. Polyaniline/PVDF Composite Films for Hydrogen Purification

In addition to chemical resistance, thermal resistance and mechanical requirement, a high performance polymeric gas separation membrane needs to have both high separation efficiency and high productivity. The optimum gas permselective membrane is achieved when the membrane material combines high selectivity with high flux (gas transport rate (GTR)). These two basic properties are determined by the membrane material and the membrane thickness.

The use of polyaniline membranes in gas separation applications has been limited due to fairly low gas transport rates through self-supported polyaniline films. As the gas flux through a polymer membrane is inversely

proportional to the membrane thickness, the thickness of the selective polyaniline must be reduced to achieve sufficient gas transport rates. One way to reduce the membrane thickness is to prepare a composite membrane consisting of a thin film supported on a porous substrate. These membranes are classified on the basis of whether the support material controls the separation properties. If the selective polyaniline layer has a large number of defects, the transport behaviour of permeating gases through the polyaniline films can be described by Knudsen diffusion [329]. If the selective polyaniline layer is defect-free, the gas transport of composite membranes is similar to that in the dense self-supported polyaniline film, which can be described by the *solution-diffusion* mechanism.

A novel method was developed [327] and used (see Section 4.2.1; Chapter 3) to prepare an ultrathin polyaniline membrane supported on highly permeable PVDF substrate. A schematic cross-section of a polyaniline/PVDF composite membrane is shown in Figure 4.29.

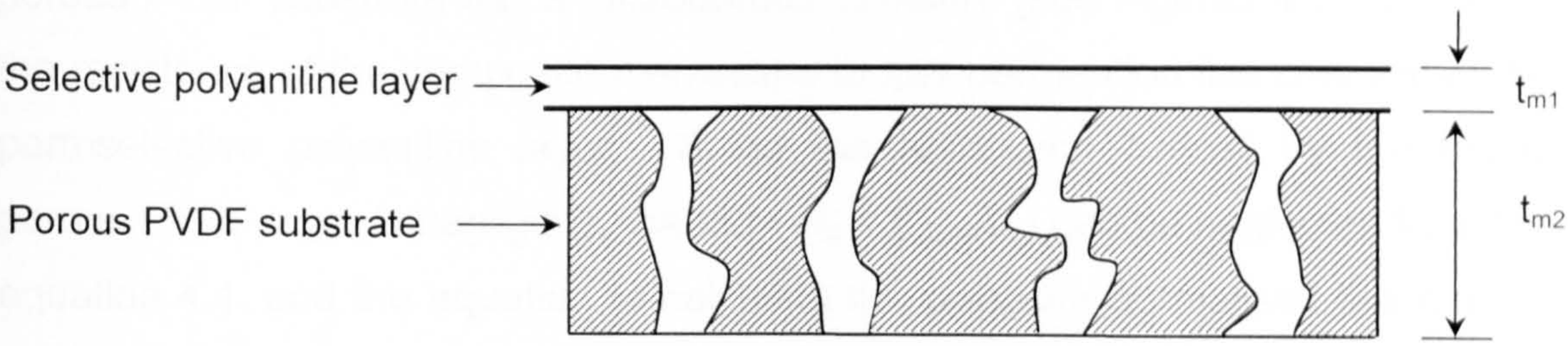

Figure 4. 29 Schematic cross section of a polyaniline/PVDF composite membrane.

Using the expression for the resistances in series, the equation to calculate the flux (GTR) through polyaniline/PVDF composite membrane can be written as;

$$J_{(A)} = \frac{\Delta p}{R_{total}} \qquad (4.3)$$

where,

$$R_{total} = R_1 + R_2 = \frac{t_{m1}}{P_{1(A)}} + \frac{t_{m2}}{P_{2(A)}} \qquad (4.4)$$

where Δp is the pressure difference across the membrane, R_{total} is the total resistance offered by the selective polyaniline layer (R_1) and porous PVDF layer

(R_2), t_{m1} and t_{m2} are the thicknesses of the selective polyaniline layer and porous PVDF layer, respectively. $P_{1(A)}$ and $P_{2(A)}$ are the permeability coefficients of the selective polyaniline layer and porous PVDF layer of gas A, respectively.

The ideal selectivity of the membrane for gas A over gas B, $\alpha_{A/B}$, can be calculated from equation 2.30. However, the equation to calculate the ideal selectivity of a composite membrane can be modified and written from equation 2.30 as;

$$\alpha_{A/B} = \frac{P_{1(A)}/t_{m1} + P_{2(A)}/t_{m2}}{P_{1(B)}/t_{m1} + P_{2(B)}/t_{m2}} \qquad (4.5)$$

It is apparent from the expression that the ideal selectivity of the composite membrane is determined by both layers of composite structure (selective polyaniline layer and porous PVDF substrate). However, the highly porous PVDF substrate has a microporous structure (see Figures 4.17 and 4.18) the resistance of the composite membrane to gas permeation lies only within the permselective polyaniline layer. Since the resistance offered by the highly porous PVDF layer is negligible, the term $R_2 = P_{2(A)}/t_{m2}$ can be neglected from the equation 4.4, and the equation to calculate the pressure normalised flux can be rewritten as;

$$\left(\frac{J_{(A)}}{\Delta p}\right) = \left(\frac{P_{1(A)}}{t_{m1}}\right) \qquad (4.6)$$

and the equation to calculate the ideal (pure gas) selectivity becomes;

$$\alpha_{A/B} = \frac{P_{1(A)}/t_{m1}}{P_{1(B)}/t_{m1}} \qquad (4.7)$$

Henceforth, the above expressions (equations 4.6 and 4.7) were used to calculate permeance and ideal separation efficiencies of various penetrant gases for undoped ultrathin polyaniline membranes.

As discussed earlier, the bursting pressure value for the ultrathin polyaniline film (selective polyaniline film thickness = 500 nm) was calculated to be 0.6 bar (0.06 MPa), assuming the linear relationship between calculated

bursting pressure (from the stress-strain curve) and polyaniline film thickness. A test was performed to evaluate the bursting pressure of the polyaniline/PVDF composite film (total film thickness = 60 μm). The bursting pressure was measured by mounting the polyaniline/PVDF composite membrane in the permeation cell and gradually pressuring the upstream section of the permeation cell. The bursting pressure measured for the ultrathin polyaniline film to be was 4.3 bar (± 0.2 bar), which shows the PVDF support layer increased the mechanical strength of the composite film. Hence, to prevent the polyaniline/PVDF composite film from bursting during the gas permeation experiment, the experiments were conducted, using the pure gas permeation method (see Section 5.3.2.4; Chapter 3), in the feed pressure range of 0.2 to 1.5 bar (0.02 to 0.15 MPa) and room temperature (21 ± 2 C).

The ultrathin polyaniline films with the selective layer thicknesses between 0.4 and 1.37 μm were analysed with various pure gases – H_2, CO_2, O_2, N_2, CH_4, C_2H_4, C_2H_6, C_3H_6 and C_3H_8. The polyaniline/PVDF composite membranes were dried overnight in a vacuum oven at 60 C, and a single gas permeation experiment was conducted with the method described in Section 5.3.2.4 (see Chapter 3).

The pressure normalised flux values (in GPU) and permeabilities (in Barrer, bracketed) of various gases through undoped ultrathin polyaniline membranes (selective polyaniline layer thickness between 0.4 and 1.37 μm) are summarised in Table 4.10.

Table 4. 10 Pure gas permeance (in GPU) and permeability (in Barrer, bracketed) of various gases through undoped ultrathin polyaniline membranes supported on PVDF substrate.

Membrane Thickness (μm)	Permeance (GPU*) and Permeability (Barrer**, bracketed)								
	H_2	CO_2	O_2	N_2	CH_4	C_2H_4	C_2H_6	C_3H_6	C_3H_8
1.37	3.635 (4.98)	1.058 (1.45)	0.223 (0.31)	0.035 (0.048)	0.0093 (0.013)	0.286 (0.39)	0.086 (0.12)	0.044 (0.059)	0.0067 (0.009)
0.63	25.99 (16.4)	4.916 (3.10)	1.575 (0.99)	0.273 (0.172)	0.0796 (0.050)	1.474 (0.93)	0.302 (0.19)	0.519 (0.327)	0.1081 (0.068)
0.448	1315 (590)	433.2 (194)	132.4 (59.4)	29.59 (13.26)	4.343 (1.946)	111.1 (49.7)	30.25 (13.6)	18.10 (8.11)	4.29 (1.922)
0.4	1531 (613)	433.3 (173)	105 (42.0)	23.97 (9.589)	6.683 (2.673)	159.1 (63.6)	46.60 (18.5)	25.97 (10.39)	4.70 (1.879)

* 1 GPU = 1 x 10^6 $cm^3_{(STP)}/cm^2 \cdot s \cdot cmHg$

** 1 Barrer = 1 x 10^{-10} $cm^3_{(STP)} \cdot cm/cm^2 \cdot s \cdot cmHg$

In Figure 4.30 the permeance (pressure normalised flux) values of various gases through polyaniline/PVDF composite film are plotted.

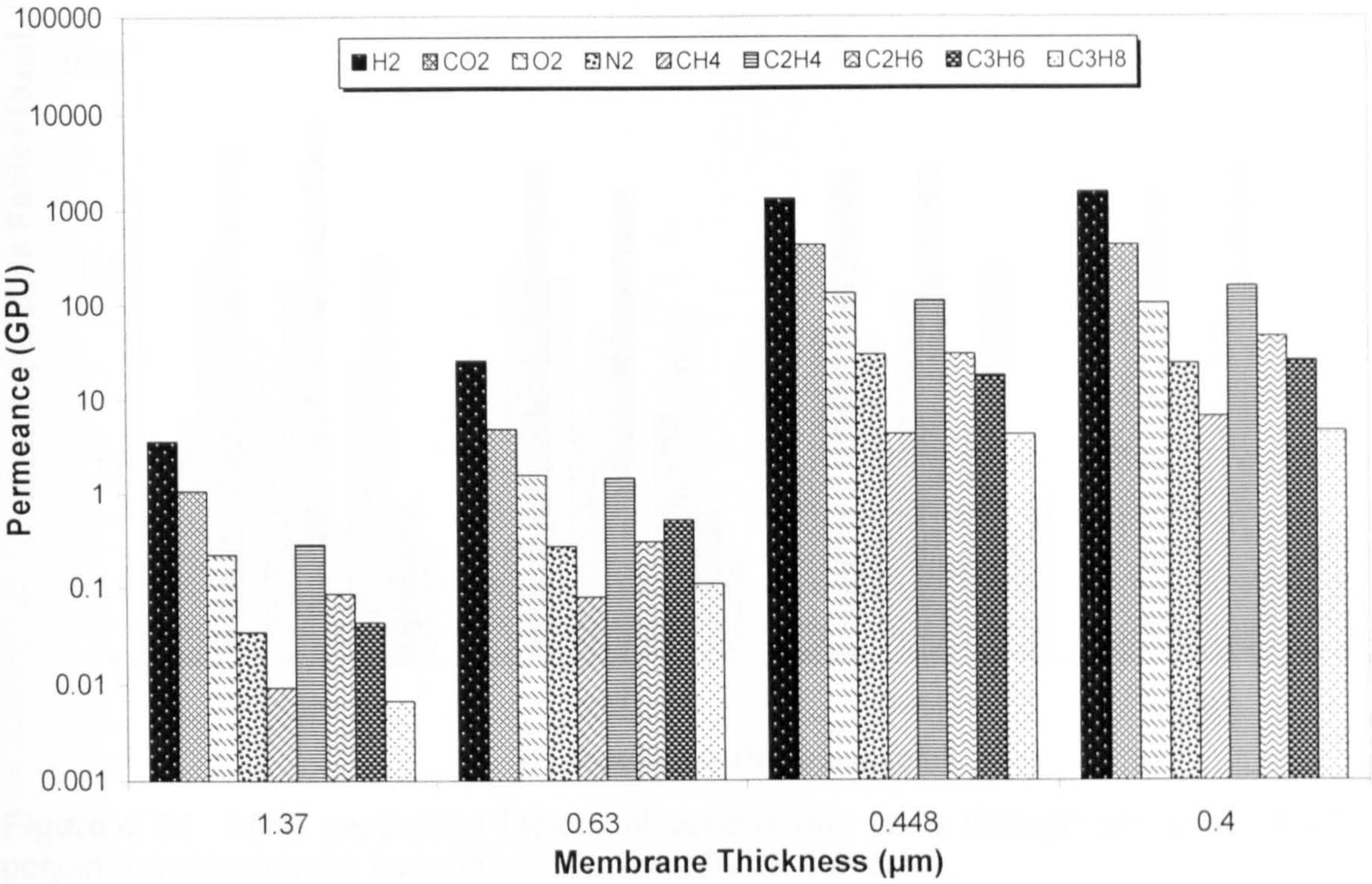

Figure 4. 30 The permeance of various permeating gases through undoped ultrathin polyaniline membranes supported on PVDF substrate.

The ideal separation efficiencies of various gas pairs for undoped ultrathin polyaniline membranes, calculated using equation 4.7, are summarised in Table 4.11 and plotted in Figure 4.31.

Table 4. 11 Effect of polyaniline film thickness on ideal selectivities of various gas pairs through ultrathin polyaniline membranes.

	Ideal Separation Efficiency ($\alpha_{A/B}$)			
	1.371 μm	**0.63 μm**	**0.448 μm**	**0.4 μm**
H_2/CO_2	3.43	5.29	3.03	3.53
H_2/O_2	16.3	16.5	9.93	14.6
H_2/N_2	104	95.2	45.1	63.9
H_2/CH_4	392	326	302	229
H_2/C_2H_4	41.9	85.9	43.5	32.9
H_2/C_2H_6	12.7	17.6	11.9	9.63
H_2/C_3H_6	83.4	50.1	72.7	58.9
H_2/C_3H_8	540	240	306	326
CO_2/O_2	4.73	3.12	3.27	4.13
CO_2/N_2	30.2	18.1	14.6	18.1
CO_2/CH_4	114	61.7	99.7	64.8
O_2/N_2	6.37	5.76	4.47	4.38
N_2/CH_4	3.78	3.43	6.81	3.59

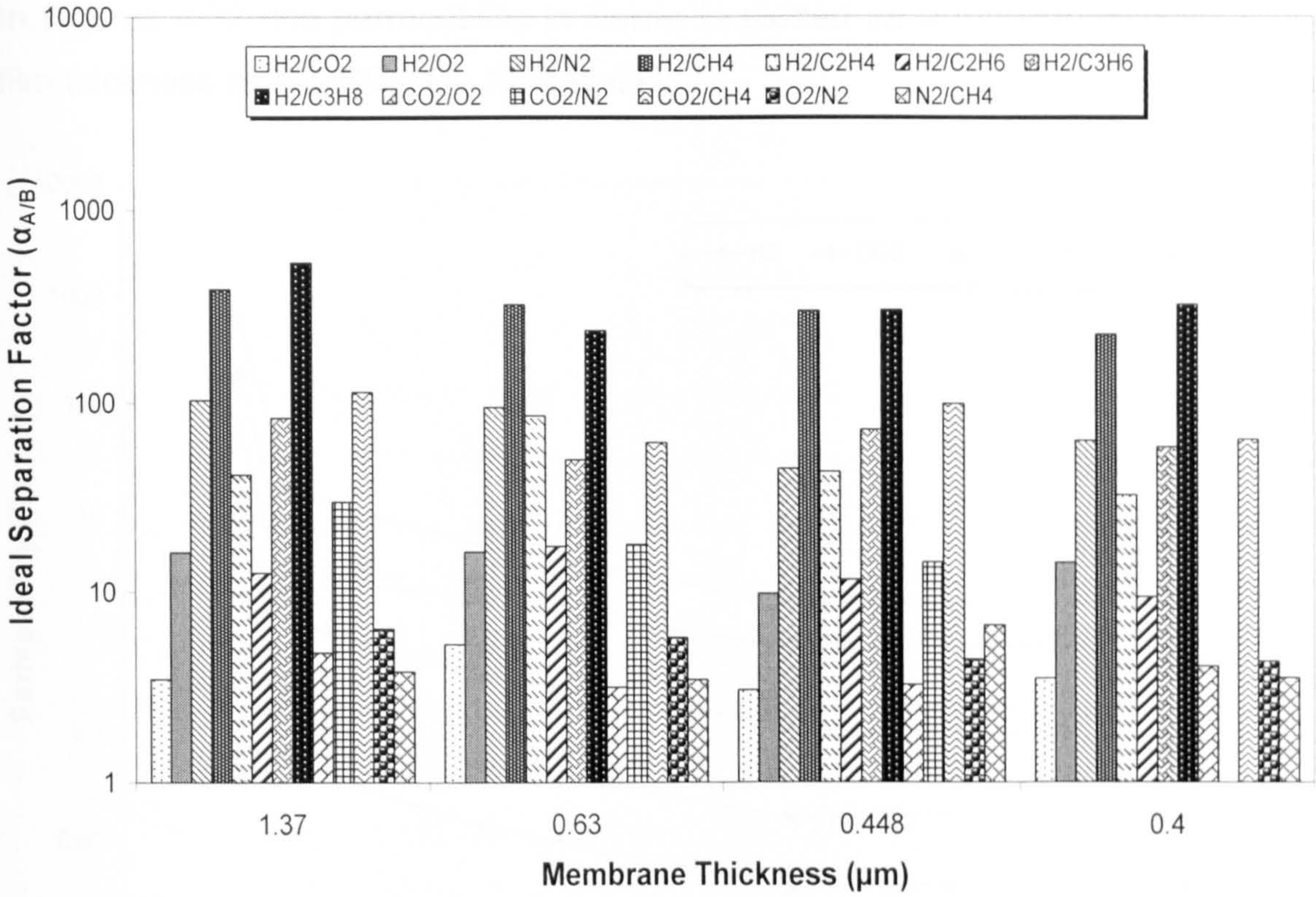

Figure 4. 31 Ideal separation factors of various gas pairs through undoped ultrathin polyaniline membranes supported on porous PVDF substrate.

In Table 4.12, the calculated ideal separation efficiency values for polyaniline/PVDF composite membranes are compared with the data published by Wang *et al.* [62]

Table 4. 12 A comparison of published ideal selectivity data for ultrathin polyaniline films supported on porous substrate with the results obtained in this work.

Researcher	**Ideal separation factor ($\alpha_{A/B}$)**					
	H_2/CO_2	**H_2/O_2**	**H_2/N_2**	**CO_2/O_2**	**CO_2/N_2**	**O_2/N_2**
Wang *et al.* (film thickness: 0.178 μm)	2.3	9.9	75.2	4.3	32.7	5.6
This work: PAni/PVDF[a] composite film (film thickness: 0.63 μm)	5.3	16.5	95.2	3.1	18.0	5.8

[a] polyaniline nano-film membrane supported on porous PVDF substrate.

It is apparent from Table 4.12 that the selectivity values obtained for ultrathin polyaniline films were similar to that of obtained by Wang *et al.* [62]. Polyaniline films with a selective polyaniline layer thickness below 1 μm showed different permeation behaviours than intermediate or thick polyaniline films.

In Figures 4.32, the permeability in Barrer is plotted as a function of polyaniline film thickness for H_2, CO_2, O_2, N_2 and CH_4.

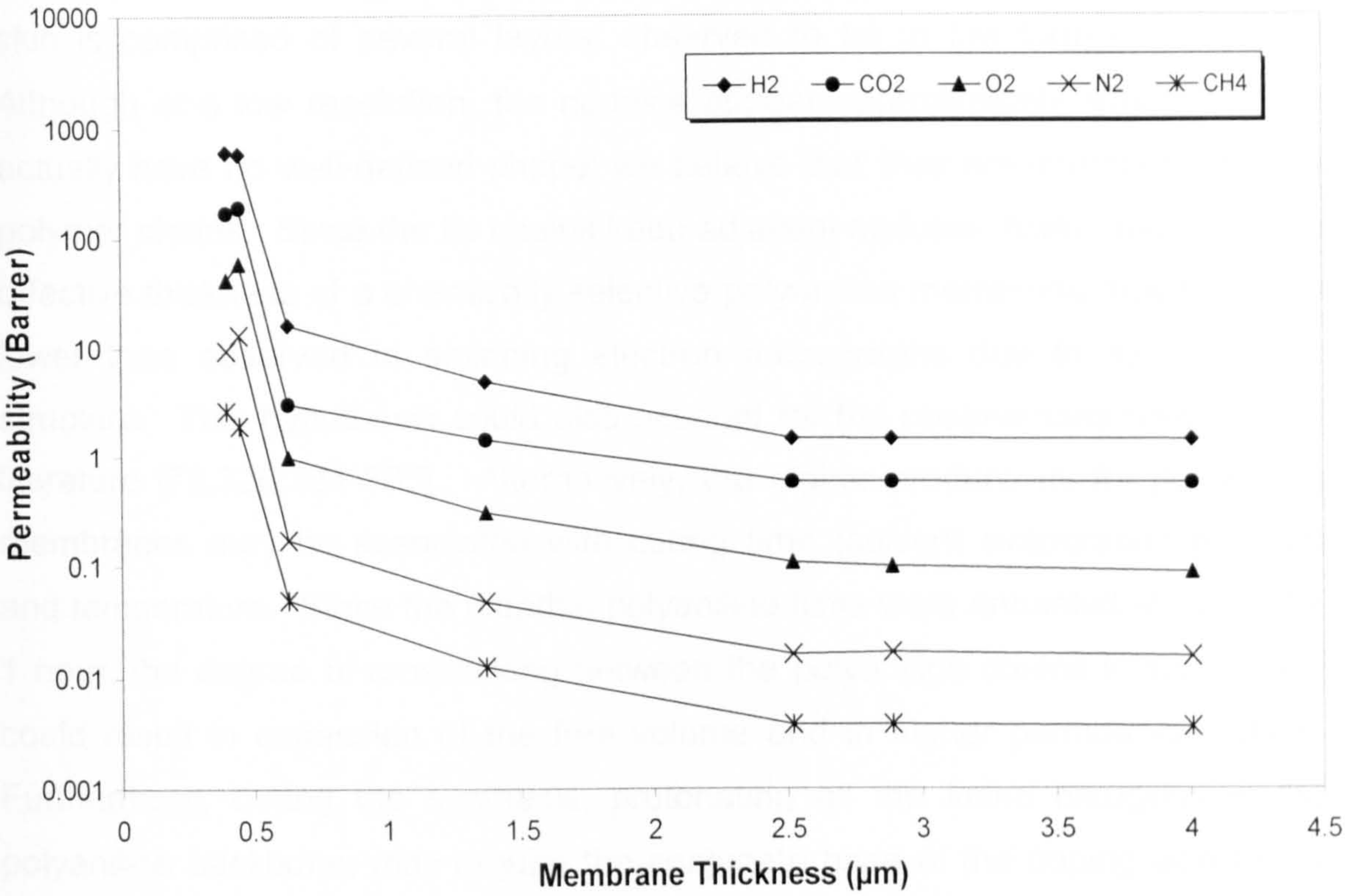

Figure 4. 32 Permeability of various gases (H_2, CO_2, O_2, N_2 and CH_4) through polyaniline membranes in Barrers.

It is apparent from the Figure 4.32 that the thickness of the selective polyaniline membrane affects the permeability of the permeating gases through polyaniline films. The permeability values obtained for all permeating gases were significantly higher in the case of ultrathin polyaniline membranes supported on a porous PVDF substrate. The permeability increased almost linearly with decreasing polyaniline film thickness. The increase in permeability, which was contrary to previously widely held views, of various gases for ultrathin polyaniline membranes can be explained by chemical structure of polyaniline (see Figure 4.33).

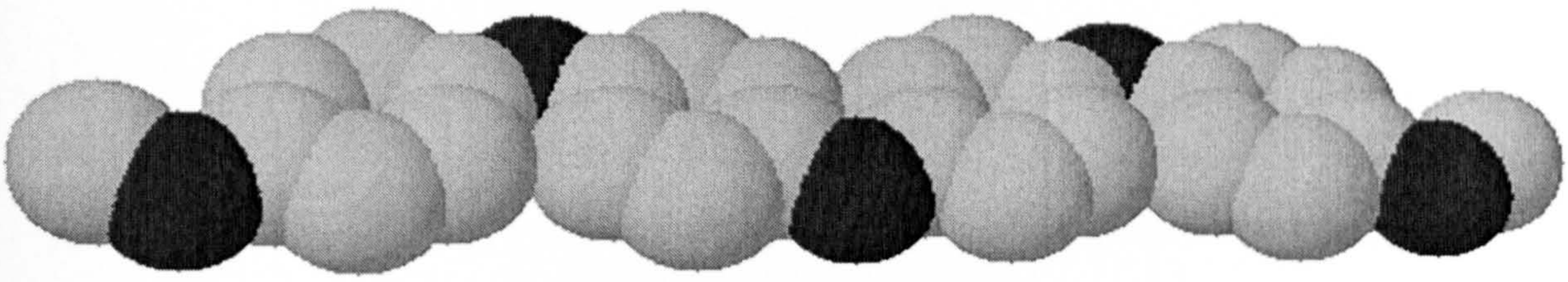

Figure 4. 33 3 – D structure of emeraldine base form of polyaniline.

The dense skin morphology depicted is based on photomicrographs of the actual self-supported polyaniline films as well as of ultrathin polyaniline membranes supported on a porous PVDF substrate. It is thought that the dense skin is comprised of several layers, observed to be in the form of *"nodules"*. Although at a low resolution, the nodules appear approximately spherical, they actually have no well-defined shape; we believe that they are interconnected by polymer chains. Since the tie chains keep adjacent nodules *"fused"* together, the effective thickness of a chemically selective polyaniline membrane may be much lower than observed in scanning electron micrographs due to its molecular structure. This hypothesis could also account for the observations noted in the literature [78,326,331-335]. Alternatively, the higher productivity for polyaniline membranes may be associated with curing time (solvent evaporation method) and temperature. Since the ultrathin polyaniline films were annealed at 120 C for 1 hour, the degree of crosslinking between the polyaniline chains is less, which could result in expansion of the free volume and in higher permeance values. Furthermore, during the synthesis, protonating all the imine nitrogens in the polyaniline backbone, may require the conjugate base of the doping acid to act as a counterion to maintain electroneutrality in the salt form of polyaniline. The close association of this counterion with the polymer backbone means that the polymer microstructure must distort to accommodate the extra mass. This distortion remains after the removal of the counterion with ammonium hydroxide and is likely to an increase in free volume in the film that results in greater permeability of gases over the polyaniline membranes.

The effect of polyaniline film thickness on the pure gas selectivity of various gas pairs was examined. In Figures 4.34 and 4.35, the ideal selectivities for various gas pairs through polyaniline membranes are plotted as a function of selective polyaniline layer thickness.

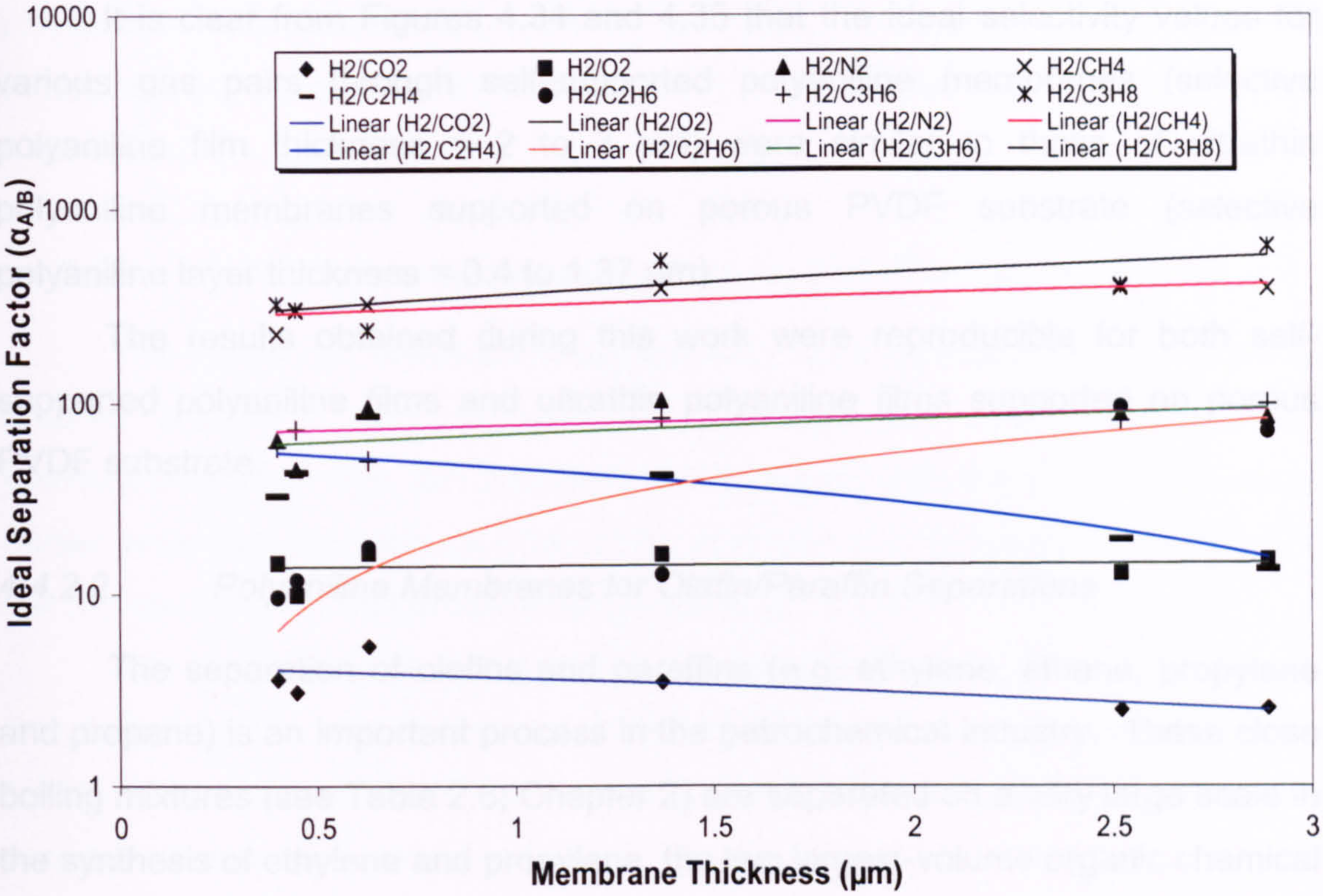

Figure 4. 34 Effect of polyaniline film thickness on ideal separation factor values of various gas pairs for polyaniline membranes.

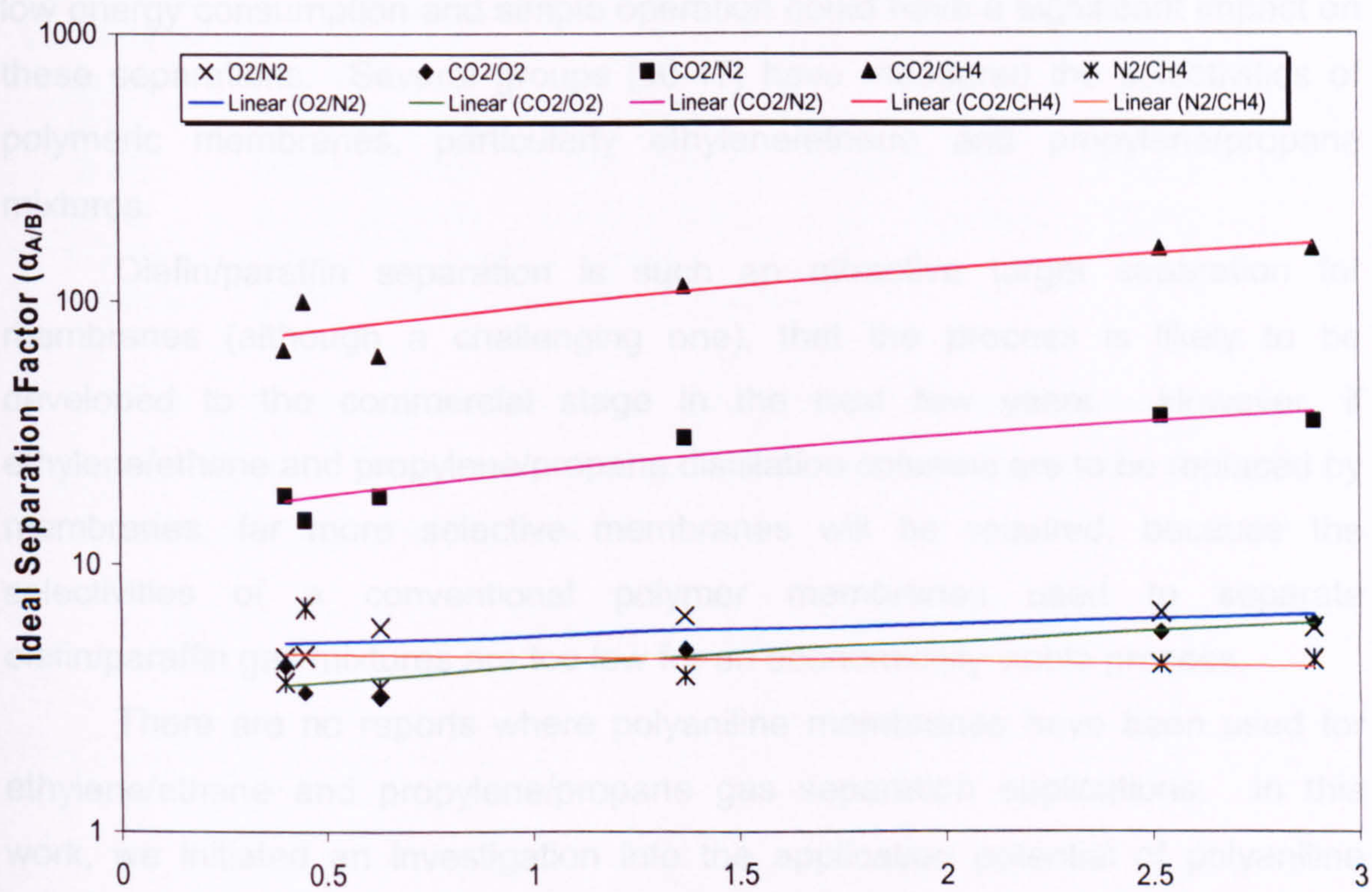

Figure 4. 35 Effect of polyaniline film thickness on ideal separation factor values of various gas pairs for polyaniline membranes.

It is clear from Figures 4.34 and 4.35 that the ideal selectivity values for various gas pairs through self-supported polyaniline membranes (selective polyaniline film thickness = 2 to 3 μm) were similar to those of ultrathin polyaniline membranes supported on porous PVDF substrate (selective polyaniline layer thickness = 0.4 to 1.37 μm).

The results obtained during this work were reproducible for both self-supported polyaniline films and ultrathin polyaniline films supported on porous PVDF substrate.

4.4.2.2. Polyaniline Membranes for Olefin/Paraffin Separations

The separation of olefins and paraffins (e.g. ethylene, ethane, propylene and propane) is an important process in the petrochemical industry. These close boiling mixtures (see Table 2.6; Chapter 2) are separated on a very large scale in the synthesis of ethylene and propylene, the two largest-volume organic chemical feed stocks. Since the mixtures are close-boiling, large towers and high reflux ratios are required to achieve good separation. Membrane separations with their low energy consumption and simple operation could have a significant impact on these separations. Several groups [30-47] have measured the selectivities of polymeric membranes, particularly ethylene/ethane and propylene/propane mixtures.

Olefin/paraffin separation is such an attractive target separation for membranes (although a challenging one), that the process is likely to be developed to the commercial stage in the next few years. However, if ethylene/ethane and propylene/propane distillation columns are to be replaced by membranes, far more selective membranes will be required, because the selectivities of a conventional polymer membranes used to separate olefin/paraffin gas mixtures are too low for an economically viable process.

There are no reports where polyaniline membranes have been used for ethylene/ethane and propylene/propane gas separation applications. In this work, we initiated an investigation into the application potential of polyaniline membranes for these separations. In the following sub-sections, the gas transport properties of self-supported polyaniline films (film thickness = 2 to 4 μm) as well as ultrathin polyaniline films supported on PVDF substrate (selective

polyaniline layer thickness = 0.4 to 0.8 μm), in respect to olefin/paraffin (ethylene/ethane, and propylene/propane) separations, are presented and discussed.

4.4.2.2.1. Self-supported Polyaniline Films for Olefin/Paraffins Separations

The single gas permeation experiments were conducted using ethylene, ethane, propylene and propane for self-supported undoped polyaniline membranes (polyaniline film thickness = 2 to 4 μm) with the method discussed earlier in Section 5.3.2.4 (see Chapter 3), at a feed side pressure between 1 to 4 bar (0.1 to 0.4 MPa) and ambient temperature (21 ± 2 C).

The permeance (in GPU) and permeability (in Barrers, bracketed) values, calculated at room temperature, i.e. 21 ± 2 C and upstream pressure of 4 bar (0.4 MPa), of ethylene, ethane, propylene and propane for self-supported polyaniline membranes are summarised in Table 4.13.

Table 4. 13 Permeance (in GPU) and permeability (in Barrers, bracketed) of ethylene, ethane, propylene and propane through undoped self-supported polyaniline membranes.

Membrane Thickness	**Productivity (GPU*) and Permeability (Barrers**)**			
(μm)	**C_2H_4**	**C_2H_6**	**C_3H_6**	**C_3H_8**
4.01	0.017 (0.072)	0.004 (0.017)	0.04 (0.0146)	0.0004 (0.0018)
2.89	0.037 (0.108)	0.007 (0.021)	0.005 (0.0148)	0.0008 (0.0023)
2.52	0.030 (0.076)	0.006 (0.016)	0.007 (0.0183)	0.0009 (0.0037)

* 1 GPU = 1×10^{6} $cm^3_{(STP)}/cm^2 \cdot s \cdot cmHg$

** 1 Barrer = 1×10^{-10} $cm^3_{(STP)} \cdot cm/cm^2 \cdot s \cdot cmHg$

The pressure normalised flux (productivity or permeance) values of ethylene, ethane, propylene and propane for self-supported polyaniline membranes are plotted in Figure 4.36.

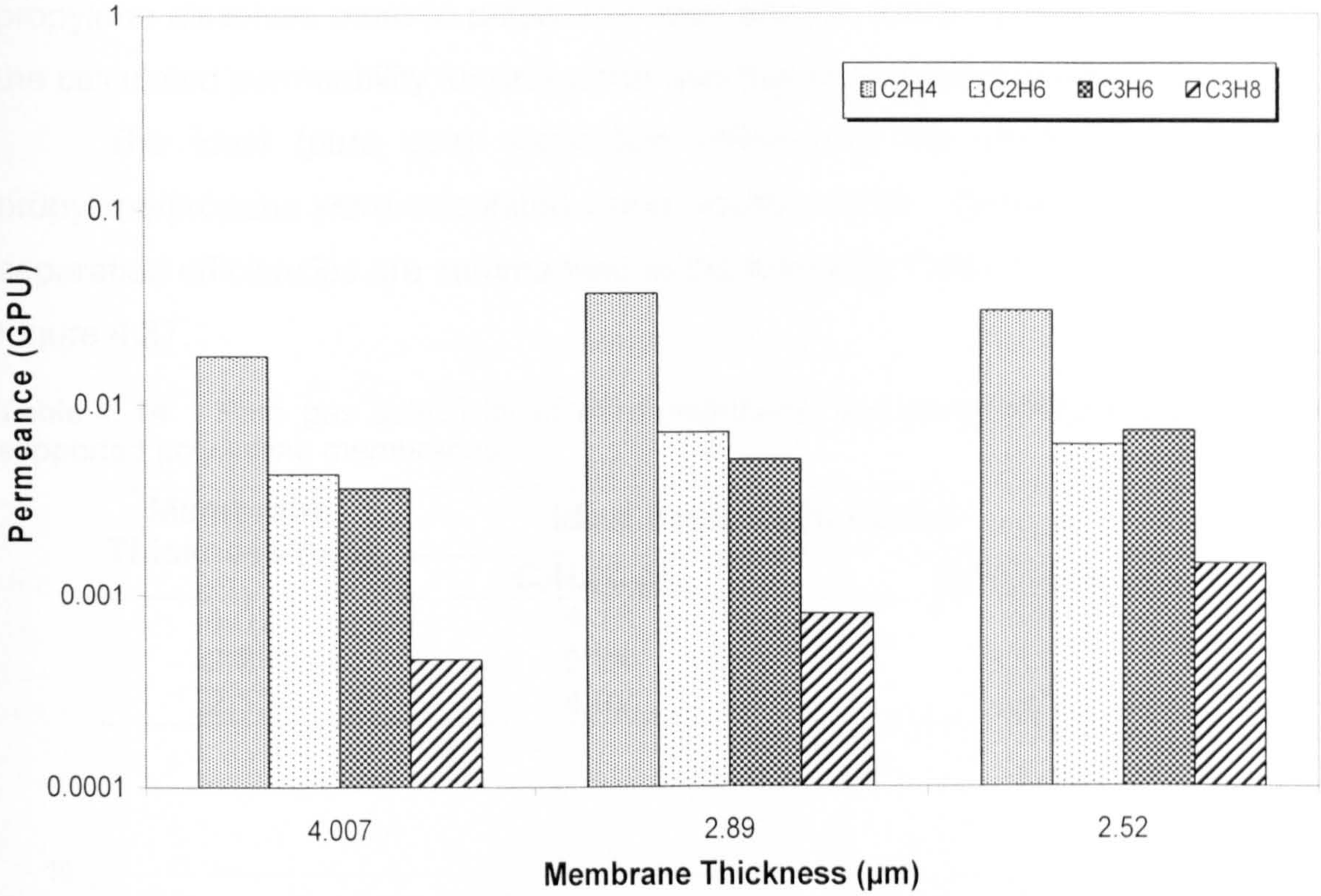

Figure 4. 36 Pressure normalised flux values of ethylene, ethane, propylene and propane through undoped self-supported polyaniline membranes.

As discussed earlier, the permeability of selected test gases through undoped polyaniline (EB) films essentially followed a size dependent (kinetic diameter) relationship. However, the exceptions from this trend were C_2H_4 (3.9 Å), C_2H_6 (4.0 Å), C_3H_6 (4.4 Å) and C_3H_8 (3.96 Å), since their permeability values were higher than CH_4 (3.80 Å), even though the kinetic diameters of C_2H_4, C_2H_6, C_3H_6 and C_3H_8 are larger molecules than CH_4. According to the kinetic diameters of the permeating gases (ethylene, ethane, propylene and propane) the permeability order should have been:

$$C_2H_4\ (3.90\ Å) > C_3H_8\ (3.96\ Å) > C_2H_6\ (4.0\ Å) > C_3H_6\ (4.40\ Å)$$

and the permeability order through polyaniline membranes observed to be was:

$$C_2H_4\ (3.90\ Å) > C_3H_6\ (4.40\ Å) > C_2H_6\ (4.0\ Å) > C_3H_8\ (3.96\ Å)$$

This was, we believe, because of a relatively higher solubility of ethylene and propylene in the polyaniline membranes than ethane and propane. The

propylene dissolves more in polyaniline than ethane and propane, and therefore the calculated permeability for propylene was higher than ethane and propane.

The ideal (pure gas) separation efficiencies for ethylene/ethane and propylene/propane were calculated using equation 2.30. These calculated ideal separation efficiencies are summarised in the following Table 4.14, and plotted in Figure 4.37.

Table 4. 14 Pure gas selectivity of ethylene/ethane and propylene/propane for self-supported polyaniline membranes.

Membrane Thickness (μm)	Ideal Separation Factor ($\alpha_{A/B}$)	
	C_2H_4/C_2H_6	C_3H_6/C_3H_8
4.01	4.13	7.98
2.89	5.24	6.39
2.52	4.92	4.93

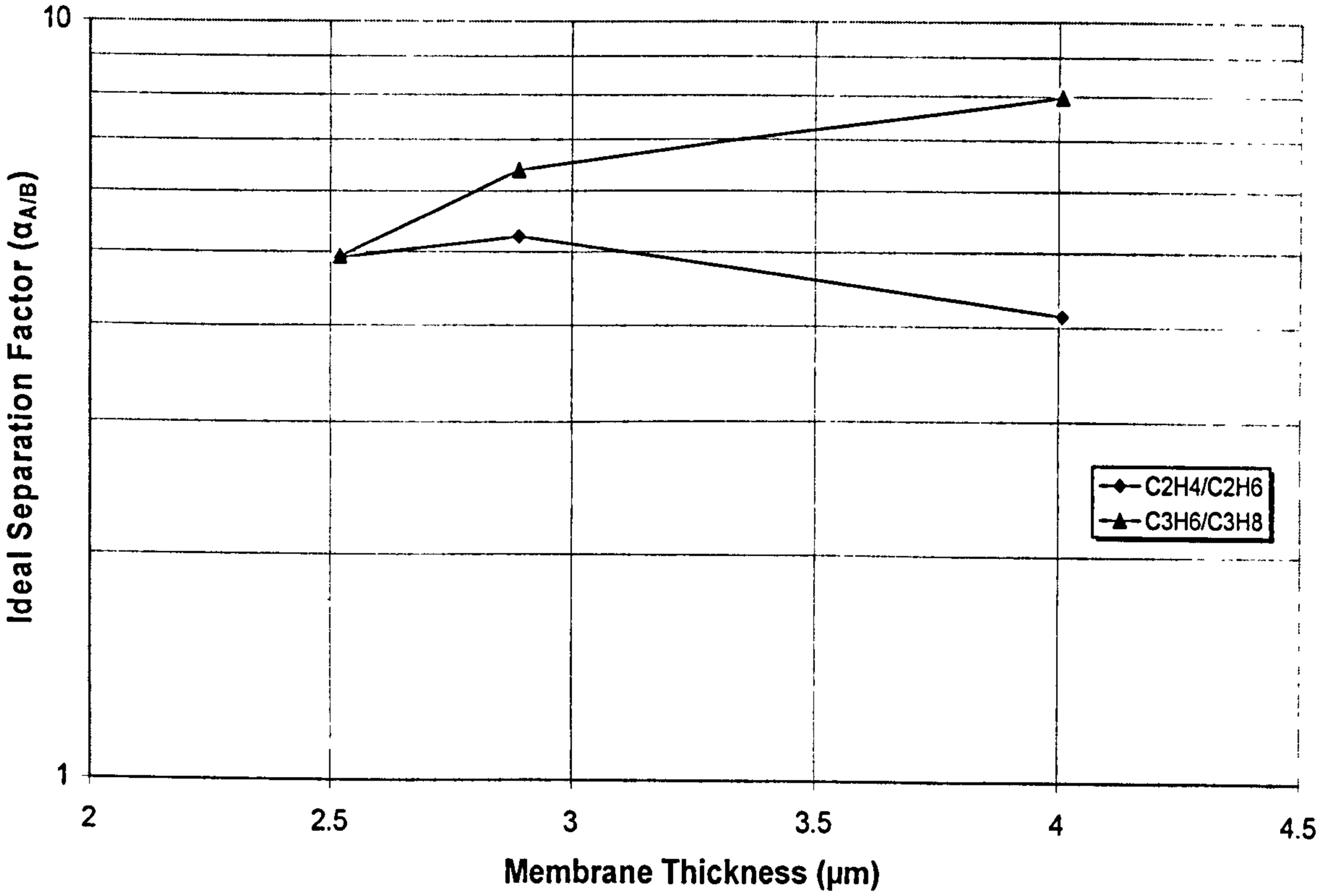

Figure 4. 37 Ideal separation factors for ethylene/ethane and propylene/propane through self-supported polyaniline films.

The pure gas selectivity values for various gas pairs such as CO_2/C_2H_4, CO_2/C_2H_6, CO_2/C_3H_6, CO_2/C_3H_8, C_2H_4/CH_4, C_2H_6/CH_4, C_3H_6/CH_4, C_3H_8/CH_4, C_2H_4/N_2, C_2H_6/N_2, C_3H_6/N_2, and N_2/C_3H_8 were also calculated using equation 2.30. These calculated ideal selectivities are summarised in Table 4.15, and plotted in Figure 4.38.

Table 4. 15 Effect of polyaniline film thickness on ideal (pure gas) separation factors of various gas pairs through self-supported polyaniline membranes.

	Ideal Separation Factor ($\alpha_{A/B}$)		
	4.00 µm	**2.89 µm**	**2.52 µm**
CO_2/C_2H_4	2.25	5.51	7.52
CO_2/C_2H_6	9.31	28.8	36.97
CO_2/C_3H_6	11.1	40.14	31.3
CO_2/C_3H_8	87.9	256	154
C_2H_4/CH_4	27.5	28.4	24.6
C_2H_6/CH_4	6.65	5.42	5.01
C_3H_6/CH_4	5.62	3.89	5.90
C_3H_8/CH_4	1.42	1.64	0.84
C_2H_4/N_2	17.9	6.14	4.76
C_2H_6/N_2	4.35	1.17	0.97
C_3H_6/N_2	3.67	0.84	1.14
N_2/C_3H_8	2.17	7.61	4.31

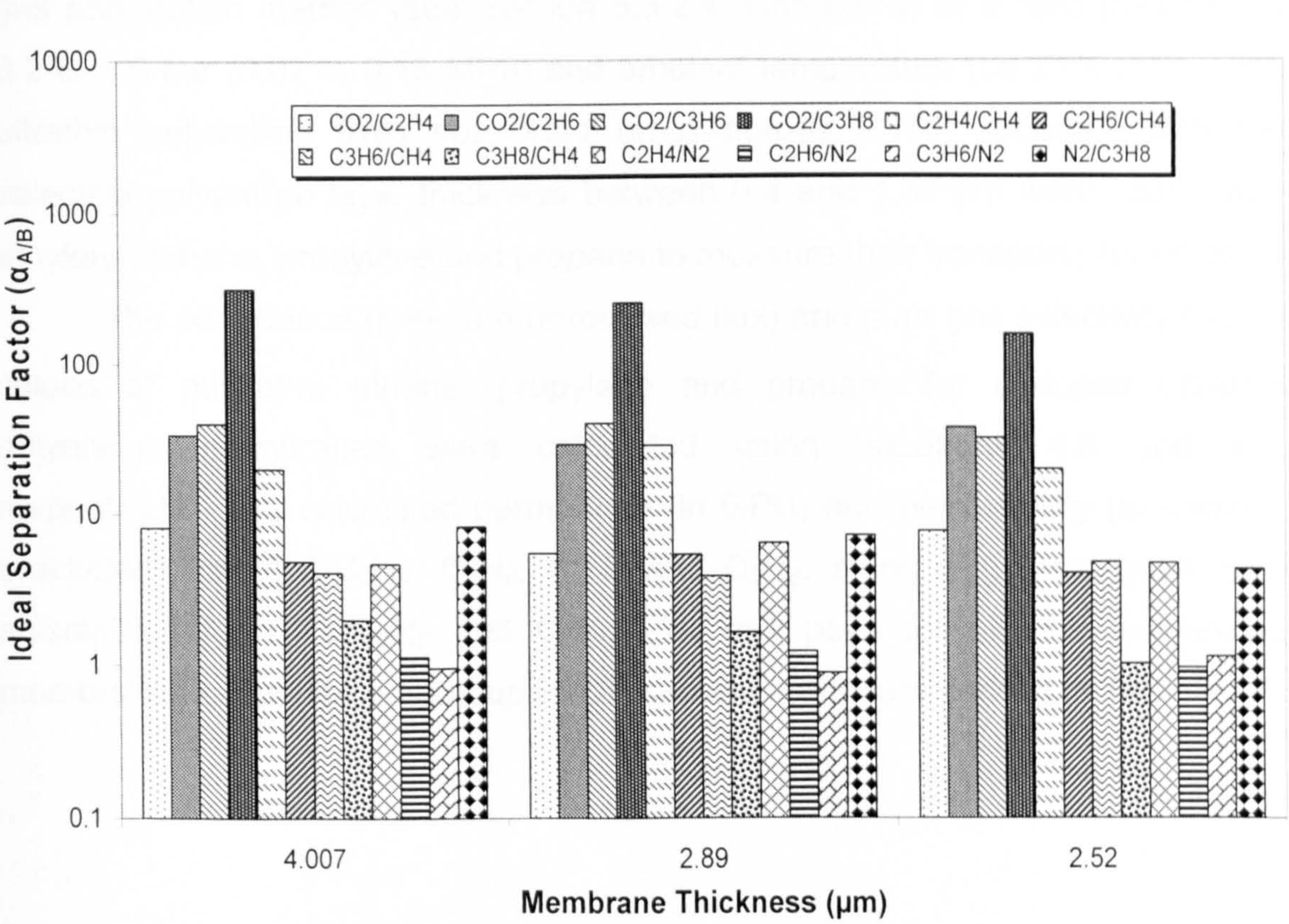

Figure 4. 38 Ideal separation factors for various gas pairs as a function of self-supported polyaniline membrane thickness.

Table 4.16 shows a comparison of published selectivity data for hydrocarbons in the literature with the data obtained for self-supported polyaniline films in this work.

Table 4. 16 A comparison of published selectivity data for hydrocarbons with current work.

Ideal Selectivity ($\alpha_{A/B}$)	Researcher		
	Pinnau *et al.* (Hyflon®) [200]	**Krol *et al.* (Polyimide) [184]**	**This work (Polyaniline Films*)**
H_2/C_3H_6	100	-----	*101*
H_2/C_3H_8	110	-----	*757*
C_3H_6/C_3H_8	1.10	21.0	*7.98*
CO_2/C_3H_6	-----	-----	*40.1*
CO_2/C_3H_8	8.70	-----	*256*
C_3H_6/N_2	13.0	-----	*3.67*
N_2/C_3H_8	-----	-----	*7.61*

* Undoped self-supported polyaniline films

4.4.2.2.2. Polyaniline/PVDF composite Films for Olefin/Paraffin Separations

The single gas permeation measurements were conducted using the pure gas permeation method (see Section 5.3.2.4; Chapter 3) at a feed pressure of 0.2 to 1.5 bar (0.02 to 0.15 MPa) and ambient temperature (i.e 21 ± 2 C). The ultrathin polyaniline films supported on a porous PVDF substrate with the selective polyaniline layer thickness between 0.4 and 1.37 μm were tested with ethylene, ethane, propylene and propane to measure their transport properties.

The permeance (pressure normalised flux) and pure gas selectivity ($\alpha_{A/B}$) values of ethylene, ethane, propylene and propane for undoped ultrathin polyaniline membranes were calculated using equations 4.6 and 4.7, respectively. The calculated permeance (in GPU) and permeability (in Barrers, bracketed) data for C_2H_4, C_2H_6, C_3H_6 and C_3H_8, along with ideal (pure gas) selectivities for C_2H_4/C_2H_6 and C_3H_6/C_3H_8 gas pairs for ultrathin polyaniline membranes supported on porous PVDF substrate are summarised in Table 4.17.

Table 4. 17 Permeance (in GPU) and permeability (in Barrers, bracketed) and pure gas selectivity of olefins (ethylene, propylene) and paraffins (ethane, propane).

Membrane Thickness (μm)	Permeance (GPU*) and Permeability (Barrers**)				Pure gas Selectivity ($\alpha_{A/B}$)	
	C_2H_4	C_2H_6	C_3H_6	C_3H_8	C_2H_4/C_2H_6	C_3H_6/C_3H_8
1.37	0.286 (0.392)	0.086 (0.119)	0.044 (0.059)	0.0067 (0.0092)	3.30	6.48
0.63	1.474 (0.929)	0.302 (0.191)	0.519 (0.327)	0.1081 (0.0681)	4.88	4.80
0.448	111.1 (49.73)	30.25 (13.55)	18.10 (8.113)	4.290 (1.922)	3.67	4.22
0.4	159.1 (63.65)	46.60 (18.64)	25.97 (10.39)	4.698 (1.879)	3.41	5.53

* 1 GPU = 1 x 10^6 $cm^3_{(STP)}$ /cm^2 · s · cmHg

** 1 Barrer = 1 x 10^{-10} $cm^3_{(STP)}$ · cm/cm^2 · s · cmHg

In Figures 4.39 and 4.40, the permeance (in GPU) of ethylene, ethane, propylene and propane and ideal separation efficiency of C_2H_4/C_2H_6 and C_3H_6/C_3H_8 gas pairs for polyaniline/PVDF composite membranes (selective polyaniline layer thickness between 0.4 and 1.37 μm) are plotted, respectively.

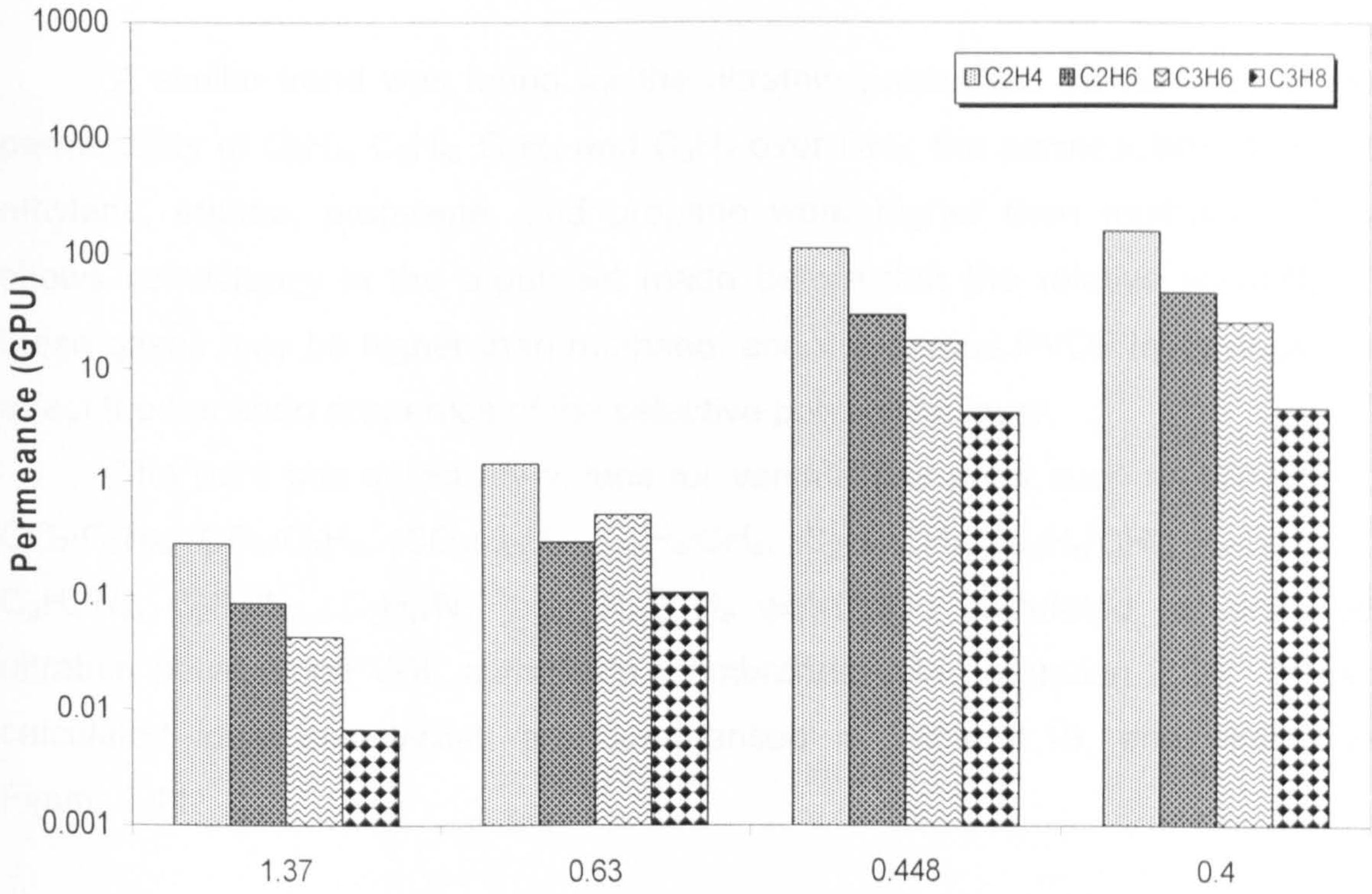

Figure 4. 39 The permeance (in GPU) of ethylene, ethane, propylene and propane through undoped ultrathin polyaniline membranes supported on PVDF substrate.

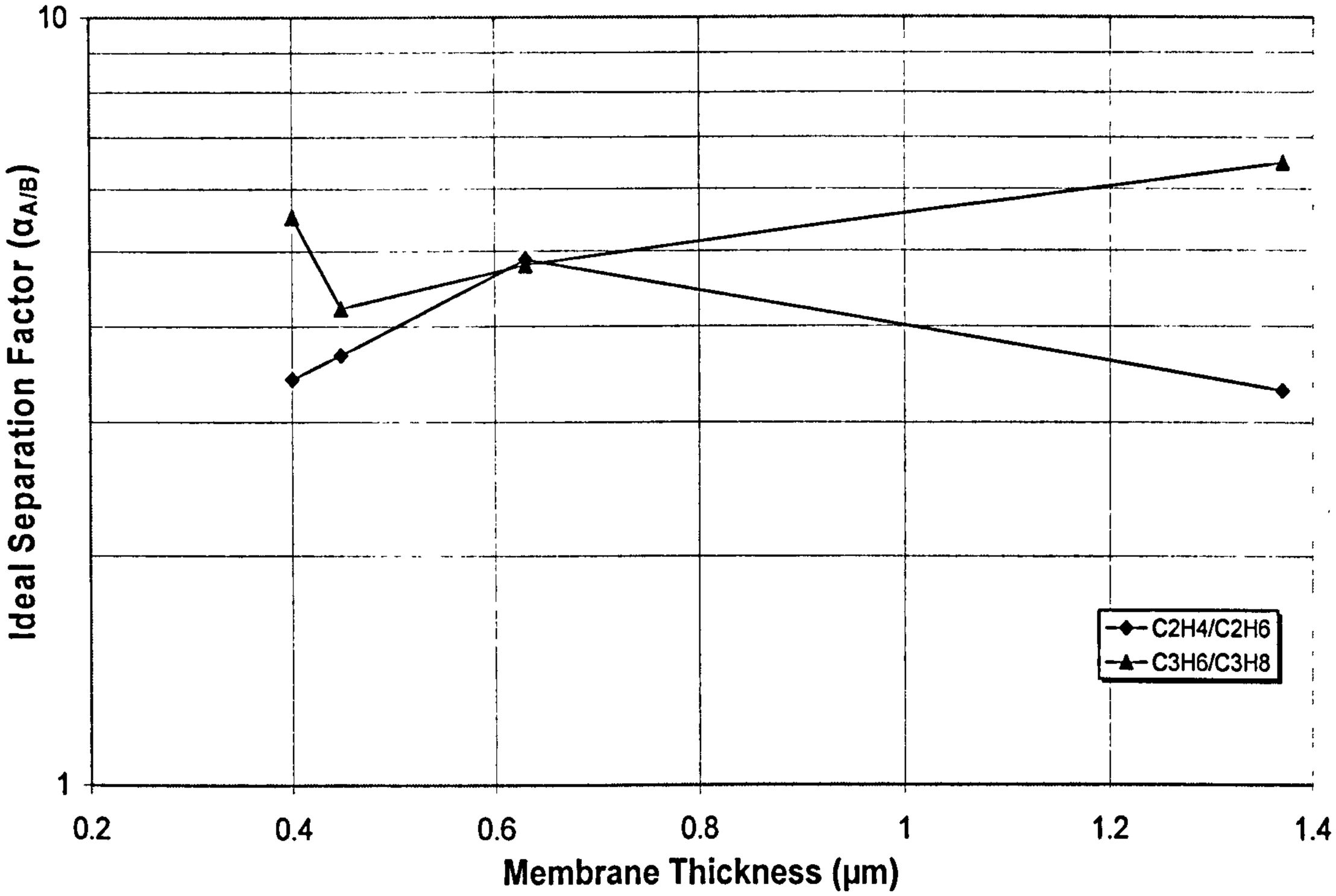

Figure 4. 40 Ideal separation factor values of C_2H_4/C_2H_6 and C_3H_6/C_3H_8 gas pairs through undoped ultrathin polyaniline membranes supported on porous PVDF substrate.

A similar trend was found for the ultrathin polyaniline membranes to the permeability of C_2H_4, C_2H_6, C_3H_6 and C_3H_8 over CH_4; the permeability values of ethylene, ethane, propylene, and propane were higher than methane. This shows consistency in the argument made before that the relative solubility of these gases may be higher than methane, and the porous PVDF layer does not affect the transport properties of the selective polyaniline layer.

The pure gas selectivity values for various gas pairs such as CO_2/C_2H_4, CO_2/C_2H_6, CO_2/C_3H_6, CO_2/C_3H_8, C_2H_4/CH_4, C_2H_6/CH_4, C_3H_6/CH_4, C_3H_8/CH_4, C_2H_4/N_2, C_2H_6/N_2, C_3H_6/N_2, and N_2/C_3H_8 were also calculated for undoped ultrathin polyaniline/PVDF composite membranes using equation 2.30. These calculated ideal selectivities are summarised in Table 4.18, and plotted in Figure 4.41.

Table 4. 18 Ideal selectivities of various gas pairs as a function of ultrathin polyaniline membrane thickness.

	Ideal Separation Factor ($\alpha_{A/B}$)			
	1.371 μm	**0.63 μm**	**0.448 μm**	**0.4 μm**
CO_2/C_2H_4	3.70	3.33	3.90	2.72
CO_2/C_2H_6	12.2	16.3	14.3	9.31
CO_2/C_3H_6	24.3	9.47	23.9	16.7
CO_2/C_3H_8	157	45.5	100	92.2
C_2H_4/CH_4	30.9	18.5	25.6	23.8
C_2H_6/CH_4	9.35	3.79	6.96	6.97
C_3H_6/CH_4	4.70	6.51	4.17	3.89
C_3H_8/CH_4	1.38	0.74	1.01	1.42
C_2H_4/N_2	8.17	5.40	3.75	6.64
C_2H_6/N_2	2.47	1.11	1.02	1.94
C_3H_6/N_2	1.21	1.90	0.61	1.08
N_2/C_3H_8	5.21	4.52	6.90	5.10

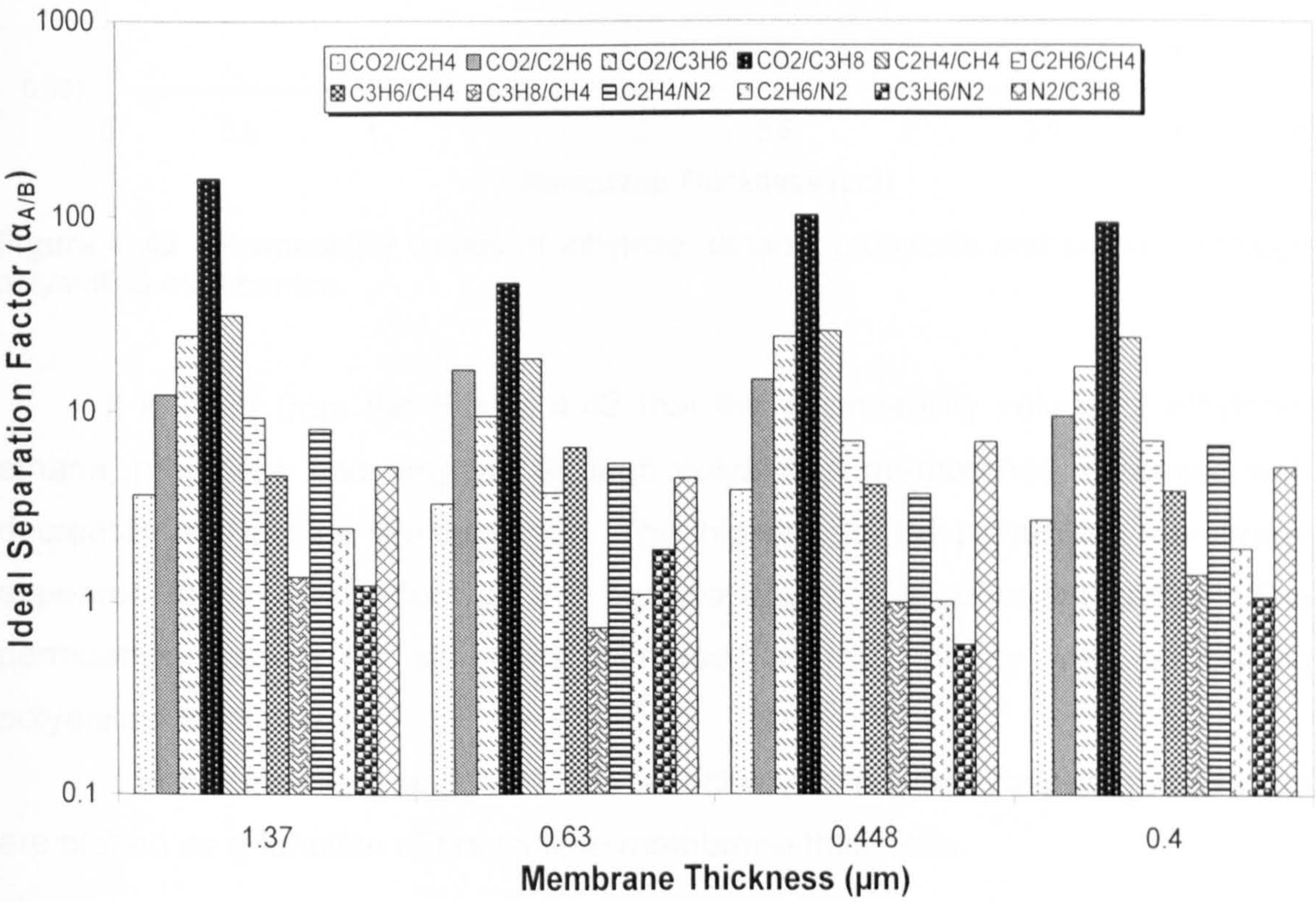

Figure 4. 41 Ideal separation factor values of various gas pairs through undoped ultrathin polyaniline membranes supported on porous PVDF substrate.

In Figure 4.42, the permeability values (in Barrers) for C_2H_4, C_2H_6, C_3H_6 and C_3H_8 is plotted as a function of polyaniline membrane thickness.

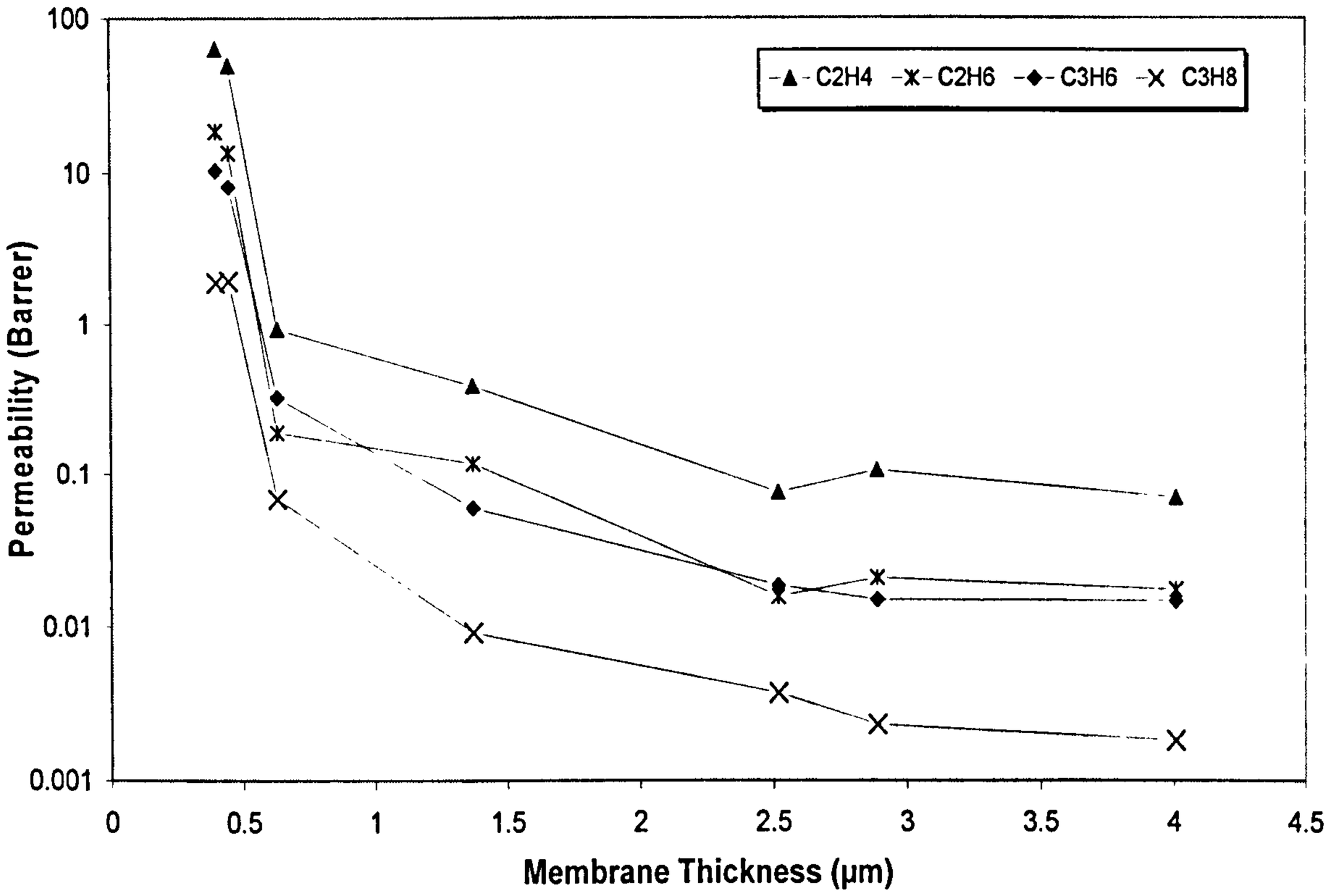

Figure 4. 42 Permeability values of ethylene, ethane, propylene and propane through polyaniline membranes.

It is clear from the Figure 4.42 that the permeability values of ethylene, ethane, propylene and propane through polyaniline membranes increased with decreasing polyaniline film thickness. The thickness of the polyaniline membrane appeared to have an effect on the permeability of the penetrant gases. The permeability values for all gases increased almost linearly with decreasing polyaniline thickness.

In Figures 4.43 and 4.44, the selectivity values for various gas pairs to are plotted as a function of polyaniline membrane thickness.

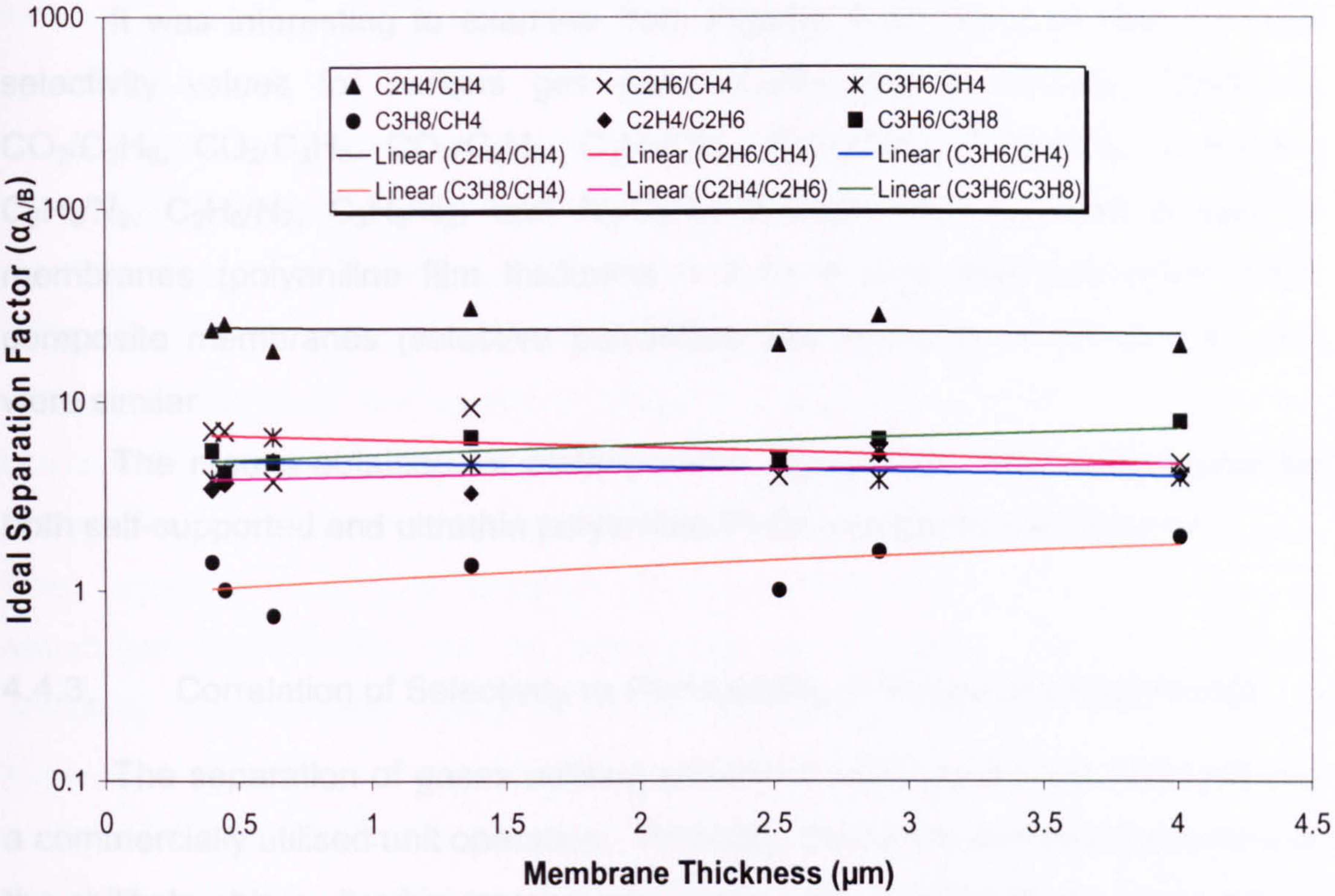

Figure 4. 43 Ideal separation factor values of C_2H_4/C_2H_6, C_3H_6/C_3H_8, C_2H_4/CH_4, C_2H_6/CH_4, C_3H_6/CH_4, and C_3H_8/CH_4 as a function of selective polyaniline film thickness.

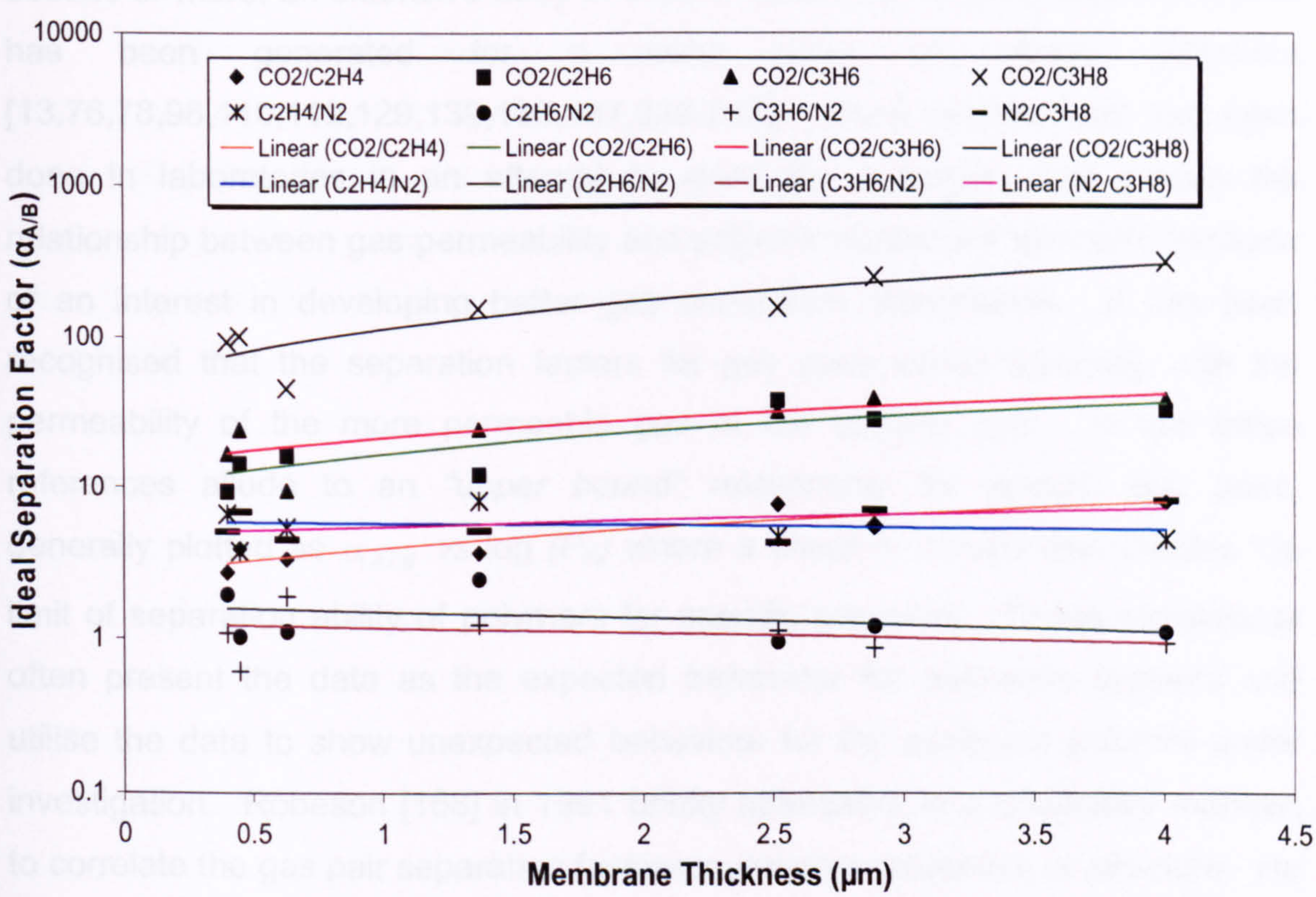

Figure 4. 44 Ideal separation factor values of CO_2/C_2H_4, CO_2/C_2H_6, CO_2/C_3H_6, CO_2/C_3H_8, C_2H_4/N_2, C_2H_6/N_2, C_3H_6/N_2, and N_2/C_3H_8 as a function of selective polyaniline film thickness.

It was interesting to examine from Figures 4.43 and 4.44 that the ideal selectivity values for various gas pairs (C_2H_4/C_2H_6, C_3H_6/C_3H_8, CO_2/C_2H_4, CO_2/C_2H_6, CO_2/C_3H_6, CO_2/C_3H_8, C_2H_4/CH_4, C_2H_6/CH_4, C_3H_6/CH_4, C_3H_8/CH_4, C_2H_4/N_2, C_2H_6/N_2, C_3H_6/N_2, and N_2/C_3H_8) through self-supported polyaniline membranes (polyaniline film thickness = 2 to 4 μm), and polyaniline/PVDF composite membranes (selective polyaniline film thickness = 0.4 to 1.37 μm) were similar.

The results obtained for olefin/paraffin separations were reproducible for both self-supported and ultrathin polyaniline/PVDF composite membranes.

4.4.3. Correlation of Selectivity *vs* Permeability of Polyaniline Membranes

The separation of gases utilising polymeric membranes has emerged into a commercially utilised unit operation. Probably, the key to this development was the ability to obtain ultrathin membranes (of the order of 1000 Å) via improvement of asymmetric membranes of thin-film composite fabrication. Over the past decade or more, an extensive body of experimental data on permeation of gases has been generated for a wide array of glassy polymers [13,76,78,96,110,112,129,139,168,187,336-342]. Much of this work has been done in laboratories in an attempt to learn the principles that govern the relationship between gas permeability and polymer repeat unit structure because of an interest in developing better gas separation membranes. It has been recognised that the separation factors for gas pairs varies inversely with the permeability of the more permeable gas of the specific pair. In fact these references allude to an *"upper bound"* relationship for specific gas pairs, generally plotted as $\alpha_{A/B}$ *vs* log (P_A) where a linear or curved line denotes the limit of separation ability of polymers for specific gas pairs. These correlations often present the data as the expected behaviour for polymeric systems and utilise the data to show unexpected behaviour for the particular polymer under investigation. Robeson [168] in 1991 briefly attempted, in a qualitative manner, to correlate the gas pair separation factors to polymer properties or structure. He defined the upper bound limit for most gas mixtures by compiling the permeability data from over 300 references. The data demonstrated the *"upper bound"*

concept for the limits of ideal selectivities for specific values of permeabilities for specific gas pairs.

The permeability of a penetrant in the membrane, defined as a thickness normalised flux, can be expressed as a product of a kinetic factor *D*, the diffusion coefficient, and a thermodynamic factor *S*, the sorption coefficient (see equation 2.29; Chapter 2). The sorptivity, *S*, is measured as the secant slope of the sorption isotherm at the upstream pressure conditions when the downstream pressure of the membrane is negligible. The diffusivity, *D*, is determined by taking the ratio of penetrant permeability and the sorption coefficient. Following from equation 2.32 (see Chapter 2), the permselectivity of practical gas separation membranes can be interpreted as a product of diffusivity and solubility. The sorption selectivity, S_A/S_B, has proven difficult to adjust without seriously off-setting the diffusivity selectivity for nonporous polymeric materials [336]. On the other hand, the separation of common gas pairs is accomplished by a size selective sieving mechanism (thus diffusion controlling), and adjustment of the diffusivity selectivity has been the major tool used in moving from the 1980 upper bound limit to 1991 upper bound limit [14,330].

Practical gas separation membranes need to be highly permeable to one of the mixture components while significantly rejecting the others. The benefits achievable with tailored glassy polymer structures seem to be approaching a limit, as shown in the extensive trade-off data for gas permeability and selectivity (see Figure 4.45) which is an adaptation of a similar figure published in 1991 [168].

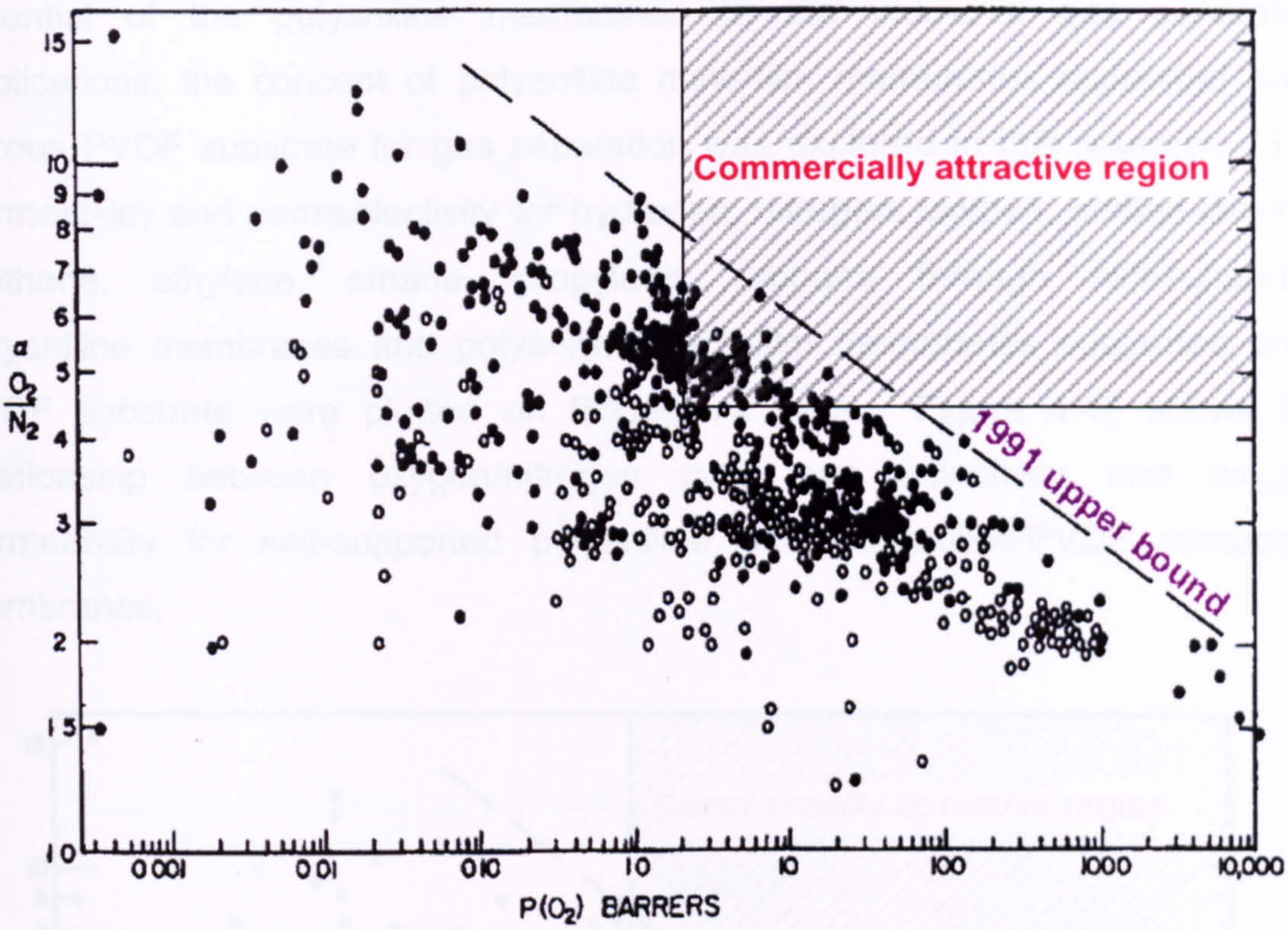

Figure 4. 45 Oxygen/nitrogen selectivity as a function of oxygen permeability for all known membrane materials as of 1991 (Robeson's plot of oxygen permeability and oxygen/nitrogen selectivity).

(○) rubbery polymers, and (●) glassy polymers.

Molecular sieving materials like zeolites and carbon molecular sieves (CMS) lie above the upper bound for polymers on this trade-off curve [330]. The research on facilitated selective carriers, block-copolymers, polymer nano-composites, carbon membranes and surface modified glass membranes is being carried out to work in the commercially attractive region (the shaded area on Figure 4.45) [343]. Understanding why polymeric membranes have been unable to achieve selectivities of the same orders as zeolites or CMS is both scientifically and technologically interesting.

The challenge, therefore, is to identify and introduce the missing key elements in polymeric materials to boost performance above the upper bound and approach that of molecular sieving materials. Self-supported polyaniline membranes and polyaniline/PVDF composite membranes were produced and analysed during this work. It was observed from the gas permeation measurements that the productivity of the various gases through dense self-supported polyaniline films was fairly low. To expand the application

potential of the polyaniline membranes to the industrial gas separation applications, the concept of polyaniline nano-film membranes supported on a porous PVDF substrate for gas separation was explored in this research. The permeability and permselectivity for hydrogen, nitrogen, oxygen, carbon dioxide, methane, ethylene, ethane, propylene, propane through self-supported polyaniline membranes and polyaniline nano-film membranes supported on a PVDF substrate were plotted on Robeson's plots. Figure 4.46 shows the relationship between oxygen/nitrogen pure gas selectivity and oxygen permeability for self-supported polyaniline and polyaniline/PVDF composite membranes.

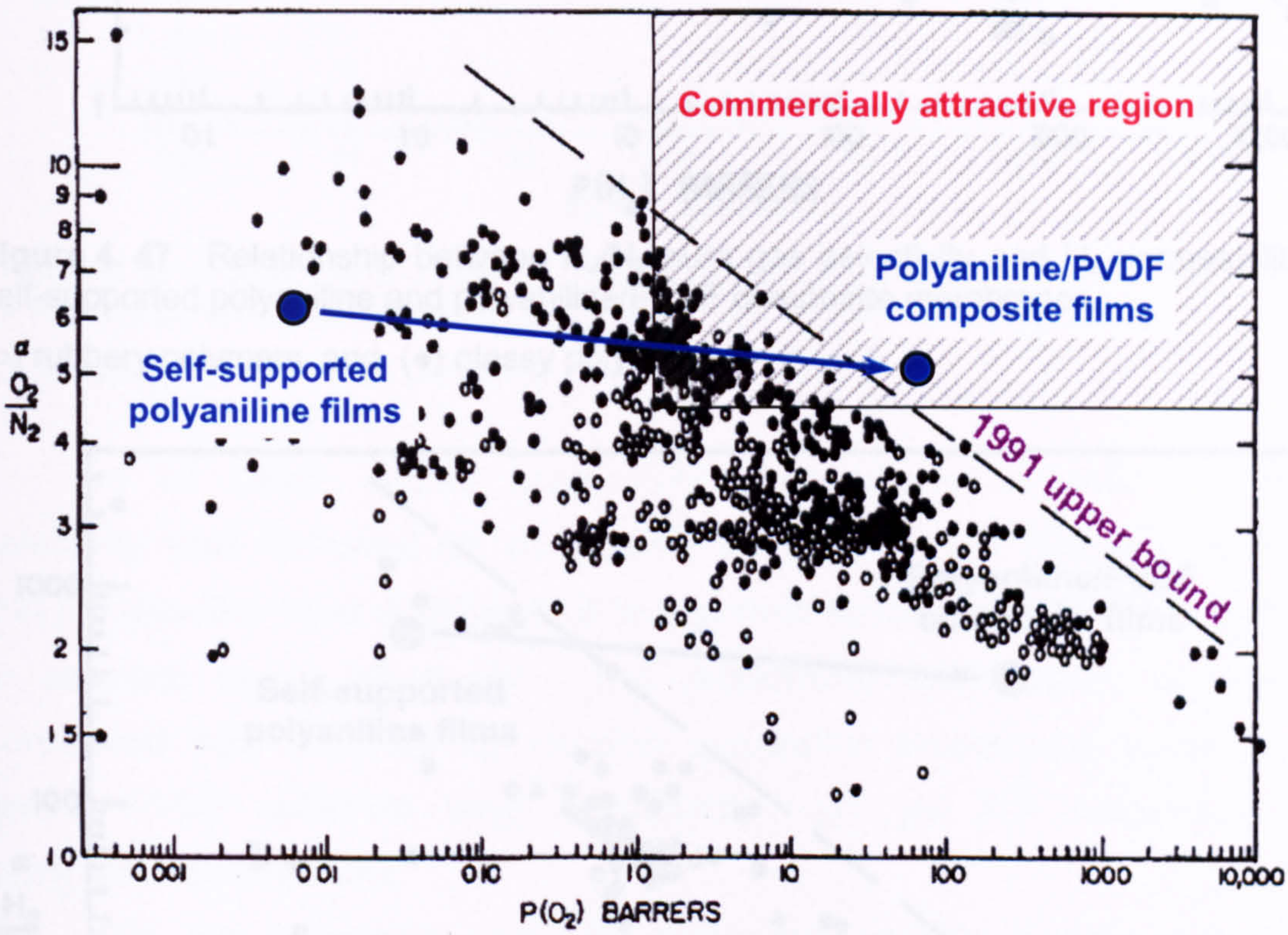

Figure 4. 46 Relationship between O_2/N_2 pure gas selectivity and O_2 permeability for self-supported polyaniline and polyaniline/PVDF composite membranes. (○) rubbery polymers, and (●) glassy polymers.

Similarly, the relationship between H_2/N_2 pure gas selectivity and H_2 permeability, H_2/CH_4 pure gas selectivity and H_2 permeability, and CO_2/CH_4 permselectivity and CO_2 permeability for self-supported polyaniline membranes and polyaniline/PVDF composite membranes are plotted in Figures 4.47, 4.48 and 4.49, respectively.

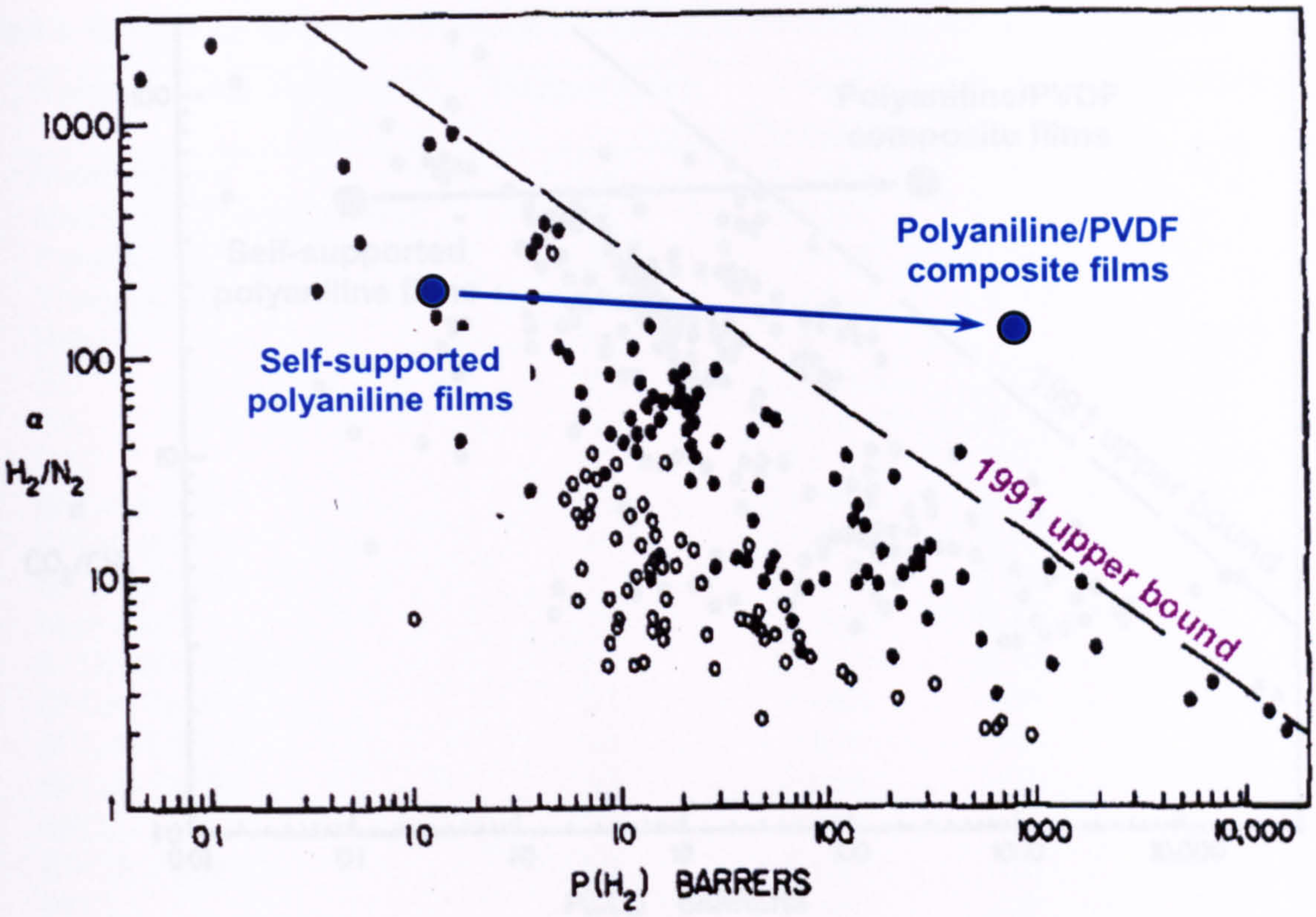

Figure 4. 47 Relationship between H_2/N_2 pure gas selectivity and H_2 permeability for self-supported polyaniline and polyaniline/PVDF composite membranes.

(○) rubbery polymers, and (●) glassy polymers.

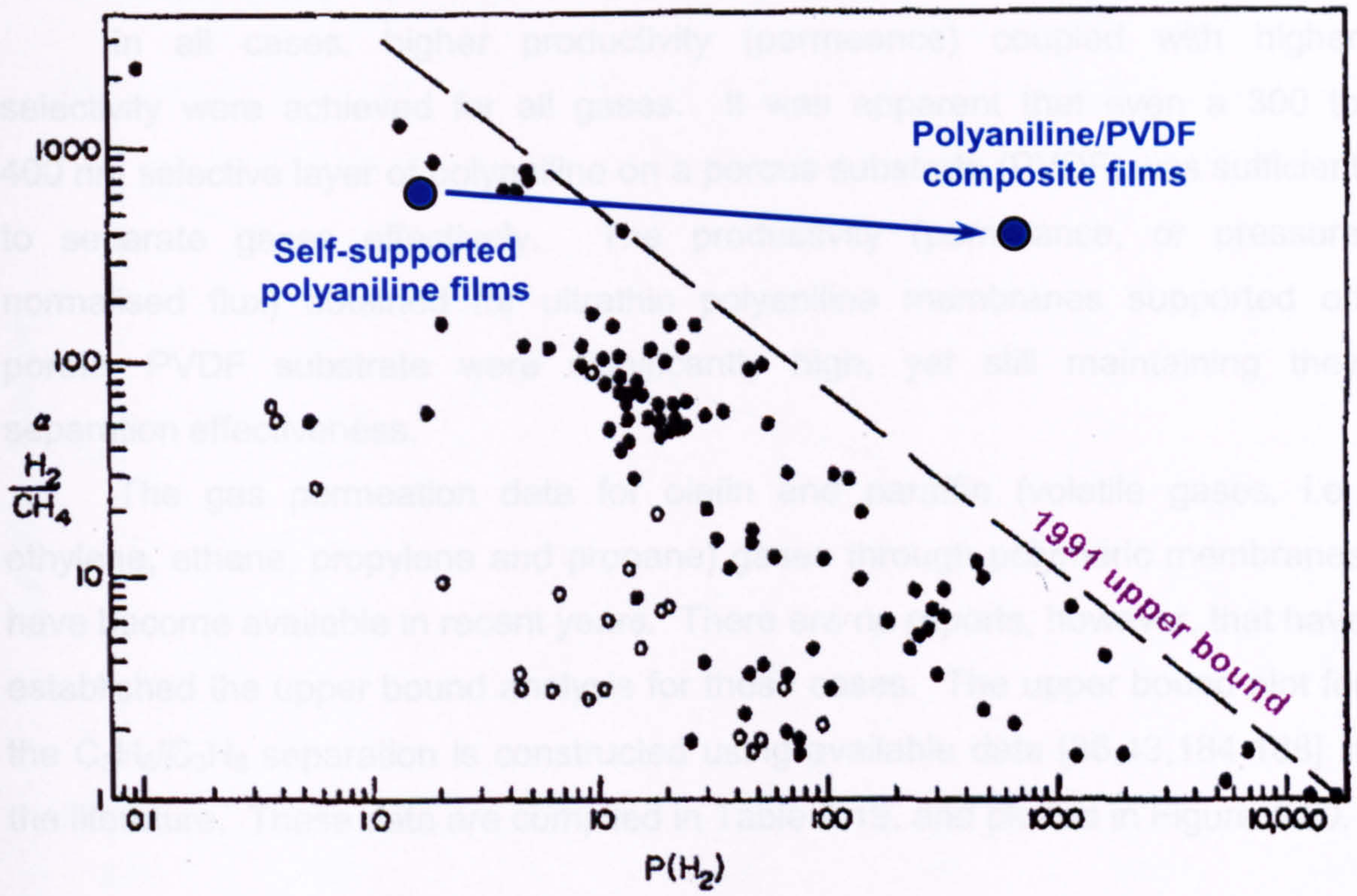

Figure 4. 48 Relationship between H_2/CH_4 pure gas selectivity and H_2 permeability for self-supported polyaniline and polyaniline/PVDF composite membranes.

(○) rubbery polymers, and (●) glassy polymers.

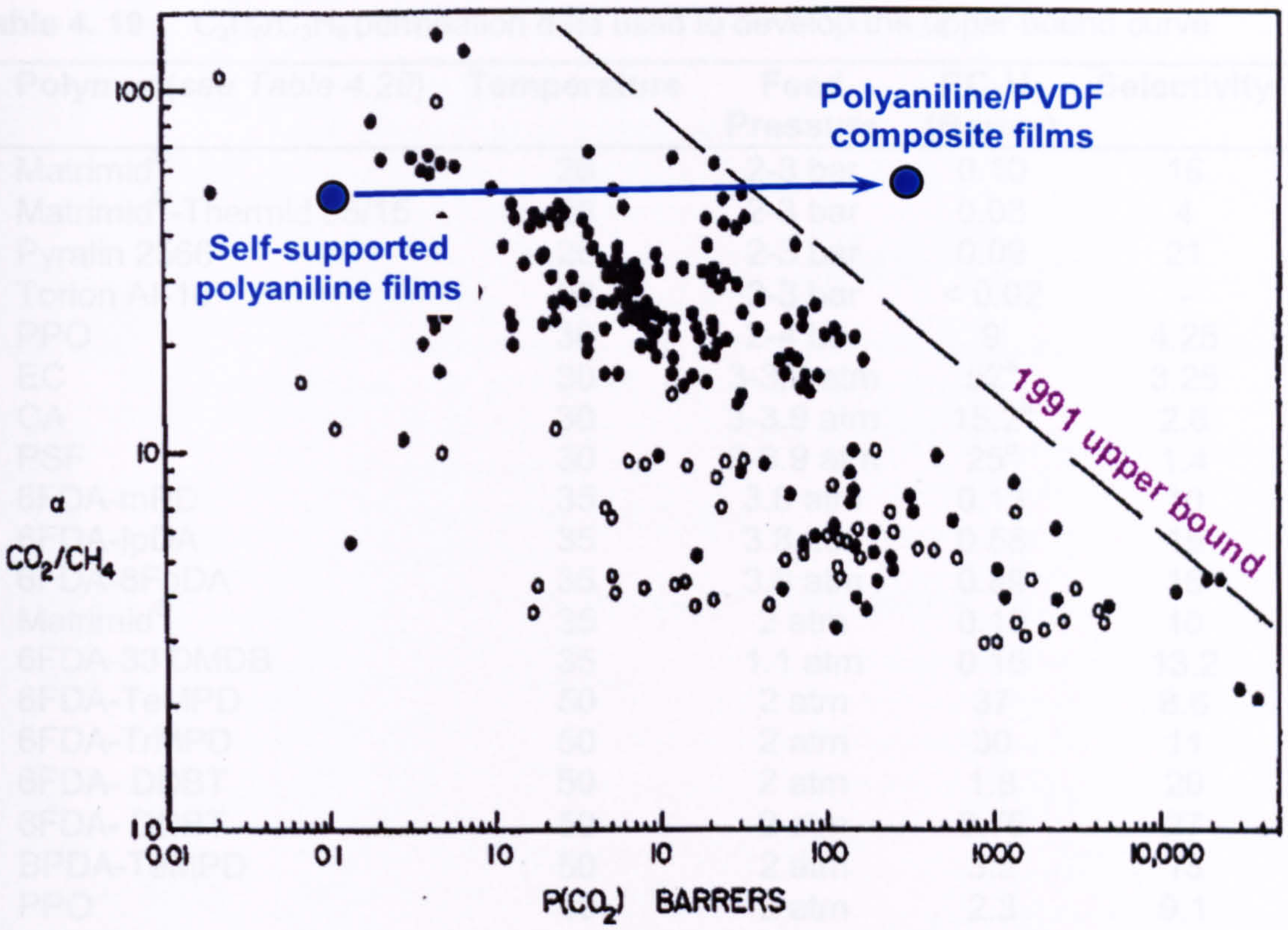

Figure 4. 49 Relationship between CO_2/CH_4 pure gas selectivity and CO_2 permeability for self-supported polyaniline and polyaniline/PVDF composite membranes.

(○) rubbery polymers, and (●) glassy polymers.

In all cases, higher productivity (permeance) coupled with higher selectivity were achieved for all gases. It was apparent that even a 300 to 400 nm selective layer of polyaniline on a porous substrate (PVDF) was sufficient to separate gases effectively. The productivity (permeance, or pressure normalised flux) obtained for ultrathin polyaniline membranes supported on porous PVDF substrate were significantly high, yet still maintaining their separation effectiveness.

The gas permeation data for olefin and paraffin (volatile gases, i.e., ethylene, ethane, propylene and propane) gases through polymeric membranes have become available in recent years. There are no reports, however, that have established the upper bound analysis for these cases. The upper bound plot for the C_3H_6/C_3H_8 separation is constructed using available data [36,43,184-188] in the literature. These data are compiled in Table 4.19, and plotted in Figure 4.50.

Table 4. 19 C_3H_6/C_3H_8 permeation data used to develop the upper bound curve.

Polymer (*see Table 4.20*)	**Temperature**	**Feed Pressure**	**PC_3H_6 (Barrer)**	**Selectivity**
Matrimid®	26	2-3 bar	0.10	16
Matrimid®-Thermid 85/15	26	2-3 bar	0.03	4
Pyralin 2566	26	2-3 bar	0.09	21
Torlon AI-10	26	2-3 bar	< 0.02	-
PPO	30	2-4 bar	9	4.25
EC	30	3-3.9 atm	52[a]	3.25
CA	30	3-3.9 atm	15.2[a]	2.6
PSF	30	3-3.9 atm	25[a]	1.4
6FDA-mPD	35	3.8 atm	0.13	10
6FDA-IpDA	35	3.8 atm	0.58	15
6FDA-6FpDA	35	3.8 atm	0.89	16
Matrimid®	35	2 atm	0.10	10
6FDA-33'DMDB	35	1.1 atm	0.15	13.2
6FDA-TeMPD	50	2 atm	37	8.6
6FDA-TrMPD	50	2 atm	30	11
6FDA- DDBT	50	2 atm	1.8	20
6FDA- DDBT	50	2 atm	0.76	27
BPDA-TeMPD	50	2 atm	3.2	13
PPO	50	2 atm	2.3	9.1
P4MP	50	2 atm	54	2
1.2PB	50	2 atm	260	1.7
PDMS	50	2 atm	6600	1.1
6FDA-ODA	100	2 atm	0.48	11

[a] Mixed gas results : 55% propylene / 45% propane feed.

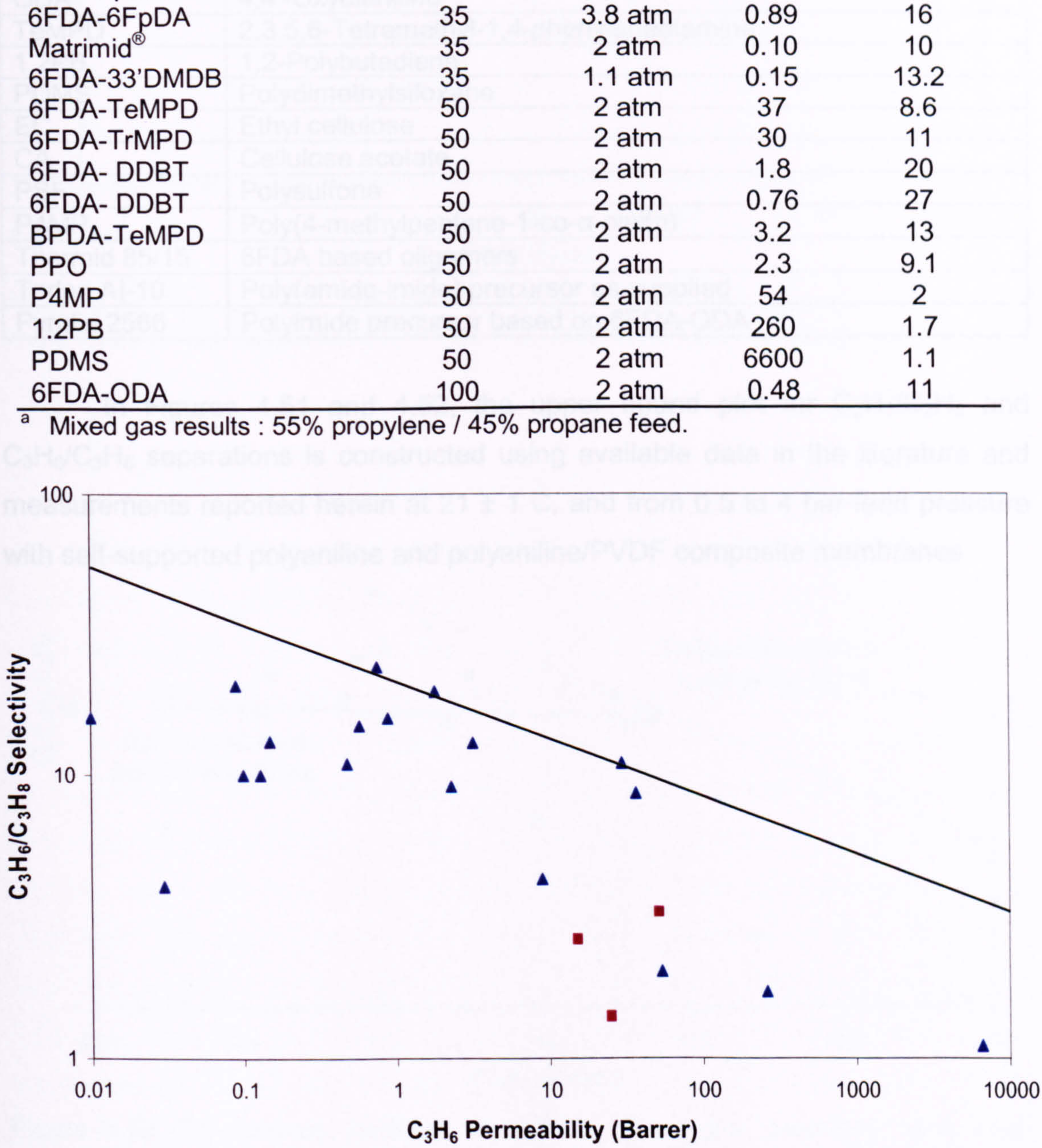

Figure 4. 50 C_3H_6/C_3H_8 experimental upper bound on pure gas permeation data over the range 1-4 atm feed pressure. (▲) pure gas experiments, (■) mixed gas results.

Table 4. 20 List of abbreviations and corresponding technical names.

Abbreviation	Chemical name
6FDA	4,4'-(Hexafluoro-isopropylidene)diphthalic anhydride
6FpDA (BAAF)	4,4'-(Hexafluoro-isopropylidene)dianiline
TrMPD (DAM)	Trimethylphenylinediamine
DDBT	Dimethyl-3,7-diaminodiphenylthiophene-5,5-dioxide
33'DMDB	3,3'-Dimethyl-4,4'diaminophenyl
Matrimid®	3,3', 4,4'-Benzophenone tetracarboxylic dianhydride and 5(6)-amino-1-(4' aminophenyl)-1,3-trimethylindane
BPDA	3,3', 4,4'-Biphenyltetracarboxylic dianhydride
mPD	1,3-Phenylenediamine
IPDA	4,4'-(Isopropylidene)dianiline
ODA	4,4'-Oxydianiline
TeMPD	2,3,5,6-Tetramethyl-1,4-phenylenediamine
1.2PB	1,2-Polybutadiene
PDMS	Polydimethylsiloxane
EC	Ethyl cellulose
CA	Cellulose acetate
PSF	Polysulfone
P4MP	Poly(4-methylpentene-1-co-α-oleifn)
Thermid 85/15	6FDA based oligomers
Torlon AI-10	Poly(amide-imide) precursor as supplied
Pyralin 2566	Polyimide precursor based on 6FDA-ODA

In Figures 4.51 and 4.52, the upper bound plot for C_2H_4/C_2H_6 and C_3H_6/C_3H_8 separations is constructed using available data in the literature and measurements reported herein at 21 ± 1 C, and from 0.5 to 4 bar feed pressure with self-supported polyaniline and polyaniline/PVDF composite membranes.

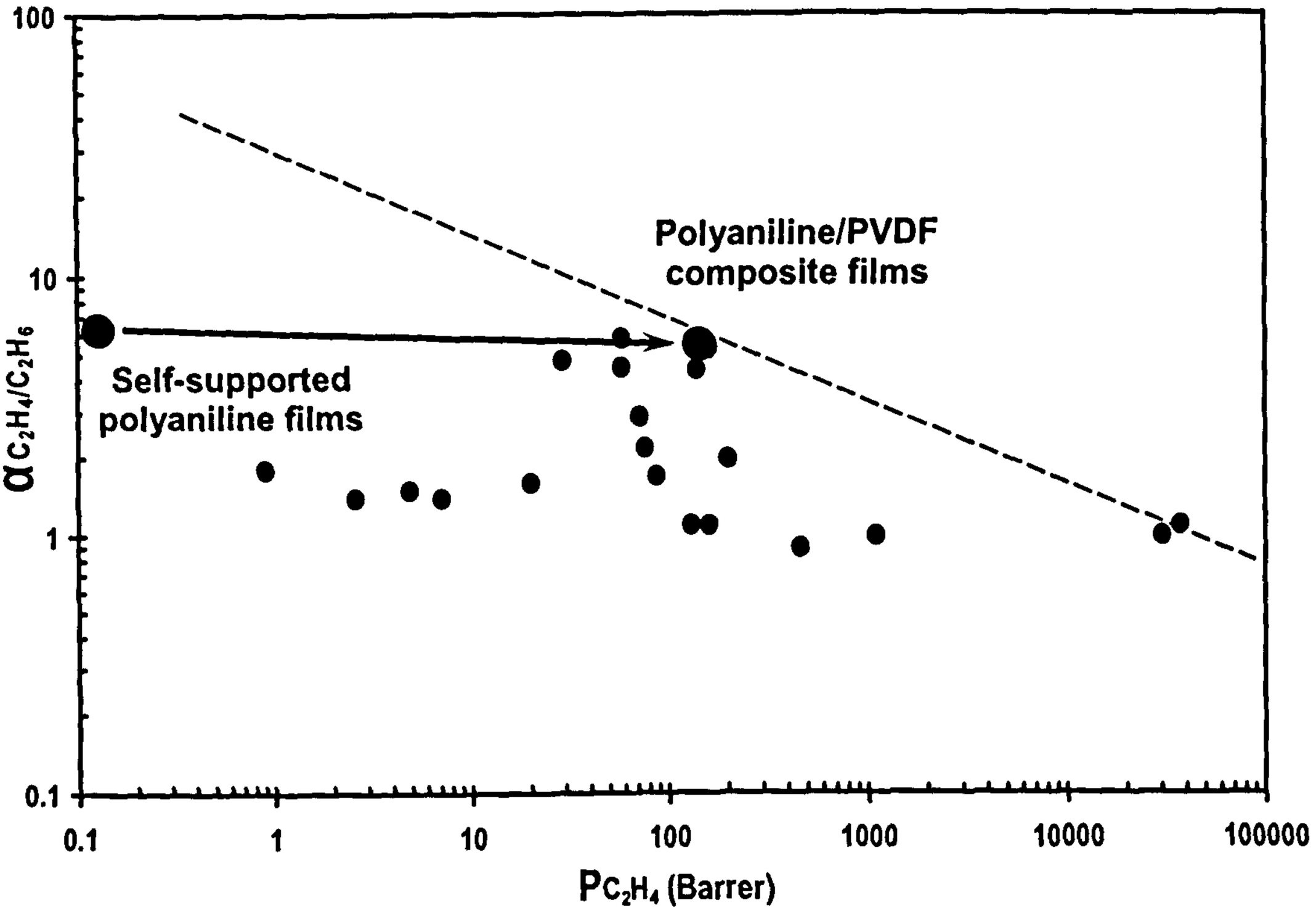

Figure 4. 51 Relationship between C_2H_4/C_2H_6 pure gas selectivity and C_2H_4 permeability for self-supported polyaniline and polyaniline/PVDF composite membranes.

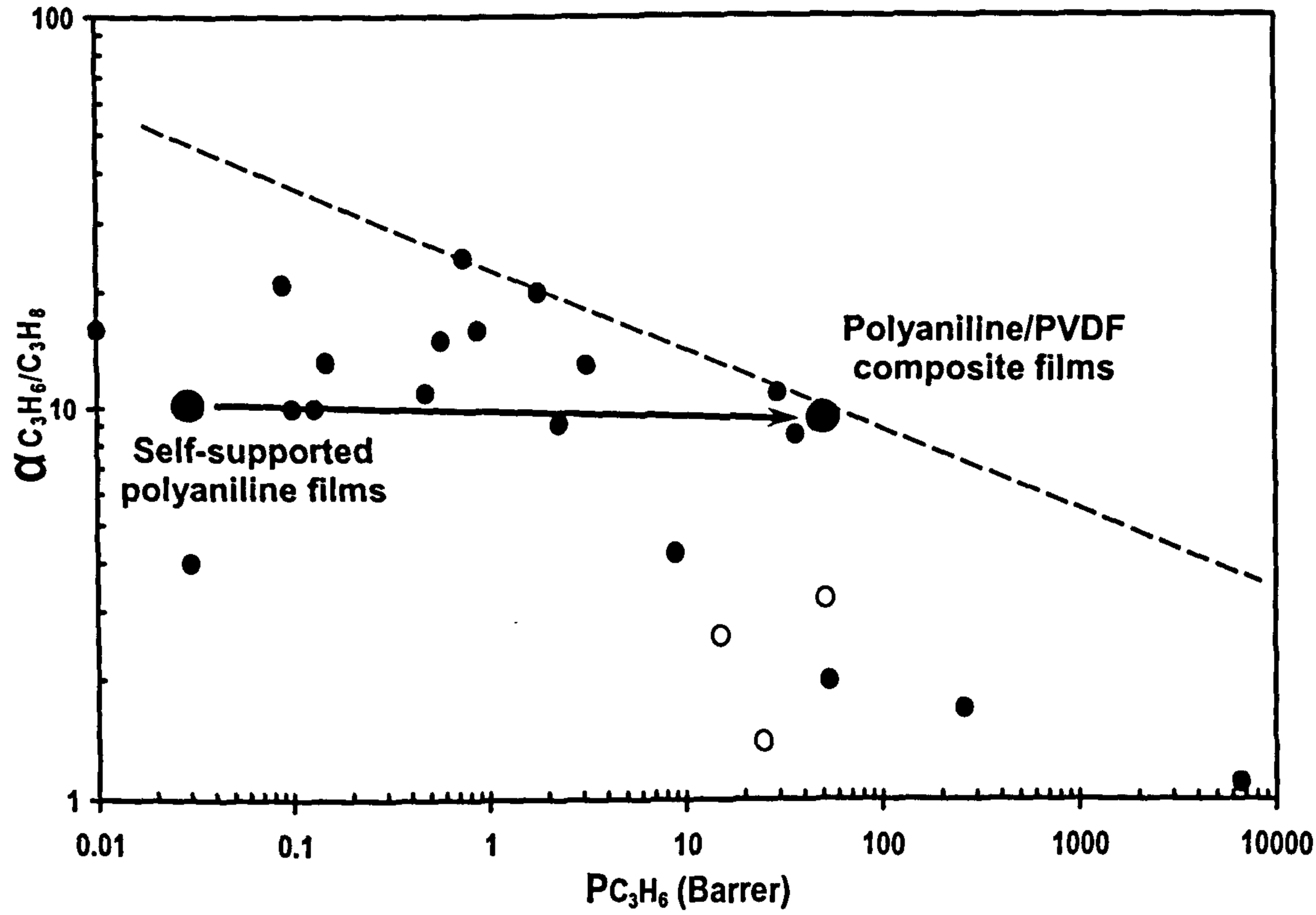

Figure 4. 52 Relationship between C_3H_6/C_3H_8 pure gas selectivity and C_3H_6 permeability for self-supported polyaniline and polyaniline/PVDF composite membranes

(•) pure gas experiment results, and (○) mixed gas experiment results.

The remarkable separation performance of silver based polymer membranes using the concept of facilitated transport for olefin/paraffin separations has been published elsewhere [21-48]. However, limited work has been done to develop new membranes which combine increased selectivities and higher productivity for these separations. The use of polyaniline membranes has been proposed for these applications (olefin/paraffin gas separations) due to their excellent chemical stability against the gas streams containing high levels of plasticising, condensable vapours. However, the permeability for self-supported polyaniline membranes for C_2H_4 and C_3H_6 were far too low. It was clear from the above figures (Figures 4.50 and 4.51) that the use of polyaniline nano-film membranes resulted in substantially higher productivities for C_2H_4 and C_3H_6.

Furthermore, polyaniline is a dopable material, so it can be doped with Ag(I) (a Group I-B metal ion) to facilitate transport of olefins through the polyaniline films. Hence, it is important, and recommended, to measure the effect of doping, dedoping and controlled redoping of Ag(I) on permeance and separation efficiency of ethylene and propylene through polyaniline membranes in the future work.

4.4.4. Mixed Gas Permeation Experiments

Polymeric membranes have been successfully used in many gas separation applications. Their success has been largely based on their mechanical and thermal stability, along with good separation properties. Understanding the transport phenomena of the target gases through membranes is the foundation of realising effective separation of a mixed gas and selecting the appropriate feed conditions. Generally, the permeation behaviour of pure gas through a membrane depends mainly on the properties of the gas, the membrane and the feed conditions. As for the gas mixture, the transport behaviour of one component through a membrane is affected by the presence of other penetrants so that it deviates from that of the pure gas. Hence, it is difficult to evaluate the relative contribution of diffusion coupling or competitive solubility effects on the membrane selectivity from the use of single (pure) gas permeation data. In the actual membrane separation application, to optimise the separation design and determine the proper feed conditions, it is necessary to establish a mathematical

model based on the available experimental data. The model can be used as a powerful tool to evaluate or predict the performance of the separation system at various feed conditions for a specific gas pair-membrane system.

In this study, based on the permeation behaviour of binary gas mixtures (i.e. O_2-N_2, O_2-CO_2 and N_2-CO_2) through self-supported polyaniline membranes (polyaniline film thickness = 2.89 μm) and polyaniline/PVDF composite membranes (selective polyaniline layer thickness = 0.448 μm) at various feed conditions, a simple and practical mathematical model expressed in terms of feed compositions was derived to interpret the experimental data, and predict the permeation flux and the composition of the permeated stream quantitatively.

For ideal mixed gas permeation experiments in which there are no interactions between the gases, as well as no special gas-polymer interactions in the presence of the second gas, the total permeation flux of the gas mixture can be calculated form the following equation;

$$J_{total} = \frac{P_{total} \cdot \Delta p_{total}}{t_m} \tag{4.8}$$

where t_m is the membrane thickness, Δp_{total} is the total pressure difference across the polymeric membrane, and J_{total} and P_{total} are the total permeation flux and total permeability of the mixed gases, respectively.

The total permeation flux and total pressure difference across the polymeric film can be calculated from following equations;

$$J_{total} = J_1 + J_2 \tag{4.9}$$

$$\Delta p_{total} = (p_{i,1} + p_{i,2}) - (p_{o,1} + p_{o,2}) \tag{4.10}$$

where J, p_i and p_o are the permeation flux, partial pressure of the permeating gas in the feed, and partial pressure of the permeating gas in the permeate, respectively; and the subscripts *1* and *2* denote the component gases.

Equation 4.10 can be rearranged in terms of total feed side pressure, $p_{i,total}$ and total permeate side pressure, $p_{o,total}$ as follows;

$$\Delta p_{total} = (p_{i,total} \cdot \phi_{i,1} + p_{i,total} \cdot \phi_{i,2}) - (p_{o,total} \cdot \phi_{o,1} + p_{o,total} \cdot \phi_{o,2}) \quad (4.11)$$

where ϕ_i and ϕ_o are the volume fraction of the permeating gas in the feed and permeate, respectively.

Equation 4.11 can be rearranged to;

$$\Delta p_{total} = (p_{i,total} \cdot \phi_{i,1} - p_{o,total} \cdot \phi_{o,1}) + (p_{i,total} \cdot \phi_{i,2} - p_{o,total} \cdot \phi_{o,2}) \quad (4.12)$$

Hence,

$$\Delta p_{total} = \frac{J_1 \cdot t_m}{P_1} + \frac{J_2 \cdot t_m}{P_2} \quad (4.13)$$

The permeation flux for the component *1* in a gas mixture can be calculated from the following equation 4.14.

$$J_1 = \frac{P_1 \cdot (p_{i,total} \cdot \phi_{i,1} - p_{o,total} \cdot \phi_{o,1})}{t_m} \quad (4.14)$$

Similarly for the component *2* in a gas mixture, the permeation flux can be calculated as;

$$J_2 = \frac{P_2 \cdot (p_{i,total} \cdot \phi_{i,2} - p_{o,total} \cdot \phi_{o,2})}{t_m} \quad (4.15)$$

At the beginning of the mixed gas permeation experiment (experimental time, $t = 0$), the volume fraction of the component *1* in the permeate, $\phi_{o,1} = 0$. The total permeate side pressure, $p_{o,total}$ can be neglected as the permeate side of the membrane permeation cell is under vacuum (at the beginning, the permeate side pressure = 0.561 cmHg) and $p_{i,total} >> p_{o,total}$, hence it is suitable to assume $p_{i,total} \cdot \phi_{i,1} >> p_{o,total} \cdot \phi_{o,1}$, and $p_{o,total} \cdot \phi_{o,1} \approx 0$. However, for the experimental time, $t > 0$, the volume fraction of the component *1* in the permeate, $\phi_{o,1} > 0$, but the

permeate side is still under vacuum and $p_{i,total} >> p_{o,total}$, hence at the experimental time, $t > 0$, $p_{i,total} \cdot \phi_{i,1} >> p_{o,total} \cdot \phi_{o,1}$, and $p_{o,total} \cdot \phi_{o,1} \approx 0$.

Hence, equations 4.14 and 4.15 can be rewritten as;

$$J_1 \approx \frac{P_1 \cdot (p_{i,total} \cdot \phi_{i,1})}{t_m} \quad (4.16)$$

$$J_2 \approx \frac{P_2 \cdot (p_{i,total} \cdot \phi_{i,2})}{t_m} \quad (4.17)$$

The total permeation flux, J_{total} can be calculated by substituting equations 4.16 and 4.17 to equation 4.9.

$$J_{total} = \frac{P_1 \cdot (p_{i,total} \cdot \phi_{i,1})}{t_m} + \frac{P_2 \cdot (p_{i,total} \cdot \phi_{i,2})}{t_m} \quad (4.18)$$

Hence the total permeance (pressure normalised flux) can be calculated as;

$$\frac{J_{total}}{p_{i,total}} = \frac{P_1 \cdot \phi_{i,1}}{t_m} + \frac{P_2 \cdot \phi_{i,2}}{t_m} \quad (4.19)$$

However, the complex factors such as coupling effect, plasticisation effect and concentration polarisation interact with each other and thus influence the transport of mixed gases through polymeric membranes, resulting in a deviation of the permeation behaviour of the actual binary gas mixture from that of the ideal gas mixture. Hence, it is necessary to reformulate equation 4.19, in order to predict the permeation behaviour of an actual binary gas mixture, by incorporating the effects of these complex factors on the permeability coefficient for the mixed gas system.

The actual total permeance (pressure normalised flux) of a binary gas mixture through a polyaniline membrane can be expressed as follows;

$$\frac{J_{total}}{p_{i,total}} = \frac{P_1 \cdot \phi_{i,1}}{t_m} + \frac{P_2 \cdot \phi_{i,2}}{t_m} \pm \sum \zeta \quad (4.20)$$

where, ζ is the characteristic parameter of gas-gas and gas-membrane interactions (due to coupling effects, plasticisation effects, and concentration polarisation).

4.4.4.1. Mixed Gas Permeation Measurements for Undoped Self-supported Polyaniline Membranes

The mixed gas permeation experiments for self-supported polyaniline membranes involved similar start up as the single permeation experiments, except for some modifications in the feed gas section (see Section 5.3.2.5; Chapter 3). The calibration curves were constructed for N_2, O_2 and CO_2, relating the mass spectroscopic intensity and the injected standard gas concentration under the fixed conditions (see Appendix 7). Similar operating conditions were maintained during the mixed gas permeation experiments. The detailed operational procedure to conduct mixed gas permeation measurements is described in Section 5.3.2.5 (see Chapter 3). The mixed gas permeation behaviour of O_2-N_2, CO_2-O_2 and CO2-N_2 was measured in this study.

The mixed gas permeance through a self-supported polyaniline membrane (polyaniline film thickness = 2.89 μm) for an O_2-N_2 mixed gas system was measured using a MKS Baratron pressure transducer, and plotted in Figure 4.53. The *"theoretical straight line"* in the Figures 4.53 to 4.55 corresponds to the permeance values calculated using equation 4.19, and the *"experimental values"* are the mixed gas permeance measured experimentally.

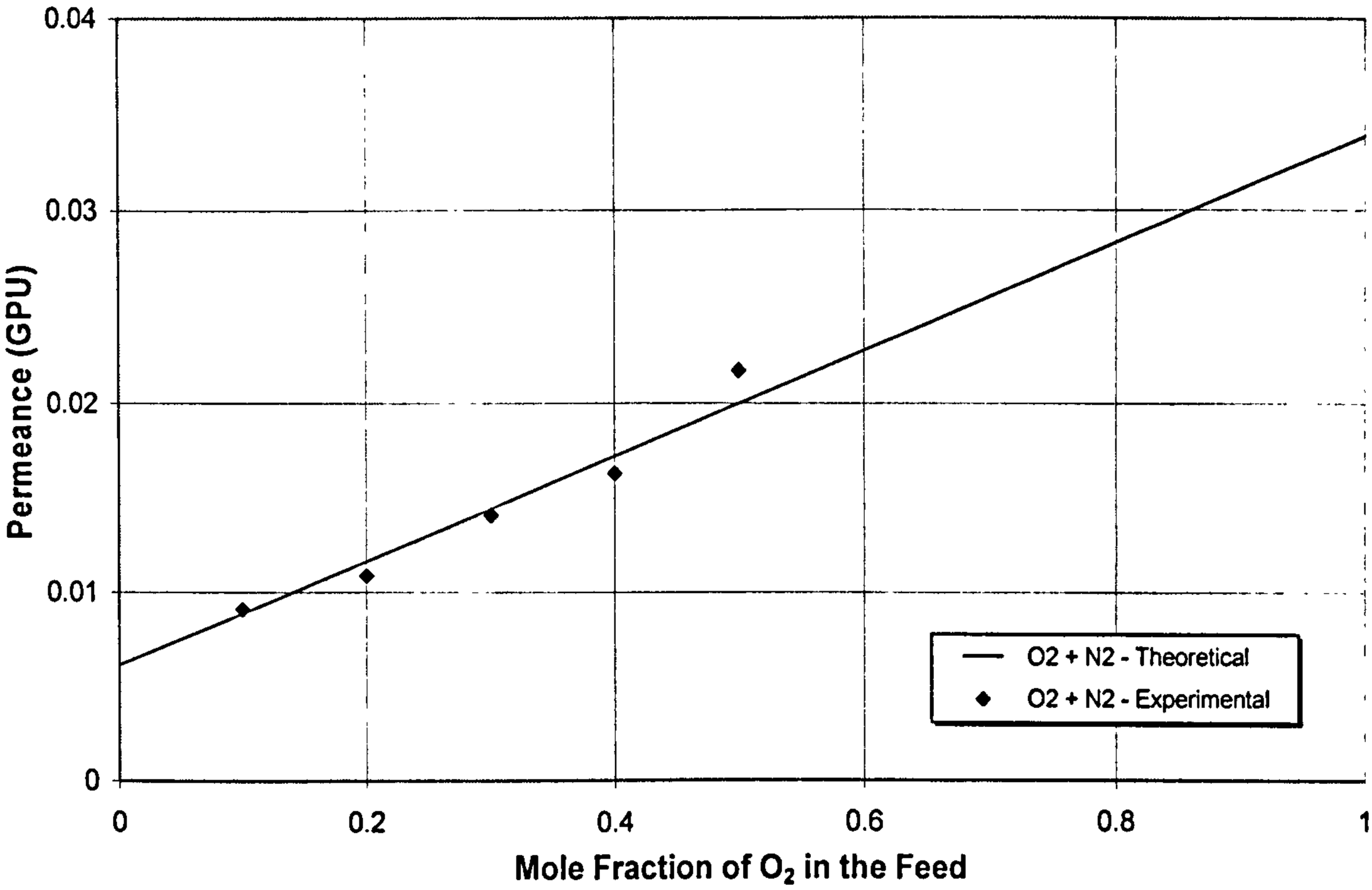

Figure 4. 53 Effect of the molar composition of O_2 in the feed gas on the total permeance for O_2-N_2 mixed gases in self-supported polyaniline films.

Similarly, the mixed gas permeance of the mixed gas system containing CO_2-O_2, and CO_2-N_2 are plotted in Figures 4.54 and 4.55, respectively.

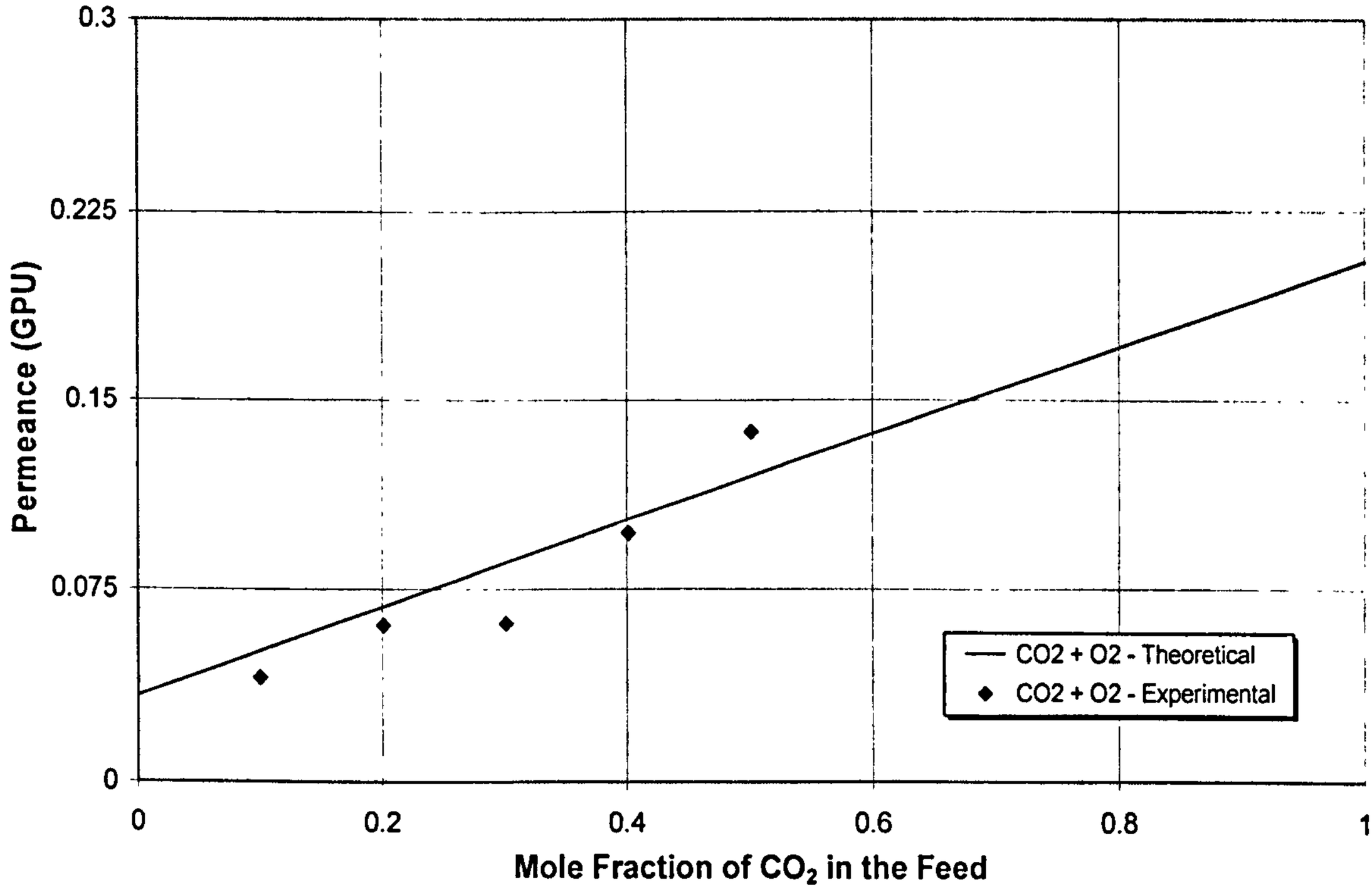

Figure 4. 54 Effect of the molar composition of CO_2 in the feed gas on the total permeance for CO_2-O_2 mixed gases in self-supported polyaniline films.

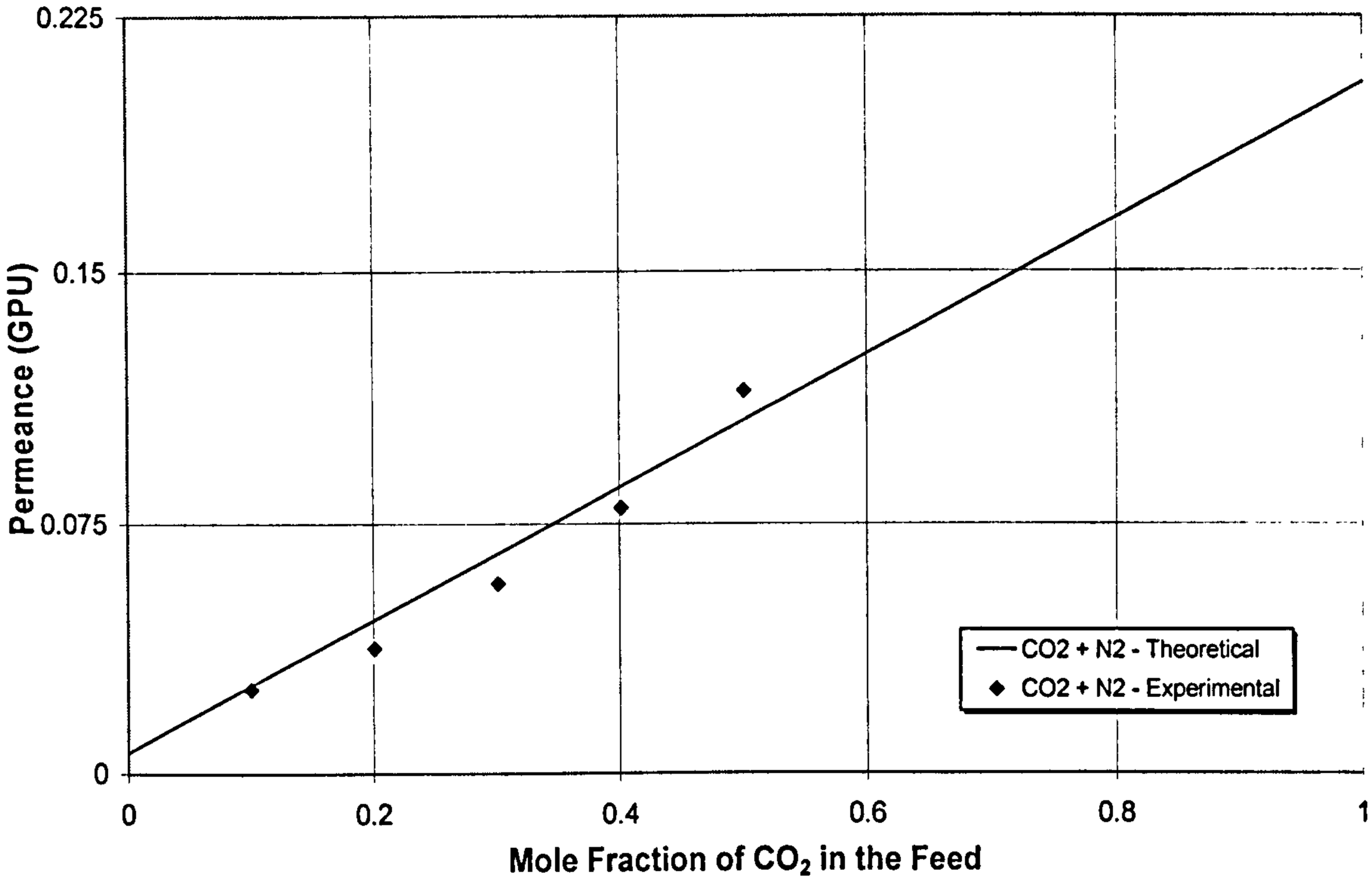

Figure 4. 55 Effect of the molar composition of CO_2 in the feed gas on the total permeance for CO_2-N_2 mixed gases in self-supported polyaniline films.

The permeance values calculated from equation 4.19 were compared (see Figures 4.53 to 4.55) with the experimental data, and found to be in a good agreement with the experimental data. The maximum errors of the model prediction are no more than 9%. Figures 4.53 to 4.55 revealed the dependence of the permeation behaviour of the binary gas mixed gases on the feed composition. The total permeation flux of O_2-N_2 mixed gas system increased with increasing the mole fraction of O_2 in the feed gases. Similarly, with the increase of the mole fraction of CO_2 in the feed gases, the total permeation flux increased for CO_2-O_2 and CO_2-N_2 binary gas systems.

The effect of the gas-gas and gas-polyaniline membrane interactions on transport properties of a binary gas system is clearly seen from Figures 4.53 to 4.55. Due to the permeating gas-gas and permeating gas-polyaniline membrane interactions the actual experimental permeance values in an O_2-N_2, CO_2-O_2 and CO_2-N_2 mixed gas systems were marginally different than the values predicted using the equation 4.19. These phenomena indicated that the contribution of the faster gas to the total permeance is dominating. Hence, development of a more accurate permeation model, involving the characteristic parameters for coupling

and plasticisation effects and concentration polarisation, is recommended in the future work for mixed gas permeation studies through polyaniline membranes.

In order to verify the application limitations of the developed permeation function, a series of mixed gases permeation experiments with different feed gas molar compositions were carried out at the feed pressure of 2 bar (0.2 MPa). The permeance and permeate gas composition data obtained for O_2-N_2 against the molar composition of O_2 in the feed gases were plotted in Figures 4.56.

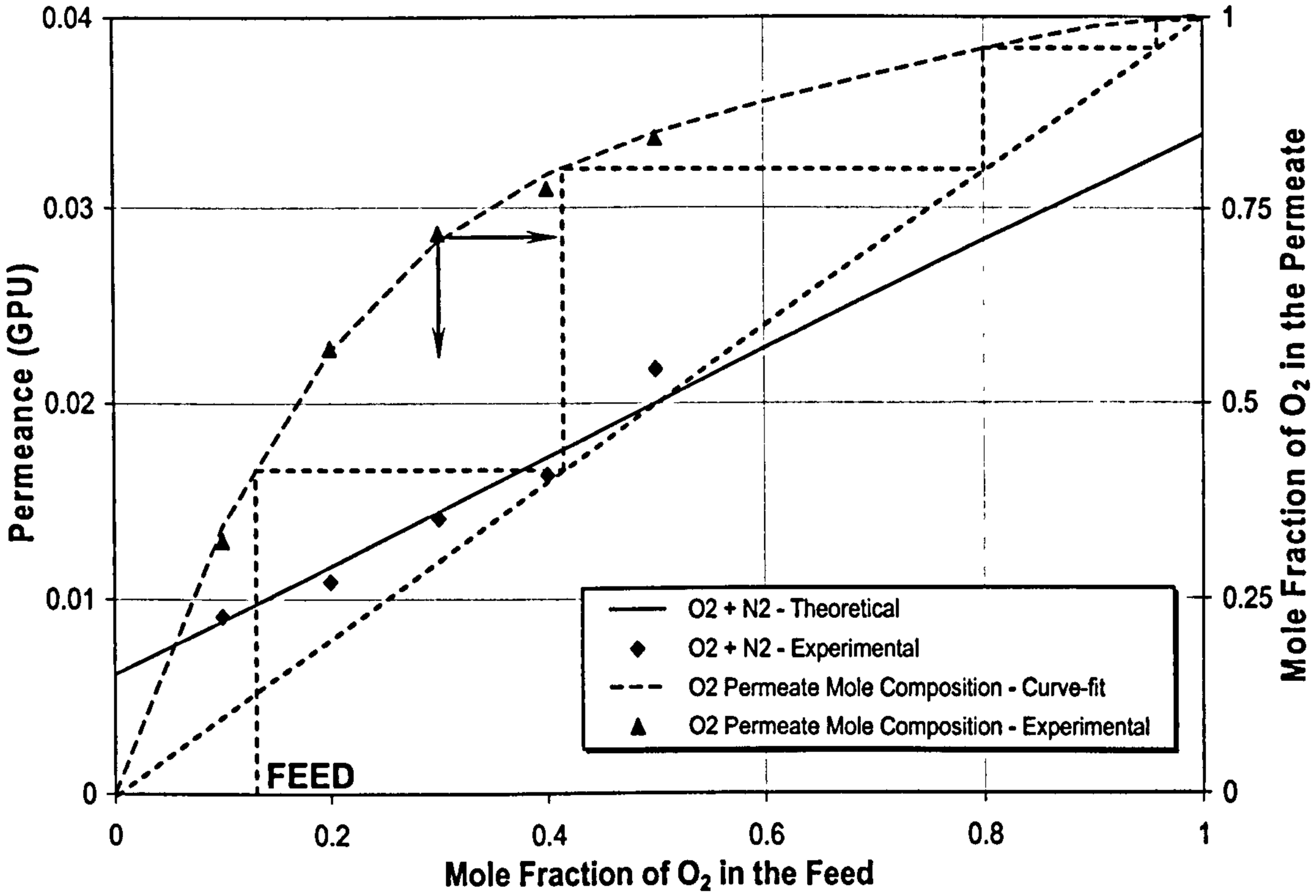

Figure 4. 56 Effect of the molar composition of the feed gases on the total permeance and mole fraction of O_2 in the permeated stream for O_2-N_2 mixed gases.

It is clear from Figure 4.56 that the total permeance and mole fraction of O_2 in the permeate (in O_2-N_2 mixed gas system) increased with increasing the mole fraction of O_2 in the feed. During the O_2-N_2 mixed gas experiment, oxygen permeates five times ($\alpha_{O_2/N_2} \sim 5$) faster than nitrogen through a polyaniline membrane. The molar fraction of oxygen in permeate can be predicted by the following equation (obtained from the mixed gas permeation experiment data);

$$y = -2.66\,x^4 + 7.49\,x^3 - 7.97\,x^2 + 4.15\,x \qquad (4.21)$$

where y = mole fraction of oxygen in the permeate and x = mole fraction of oxygen in the feed gases.

The oxygen composition values in the permeate obtained using equation 4.21 were within 0.03 mole fraction of each experimental run which represents 0.7% error in the predicted values (from equation 4.21). It is recognised that the data over a limited range of O_2 mole fractions in the feed were used to fit equation 4.21, and the limits of the equation are correct (at x = 0, y = 0 and at x = 1, y = 1). The complete curve over x = 0 to x = 1 is given to show the possible variation of mole fraction of oxygen in the permeate, y, over the complete range of mole fraction of oxygen in the feed, x.

Figure 4.57 illustrates the schematics of the polyaniline membrane module cascade with 15 : 85 by moles O_2-N_2 feed gas ratio.

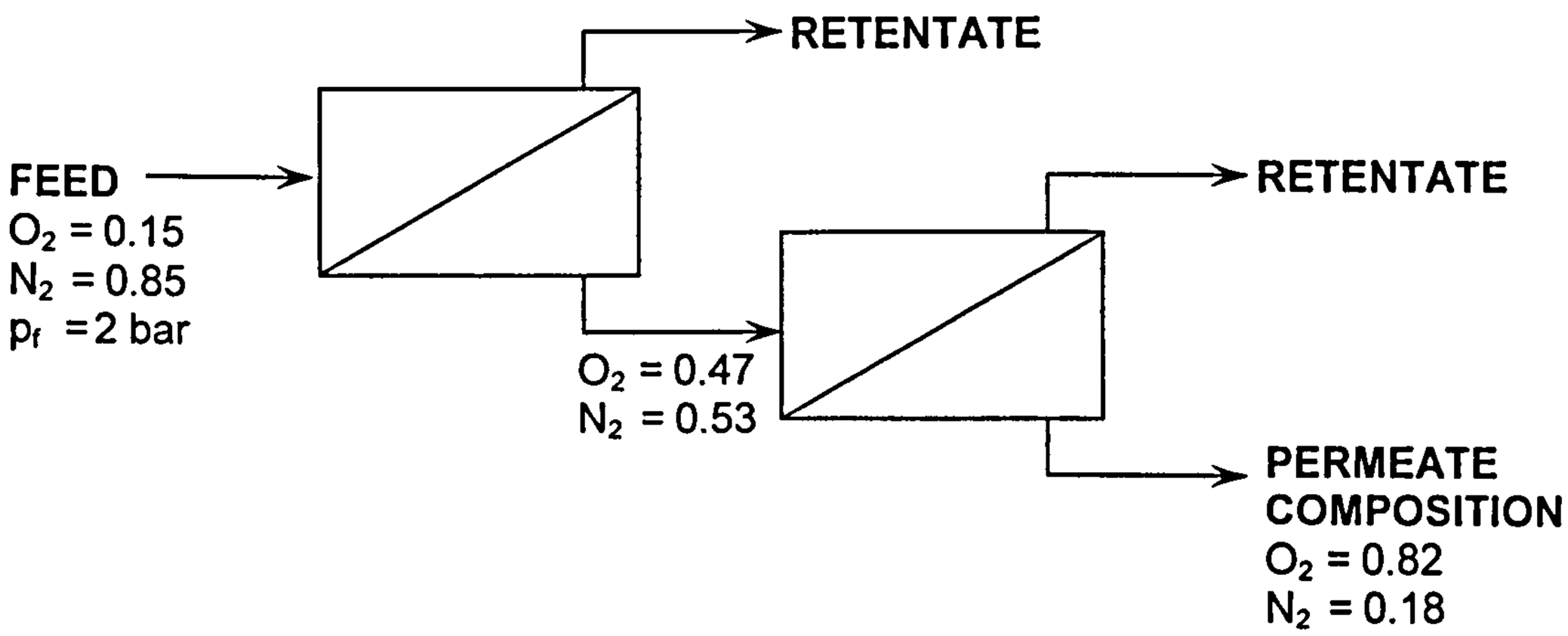

Figure 4. 57 A schematic of a two stage polyaniline membrane module for O_2-N_2 mixed gas system.

The number of membrane module stages in a membrane cascade required to achieve desired permeate oxygen composition can be estimated from a plot similar (see Figure 4.56) to the McCabe-Thiele plot used in distillation. For example, the permeate oxygen composition after the second stage in the module cascade can be calculated using equation 4.21, as the permeate stream from the stage one becomes feed stream for the second module in the cascade.

The stage cut (also defined by the ratio of the permeate flow rate per unit feed flow rate to the membrane module) is a major parameter for separation process design, since it affects the overall retentate and permeate separation factors. The stage cut for a given membrane module can be calculated by equation 4.22;

$$\textit{Stage Cut (SC)} = \textit{Permeate Flow Rate / Feed Flow Rate} \qquad (4.22)$$

A low stage cut means the highest purity of oxygen in the permeate and nitrogen in the retentate; but only small amount of oxygen can be enriched in the permeate (see Table 4.23). For example, the stage cut and oxygen purity in the permeate (mole fraction of O_2 in the permeate) values for self-supported polyaniline membrane (for 15 : 85 by volume O_2-N_2 feed gas mixture) were 1.38×10^{-5} and 0.86, respectively.

Similarly, the permeance and permeate gas composition data obtained for CO_2-O_2 and CO_2-O_2 against the molar composition of CO_2 in the feed gases were plotted in Figures 4.58 and 4.59.

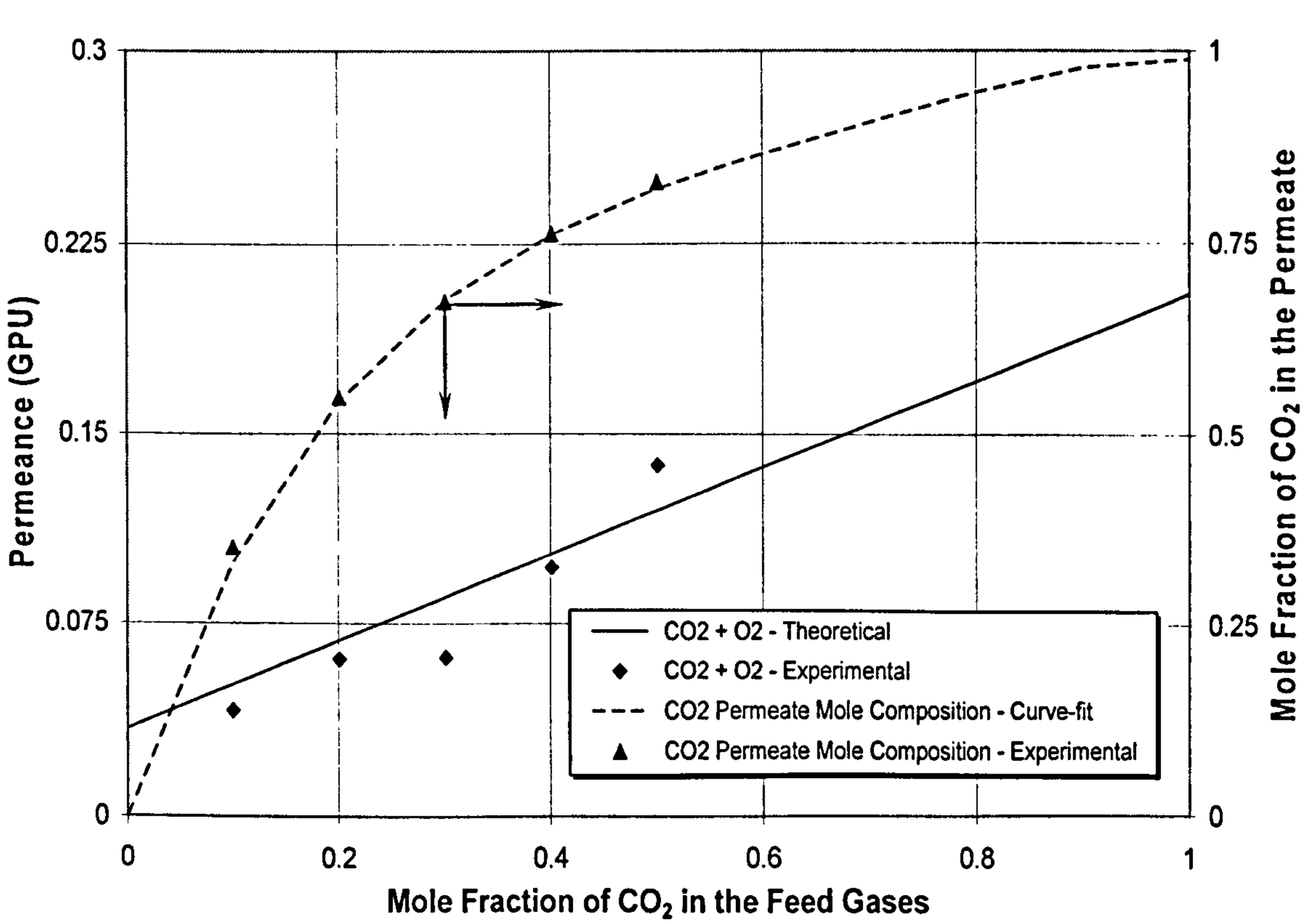

Figure 4. 58 Effect of the molar composition of the feed gases on the total permeance and mole fraction of CO_2 in the permeated stream for CO_2-O_2 mixed gases.

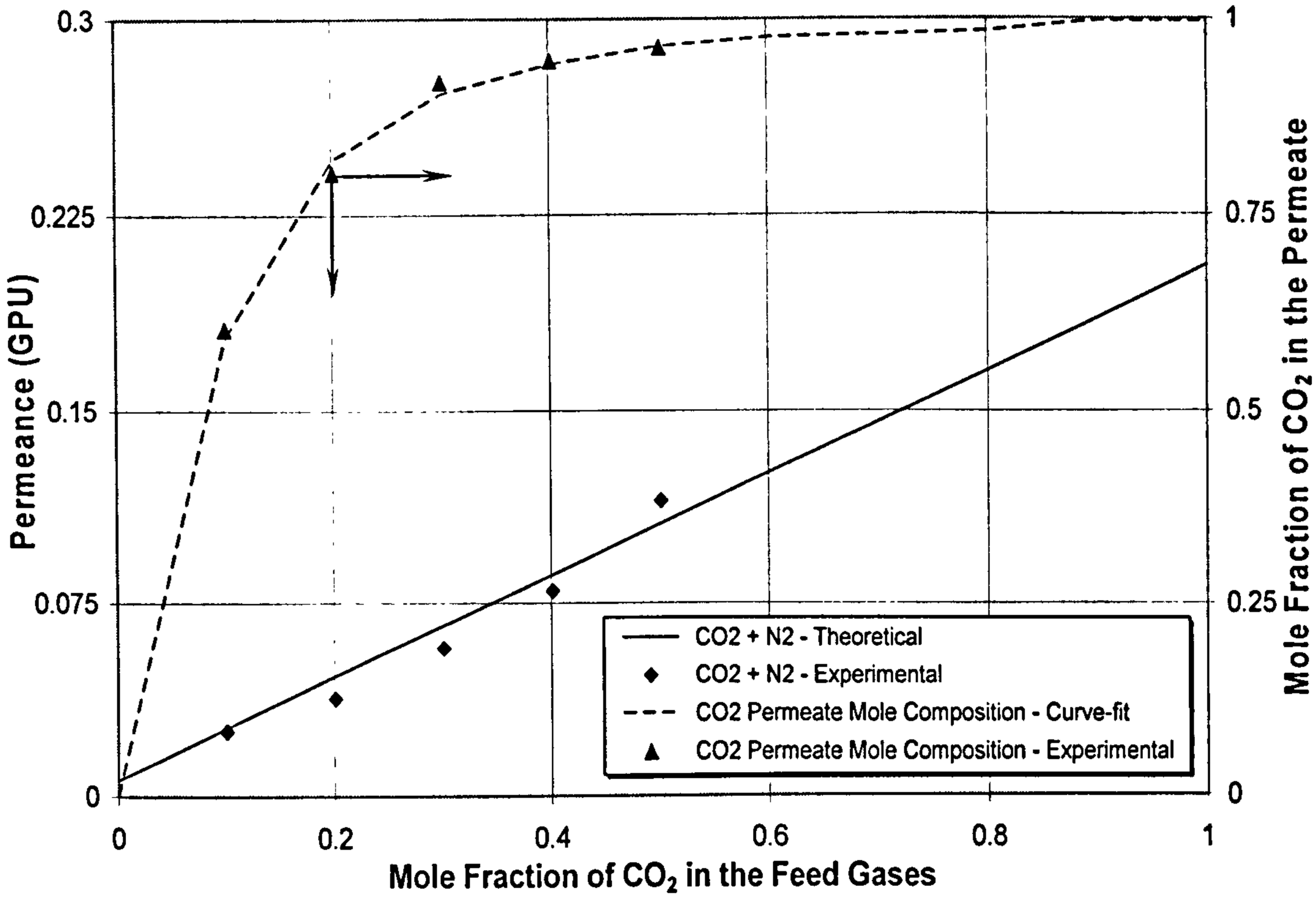

Figure 4. 59 Effect of the molar composition of the feed gases on the total permeance and mole fraction of CO_2 in the permeated stream for CO_2-N_2 mixed gases.

Similar trends, for total permeance and molar composition of CO_2 in the permeate *vs* increasing the molar composition of CO_2 in the feed gases, were observed in the CO_2-O_2, and CO_2-N_2 mixed gas permeation measurements. From the mixed gas permeation measurements, the equations to predict the molar concentration of CO_2 in the permeate for CO_2-O_2 (equation 4.23) and CO_2-N_2 (equation 4.24) mixed gas systems can be written as;

$$y = -2.91\,x^4 - 7.78\,x^3 - 7.88\,x^2 + 3.99\,x \qquad (4.23)$$

$$y = -23.66\,x^6 + 84.39\,x^5 - 121.46\,x^4 + 91.03\,x^3 - 38.25\,x^2 + 8.95\,x \qquad (4.24)$$

where y = mole fraction of CO_2 in the permeate and x = mole fraction of CO_2 in the feed gases for CO_2-O_2 (equation 4.22) and CO_2-N_2 (equation 4.23).

The stage cut values for the CO_2-O_2 and CO_2-N_2 mixed gas systems were calculated to be 8.75×10^{-5} and 7.31×10^{-5}, respectively. The stage cut values obtained for a membrane system for O_2-N_2, CO_2-O_2, and CO_2-N_2 mixed gas separation systems using a self-supported polyaniline membrane were very low,

which may partially explain the reason why polyaniline membranes have not been explored in commercial gas separation processes.

The pure gas and mixed gas selectivities for O_2-N_2, CO_2-O_2, CO_2-N_2 binary gas systems through self-supported polyaniline membranes are summarised in Table 4.21.

Table 4. 21 Pure gas and mixed gas selectivities for O_2-N_2, CO_2-O_2, CO_2-N_2 for self-supported polyaniline membranes.

	Selectivity ($\alpha_{A/B}$)		
	Pure gas (Ideal)	Mixed Gas	
		Mole Fraction	Selectivity
O_2-N_2	5.56	0.1	4.32
		0.2	5.16
		0.3	5.31
		0.4	5.33
		0.5	5.89
CO_2-O_2	6.06	0.1	4.43
		0.2	4.79
		0.3	4.58
		0.4	4.66
		0.5	4.82
CO_2-N_2	33.8	0.1	21.1
		0.2	24.7
		0.3	24.9
		0.4	25.3
		0.5	26.4

Mole Fraction = mole fraction of O_2 for O_2-N_2, and CO_2 for CO_2-O_2 and CO_2-N_2 in the feed gas

It is apparent that the mixed gas selectivity values for the O_2-N_2 binary gas system vary with molar composition of O_2 in the feed. Similarly, the mixed gas selectivities for CO_2/O_2 and CO_2/N_2 were also dependent on the molar composition of CO_2 in the feed gases. The mixed gas selectivity data for O_2-N_2, CO_2/O_2 and CO_2/N_2 binary gas systems are close to the pure-gas selectivity values. This shows that extraordinarily high permeability is not due to the microporous defects in the polyaniline films, as separation occurs. The difference between the mixed gas selectivities and pure gas selectivities was small in the case of the O_2-N_2 binary gas system, whereas it was considerable in the case of CO_2-O_2 and CO_2-N_2 binary gas systems due to the gas-gas interactions (interactions between CO_2 and O_2, and CO_2 and N_2) and gas-membrane (CO_2-polyaniline membrane) interactions. It is important to note that,

for self-supported polyaniline films, the O_2/N_2, and CO_2/O_2 and CO_2/N_2 selectivity values increased with increasing O_2, and CO_2 concentration in the feed gases, respectively.

4.4.4.2. Mixed Gas Permeation Measurements for Undoped Polyaniline/PVDF Composite Membranes

The mixed gas permeation measurement experiments were conducted through the undoped ultrathin polyaniline membranes supported on a porous substrate (selective polyaniline layer thickness = 0.448 μm) for O_2-N_2, CO_2-O_2 and CO_2-N_2 mixed gas systems. In Figures 4.60 to 4.62, the relationship between the mixed gas permeance and the mole fraction of a permeating gas is plotted. The theoretical straight lines in Figures 4.60 to 4.62 correspond to the permeance values calculated using equation 4.19, and the experimental values correspond to the mixed gas permeance measured experimentally.

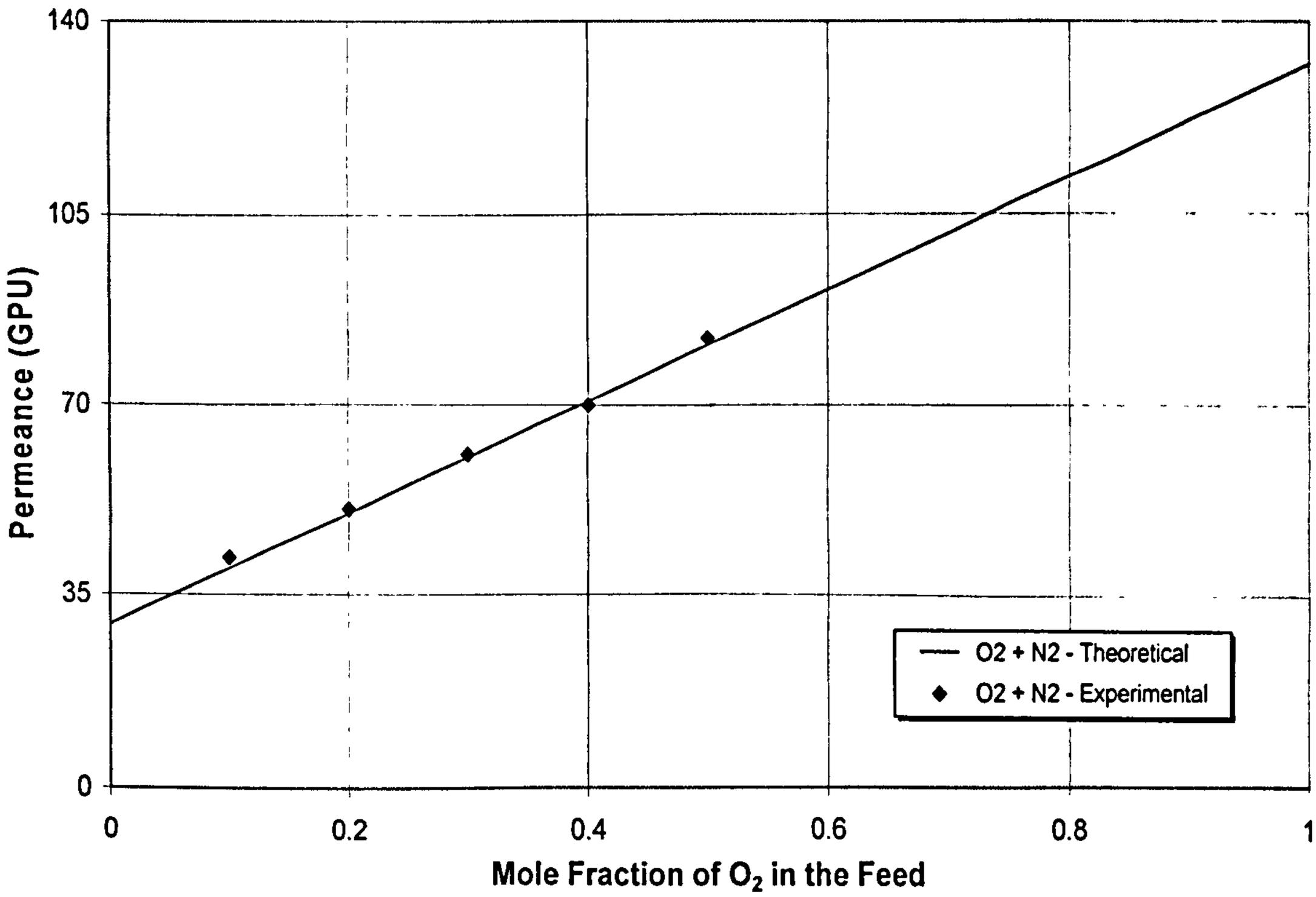

Figure 4. 60 Effect of molar composition of O_2 in the feed gas on the total permeance for O_2-N_2 mixed gases in polyaniline/PVDF composite films.

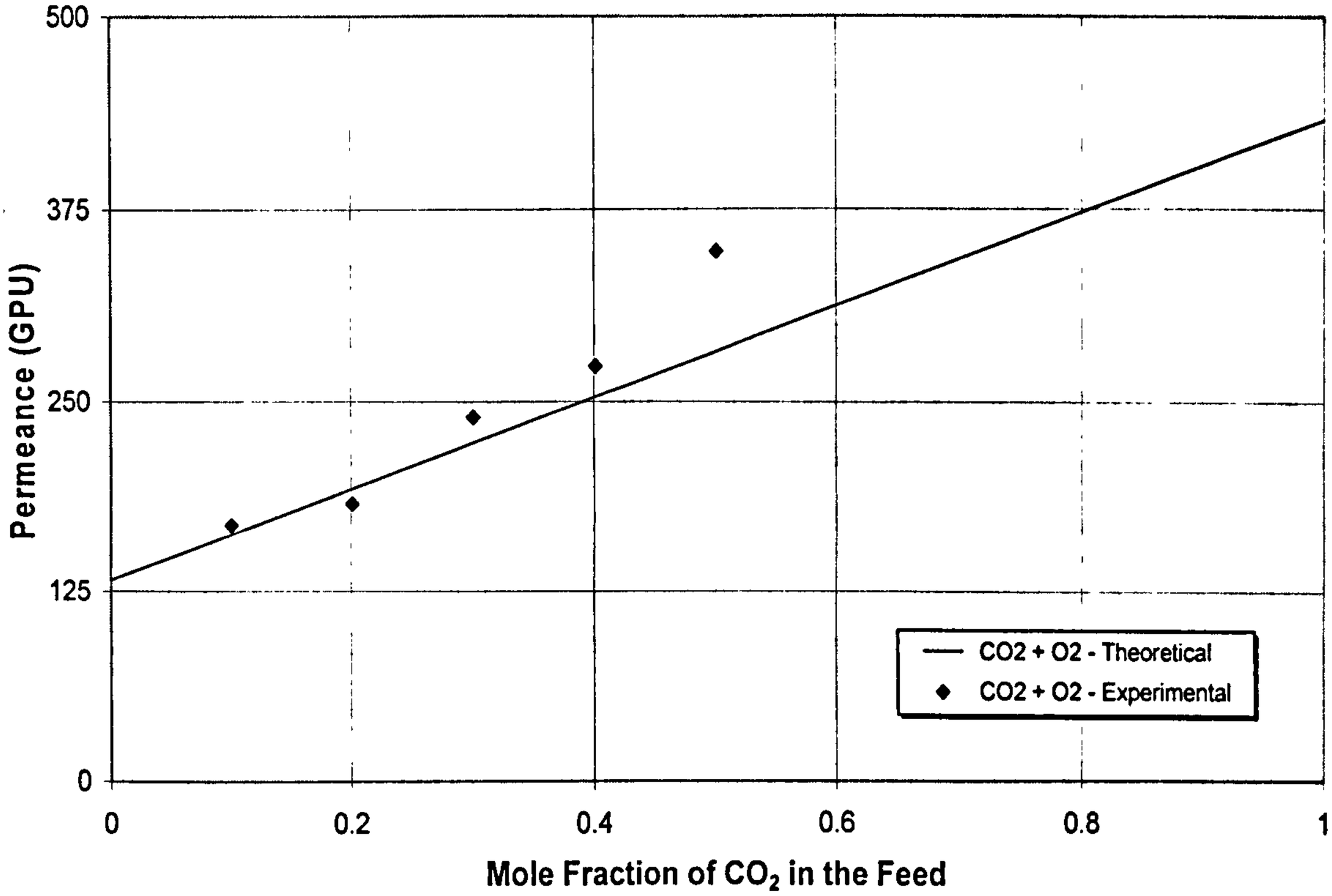

Figure 4. 61 Effect of molar composition of CO_2 in the feed gas on the total permeance for CO_2-O_2 mixed gases in polyaniline/PVDF composite films.

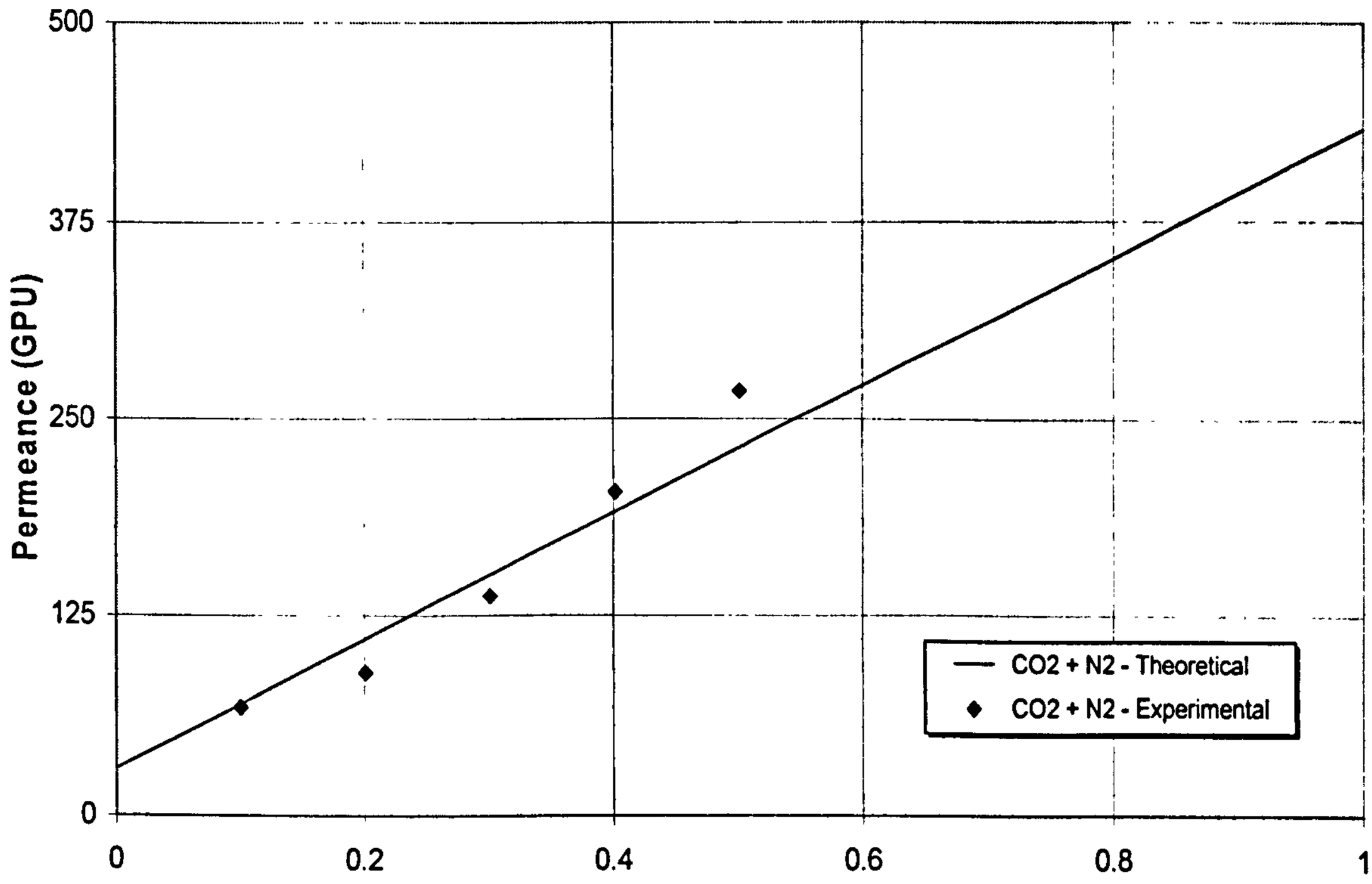

Figure 4. 62 Effect of molar composition of CO_2 in the feed gas on the total permeance for CO_2-N_2 mixed gases in polyaniline/PVDF composite films.

Similar to the results obtained for self-supported polyaniline films, the calculated permeance values using equation 4.19, for polyaniline/PVDF composite membranes, were found to be in good agreement with the experimental data, and the permeation behaviour was dependent on the mixed gases feed composition. The effects of the gas-gas and gas-polyaniline membrane interactions were also seen on transport properties of a binary gas system (for CO_2-O_2 and CO_2-N_2 mixed gas systems) for polyaniline/PVDF composite films. The permeance data measured experimentally were similar for O_2-N_2 mixed gas system, whereas marginally scattered for CO_2-O_2 and CO_2-N_2 mixed gas systems.

A series of binary gas permeation experiments (for O_2-N_2, CO_2-O_2, CO_2-N_2 mixed gas systems) with different molar compositions were conducted at 0.4 bar (0.04 MPa). In Figure 4.63 the permeance and permeate gas composition data, obtained for O_2-N_2 binary gas system, against the molar composition of O_2 in the feed gases are plotted.

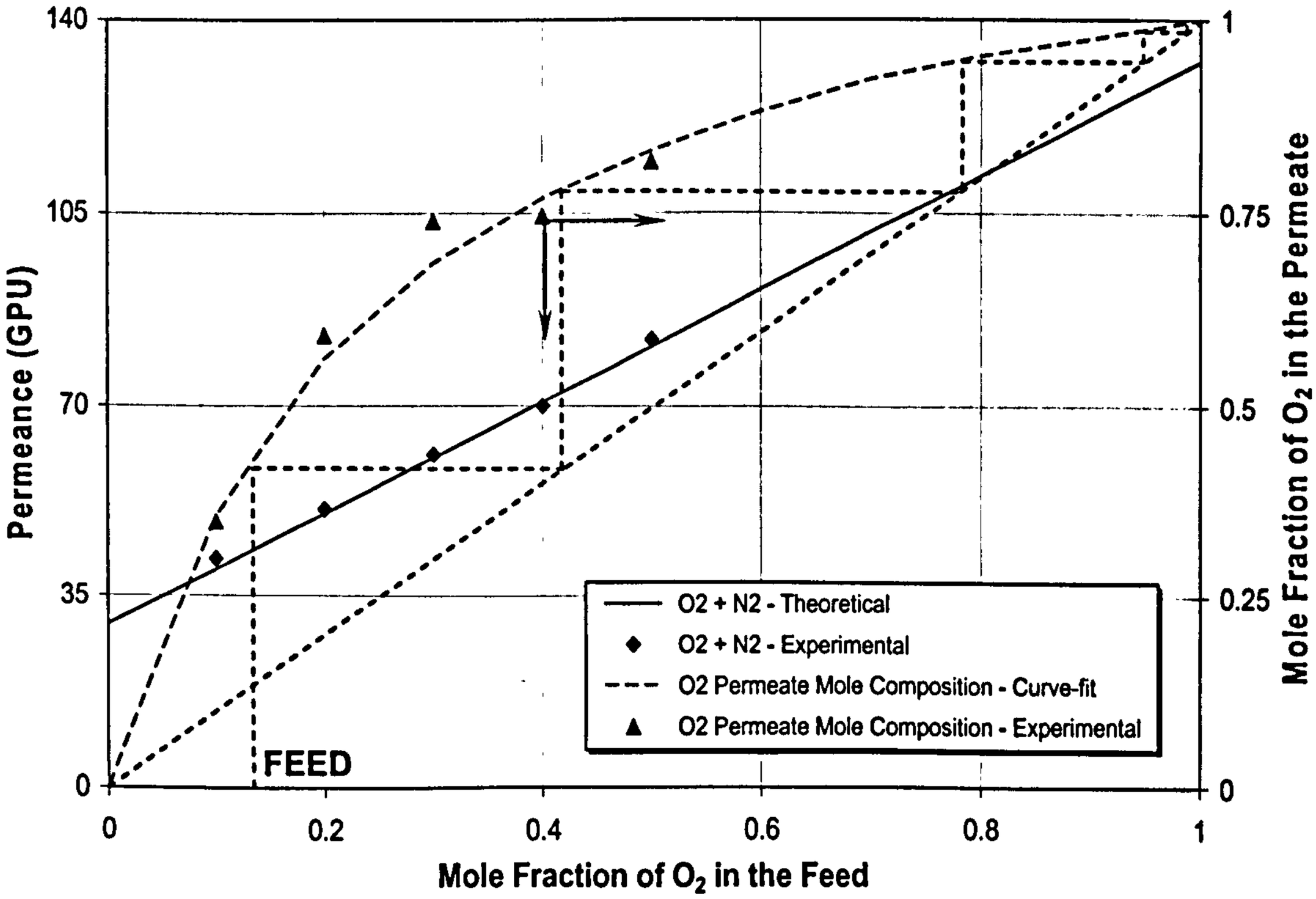

Figure 4. 63 Effect of the O_2 feed gas molar composition on the permeance and mole fraction of O_2 in the permeated stream for O_2-N_2 mixed gases.

From the mixed gas permeation data, the following equation can be developed to predict the mole fraction of the oxygen (product purity) in the permeate stream.

$$y = 4.75\,x^5 - 15.03\,x^4 + 18.76\,x^3 - 12.06\,x^2 + 4.59\,x \qquad (4.25)$$

where y = mole fraction of O_2 in the permeate, and x = mole fraction of O_2 in the feed gases.

For the same O_2 mole concentration in the feed, the number of membrane module stages in a cascade required to achieve a desired permeate oxygen composition when using self-supported polyaniline membrane (see Figure 4.56) and when using ultrathin polyaniline membranes supported on a porous PVDF substrate are similar. However, the total permeance, $P_{O_2+N_2}$, obtained for polyaniline/PVDF composite membranes is 1000 times higher than that of free standing self-supported polyaniline membranes. Hence, substantially higher productivity can be obtained for same number of modules using ultrathin polyaniline membranes for oxygen enrichment having similar product purity.

The stage cuts (calculated from equation 4.22) and oxygen product purity (molar composition of oxygen in the permeate) for 15 : 85 by moles O_2-N_2 feed gas mixture and 0.4 bar (0.04 MPa) upstream pressure for polyaniline/PVDF composite membranes were 0.01047 and 0.799, respectively.

The total permeance (permeation flux of a gas mixture) and permeate gas composition data obtained for CO_2-O_2 and CO_2-N_2 mixed gas systems against CO_2 feed molar composition were plotted in Figures 4.64 and 4.65.

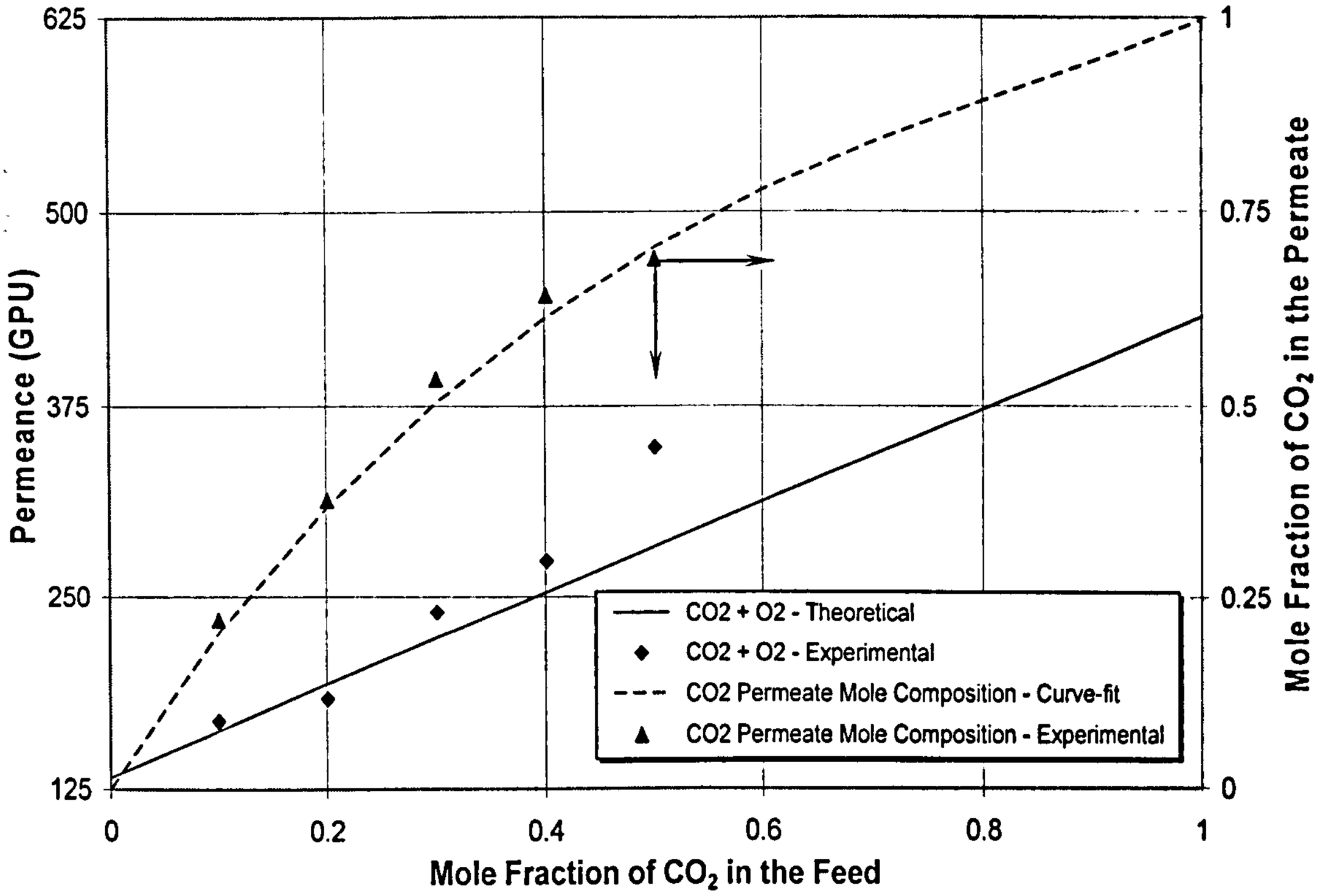

Figure 4. 64 Effect of the CO_2 molar composition in the feed on the permeance and mole fraction of CO_2 in the permeated stream for CO_2-O_2 mixed gases.

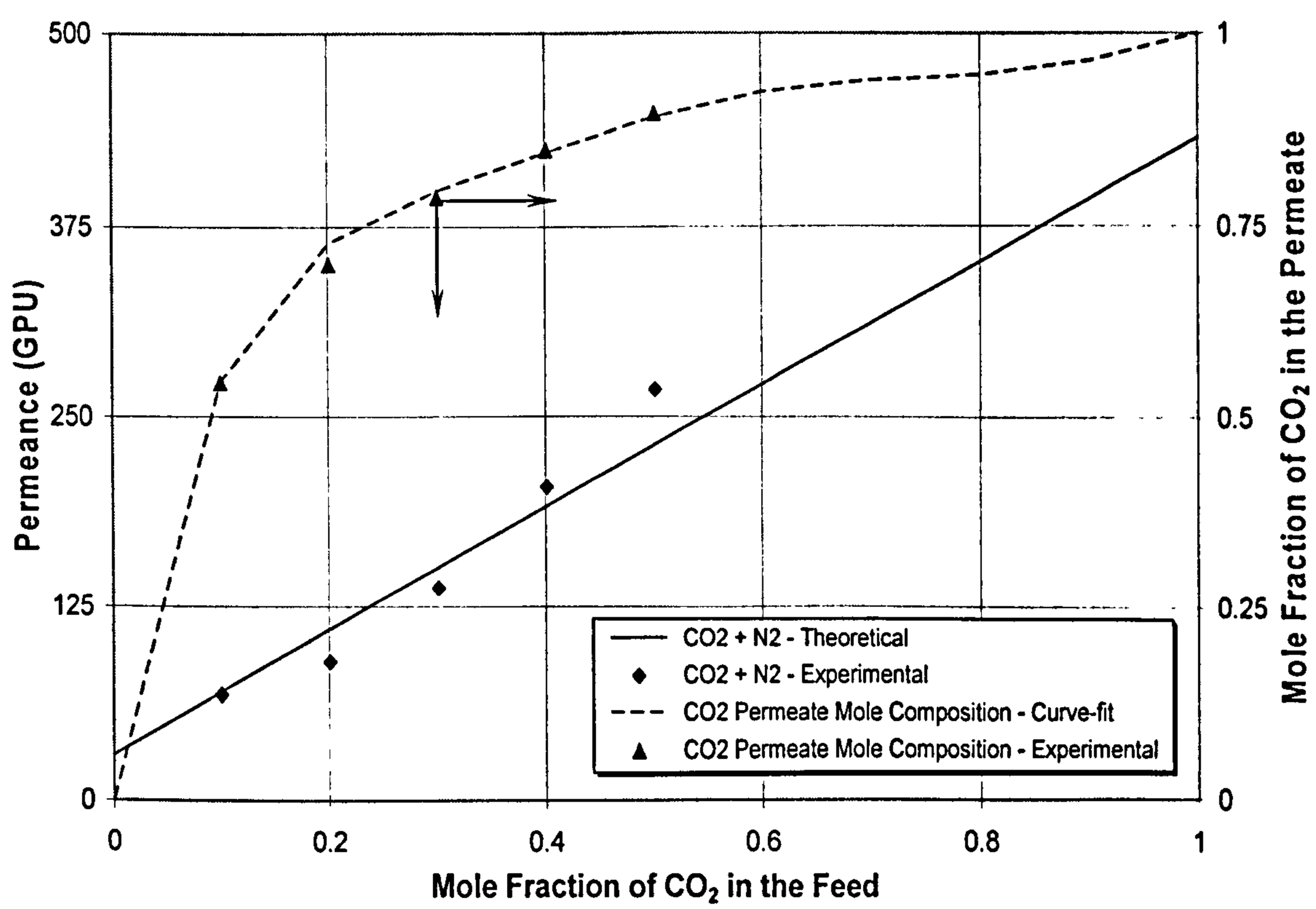

Figure 4. 65 Effect of the CO_2 feed gas molar composition on the permeance and mole fraction of CO_2 in the permeated stream for CO_2-N_2 mixed gases.

The total permeance ($P_{CO_2+O_2}$ and $P_{CO_2+N_2}$) and mole fraction of CO_2 in the permeate increased with increasing the molar composition of CO_2 in the feed gases. The equations to predict the molar concentration of CO_2 in the permeate for CO_2-O_2 and CO_2-N_2 binary gas system can be written (from the mixed gas permeation measurements) as;

$$y = 0.756\,x^3 - 1.96\,x^2 + 2.197\,x \qquad (4.26)$$

$$y = -26.57\,x^6 + 98.02\,x^5 - 142.5\,x^4 + 104.1\,x^3 - 40.63\,x^2 + 8.59\,x \qquad (4.27)$$

The stage cut values for CO_2-O_2 and CO_2-N_2 binary gas systems were calculated to be 0.0443 and 0.0341, respectively.

The pure gas (ideal) and mixed gas selectivities for O_2-N_2, CO_2-O_2, CO_2-N_2 mixed gas systems for polyaniline/PVDF composite membranes are summarised in Table 4.22.

Table 4. 22 Pure gas and mixed gas selectivities for O_2-N_2, CO_2-O_2, CO_2-N_2 for polyaniline/PVDF composite membranes.

	Selectivity ($\alpha_{A/B}$)		
	Pure gas (Ideal)	Mixed Gas	
		Mole Fraction	Selectivity
O_2-N_2	5.08	0.1	4.89
		0.2	4.73
		0.3	4.97
		0.4	5.29
		0.5	5.11
CO_2-O_2	4.13	0.1	2.38
		0.2	2.41
		0.3	2.53
		0.4	2.51
		0.5	2.46
CO_2-N_2	18.08	0.1	10.45
		0.2	9.37
		0.3	10.38
		0.4	11.1
		0.5	11.29

Mole Fraction = mole fraction of O_2 for O_2-N_2, and CO_2 for CO_2-O_2 and CO_2-N_2 in the feed gas

Similar to the results obtained for self-supported polyaniline membranes, the mixed gas selectivity values for O_2-N_2, and CO_2/O_2 and CO_2/N_2 were dependent on the molar composition of O_2, and CO_2 in the feed gases. Due to the gas-gas and gas-membrane interactions, the mixed gas selectivity values were marginally different than pure gas (ideal) selectivity values.

In Table 4.23 the stage cut and selectivity values for O_2-N_2, CO_2-O_2 and CO_2-N_2 binary gas systems for both self-supported polyaniline membranes and polyaniline/PVDF composite membranes were compared to examine the effect of polyaniline film thickness on the productivity and product purity.

Table 4. 23 A comparison of stage cut and selectivity values for O_2-N_2, CO_2-O_2 and CO_2-N_2 binary gas systems for self-supported polyaniline and polyaniline/PVDF composite membranes.

	Stage Cut (SC)				Selectivity ($\alpha_{A/B}$)			
	A		B		A		B	
	MF	SC ($x\ 10^5$)	MF	SC	MF	$\alpha_{A/B}$	MF	$\alpha_{A/B}$
O_2-N_2	0.1	0.579	0.1	0.0053	0.1	4.32	0.1	4.89
	0.2	0.693	0.2	0.0065	0.2	5.16	0.2	4.73
	0.3	0.897	0.3	0.0078	0.3	5.31	0.3	4.97
	0.4	1.037	0.4	0.0089	0.4	5.33	0.4	5.29
	0.5	1.382	0.5	0.0105	0.5	5.89	0.5	5.11
CO_2-O_2	0.1	2.608	0.1	0.0215	0.1	4.43	0.1	2.38
	0.2	3.883	0.2	0.0233	0.2	4.79	0.2	2.41
	0.3	3.924	0.3	0.0305	0.3	4.58	0.3	2.53
	0.4	6.195	0.4	0.0348	0.4	4.66	0.4	2.51
	0.5	8.751	0.5	0.0443	0.5	4.82	0.5	2.46
CO_2-N_2	0.1	1.584	0.1	0.0087	0.1	21.1	0.1	10.45
	0.2	2.380	0.2	0.0114	0.2	24.7	0.2	9.37
	0.3	3.633	0.3	0.0175	0.3	24.9	0.3	10.38
	0.4	5.076	0.4	0.0259	0.4	25.3	0.4	11.1
	0.5	7.307	0.5	0.0341	0.5	26.4	0.5	11.29

A self-supported polyaniline membranes
B polyaniline/PVDF composite membranes
MF mole fraction of O_2 for O_2-N_2, and CO_2 for CO_2-O_2 and CO_2-N_2 in the feed gas

Clearly, the thickness of the selective polyaniline layer seemed to have an effect on the productivity and product purity of the permeating gas mixture. The stage cut values obtained for O_2-N_2, CO_2-O_2 and CO_2-N_2 binary gas systems for ultrathin polyaniline membranes were significantly higher than the values obtained for self-supported polyaniline films. A number of membrane module stages in a membrane cascade required to achieve a desired permeate

composition for self-supported polyaniline membranes and for ultrathin polyaniline membranes supported on a porous PVDF substrate are similar. However, the productivity obtained for polyaniline/PVDF composite membranes is 1000 times higher than that of free standing self-supported polyaniline membranes.

The mixed gas selectivity values for self-supported polyaniline membranes and polyaniline/PVDF composite membranes are dependent on the molar composition of the feed gases. The difference between the mixed gas selectivities and pure gas selectivities was small in the case of O_2-N_2 binary gas system, whereas it was considerable in the case of CO_2-O_2 and CO_2-N_2 binary gas systems due to the gas-gas interactions (interactions between CO_2 and O_2, and CO_2 and N_2) and gas-membrane (CO_2-polyaniline membranes) interactions.

The permeance values calculated from equation 4.19 were found to be in a good agreement with the experimental data. The total permeation flux of O_2-N_2 mixed gas system increased with increasing the mole fraction of O_2 in the feed gases for both self-supported polyaniline and polyaniline/PVDF composite membranes. However, in the case of CO_2-O_2 and CO_2-N_2 binary gas systems, an increase in the total permeance does not follow the linear relationship with CO_2 feed concentration due to gas-gas interactions (interaction between CO_2-O_2 and CO_2-N_2) and CO_2-polyaniline membrane interactions. It is thought that the polar gas (CO_2) induced swelling of the polyaniline films, leading to the higher diffusion coefficient of the permeating gas mixture containing CO_2. These phenomena indicated that the contribution of the faster gas to the total permeance is dominating.

The model suggested earlier is good for achieving the accurate productivity (from equation 4.19) and product purity (from curve fit equations) values for a binary gas permeation experiments in which there are no interactions between the gases, and no special gas-polymer interactions in the presence of the second gas. However, for the gas mixtures containing one or more plasticising gases, the development of a more accurate permeation model, involving the characteristic parameters for coupling and plasticisation effects and concentration polarisation, is recommended for mixed gas permeation studies through polyaniline membranes in the future work.

Chapter 5

CONCLUSIONS & FUTURE WORK

1. CONCLUSIONS

1.1. Synthesis of Polyaniline

Polyaniline was chemically synthesised by the polymerisation of aniline in the presence of *p*-toluene sulfonic acid (*p*-TSA) using ammonium peroxodisulfate. In this research, the effect of reaction parameters such as starting reaction mixture pH, oxidant to aniline molar ratio, oxidation addition time, total reaction time, and polymerisation reaction temperature on the percentage yield, molecular weight and physical, chemical and as well as transport properties of polyaniline were investigated.

The highest polyaniline yield was obtained for the polymerisation reactions at the starting reaction solution pH of +1.0. Polyaniline yield dropped slightly for the pH values below +1.0 and sharply for the reaction solution pH above +1.5. Hence, the optimum starting reaction pH found to be was +1.0.

The polymer (polyaniline) yield increased with the use of larger amount of oxidant. The highest polyaniline percentage yield was monitored for the oxidant to aniline molar ratio of 1.20. This was due to the concentration of radical cation increased with increasing the amount of the oxidant. However, the polyaniline percentage yield dropped sharply for the oxidant to aniline ratio higher than 1.20. The excess oxidising agent decomposed the polyaniline to colourless low molecular weight products of the quinone type, and the yield of the polyaniline (EB) reduced.

The polyaniline yield also increased when the polymerisation reaction temperature was reduced. Lower reaction temperature increases the dielectric constant and this favours the production of higher molecular weight polyaniline than at room temperature, which accounts to the higher polymer yield. The percent yield increased only slightly with increasing the oxidant addition from

instantaneous addition to 8 hours. The minimum reaction time of about 15 hours was necessary for the polymerisation reactions below 0 C, whereas about 4 to 6 hours was sufficient at 0 C. The polyaniline percent yield increased only slight for the polymerisation reactions with oxidant addition time more than 4 hours and total reaction time more than 24 hours.

1.2. Characterisation of Polyaniline Powder

The as-synthesised polyaniline powder was characterised by the various polymer characterisation techniques including FTIR spectroscopy, UV-Vis spectroscopy, FEGSEM, density measurements, gel permeation chromatography.

The infrared transmittance spectra for polyaniline powder produced at different polymerisation reaction temperatures were similar to the polyaniline FTIR spectra obtained by other researchers, which endorsed the fact that the polymer synthesis route was correct and the produced polymer was pure. The ratio of quinoid rings to benzenoid rings for polyaniline was calculated from the FTIR transmittance peaks at 1580 and 1508 cm^{-1}. A ratio of quinoid/benzenoid of 0.5 to 0.53 attributed that some of the polyaniline batches contain more benzenoid rings than quinoid rings. The amount of CO_2 present increased with decreasing the polymerisation reaction temperature, which accounts for the higher transport rates of CO_2 observed through polyaniline membranes in the gas permeation experiments.

The optical absorption and exciton absorption of polyaniline was found to depend on the concentration of the polyaniline in the solvent (NMP). The UV-Vis spectra of all polyaniline samples prepared in NMP showed that at least two major absorption peaks existed in all UV-Vis spectra. The first band at ~640 nm is an indicative of a charge-transfer exciton-like transition from the highest occupied levels on benzenoid rings to the lowest occupied energy levels on quinoid rings. The second band at ~320 nm can be attributed to $\pi - \pi^*$ transition associated with the π electrons of the benzene ring. A relative intensity ratio of the peak at 640 nm to the peak at 320 nm (also known as quinoid/benzenoid ratio) was calculated from the polyaniline UV-Vis spectra. The quinoid/benzene

ratio values obtained through UV-Vis spectra were similar to the values obtained in FTIR analysis.

The morphology of the polyaniline powder was determined by the field emission scanning electron microscope (FEGSEM). Polyaniline prepared at higher temperature was obtained as a fluffy emeraldine blue powder, whereas that produced at sub-ambient temperatures was a macro-porous material. The FEGSEM images revealed that the crystallinity of polyaniline powder increased when the polymer was produced at reduced polymerisation reaction temperature.

The density of the various polyaniline batches prepared at our laboratory was measured by pycnometer. The density values of emeraldine salt form of polyaniline were higher than undoped (emeraldine base) polyaniline samples. This was because of the polymer chains contained small amount of *p*-toluenesulfonate atoms on C_6 rings. In addition to that, the density of the emeraldine base samples increased with lowering the polymerisation reaction temperature. This was because of the presence of LiCl (added for the polymerisation reactions at sub-ambient temperatures) increased the amount of ring chlorination, which accounted for the higher polymer density at lower polymerisation reaction temperature.

The weight-average and number-average molecular weight of the various polyaniline batches were calculated from the GPC chromatographs. The molecular weight of the polyaniline decreased with increasing polymerisation reaction temperature due to condensation of radical cation species which lose protons to give protonated emeraldine form. The lower polymerisation reaction temperature increases the dipole moment and this favours the production of higher molecular weight polyaniline compared to material prepared at ambient temperature.

1.3. Polyaniline Membranes

A novel method was developed to make reproducible defect-free self-supported polyaniline films with thicknesses between 2 and 6 μm, and polyaniline nano-film membranes with selective polyaniline layer thicknesses between 300 and 800 nm supported on a highly porous substrate (polyvinylidene fluoride). The mechanical and gas transport properties of free standing undoped

self-supported polyaniline films and polyaniline/PVDF composite membranes were investigated.

1.4. Characterisation of Polyaniline Membranes

The morphology (structure and thickness) of the self-supported polyaniline membranes was examined by the FEGSEM image analysis, and the continuity of the dense selective polyaniline layer in polyaniline/PVDF composite membrane was measured by the atomic force microscope (AFM). The sectional analysis of polyaniline nano-film membrane with AFM, for a scanned area, revealed that the layer had structural dips up to 5 nm and peaks up to 6 nm, which are orders of magnitude smaller than the total selective polyaniline layer thickness. This provided the evidence that the polyaniline prepared on PVDF substrate was continuous, dense and defect-free over the scanned area.

The mechanical properties of self-supported polyaniline membranes prepared from various polyaniline samples (prepared at various polymerisation reaction temperatures) were examined. The strength and toughness as measured by tensile strength and elongation break for polyaniline film samples increased with the molecular weight and crystallinity of the polymer (observed for the polyaniline samples prepared at sub-ambient polymerisation reaction temperature).

The permeation rate of a permeating gas through a polyaniline film was measured by an integral permeation method. The effect of selective polyaniline membrane thickness on the productivity (pressurised normalised flux) and the separation efficiency was investigated.

Various undoped self-supported polyaniline (EB) films (polyaniline film thicknesses between 2 and 6 μm), and polyaniline/PVDF composite membranes (selective polyaniline layer thicknesses between 300 and 800 nm) were tested to measure their transport properties for various pure gases such as H_2, CO_2, O_2, N_2, CH_4, C_2H_4, C_2H_6, C_3H_6 and C_3H_8. The permeability of selected test gases (H_2, CO_2, O_2, N_2 and CH_4) through undoped polyaniline (EB) films essentially followed a size dependent (kinetic diameter) relationship, that is;

$$H_2\ (2.89\ Å) > CO_2\ (3.30\ Å) > O_2\ (3.46\ Å) > N_2\ (3.64) > CH_4\ (3.80\ Å)$$

However, for the plasticising gases (C_2H_4, C_2H_6, C_3H_6 and C_3H_8) the permeability through undoped polyaniline membranes did not follow the size dependent relationship. According to the kinetic diameters of the permeating gases the permeability order should have been:

$$C_2H_4\ (3.90\ Å) > C_3H_8\ (3.96\ Å) > C_2H_6\ (4.0\ Å) > C_3H_6\ (4.40\ Å)$$

and the permeability order through polyaniline membranes observed to be was:

$$C_2H_4\ (3.90\ Å) > C_3H_6\ (4.40\ Å) > C_2H_6\ (4.0\ Å) > C_3H_8\ (3.96\ Å)$$

This was because of a relatively higher solubility of ethylene and propylene in the polyaniline membranes than ethane and propane. The propylene dissolves more in polyaniline than ethane and propane, and therefore the calculated permeability for propylene was higher than ethane and propane.

The ideal (pure gas) selectivities ($\alpha_{A/B}$) obtained for the gas pairs H_2/N_2 (348), H_2/O_2 (69.5), H_2/CO_2 (8.6), CO_2/O_2 (8.1), CO_2/N_2 (40.4), H_2/C_3H_8 (757), CO_2/C_3H_8 (256), in the case of undoped self supported polyaniline films, surpassed the selectivities of the majority of the conventional polymeric materials. The results obtained during this work were reproducible for both self-supported polyaniline films and ultrathin polyaniline films supported on porous PVDF substrate.

The thickness of the polyaniline membrane seemed to have an affect on the permeability of the permeating gases. The permeability obtained for all permeating gases were significantly higher in the case of ultrathin polyaniline membranes. The permeability increased almost linearly with decreasing polyaniline film thickness. However, the pure gas selectivity values for various gas pairs through ultrathin polyaniline membranes supported on porous PVDF substrate (selective polyaniline layer thickness between 0.4 and 1.37 μm) were similar to those of self-supported polyaniline membranes (selective polyaniline film thickness between 2 and 3 μm). Extraordinarily high gas transport rates (GTR) were observed for polyaniline based nano-membranes. GTR for various

gases were higher in the magnitude of 10^4 than those reported for self-supported polyaniline membranes.

From the industrial point of view productivity can be significantly increased by using ultrathin polyaniline membranes having higher productivity (permeance) and similar separation efficiency for various gas pairs.

2. RECOMMENDATIONS FOR FUTURE WORK

2.1. Polyaniline Synthesis

The organic acids such as 2-6 naphthalene disulfonic acid, 4-5 dihydroxy 2-7 naphthalene disulfonic acid, anthraquinone 2-6 disulfonic acid can be used as dopants during the synthesis. During the polymerisation of aniline, protonating all the imine nitrogens in the polyaniline backbone, requires the conjugate base of the doping acid to act as a counterion to maintain electroneutrality in the salt polyaniline. The close association of this with the polymer backbone means that the polymer microstructure must distort to accommodate the extra mass. This distortion remains after the removal of the counterion with ammonium hydroxide. *The use of the strong organic acids which are active on their both ends as a dopant is recommended in the polyaniline synthesis, which can bridge the polyaniline polymer chains (also known as "ladder cross-linking"), and increase the free volume within the polyaniline matrix.*

The GPC was used to calculate the molecular weight of the polyaniline samples prepared at various polymerisation reaction temperatures. The primary calibration curve of monodispersed polystyrene was analysed using the peak position method and the molecular weight of the polyaniline sample was calculated from the calibration curve. The higher column temperature was required for the GPC analysis because the polystyrene standards do not dissolve well in NMP. *For this reason, polyvinlypyridine standards, which are more soluble and give a better straight line fit for the graph of log (molecular weight) vs retention time, are recommended for the future GPC analysis to measure the molecular weight of polyaniline.*

2.2. Polyaniline Membranes

Self-supported polyaniline membranes were fairly impermeable compared to other polymer membrane materials, so the application potential for gas selective polyaniline membranes has been limited. To further extend the use of polyaniline membranes for industrial applications, one must find the way to enhance the productivity (permeance) and the separation efficiency. *Nano-composite materials can be incorporated in the free standing polyaniline films to achieve higher permeation rates of permeating gases.* In this research, however, the concept of ultrathin polyaniline films to increase the productivity of permeating gases was explored. It was often challenging to develop the defect-free dense ultrathin polyaniline layer on a highly porous polymer substrate; environmental dust, membrane cooking time, and cooking rate may create defects in the polyaniline layer. *The effect of membrane cooking (and annealing) time and cooking temperature on the gas transport properties may be investigated in order to understand the effect of degree of crosslinking on the gas permeability. The method, developed in our research, resulted in 60% of the ultrathin polyaniline membranes made being defect-free. To plug the micro-porous defects a thin layer of polysiloxanes can be developed on the selective polyaniline layer.*

The membrane process using the concept of facilitated transport has been considered to be an energy-saving process to separate olefins from paraffins. The permselectivities of natural and synthetic membranes can be increased by several orders of magnitude in the presence of mobile carriers, which are considered to remain within the membrane and which react reversibly and selectively with desired permeant. Remarkable separation performance of olefin/paraffin mixtures was previously reported by facilitated olefin transport through silver-based polymer membranes using the concept of facilitated transport. Since polyaniline is a dopable conjugated polymer it can be doped with Group I-B metal ions, such as silver (Ag(I)), to facilitate transport of olefins through polyaniline films. *The effect of doping, dedoping and controlled redoping of silver on the permeation rate and separation efficiency of ethylene over ethane and propylene over propane should be investigated.*

To develop the detailed permeation model explaining the diffusion of individual and mixed gas transport through polyaniline membranes for various

permeating gases, more experiments (for both, single and mixed gas permeation system) at higher feed side pressure (i.e. for the pressure range of 10 to 50 bar (1 to 5 MPa)) can be done. *A permeation model needs to be developed together with the sorption isotherms of ethylene, ethane, propylene and propane to calculate the solubility of permeating gases through polyaniline membranes.*

Chapter 6

LIST OF REFERENCES

1. Nollet, J.A. (1748), "Investigation on the causes for the ebullition of liquids", *Histoire de L'Académie Royale des Sciences,* **Année MDCCXLVIII**, 57.
2. Graham, T. (1829), "Notice of the singular inflation of bladder", *Quarterly J. Sci.*, **Vol. II**, 88.
3. Graham, T. (1833), "On the law of the diffusion of gases", *The London & Edinburgh Philosophical magazine and J. Sci.*, **Vol. II**, 175-190, 269-276, 351-358.
4. Daynes, H.A., Shakespear, G.A. (1920),"The theory of the katharometer", *Proc. Roy. Soc., Series A*, **97**, 273.
5. Daynes, H.A. (1920), "The process of diffusion through a rubber membrane", *Proc. Roy. Soc., Series A*, **97**, 286.
6. Mitchell, J.K. (1831), "On the penetrativeness of fluids", *Roy. Inst. Journ.*, **II**, 101-118, 307-321.
7. Mitchell, J.K. (1833), "On the penetration of gases", *Amer. J. Med. Sci.*, **VII**, 100.
8. Graham, T. (1863), "On the absorption and dialytic separation of gases by colloid septa", *Phil. Mag.*, **XXXII**, 401.
9. Meares, P. (1954), "The diffusion of gases through polyvinyl acetate", *J. Am. Chem. Soc.*, **76**, 3415.
10. See for example, the reviews given in Crank J., Park, G.S. (1968), *Diffusion in Polymers*, Academic Press, NY.
11. Leob, S., Sourirajan, S. (1962) "Sea water demineralization by means of an osmotic membrane", *Adv. Chem. Ser.*, **38**, 117.

12. Pinnau, I., Freeman, B.D. (1999), "Formation and modification of polymeric membranes: Overview in membrane formation and modification", in: *ACS Symposium Series 744*, I., Pinnau, B.D., Freeman, (Eds.), American Chemical Society: Washington, DC.
13. Koros, W.J., Pinnau, I. (1994), "Membrane formation for gas separation processes", in: *Polymeric Gas Separation Membranes*, D.R. Paul, Y.P. Yampol'skii (Eds.), CRC Press, Boca Raton, FL, pp 209.
14. Baker, R.W. (2002), "Future directions of membrane gas separation technology", *Ind. Eng. Chem. Res.*, **41**, 1393.
15. Rousseau, R.W. (1987), *Handbook of Separation Process Technology*, John Wiley & Sons, NY.
16. Koros, W.J., Fleming, G.K. (1993), "Membrane based gas separation", *J. Memb. Sci.*, **83**, 1.
17. Gottschlich, D.E., Roberts, D.L. (1990), "Energy minimization of separation processes using conventional/membrane hybrid systems". *DOE Report* – DE-AC-07-761D01570.
18. Hughes, R.D., Mahoney, J.A., Steigelmann, E.F. (1986), "Olefin separation by facilitated transport", in: *Recent Developments in Separation Science*, Vol-9, Li, N.N., Calo, J.M. (Eds.), CRC Press, Boca Raton, FL, pp 173.
19. Way, J.D., Noble, R.D. (1992), "Facilitated Transport", in: *Membrane Handbook*, W.S. Ho, K.K., Sirkar (Eds.), Van Nostrand, NY.
20. Eldridge, R.B. (1993), "Olefin/paraffin separation technology: A review", *Ind. Eng. Chem. Res.*, **32**, 2208.
21. Teramoto, M., Matsuyama, H., Yamashiro, T., Katayama, Y. (1986), "Separation of ethylene from ethane by supported liquid membranes containing silver nitrate as carrier", *J. Chem. Eng. Jpn.*, **19**, 419.
22. Kawakami, M., Tateishi, M., Iwamoto, S. (1987), "Selective permeation of ethylene and propylene through Rh(III)-polyethylene glycol liquid membranes", *J. Memb. Sci.*, **30**, 105.
23. Teramoto, M., Matsuyama, H., Yamashiro, T., Okamoto, S. (1989), "Separation of ethylene from ethane by a flowing liquid membrane using silver nitrate as a carrier", *J. Memb. Sci.*, **45**, 115.

24. Tsou, D.T., Blachman, M.W., Davis, J.C (1994), "Silver-facilitated olefin/paraffin separation in liquid membrane contactor system". *Ind. Eng. Chem. Res.*, **33**, 3209.

25. LeBlanc, O.H., Ward, W.J., Matson, S.L., Kimura, S.G. (1980), "Facilitated transport in ion-exchange membranes", *J. Memb. Sci.*, **6**, 339.

26. Hughes, R.D., Mahoney, J.A., Steigelmann, E.F. (1981), "Olefin separation by facilitated transport membranes", 90th AIChE National Meeting, Houston, TX. Pre-print No.1D.

27. Kraus, M.A. (1986), "Water-free hydrocarbon separation membrane and process", US Patent No. 4,614,524.

28. Kovel, C.A., Spontarelli, T. (1988), "Condensed phase facilitated transport of olefins through an ion-exchange membrane", *J. Am. Chem. Soc.*, **110**, 293.

29. Kovel, C.A., Spontarelli, T. (1988), "Facilitated transport of liquid phase olefins through perfluorosulfonate ionomer membranes", *Polym. Mater. Sci. Eng.*, **59**, 132.

30. Shukla, S.K., Pinemann, K.V. (1989), "1-butene/n-butane separation using fixed carrier membranes", Pre-prints of 6th International Symposium on Synthetic Membranes in Science and Industry. Tübingen, Germany.

31. Kovel, C.A., Spontarelli, T., Noble, R.D. (1989), "Styrene/ethylbenzene separation using facilitated transport through perfluorosulfonate ionomer membranes", *Ind. Eng. Chem. Res.*, **28**, 1020.

32. Ilinitch, O.M., Semin, G.L., Chertova, M.V., Zamaraev, K.I. (1992), "Novel polymeric membranes for separation of hydrocarbons", *J. Memb. Sci.*, **66**, 1.

33. Kovel, C.A., Spontarelli, T., Noble, R.D., Thoen, P. (1992), "Swelling and thickness effects on the separation of styrene and ethylbenzene based on facilitated transport through ionomer membranes", *Ind. Eng. Chem. Res.*, **31**, 1116.

34. Eriksen, O.I., Aksnes, E., Dahl, I.M. (1993), "Facilitated transport of ethane through Nafion membranes, part-I, water swollen membranes", *J. Memb. Sci.*, **85**, 89.

35. Ho, W.S., Dalrymple, D.C. (1994), "Facilitated transport of olefins in Ag+ containing polymer membranes", *J. Memb. Sci.*, **91**, 13.

36. Tanaka, K., Taguchi, A., Hao, J., Kita, H., Okamoto, K. (1996), "Permeation and separation properties of polyimide membranes to olefins and paraffins". *J. Memb. Sci.*, **121**, 197.

37. Yamaguchi, T., Baertsch, C., Koval, C.A., Noble, R.D., Bowman, C.N. (1996), "Olefin separation using silver impregnated ion-exchange membranes and silver/polymer blend membranes", *J. Memb. Sci.*, **117**, 151.

38. Sungpet, A., Way, J.D., Theon, P.M., Dorgen, J.R. (1997), "Reactive polymer membranes for ethylene/ethane separation", *J. Memb. Sci.*, **136**, 111.

39. Zyl van, A.J., Kerres, J.A., Cui, W., Junginger, M. (1997), "Application of new sulfonated ionomer membranes in the separation of pentene and pentane by facilitated transport", *J. Memb. Sci.*, **137**, 173.

40. Sunderrajan, S., Freeman, B.D., Pinnau, I. (1997) "Sorption and spectroscopic analysis of silver–olefin interaction in polymer electrolytes", *Polym. Mater. Sci. Eng.*, **77** (2), 267.

41. Pinnau, I., Toy, L.G., Sunderrajan, S., Freeman, B.D. (1997) "Solid electrolyte membranes for olefin/paraffin separation", *Polym. Mater. Sci. Eng.*, **77** (2), 269.

42. Zyl van, A.J., Kerres, J.A. (1999), "Development of new ionomer blend membranes, their characterisation, and their application in the perstractive separation of alkenes from alkene-alkane mixtures, II, electrical and facilitated transport properties". *J. Appl. Polym. Sci.*, **74**, 422.

43. Staudt-Bickel, C., Koros, W.J. (2000), "Olefin/paraffin separation with 6FDA-based polyimide membranes", *J. Memb. Sci.*, **170**, 205.

44. Hong, S.U., Jin, J.H., Won, J., Kang, Y.S. (2000) "Solid polymer electrolytes containing silver ions and their application to facilitated transport membranes", *Adv. Mater.*, **12**, 968.

45. Yoon, Y.S., Won, J., Kang, Y.S. (2000) "Polymer electrolyte membranes containing silver ion for facilitated olefin transport", *Macromolecules*, **33**, 3185.

46. Kim, H.S., Ryu, J.H., Kim, H., Ahn, B.S., Kang, Y.S. (2000), "Reversible olefin complexation by silver ions in dry poly(vinylmethylketone) membrane and its application to olefin/paraffin separations", *Chem. Commun.*, 1261.

47. Hong, S.U., Kim, J.Y., Kang, Y.S. (2001), "Effect of water on the facilitated transport of olefins through solid polymer electrolyte membranes", *J. Memb. Sci.*, **181**, 289.

48. Kim, Y.H., Ryu, J.H., Bae, J.Y., Kang, Y.S., Kim, H.S. (2000), "Reactive polymer membranes containing cuprous complexes in olefin/paraffin separation", *Chem. Commun.*, 195.

49. Skotheim, T.A., Elsenbaumer, R.L., Reynolds, J.R. (1986), *Handbook of Conductive Polymers*, 2nd Ed., Marcel Dekker, NY.

50. Liang, W. Martin, C.R. (1991), "Gas transport in electronically conductive polymers", *Chem. Mater.*, **3**, 390.

51. Anderson, M.R., Matts, B.R., Reiss, H., Kaner, R.B. (1991), "Conjugated polymer films for gas separations", *Science*, **252**, 1412.

52. Anderson, M.R., Matts, B.R., Reiss, H., Kaner, R.B. (1991), "Gas separation membranes: a novel application for conducting polymers", *Synth. Met.*, **41-43**, 1151.

53. Anderson, M.R. (1992), "An investigation of conducting polymer materials as gas separation membranes", *Dissertation*, University of California, USA.

54. Martin, C.R., Liang, W., Menon, V., Parthasarathy, R., Parthasarathy, A. (1993), "Electronically conductive polymers as chemically-selective layers in membrane based separation", *Synth. Met.*, **55-57**, 3766.

55. Matts, B.R., Anderson, M.R., Conklin, J.A., Reiss, H., Kaner, R.B. (1993), "Morphological modification of polyaniline films for separation of gases", *Synth. Met.*, **57**, 3655.

56. Kuwabata, S., Charles, R. (1994), "Investigation of the gas transport properties of polyaniline", *J. Membr. Sci.*, **91**, 1.

57. Kaner R.B., Anderson, M.R., Reiss, H., Mattes, B.R. (1994), "Membrane having selective permeability", US Patent No. 5,358,556.

58. Rebattet, L, Excoubes, M., Genies, E., Pineri, M. (1995), "Effect of doping treatment on gas permeation properties and separation factors of polyaniline membranes", *J. Appl. Polym. Sci.*, **57**, 1595.

59. Chang, M.-J., Liao, Y.-H., Myerson, A.S., Kwei, T.K. (1996), "Gas transport properties of polyaniline membranes", *J. Appl. Polym. Sci.*, **62**, 1427.

60. Conklin, J.A., Su, T.M., Haung, S.-C., Kaner, R.B. (1998), "Gas and liquid separation application of polyaniline", in: *Handbook of Conducting Polymers*, T.A., Skotheim, R.L., Elsenbaumer, J.R., Reynolds (Eds.), 2nd Ed., Marcel Dekker, NY, pp 945-956.

61. Wang, H.-L., Mattes, B.R. (1999), "Gas transport and sorption in polyaniline thin films", *Synth. Met.*, **102**, 1333.

62. Wang, H.-L., Mattes, B.R. (2004), "Permeable polyaniline articles for gas separation", US Patent No. 6,797,325 B2.

63. Stafström, S., Bredas, J.L., Epstein, A.J., Woo, H.S., Tanner, D.B., Haung, W.S., MacDiarmid, A.G. (1987), "Polaron lattice in highly conductive polyaniline: theoretical and optical studies", *Phys. Rev. Lett.*, **59**, 1464.

64. Chiang, J.C., MacDiarmid, A.G. (1986), "Polyaniline: protonic acid doping of the emeraldine form to the metallic regime", *Synth. Met.*, **13**, 193.

65. Epstein, A.J., Ginder, J.M., Zuo, F., Bigelow, R.W., Woo, H.S., Tanner, D.B., Richter, A.F., Haung, W.S., MacDiarmid, A.G. (1987), "Insulator-to-metal transition in polyaniline", *Synth. Met.*, **18**, 303.

66. Libert, J, Bredas, J.L, Epstein, A.J. (1995), "Theoretical study of *p*- and *n*- type doping of the leucoemeraldine base form of polyaniline: Evolution of the geometric and electronic structure", *Phys. Rev. B,* **51**, 5711.

67. Libert, J., dos Santos, D.A., Bredas, J.L. (1997), "From neutral oligoanilines to polyanilines: A theoretical investigation of the chain-length dependence of the electronic and optical properties", *Phys. Rev. B*, **56**, 8638.

68. Lei, W., Kocherginsky, N.M. (1999), "Doping-dependent ion selectivity of polyaniline membranes", *Synth. Met.*, **106**, 19.

69. Crank, J. (1975), *The Mathematics of Diffusion*, 2nd Ed., Oxford Science Publications, Oxford.

70. Comyn, J. (1985), *Polymer Permeability*, Elsevier Applied Science, London.
71. Vieth, W.R. (1991), *Diffusion In and Through Polymers: Principles and Applications*, Hanser, New York.
72. Koros, W.J., Chern, R.T. (1987), "Separation of gaseous mixtures using polymer membranes", in: *Handbook of Separation Process Technology*, R.W., Rousseau (Ed.), John Wiley & Sons, NY.
73. Ghosal, K. Freeman, B.D. (1994), "Gas separation using polymer membranes: An overview", *Polym. for Adv. Tech.*, **5**, 673.
74. Paul, D.R., Yampol'skii, Y.P. (1994), *Polymeric Gas Separation Membranes*, CRC Press, Boca Raton, FL.
75. Crank J., Park, G.S. (1968), *Diffusion in Polymers*, Academic Press, NY.
76. Kesting, R.E., Fritzsche, A.K. (1993), *Polymeric Gas Separation Membranes*, John Wiley & Sons, NY.
77. Stannett, V. (1978), "The transport of gases in synthetic polymeric membranes: An historic perspective", *J. Memb. Sci.*, **3**, 97.
78. Stern, S.A. (1994), "Polymers for gas separations: The next decade", *J. Memb. Sci.*, **94**, 1.
79. Smith, B.E., Wessling, M., Smolders, C.A. (1991), "Diffusion through rubbery and glassy polymer membranes", *Macromolecular Symposia*, **45**, 237.
80. Felder, R.M. (1978), "Estimation of gas transport coefficients from differential permeation, integral permeation, and sorption rate data", *J. Memb. Sci.*, **3**, 15.
81. Frisch, H.L. (1980), "Sorption and transport in glassy polymers: A review", *Polym. Engg. Sci.*, **20**, 12.
82. Koros, W.J., Ma, Y.H., Shimidzu, T. (1996), "Terminology for membranes and membrane processes", *J. Memb. Sci*, **120**, 149.
83. Silvis, H.C. (1997), "Recent advances in polymers for barrier applications", *Trends Polym. Sci.*, **5**, 75.
84. Naylor, T. deV. (1989), "Permeation properties", in: *Comprehensive Polymer Science*, S.G., Allen, J.C., Bevington, (Eds.), Pergamon Press, NY, 643.

85. Freeman, B.D., Pinnau, I. (1997), "Separation of gases using solubility-selective polymers", *Trends Polym. Sci.*, **5**, 167.

86. Wang, X., Spencer, H.G. (1997), "Polymer membranes for use in food processing", *Trends Polym. Sci.*, **5**, 38.

87. Vieth, W.R. (1988), *Membrane Systems: Analysis and Design*, John Wiley & Sons., NY.

88. Baker, R.W., Cussler, E.L., Eykamb, W., Koros, W.J., Riley, R.L., Strathmann, H. (1991), *Membrane Separation Systems: Recent Development and Future Directions*, Noyes Data Corporation, Park Ridge, NJ.

89. Bitter, J.G.A. (1991), *Transport Mechanisms in Membrane Separation Processes*, Plenum Chemical Engineering Series, Plenum Press, NY.

90. Noble, R.D., Stern, S.A. (1995), *Membrane Separations Technology: Principles and Applications*, Elsevier, Amsterdam.

91. Starzak, M.E. (1984), *The Physical Chemistry of Membranes*, Academic press, OL.

92. Neogi, P. (1996), *Diffusion in Polymers*, Marcel Dekker Inc., NY.

93. Koros, W.J. (1990), *Barrier Polymers and Structures*, ACS Symposium Series, vol. 423, American Chemical Society, Washington D.C..

94. Matsuura, T. (1994), *Synthetic Membranes and Membrane Separation Processes*, CRC Press.

95. Felder, R.M., Huvard, G.S. (1980), "Permeation, diffusion, and sorption of gases and vapours", in: *Methods of Experimental Physics*, 16c, Chapter 17, Academic Press, NY.

96. Koros, W.J., Hellums, M.W. (1989), "Transport properties", in: *Encyclopaedia of Polymer Science and Engineering*, H. F. Mark, N. M. Bikales, C. G. Overberger, G. Mendes, (Eds.), 2nd Eds, John Wiley & Sons, NY.

97. Rautenbach R., Albrecht, R. (1989), *Membrane Processes*, John Wiley & Sons, NY.

98. Kesting, R.E. (1985), *Synthetic Polymeric Membranes*, 2nd Ed., John Wiley & Sons, NY.

99. Toshima, N. (1992), *Polymers for Gas Separation*, VCH, Deerfield Beach, FL.

100. Mulder, M. (1991), *Basic Principles of Membrane Technology*, Kluwer Academic, Dordrecht.

101. Osada, Y., Nakagawa, T (1992), *Membrane Science and Technology*, Marcel Dekker, NY.

102. Frisch, H.L. (1991), "Fundamentals of membrane transport", *Polymer*, **23**, 445.

103. Cussler, E.L. (1984), *Diffusion: Mass Transfer in Fluid Systems*, Cambridge University Press, NY; also 2nd Eds. (1997), Cambridge University Press, NY.

104. Odani, H., Uyeda, T. (1991), "Theories of sorption and transport in polymer membranes", *Polymer*, **23**, 467.

105. Stannett, V.T., Koros, W.J., Paul, D.R., Lonsdale, H.K., Baker, R.W. (1979), "Recent advances in membrane science and technology", *Adv. Polym. Sci.*, **32**, 69.

106. Matson, S.L., Lopez, J., Quin, J.A. (1983), "Separation of gases with synthetic membranes", *Chem. Eng. Sci.*, **38**, 503.

107. Zolandz, R.R., Fleming, G.K. (1992), "Gas permeation", in: *Membrane Handbook*, W.S.W. Ho, K.K. Sirkar (Eds.), Van Nostrand Reinhold, NY, pp 17-101.

108. Rogers, C.E. (1965), "Solubility and diffusivity", in: *Physics and Chemistry of the Organic Solid State*, D. Fox, M.M. Labes, A. Weissberger (Eds.), Interscience, NY, pp 509-635.

109. Barrer, R.M. (1975), "Formal theory of diffusion through membranes", in: *Permeability of Plastic Films and Coatings to Gases, Vapours, and Liquids*, H.B. Hopfenberg (Ed.), Plenum Press, NY, pp 113-124.

110. Stern, S.A., Frisch, H.L. (1981), "Selective permeation of gases through polymers", *Annu. Rev. Mater. Sci.*, **11**, 523.

111. Frisch, H.L., Stern, S.A. (1983), "Diffusion of small molecules in polymers, *CRC Crit. Rev. Solid State Mater. Sci.*, **11**, 123.

112. Stern, S.A., Trohalaki, S. (1990), "Gas diffusion in rubbery and glassy polymers", *ACS Symp. Ser.*, **423**, 22.

113. Kimura, S., Hirose, T. (1992), "Theory of membrane permeation", in: *Polymers for Gas Separation*, N. Toshima (Ed.), VCH, NY, pp 15-49.

114. Husk, G.R., Cassidy, C.E., Gebert, K.L. (1988), "Synthesis and characterisation of a series of polyimides", *Macromolecules*, **21**, 1234.

115. Smit, E. (1991), "Modelling the diffusion of gases through membranes of novel polyimides", PhD Thesis, University of Twente, The Netherlands.

116. Puleo, A.C. (1988), "The effects of pendant groups on gas sorption and transport in polymers", PhD Thesis, University of Texas, Austin, TX.

117. Pitzer, K.S., Brewer, L. (1961), *Thermodynamics* (revision of Lewis and Randall), 2nd Ed., McGraw-Hill Publications, NY.

118. Soltanieh, M., Gill, W.N. (1981), "Reverse osmosis", *Chem. Eng. Commun.*, **12**, 279.

119. Onsager, L. (1931), "Reciprocal relations in irreversible processes - I", *Phys. Rev.*, **37**, 405.

120. Onsager, L. (1931), "Reciprocal relations in irreversible processes - II", *Phys. Rev.*, **38**, 2265.

121. Reid, C.E., Breton, E.J (1959), "Water and ion flow across cellulosic membranes", *J. Appl. Polym. Sci.*, **1**, 133.

122. Sourirajan, S. (1970), *Reverse Osmosis*, Academic Press, NY.

123. Fick, A. (1855), "Ueber diffusion", *Phil. Mag.*, **X**, 30.

124. Jost, W. (1960), *Diffusion in Solids, Liquids, Gases*, Academic Press, NY.

125. Wijmans, J.G. (2004), "The role of permeant molar volume in the solution-diffusion model transport equations", *J. Memb. Sci.*, **237**, 39.

126. Wijmans, J.G., Baker, R.W. (1995), "The solution-diffusion model: A review", *J. Memb. Sci.*, **107**, 1.

127. Costello, L.M., Koros, W.J (1992), "Temperature dependence of gas sorption and transport properties in polymers: measurement and applications", *Ind, Eng. Chem. Res.*, **31**, 2708.

128. Kim, T.H. (1988), "Gas Sorption and Permeation in a Series of Aromatic Polyimides". Ph. D. dissertation, University of Texas at Austin, TX.

129. Kim, T.H., Koros, W.J., Husk, G.R., O'Brien, K.C. (1988), "Relationship between gas separation properties of aromatic polyimides", *J. Memb. Sci.*, **37**, 45.

130. Stannett, V., Hopfenberg, H.B., Petropoulos, J.H. (1972), "Diffusion in polymers", *MTP Int. Rev. Sci., Macromol. Sci.*, **8**, 329.

131. Hopfenberg, H.B., Stannett, V. (1973), "The diffusion and sorption of gases and vapours in glassy polymers", in: *The Physics of Glassy Polymers*, R.N. Haward (Ed.), Wiley, NY, pp 504-547.

132. Rogers, C.E. (1985), "Permeation of gases and vapours in polymers", in: *Polymer Permeability*, J. Conyn (Ed.), Elsevier, NY, pp 11-73.

133. Kumins, C.A., Kwei, T.K. (1968), "Free volume and other theories", in: *Diffusion in Polymers*, J. Crank, G.S. Park (Eds.), Academic Press, NY, pp 107-140.

134. Rogers, C.E., Machin, D. (1972), "The concentration dependence of diffusion coefficients in polymer penetrant systems", *CRC Crit. Rev. Macromol. Sci.*, 245.

135. Yampol'skii, Y.P. (1989), "Sorption and gas and vapour permeability in membranes based on glassy polymers, role of free volume", in: *Advances in Membrane Phenomena and Processes*, A.M. Mika, T.Z. Winnicki (Eds.), Wroclaw Technical University Press, Wroclaw, pp 129-146.

136. Fujita, H. (1964), "Diffusion in polymer-diluent systems", *Fortschr. Hochpolym. Forsch.*, **3**, 1.

137. Flory P.J. (1969), *Principles of Polymer Chemistry*, Ithaca, Cornell University, NY.

138. Vrentas, J.S., Duda, J.L. (1986), "Diffusion", in: *Encyclopedia of Polymer Science*, J.I. Kroschwitz (Ed.), 2nd ed., Vol. 5, John Wiley & Sons, NY.

139. Stern, S.A., Kulkarni, S.S., Frisch, H.L. (1983), "Test of a free volume model of gas permeation through polymer membranes, pure CO_2, CH_4, C_2H_4 and C_3H_8 in polyethylene", *J. Polym Sci., Polym. Phys.*, **21**, 467.

140. Fujita, H., Kishimoto, A., Matsumoto, K. (1960), "Concentration and temperature dependence of diffusion coefficients for systems polymethyl acrylate and n-alkyl acetates", *Trans. Faraday Soc.*, **56**, 424.

141. Chern, R.T., Koros, W.J., Sanders, E.S., Chen, S.H. Hopfenberg, H.B. (1983), "Implications of the Dual Mode Sorption and Transport Models for Mixed Gas Permeation", in: *Industrial Gas Separations*, T.E. Whyte, C.M. Yon, E.H. Wagener (Eds.), ACS Symp. Serial No. 233, American Chemical Society, Washington-DC.

142. Paul, D.R., Koros, W.J. (1976), "Effect of partially immobilizing sorption on permeability and the diffusion time-lag", *J. Polym. Sci., Polym. Phys.*, **14**, 675.

143. Koros, W.J., Paul, D.R., Huvard, G.S. (1979), "Energetics of gas sorption in glassy polymers", *Polymer*, **20**, 956.

144. Petropoulos, J.H. (1970), "Quantitative analysis of gaseous diffusion in glassy polymers", *J. Polym. Sci.*, **2**, 1979.

145. Koros, W.J., Chern, R.T., Stannett, V., Hopfenberg, H.B. (1981), "A model for permeation of mixed gases and vapours in glassy polymers", *J. Polym. Sci., Polym. Phys.*, **19**, 1513.

146. Chan, A.H., Koros, W.J., Paul, D.R. (1978), "Analysis of hydrocarbon gas sorption and transport in ethyl cellulose using the dual-mode sorption/partial immobilization models", *J. Memb. Sci.*, **3**, 117.

147. Koros, W.J., Chan, A.H., Paul, D.R. (1977), "Sorption and transport of various gases in polycarbonates", *J. Memb. Sci.*, **2**, 165.

148. Koros, W.J., Paul, D.R. (1978), "Transient and steady state permeation in poly(ethylene- terephthalate) above and below the glass transition", *J. Polym. Sci., Polym. Phys.*, **16**, 2171.

149. Barrer, R.M. (1984), "Diffusivities in glassy polymers for the dual-mode sorption model", *J. Memb. Sci.*, **18**, 25.

150. Fredrickson, G.H., Helfand, E. (1985), "Dual-mode transport of penetrant in glassy polymers", *Macromolecules*, **18**, 2201.

151. Pace, R.J., Datyner, A. (1979), "Statistical mechanical model for diffusion of simple penetrants in polymers, I - theory", *J. Polym. Sci., Polym. Phys.*, **17**, 437.

152. Pace, R.J., Datyner, A. (1979), "Statistical mechanical model for diffusion of simple penetrants in polymers, I - theory", *J. Polym. Sci., Polym. Phys.*, **17**, 1675.

153. Breck, D.W. (1974), *Zeolite Molecular Sieves*, John Wiley & Sons, NY.

154. Shah, V.M., Stern, S.A., Ludovice, P.J. (1989), "Estimation of the free volume in polymers by means of Monte Carlo technique", *Macromolecules*, **22**, 4660.

155. Trohalaki, S., Rigby, D., Kloczkowski, A., Mark, J.E., Roe, R.J. (1991), "Estimation of diffusion coefficients for small molecular penetrants in amorphous polyethylene", in: *Computer Simulation of Polymers*, R.J. Roe (Ed.), Prentice Hall, Englewood Cliffs, NJ, pp 220-232.

156. Takeuchi, H., Okazaki, K. (1990), "Molecular dynamics simulation of diffusion of simple gas molecules in short chain polymer", *J. Chem. Phys.*, **92**, 5643.

157. Trohalaki, S., Kloczkowski, A., Mark, J.E., Roe, R.J. (1992), "Molecular dynamics simulation of small molecule diffusion in polyethylene", *Polym. Prepr. Am. Chem. Soc., Div. Polym. Chem.*, **33**, 629.

158. Pant, P.V.K., Boyd, R.H. (1993), "Molecular dynamics simulation of small penetrants in polymers", *Macromolecules*, **26**, 679.

159. Müller-Plathe, F. (1991), "Calculation of the free energy for gas absorption in amorphous polypropylene", *Macromolecules*, **24**, 6475.

160. Sok, R.M., Berendsen, H.J.C. (1992), "Molecular dynamics simulation of the transport of small molecules across a polymer membrane", *Polym. Prepr. Am. Chem. Soc., Div. Polym. Chem.*, **33**, 641.

161. Barrie, J.A. (1968), "Water in polymers", in: *Diffusion in Polymers*, J. Crank, G.S. Park (Eds.), Academic Press, NY.

162. Chiou, J.S., Barlow, J.W., Paul, D.R. (1985), "Plasticisation of glassy polymers by CO_2", *J. Appl. Polym. Sci.*, **30**, 2633.

163. Sanders, E.S. (1988), "Penetrant induced plasticisation and gas permeation in glassy polymers", *J. Memb. Sci.*, **37**, 63.

164. Van Amerongen, G. J. (1964), "Diffusion in elastomers", *Rubb. Chem. Tech.*, **37**, 1065.

165. Mauze, G.R., Stern, S.A. (1983), "The dual mode solution and transport of water in Poly(acrylonitrile)", *Polym .Eng. & Sci.*, **24**, 548.

166. Kamiyu, Y., Kirose, T., Mizoguchi, K., Naito, Y. (1986), "Gravimetric study of high pressure sorption of gases in polymers", *J. Polym. Sci.*, **24**, 1525.

167. Kamiyu, Y., Kirose, T., Mizoguchi, K., Terada, K. (1988), "Sorptive dilation of poly(vinyl benzoate) and poly(vinyl butyral) by carbon dioxide", *J. Polym. Sci., Polym. Phy.*, **26**, 1409.

168. Robeson, L.M. (1991), "Correlation of separation factor versus permeability for polymeric membranes", *J. Memb. Sci.*, **62**, 165.

169. Stern, S.A. (1986), "New developments in membrane processes for gas separations", *MMI Press Symp.*, **5**, 1.

170. Cabasso, I. (1987), "Membranes", in: *Encyclopaedia of Polymer Science and Engineering*, J.I. Kroschwitz (Ed.), Vol. 9, 2nd Ed., Wiley, NY, pp 509-579.

171. Hayes, R.A. (1989), "Polyimide gas separation membranes", US Patent No. 4,880,442.

172. Kusuki, Y., Yoshinaga, T., Shimazaki, H. (1992), "Aromatic polyimide double layered hollow filamentary membrane and process for producing same", US Patent No. 5,141,642.

173. Kluiter, S.C.A (2001), "Status review on membrane systems for hydrogen separation", Intermediate Report EU Project, *MIGREYD NNEU-2001-670.*

174. Engler, Y., Dupuis, G (2000), "Process for recovering olefins", US Patent No. 6,141,988.

175. Barchas, R., Hickey, T. (1992), "Membrane separation process for cracked gas", US Patent No. 5,082,481.

176. D'Aquino, R., Ondrey, G. (1999), "Refiners get cracking on petrochemicals", *Chem. Eng.*, 30.

177. West, J. (1996), *International Petroleum Encyclopaedia*. PennWell Publishing Co., Oklahoma, USA.

178. Humphrey, J.L., Seibert, A.F., Koort, R.A. (1991), "Separation technologies advances and priorities", US Department of Energy Report.

179. Barron, T.S., Heist, J.A., Hunt, K.M., Wroble, P.J. (1987), "Industrial application of freeze concentration technology", Final Report to Electric Power Research Institute, *EM-5232-1*.

180. Wilson, R.B., Brown, A. (1994), "Evaluation of separation processes in petroleum refining", SRI Report, SRI International.

181. Semenova, S.I. (2004), "Polymer membranes for hydrocarbon separation and removal", *J. Memb. Sci.*, **231**, 189.

182. Herberhold, M. (1974), *Metal ð-Complexes: Part II: Specific Aspects*, Vol. 2, Elsevier Publications, Amsterdam.

183. Heβ, S., Scharfenberger, G., Staudt-Bickel, C., Lichtenthaler, R.N. (2002), "Propylene/propane separation with copolyimides containing benzo-15-crown-5-ether to incorporate silver ions", *Desalination*, **145**, 359.

184. Krol, J.J., Boerrigter, M., Koops, G.H. (2001), "Polyimide hollow fibre gas separation membranes: preparation and the suppression of plasticisation in propane/propylene environments", *J. Memb. Sci.*, **184**, 275.

185. Sridhar, S., Khan, A.A. (1999), "Simulation studies for the separation of propylene and propane by ethylcellulose membrane", *J. Memb. Sci.*, **159**, 209.

186. Bai, S., Sridhar, S., Khan, A.A. (1998), "Metal-ion mediated separation of propylene from propane using PPO membranes", *J. Memb. Sci.*, **147**, 131.

187. Okamoto, K., Noborio, K., Hao, J., Tanaka, K., Kita, H. (1997), "Permeation and separation properties of polyimide membranes to 1,3-butadiene and *n*-butane", *J. Memb. Sci.*, **134**, 171.

188. Burns, R.L., Koros, W.J. (2003), "Defining the challenges for C_3H_6/C_3H_8 separation using polymeric membranes", *J. Memb. Sci.*, **211**, 299.

189. Kim, J.K., Won, J., Kang, Y.S. (2004), "Olefin-induced dissolution of silver salts physically dispersed in inert polymers and their application to olefin/paraffin separation", *J. Memb. Sci.*, **241**, 403.

190. Hong, S.U., Jin, J.H., Won, J., Kang, Y.S. (2000), "Polymer-salt complexes containing silver ions and their application to facilitated olefin transport membranes", *Adv. Mater.*, **12**, 968.

191. Kim, J.H., Min, B.R., Kim, C.K., Won, J., Kang, Y.S. (2001), "Role of transient cross-links for transport properties in silver-polymer electrolytes", *Macromolecules*, **34**, 6052.

192. Kim, J.H., Min, B.R., Kim, C.K., Won, J., Kang, Y.S. (2002), "Spectroscopic interpretation of silver ion complexation with propylene in silver polymer electrolytes", *J. Phys. Chem. B*, **106**, 2786.

193. Kim, J.H., Min, B.R., Won, J., Kang, Y.S. (2002), "Complexation mechanism of olefin with silver ions dissolved in polymer matrix and its effect on facilitated olefin transport", *Chem. Eur. J.*, **8**, 650.

194. Kim, J.H., Min, B.R., Kim, C.K., Won, J., Kang, Y.S. (2002), "New insights into the coordination mode of silver ions dissolved in poly(2-ethyl-2-oxazoline) and its relation to facilitated olefin transport", *Macromolecules*, **35**, 5250.

195. Kim, J.H., Min, B.R., Kim, Joo, S.H., C.K., Won, J., Kang, Y.S. (2003), "Role of polymer matrix in polymer/silver complexes for structure, interactions and facilitated olefin transport", *Macromolecules*, **36**, 6183.

196. Kim, J.H., Min, B.R., Kim, C.K., Won, J., Kang, Y.S. (2002), "Ionic interaction behavior and facilitated olefin transport in PVP:$AgCF_3SO_3$ electrolytes: effect of molecular weight", *J. Polym. Sci. B*, **40**, 1813.

197. Kim, J.H., Min, B.R., Lee, K.B., Won, J., Kang, Y.S. (2002), "Coordination structure of various ligands in crosslinked PVA to silver ions for facilitated olefin transport", *Chem. Commun.*, 2732.

198. Kim, J.H., Min, B.R., Kim, C.K., Won, J., Kang, Y.S. (2003), "Facilitated transport of ethylene across polymer membranes containing silver salt: effect of HBF_4 on the photoreduction of silver ions", *J. Membr. Sci.*, **212**, 283.

199. Kim, J.H., Min, B.R., Won, J., Kang, Y.S. (2003), "Revelation of facilitated olefin transport through silver-polymer complex membranes using anion complexation", *Macromolecules*, **36**, 4577.

200. Pinnau, I., Toy, L.G., Casillas, C. (1997), "Olefin separation membrane and process", US Patent No. 5,670,051.

201. Sunderrajan, S., Freeman, B.D., Hall, C.K., Pinnau, I. (2001), "Propane and propylene sorption in solid polymer electrolytes based on poly(ethylene oxide) and silver salts", *J. Membr. Sci.*, **182,** 1.

202. Merkel, T.C., He, Z., Morisato, A., Pinnau, I. (2003), "Olefin/paraffin solubility in a solid polymer electrolyte membrane", *Chem. Commun.*, 1596.

203. Kim, J.K., Won, J., Kang, Y.S. (2004), "Olefin-induced dissolution of silver salts physically dispersed in inert polymers and their application to olefin/paraffin separation", *J. Memb. Sci.*, **241**, 403.

204. Ito, A., Hwang, S.T. (1989). "Permeation of propane and propylene through cellulosic polymer membranes", *J. Appl. Polym. Sci.*, **38**, 483.

205. Norden, B., Krutmeijer, E. (2000), "The Nobel Prize in chemistry, 2000: Conductive Polymers", The Royal Swedish Academy of Sciences, Stockholm, Sweden.

206. Shirakawa, H., Ikeda, S. (1980), "Preparation and morphology of as-prepared and highly stretch-aligned polyacetylene", *Synth. Met.*, **1**, 175.

207. Fincher, C.R., Peebles, D.L., Heeger, A.J., Druy, M.A., Matsumura, Y., MacDiarmid, A.G., Shirakawa, H., Ikeda, S. (1978), "Anisotropic optical properties of pure and doped polyacetylene", *Solid. State. Commun.*, **27**, 489.

208. Chiang, C.K., Fincher, C.R., Park, Y.W., Heeger, A.J., Shirkawa, H., Louis, E.J., Gau, S.C., MacDiarmid, A.G. (1997), "Electrical conductivity in doped polyacetylene", *Phys. Rev. Lett.*, **39**, 1098.

209. Dogan, S., Akbulut, U., Yalcin, T., Suzer, S., Toppare, L. (1993), "Conducting polymer of aniline II. a composite as a gas sensor", *Synth. Met.*, **60**, 27.

210. Kabayashi, T., Yoneyama, H., Tamura, H. (1984), "Polyaniline film-coated electrodes as electrochromic display device", *J. Electro. Chem.*, **161**, 419.

211. Paul, E.W., Ricco, A.J., Wrighton, M.S. (1995), "Resistance of polyaniline films as a function of electrochemical potential and the fabrication of polyaniline-based microelectronic devices", *J. Phys. Chem.*, **89**, 1441.

212. Cao, Y., Treacy, G.M., Smith, P, Heeger, A.J. (1992), "Solution-cast films of polyaniline: optical-quality transparent electrodes", *Appl. Phys. Lett.*, **60**, 2711.

213. Parkhutik, V., Martinez-Duart, J., Diaz Calleja, R., Matveeva, E.S. (1993), "Deposition of polyaniline films onto porous silicon layers", *J. Electrochem Soc.*, **140**, L94.

214. Winokur, M.J., Chunwachirasiri, W. (2003), "Nanoscale structure/property relationship in conjugated polymers: Implications for current and future device applications", *J. Polym. Sci.*, **41**, 2630.

215. Green, A.G., Woodhead, A.E. (1910), "Aniline-black and allied compounds, Part I", *J. Chem. Soc.* **97**, 2388.

216. Kang, E.T., Neoh, K.G., Tan, K.L. (1998), "Polyaniline: A polymer with many interesting intrinsic redox states", *Prog. Polym. Sci.*, **23**, 277.

217. Genies, E.M., Boyle, A., Lapkowski, M., Tsintavis, C. (1990), "Polyaniline: A historical survey", *Synth. Met.*, **36**, 139.

218. Gospodinova, N., Terlemezyan, L. (1998), "Conducting polymers prepared by oxidative polymerisation: Polyaniline", *Prog. Polym. Sci.*, **23**, 1443.

219. Syed, A.A., Dinesan, M.K. (1991), "Review: Polyaniline – a novel polymeric material", *Talanta*, **38**, 815.

220. Anand, J., Palaniappan, S., Sathyanarayana, D.N. (1998), "Conducting polyaniline blends and composites", *Prog. Polym. Sci.*, **23**, 993.

221. Amano, K., Ishikawa, H., Kobayashi, A., Satoh, M. Hasegawa, E. (1994), "Thermal stability of chemically synthesised polyaniline", *Synth. Met.*, **62**, 229.

222. Pyo, M., Reynolds, J.R., Warren, L.F.O., Marcy, H.O. (1994), "Long term switching stability of polypyrrole", *Synth. Met.*, **68**, 71.

223. Ray, A., Asturias, G.E., Kershner, D.L., Richter, A.F., MacDiarmid. A.G., Epstein, A.J. (1989), "Polyaniline: Doping, structure and derivatives", *Synth. Met.*, **29**, 141.

224. Khor, S.H., Neoh, K.G., Kang, E.T. (1990), "Synthesis and characterisation of some polyaniline-organic acceptor complexes", *J. Appl. Polym. Sci.*, **40**, 2015.

225. Salaneck, W.R., Lundström I, Haung, W.S., MacDiarmid, A.G. (1986), "A two dimentional surface 'state diagram' for polyaniline", *Synth. Met.*, **13**, 291.

226. Nakajima, T., Toyosawa, S., Kijima, S., Arai, K., Maeda, Y., Osawa, M., Kawagoe, T., Iino, Y., Osawa, R. (1990), "Polyaniline", US Patent No. 4,904,553.

227. Bredas, J.L., Silbey, R. (1991), *Conjugated polymers: The novel science and technology of highly conducting and nonlinear optically active materials*, Kluwer Academic Press, Dordrecht, Netherlands.

228. MacDiarmid, A.G., Chiang, J.C., Richter, A.F., Epstein, A.J. (1987), "Polyaniline: a new concept in conducting polymers", *Synth. Met.*, **18**, 285; and references therein.

229. Furukawa, Y., Hara, T., Hyodo, Y., Harada, I. (1986), "Vibrational spectra of polyaniline and its ^{15}N- and ^{2}H-substituted derivatives in as-polymerized, alkali-treated and reduced states", *Synth. Met.*, **16**, 189.

230. Yang, S.M., Chen, J.T. (1995), "The effect of synthesis conditions on the properties of polyaniline film", *Synth. Met.*, **69**, 153.

231. Wang, H.L., Romero, R.J., Mattes, B.R., Zhu, Y., Winokur, M.J. (2000), "Effect of processing conditions on the properties of high molecular weight conductive polyaniline fibre", *J. Polym. Sci., Polym. Phys.*, **38**, 194.

232. Stejskal, J., Riede, A., Hlavata, D., Prokes, J., Helmstedt, M., Holler, P. (1998), "The effect of polymerisation temperature on molecular weight crystallinity, and electrical conductivity of polyaniline", *Synth. Met.*, **96**, 55.

233. Angelopoulos, M., Dipietro, R., Zheng, W.G., MacDiarmid, A.G. (1997), "Effect of selected processing parameters on solution properties and morphology of polyaniline and impact on conductivity", *Synth. Met.*, **84**, 35.

234. Demoustier-Champagne, S., Stavaux, P.Y. (1999), "Effect of electrolyte concentration and nature on the morphology and the electrical properties of electropolymerised polypyrrole nanotubules", *Chem. Mater.*, **11**, 829.

235. Sabatani, E., Gafni, Y., Rubinstein, I. (1995), "Morphology control in electrochemically grown conducting polymer films. 3. a comparative stydy of polyaniline films on bare gold and on gold pretreated with p-aminothiophenol", *J. Phys. Chem.*, **99**, 12305.

236. MacDiarmid, A.G., Epstein, A.J. (1995), "Secondary doping in polyaniline, *Synth. Met.*, **69**, 85.

237. Salzer, C.Z., Elliott, C.M. (2000), "Quantitative in situ studies of ionic doping of polypyrrole employing rotated ring disk electrode voltammetry", *Chem. Meter.*, **12**, 2099.

238. Lee, D., Swager, T.M. (2003), "Defining space around conducting polymers: reversible protonic doping of a canopied polypyrrole", *J. Am. Chem. Soc.*, **125**, 6870.

239. Hatchett, D.W., Josowicz, M., Janata, J. (1999), "Acid doping of polyaniline: spectroscopic and electrochemical studies", *J. Phys. Chem. B.*, **103**, 10992.

240. Polk, B.J., Potje-Kamloth, K., Josowicz, M., Janata, J. (2002), "Role of protonic and charge transfer doping in solid state polyaniline", *J. Phys. Chem. B.*, **106**, 11457.

241. Hardaker, S.S., Gregory, R.V. (1999), "*Polyaniline*", in: *Polymer Data Handbook*, J. Mark (Ed.), Oxford University Press, Oxford.

242. Braun, D., Heeger A.J. (1991), "Visible light emission from semi-conducting polymer diodes", *App. Phy. Lett.*, **58**, 1982.

243. Epstein, A.J., Woo, H.S., Tanner, D.B., Haung, W.S., MacDiarmid, A.G. (1987), "Polaron lattice in highly conducting polyaniline: Theoretical and optical studies", *Phys. Rev. Lett.*, **59**, 1464.

244. Avlyanov, J.K., Min, Y., MacDiarmid, A.G., Epstein, A.J. (1995), "Polyaniline: conformational changes induced in solution by variation of solvent and doping level", *Synth. Met.*, **72**, 65; and references therein.

245. Yang, C.Y., Cao, Y., Smith, P., Heeger, A.J. (1993), "Morphology of conductive, solution-processed blends of polyaniline and poly(methyl methacrylate)", *Synth. Met.*, **53**, 293; and references therein.

246. Angelopoulos, M., Asturias, G.E., Ermer, S.P., Ray, A., Scherr, E.M, MacDiarmid, A.G., Akhtar, M., Kiss, Z., Epstein, A.J. (1988), "Polyaniline: solutions, films and oxidation state", *Mol. Cryst. Liq. Cryst.*, **160**, 151.

247. Tang, X., Sun, Y., Wei, Y. (1988), "Molecular weight of chemically polymerised polyaniline", *Makromol. Chem.*, **9**, 829.

248. Angelopoulos, M., Ray, A., MacDiarmid, A.G., Epstein, A.J. (1987), "Polyaniline: Processability from aqueous solutions and effect of water vapour on conductivity", *Synth. Met.*, **21**, 21.

249. Epstein, A.J., Joo, J., Wu, C.Y., Benatar, A., Faust, C.F., Zegarski, J. (Jr), MacDiarmid, A.G (1993), "Polyanilines: Recent advances in processing and applications to welding of plastics", in: *Intrinsically Conducting Polymers*, Aldissi, M. (Ed.), Kluwer Academic, Dordrecht, pp. 165.

250. Cao, Y., Smith, P., Heeger, A.J. (1992), "Counter-ion induced processibility of conducting polyaniline and of conducting polyblends of polyaniline in bulk polymers", *Synth. Met.*, **48**, 91.

251. Aldissi, M. (1992), *Intrinsically Conducting Polymers: An Emerging Technology*, NATO-ASI series, Vol. E246, Kluwer Academic, Dordrecht.

252. Salaneck, W.R., Clark, D.T., Samuelsen, E.J. (1991), *Science and Applications of Conducting Polymers*, Adam Hilger, Bristol.

253. Prasad, P.N., Mark, J.E., Fai, T.J. (1995), *Polymers and Other Advanced Materials. Emerging Technologies and Business Opportunities*, Plenum Press, London.

254. Cao, Y. Smith, P., Heeger, A.J. (1993), "Counter-ion induced processibility of conducting polyaniline", *Synth. Met.*, **57**, 3514.

255. Xia, Y.N., Wiesinger, J.M., MacDiarmid, A.G., Epstein A.J. (1995), "Camphorsulfonic acid fully doped polyaniline emeraldine salt: conformations in different solvents studied by an ultraviolet/visible/near infrared spectroscopic method", *Chem. Mater.*, **7**, 443.

256. Majidi, M.R., Kane-Maguire, L.A.P., Wallace, G.G. (1994), "Enantioselective electropolymerisation of aniline in presence of (+) –or (-) - camphorsulfonate ion: a facile route to conducting polymers with preferred one-screw-sense helicity", *Polymer*, **35**, 3113.

257. Rozsnyai, L.F., Wrighton, M.S. (1996), "Controlling the adhesion of conducting polymer films with patterned self-assembled monolayers", *Chem. Mater.*, **8**, 309.

258. Liu, G., Freund, M.S. (1996), "Nucleophilic substitution reactions of polyaniline with substituted benzenediazonium ions: a facile method for controlling the surface chemistry of conducting polymers", *Chem. Mater.*, **8**, 1164.

259. MacDiarmid, A., Manohar, S.K. (1994), "High molecular weight polyanilines and synthetic methods therefore", US Patent No. 5,276,112.

260. Järvinen, H, Laakso, J, Auvinen, I., Silvasti, E. (1995), "Method for preparing polyaniline", US Patent No. 5,436,317.

261. Palaniappan, S., Chellachamy, A.A. (2003), "Process for the preparation of polyaniline salt", US Patent No. 6,630,567 B1.

262. Subramaniam, R., Deshpande, S.D. (2005), "Process for preparation of conducting polyaniline", US Patent No. 6,900,282 B2.

263. Adams, P.N., Laughlin, P.J., Monkman, A.P. (1996), "Synthesis of high molecular weight polyaniline at low temperature", *Synth. Met.*, **76**, 157.

264. Adams, P.N., Laughlin, P.J., Monkman, A.P., Kenwright, A.M. (1996), "Low temperature synthesis of high molecular weight polyaniline", *Polymer*, **37**, 3411.

265. Adams, P.N., Abell, L, Middleton, A., Monkman, A.P. (1997), "Low temperature synthesis of high molecular weight polyaniline using dichromate oxidant", *Synth. Met.*, **84**, 61.

266. Geng, Y., Li, J., Sun, Z., Jing, X., Wang, F. (1998), "Polymerisation of aniline in an aqueous system containing organic solvents", *Synth. Met.*, **96**, 1.

267. Genies, E.M., Syed, A.A., Tsintavis, C. (1985), "Electrochemical study of polyaniline in Aqueous and organic medium, redox and kinetic properties", *Mol. Cryst. Liq. Cryst.*, **121**, 181.

268. Masao, A., Akira, O., Hiroyuki, H., Minoru, E., Shinya, A., Keiji, N., Keiko, M., Yasuhiro, U., Michio, U (1998), "Organic polymer, conducting organic polymer, production methods and uses of the same", US Patent No. 5,728,321.

269. Sun, Z., Geng, Y., Li, J., Jing, X., Wang, F. (1997), "Chemical polymerisation of aniline with hydrogen peroxide as oxidant", *Synth. Met.*, **84**, 99.

270. Yasuda, A., Shimidzu, T. (1993), "Chemical and electrochemical analysis of polyaniline prepared with $FeCl_3$", *Synth. Met.*, **61**, 239.

271. Mažeikienė R., Malinauskas, A. (2000), "Deposition of polyaniline on glass and platinum by autocatalytic oxidation of aniline with dichromate", *Synth. Met.*, **108**, 9.

272. Tzou, K., Gregory, R.V. (1992), "Kinetic study of the chemical polymerisation of aniline in aqueous solution", *Synth. Met.*, **47**, 267.

273. Adams, P.N., Apperley, D.C., Monkman, A.P. (1993), "A comparison of the molecular weights of polyaniline samples obtained from gel permeation chromatography and solid state ^{15}N n.m.r. spectroscopy", *Polymer*, **34**, 328.

274. Kenwright, A.M., Feast, W.J., Adams, P., Milton, A.J., Monkman, A.P., Say, B.J. (1992), "Solution state carbon-13 nuclear magnetic resonance studies of polyaniline", *Polymer*, **33**, 4292.

275. Bikales, N. (1971), *Characterisation of Polymers*, Wiley-Interscience, John Wiley & Sons, NY.

276. Fukuda, T., Takezoe, H., Ishikawa, K., Fukuda, A., Wood, H.S., Jeong, S.K., Oh, E.J., Suh, J.S. (1995), "IR and Raman studies in three polyanilines with different oxidation levels", *Synth. Met.*, **69**, 175.

277. Gazotti, W.A., De Paoli M.-A. (1996), "High yield preparation of a soluble polyaniline derivative", *Synth. Met.*, **80**, 263.

278. Trchová, M., Sapurina, I., Prokeš, J., Stejskal, J. (2003), "FTIR spectroscopy of ordered polyaniline films", *Synth. Met.*, **135**, 305.

279. Chen, S.A., Lee, H.T. (1993), "Polyaniline plasticised with 1-methyl, 2-pyrrolidone: structure and doping behaviour", *Macromolecules*, **26**, 3254.

280. Lux, F., Samuelsen, E.J., Kang, E.T. (1995), "A new assessment of the crystalline structure of undoped and doped aniline oligomers and polymers", *Synth. Met.*, **69**, 167.

281. Dominis, A.J., Spinks, G.M., Kane-Maguire, A.P., Wallace, G.G. (2002), "A dedoping/redoping study of organic soluble polyaniline", *Synth. Met.*, **129**, 165.

282. Albuquerque, J.E., Mattoso, L.H.C., Balogh, D.T., Faria, R.M., Masters, J.G., MacDiarmid, A.G. (2000), "A simple method to estimate the oxidation state of polyanilines", *Synth. Met.*, **113**, 19.

283. Lindfors, T., Kvarnström, C., Ivaska, A. (2002), "Raman and UV-vis spectroscopic study of polyaniline membranes containing a bulky cationic additive", *J. Elect. Chem.*, **518**, 131.

284. Yang, D., Mattes, B.R. (2002), "Polyaniline emeraldine base in N-methyl-2-pyrrolidinone containing secondary amine additives: B. characterisation of solutions and thin films", *Synth. Met.*, **129**, 249.

285. Hanton, S.D. (2001), "Mass spectrometry of polymers and polymer surfaces", *Chem. Rev.*, **101**, 527.

286. Jackson, C.A., Simonsick, W.J. (Jr.) (1997), "Application of mass spectrometry to the characterisation of polymers", *Curr. Opin. Sol. State Mater. Sci.*, **2**, 661.

287. Karas, M., Hillenkamp, F. (1988), "Laser desorption ionisation of proteins with molecular masses exceeding 10,000 Daltons", *Anal. Chem.*, **60**, 2269.

288. Moore, J.C. (1964), "Gel permeation chromatography. I. a new method for molecular weight distribution of high polymers", *J. Polym. Sci.*, **A2**, 835.

289. Quivoron, C. (1984), "Use for polymer analysis", in: *Steric Exclusion Liquid Chromatography of Polymers*, J. Janča (Ed.), Marcel Dekker, Inc. NY.

290. Pellegrino, J. (2003), "The use of conducting polymers in membrane based separations", *Ann. N.Y. Acad. Sci.*, **984**, 289.

291. Wessling, B. (1999), "Polyaniline on the metallic side of the insulator-to-metal transition due to dispersion: the basis for successful nano-technology and industrial applications of organic metals", *Synth. Met.*, **102**, 1396; and references therein.

292. Shacklette, L., Han, C. (1994), "Solubility and dispersion characteristics of polyaniline", *Mat. Res. Soc.:Symp. Proc.*, **328**, 157.

293. Wessling, B. (1991), "On the structure of binary conductive polymer/solvent systems", *Synth. Met.*, **41**, 907.

294. Monkman, A.P., Adams, P.N. (1991), "Optical and electronic properties of stretch-oriented solution-cast polyaniline films", *Synth. Met.*, **40**, 87.

295. Cao, Y., Qiu, J., Smith, P. (1995), "Effect of solvents and co-solvents on the processibility of polyaniline: I. solubility and conductivity studies", *Synth. Met.*, **69**, 187.

296. Illing, G., Hellgardt, K., Wakeman, R. J., Jungbauer, A. (2001), "Preparation and characterisation of polyaniline based membranes for gas separations", *J. Memb. Sci.*, **184**, 69.

297. Pinnau, I, He, Z., Da Costa, A.R., Amo, K.D., Daniels, R. (2002), "Gas separation using C_{3+} hydrocarbon resistant membranes", US Patent No. 6,361,582 B1.

298. Jozefowicz, M.E., Laversanne, R., Javadi, H.H.S., Epstein, A.J., Pouget, J.P., Tang, X., MacDiarmid, A.G. (1989), "Multiple lattice phases and polaron-lattice-spinless-defect competition in polyaniline", *Phys. Rev. B.*, **39**, 12958.

299. ISO Standards (1993), "Plastics - determination of tensile properties - part 2: test conditions for moulding and extrusion plastics", ICS 83.080.01.

300. Pye, D.G., Hoehn, H.H., Paner, M. (1976), "Measurement of gas permeability of polymers. I. permeabilities in constant volume/variable pressure apparatus", *J. Appl. Sci.*, **20**, 1921.

301. Wei, Y., Jang, G.W., Chan, C.C. Hsuen, K.F., Hariharan, R., Patel, S.A., Whitecar, C.K. (1990), "Polymerisation of aniline and alkyl ring substituted anilines in the presence of aromatic additives", *J. Phys. Chem.*, **94**, 7716.

302. Mattoso, L.H.C., Manohar, S.K., MacDiarmid, A.G., Epstein, A.J. (1995), "Studies on chemical synthesis and on characteristics of polyaniline derivatives", *J. Polym. Sci., Part A: Polym. Chem.*, **33**, 1227.

303. Wei, Y., Tang, X., Sun, Y., Focke, W.W. (1989), "A study of the mechanism of aniline polymerisation", *J. Polym. Sci., Part A: Polym. Chem.*, **27**, 2385.

304. Genies, E.M., Lapkowski, M. (1987), "Polyaniline films. electrochemical redox mechanisms", *Synth. Met.*, **24**, 61.

305. Mohilner, D.M., Adams, R.N., Argersinger, W.J. (1962), "Investigation of the kinetics and mechanism of the anodic oxidation of aniline in aqueous sulphuric acid solution at a platinum electrode", *J. Am. Chem. Soc.*, **84**, 3618.

306. Breitenbach, M., Heckner, K.H. (1971), "Untersuchungen zur kinetic der anodischen oxidation von aniline in azetonitril an der rotierenden platinelektrode", *J. Electro-anal. Chem.*, **29**, 309.

307. Breitenbach, M., Heckner, K.H. (1971), "Elektrochemische untersuchungen der bildung and elgenschaften von polyanilinfilmen auf platin- und kohleelektronden", *J. Electro-anal. Chem.*, **43**, 267.

308. Sasaki, K., Kaya, M., Yano, J., Kitani, A., Kunai, A. (1986), "Growth mechanism in the electropolymerisation of aniline and *p*-aminodiphenylamine", *J. Electro-anal. Chem.*, **215**, 401.

309. Ohsaka, T., Ohnuki, Y., Oyama, N., Katagiri, G., Kamisako, K. (1984), "IR absorption spectroscopic identification of electroactive and electroinactive polyaniline films prepared by the electrochemical polymerisation of aniline", *J. Electro-anal. Chem.*, **161**, 399.

310. Nalawade, S.P., Picchioni, F., Marsman, J.H., Janssen, L.P.B.M. (2006), "The FTIR studies of interactions of CO_2 and polymers having different chain groups", *J. Supercrit. Fluids*, **36**, 236.

311. Zheng, W., Angelopoulos, M., Epstein, A.J., MacDiarmid, A.G. (1997), "Concentration dependence of aggregation of polyaniline in NMP solution and properties of resulting cast films", *Macromolecules*, **30**, 7634.

312. Cao, Y., Li, S., Xue, Z., Guo, D. (1986), "Spectroscopic and electrical characterisation of some aniline oligomers and polyaniline", *Synth. Met.*, **16**, 305.

313. Tang, J., Jing, X., Wang, B., Wang, F. (1988), "Infrared spectra of soluble polyaniline", *Synth. Met.*, **24**, 231.

314. Harada, I., Furukawa, Y., Ueda, F. (1989), "Vibrational spectra and structure of polyaniline and related compounds", *Synth. Met.*, **29**, 303.

315. Wan, M. (1992), "Absorption spectra of thin film of polyaniline", *J. Polym. Sci., Part A: Polym. Chem.*, **30**, 543.

316. Zuo, F., McCall, R.P., Ginder, J.M., Roe, M.G., Leng, J.M., Epstein, A.J., Asturias, G.E., Ermer, S.P., Ray, A., MacDiarmid, A.G. (1989), "Solution studies of the emeraldine oxidation state of polyaniline", *Synth. Met.*, **29**, 445.

317. Haung, W.S., MacDiarmid, A.G. (1993), "Optical properties of polyaniline", *Polymer*, **34**, 1833.

318. Zheng, W.Y., Levon, K., Laakso, J., Oesterholm, J.E. (1994), "Characterisation and solid state properties of processable *N*-alkylated polyanilines in natural state", *Macromolecules*, **27**, 7754.

319. Zheng, W., Min, Y., Lee, S.J., MacDiarmid, A.G., Angelopoulos, M., Liao, Y.H., Epstein, A.J. (1996), "The molecular conformation of non-doped polyaniline and its effect on the properties of doped polyaniline", *Mater. Res. Soc. Symp. Proc.*, **413**, 535.

320. Ohtani, A., Abe, M., Ezeo, M., Doi, T., Miyata, T., Miyake, A. (1993), "Synthesis and properties of high molecular weight soluble polyaniline and its application to the 4MB-capacity barium ferrite floppy disk's antistatic coating", *Synth. Met.*, **57**, 3696.

321. Oh, E.J., Min, Y., Wiesinger, J.M., Manoher, S.K., Sherr, E.M., Prest, P.J., MacDiarmid, A.G., Epstein, A.J. (1993), "Polyaniline: dependency of selected properties on molecular weight", *Synth. Met.*, **55**, 977.

322. Mattoso, L.H.C., MacDiarmid, A.G., Epstein, A.J. (1994), "Controlled synthesis of high molecular weight polyaniline and poly(*o*-methoxyaniline)", *Synth. Met.*, **68**, 1.

323. Boara, G., Sparpaglione, M. (1995), "Synthesis of polyanilines with high electrical conductivity", *Synth. Met.*, **72**, 135.

324. Adams, P.N., Monkman, A.P. (1997), "Characterisation of high molecular weight polyaniline synthesised at -40 C using a 0.25:1 mole ratio of persulfate oxidant to aniline", *Synth. Met.*, **87**, 165.

325. Vilčnik, M., Žigon, M., Zupan, M., Šebenik, A. (1998), "Influence of polymerisation parameters on the molecular weight of polyaniline", *Acta Chim. Slov.*, **45**, 173.

326. Pfromm, P.H., Pinnau, I., Koros, W.J. (1990), "Gas transport through asymmetric membranes: a comparison to isotropic film transport properties", *J. Memb. Sci.*, **48**, 2161.

327. Gupta, Y., Hellgardt, K., Wakeman, R.J. (2006), "Enhanced permeability of polyaniline based nano-membranes for gas separation", *J. Memb. Sci.*, **282**, 60.

328. Athayde, A.L., Baker, R.W., Nguyen, P. (1994), "Metal composite membranes for hydrogen separation", *J. Memb. Sci.*, **94**, 299.

329. Schofield, R.W., Fane, A.G., Fell, C.J.D. (1990), "Gas and vapour transport through microporous membranes. I – Knudsen-Poiseuille transport", *J. Memb. Sci.*, **53**, 59.

330. Singh, A., Koros, W.J. (1996), "The significance of entropic selectivity for advanced gas separation membranes", *Ind. Eng. Chem. Res.*, **35**, 1231.

331. Nagai, K., Masuda, T., Nakagawa, T., Freeman, B.D., Pinnau, I. (2001), "Poly[1-(trimethylsilyl)-1-propyne] and related polymers: Synthesis, properties and functions", *Polymer Science*, **26**, 721.

332. Nakagawa, T., Fujisaki, S., Nakano, H., Higuchi, A. (1994), "Physical modification of poly[1-(trimethylsilyl)-1-propyne] membranes for gas separation", *J. Membrane Sci.*, **94**, 183.

333. Jordan, S.M., Henson, M.A., Koros, W.J. (1990), "The effect of carbon dioxide conditioning on the permeation behaviour of hollow fibre asymmetric membranes", *J. Membrane Sci.*, **54**,102.

334. White, L.S., Blinka, T.A., Kloczewski, H.A., Wang, I. -F. (1995), "Properties of polyimide gas separation membrane in natural gas streams", *J. Membrane Sci.*, **103**, 73.

335. Wang, Z., Chen, T., Xu, J. (1997), "Novel, poly(aryl ether ketone)s containing various pendant groups. II. gas transport properties", *J. Appl. Polym. Sci.*, **64**, 1725.

336. Koros, W.J., Coleman, M.R., Walker, D.R.B. (1992), "Controlled permeability of polymer membranes", *Ann. Rev. Mater. Sci.*, **22**, 47.

337. McHattie, J.S., Koros, W.J., Paul, D.R. (1991), "Gas transport properties of polysulfones: 1. Role of summery of methyl group placement on bisphenol rings", *Polymer*, **33**, 1701.

338. Muruganandam, N., Paul, D.R. (1987), "Evaluation of substituted polycarbonated and a blend with polystyrene as gas separation membranes", *J. Memb. Sci.*, **34**, 185.

339. Aitken, C.L., Koros, W.J., Paul, D.R. (1993), "Gas transport properties of biphenol polysulfones", *Macromolecules*, **25**, 3651.

340. Aitken, C.L., Koros, W.J., Paul, D.R. (1992), "Effect of structural symmetry of gas transport properties of polysulfones", *Macromolecules*, **25**, 3424.

341. McHattie, J.S., Koros, W.J., Paul, D.R. (1991), "Effect of isopropylidene replacement of gas transport properties of polycarbonates", *J. Polym. Sci., Part B, Polym. Phys.*, **29**, 731.

342. Mohr, J.M., Paul, D.R., Tullos, G.L., Cassidy, P.E. (1991), "Gas transport properties of a series of poly(ether ketone) polymers", *Polymer*, **32**, 2387.

343. Gupta, Y., Wakeman, R.J., Hellgardt, K. (2006), "The potential of polyaniline nano-membranes for gas separation", *10th Nordic Filtration Symposium*, Trondheim, Norway.

Appendix 1

LIST OF SYMBOLS

A_m	Membrane surface area	(cm^2)
C'	Geometrical parameter that depends on pore system	
D	Diffusion coefficient	($cm^2\ s^{-1}$)
D_D	Mobility (diffusion) of the dissolved components	($cm^2\ s^{-1}$)
D_{eff}	Effective diffusion coefficient	($cm^2\ s^{-1}$)
D_H	Mobility (diffusion) of the Langmuir sorbed components	($cm^2\ s^{-1}$)
D_i	Surface diffusion coefficient	($cm^2\ s^{-1}$)
D_T	Thermodynamic diffusion coefficient	($cm^2\ s^{-1}$)
E	Activation energy	($kJ\ mol^{-1}$)
F_k	Driving force (such as chemical potential) of component *'k'*	($cmHg\ cm^3\ mol^{-1}$)
J	Permeation rate (flux)	($cm^3\ cm^{-2}\ s^{-1}$)
J_p	Total permeate flux (for mixed-gas system)	($cm^3\ cm^{-2}\ s^{-1}$)
J_{vf}	Volumetric flux of the gas on the feed side	($cm^3\ cm^{-2}\ s^{-1}$)
J_{vp}	Volumetric flux of the gas in the permeate side	($cm^3\ cm^{-2}\ s^{-1}$)
K_i	Sorption coefficient of *'i'*	($cmHg^{-1}$)
L_{ik}	Phenomenological coefficient	
M_n	Number average molecular weight	
M_w	Weight average molecular weight	
P	Permeability coefficient	($cm^3\ cm\ cm^{-2}\ s^{-1}\ cmHg^{-1}$)
P_0	Permeability at STP	($cm^3\ cm\ cm^{-2}\ s^{-1}\ cmHg^{-1}$)
P_i	Permeability coefficient of the component *'i'*	($cm^3\ cm\ cm^{-2}\ s^{-1}\ cmHg^{-1}$)
P_j	Permeability coefficient of the component *'j'*	($cm^3\ cm\ cm^{-2}\ s^{-1}\ cmHg^{-1}$)
P_{total}	Total permeability coefficient (for mixed-gas system)	($cm^3\ cm\ cm^{-2}\ s^{-1}\ cmHg^{-1}$)
R	Ideal Gas constant	($cm^3\ cmHg\ cm^{-1}{}_{STP}\ K^{-1}$)
R_s	Stoke's radius of the solute	(cm)
S	Solubility coefficient	($cm^3{}_{gas}\ cm^{-3}{}_{polymer}\ cmHg^{-1}$)
T	Temperature	(K)
V	Specific volume of the polymer	($cm^3\ g^{-1}$)
V_d	Downstream volume of the permeation cell	(cm^3)
V_f	Fractional free volume	(cm^3)
V_g	Actual glassy specific volume	(cm^3)
V_l	Equilibrium volume of densified glass	(cm^3)
ΔE_D	Activation energy for diffusion	($kJ\ mol^{-1}$)

ΔE_p	Activation energy for permeation	(kJ mol^{-1})
ΔH_D	Henry type sorption enthalpy	(kJ mol^{-1})
ΔH_H	Langmuir type sorption enthalpy	(kJ mol^{-1})
ΔH_s	Partial molar enthalpy of the sorption	(kJ mol^{-1})
b	Langmuir's hole affinity constant	($cmHg^{-1}$)
c^*	Effective total concentration of the sorbed penetrant	(g cm^{-3}) or (mol cm^{-3})
c_D	Sorption described by Henry's law relation	(mol cm^{-3})
c_g	Concentration of solute at glass transition temperature	(g cm^{-3}) or (mol cm^{-3})
c_H	Sorption described by Langmuir's "hole filling" process	(mol cm^{-3})
c'_H	Langmuir's capacity constant	(mol cm^{-3}) or (cm^3_{STP} cm^{-3})
$c_{i,0}$	Concentration of *'i'* in the feed	(g cm^{-3}) or (mol cm^{-3})
$c_{i,0(m)}$	Concentration of *'i'* on the feed side membrane surface	(g cm^{-3}) or (mol cm^{-3})
c_{i,t_m}	Concentration of *'i'* in the permeate	(g cm^{-3}) or (mol cm^{-3})
$c_{i,t_m(m)}$	Concentration of *'i'* on the permeate side membrane surface	(g cm^{-3}) or (mol cm^{-3})
f_{kj}	Free frictional coefficient	
f_{km}	Frictional coefficient	
k_D	Henry's law solubility coefficient	(cm^3_{STP} $cm^{-3}_{polymer}$ $cmHg^{-1}$)
m_i	Molar weight of *'i'*	(mol)
n_i	Mole fraction	(mol mol^{-1})
$n_{i(0)}$	Mole fraction of *'i'* in the feed	(mol mol^{-1})
$n_{i(m)}$	Mole fraction of *'i'* on the feed side membrane surface	(mol mol^{-1})
n_{i,t_m}	Mole fraction of *'i'* in the permeate	(mol mol^{-1})
$n_{i,t_m(m)}$	Mole fraction of *'i'* on the permeate side membrane surface	(mol mol^{-1})
p_0	Feed side pressure	(cmHg)
p_f	Feed side pressure	(cmHg)
p_o	Vapour pressure of the penetrant	(cmHg)
p_{t_m}	Permeate side pressure	(cmHg)
p_i^{sat}	Saturated vapour pressure	(cmHg)
t_m	Thickness of the polymeric membrane	(cm)
u_k	linear velocity of solute *'k'*	(cm s^{-1})
u_j	Linear velocity of solute *'j'*	(cm s^{-1})
u_i	Mobility coefficient of the penetrant	(cm^2 s^{-1})
v_H	Excess free volume	(cm^3)
$v_{H(c)}$	Excess free volume per unit volume of the penetrant polymer system	
w_i	Weight of the fraction	(g)
x_i	Molar fraction of the component *'i'* in the feed	(mol mol^{-1}_{total})

x_j	Molar fraction of the component *'j'* in the feed	(mol mol^{-1}_{total})
y_i	Molar fraction of the component *'i'* in the permeate	(mol mol^{-1}_{total})
y_j	Molar fraction of the component *'j'* in the permeate	(mol mol^{-1}_{total})
α_{ij}	Separation factor	
μ_i^o	Reference chemical potential of pure *'i'*	(cm^3 cmHg mol^{-1})
$\mu_{i,o}$	Chemical potential of *'i'* in the feed	(cm^3 cmHg mol^{-1})
$\mu_{i,o(m)}$	Chemical potential of *'i'* on the feed side membrane surface	(cm^3 cmHg mol^{-1})
μ_{i,t_m}	Chemical potential of *'i'* in the permeate	(cm^3 cmHg mol^{-1})
$\mu_{i,t_m(m)}$	Chemical potential of *'i'* on the permeate side membrane surface	(cm^3 cmHg mol^{-1})
ρ	Density of the pure gas	(g cm^{-3})
ρ_m	Molar density of the membrane phase	(mol cm^{-3})
ρ_{total}	Density of the gas mixture (for mixed-gas system)	(g cm^{-3})
σ	Characteristic parameter for the solubility dependence on the concentration	
ϕ	Local volume fraction of the penetrant in the polymer	(cm^3 cm^{-3}_{total})
ϕ_p	Volume fraction of the polymer	(cm^3 cm^{-3}_{total})
ϕ_{fs}^o	Fractional free volume of the penetrant in pure polymer	(cm^3)
$\bar{\upsilon}$	Molar Volume	(cm^3 mol^{-1})
υ_i	Molar volume of the component *'i'*	(cm^3 mol^{-1})
$\upsilon_{i(m)}$	Molar volume of *'i'* in the feed side membrane surface	(cm^3 mol^{-1})
ζ	Characteristic parameter of gas-gas and gas-membrane interactions	
χ	Flory-Huggins parameter	
γ	Characteristic parameter of penetrant to plasticise the	
γ_i	Activity coefficient linking the mole fraction activity	
$\gamma_{i(m)}$	Activity coefficient linking the mole fraction activity in the membrane surface	
δ	Thickness of the layer of unmixed fluid on the feed side membrane surface	(cm)
$\Delta\alpha$	Difference between thermal expansion and compressibility coefficient above glass transition temperature	

$\Delta\beta$	Difference between thermal expansion and compressibility coefficient below glass transition temperature	
$\left(\frac{dc_{i(m)}}{dx}\right)$	Concentration gradient in membrane	(g cm^{-3} cm^{-1})
$\left(\frac{dp}{dt_m}\right)$	Pressure gradient across the membrane	(cmHg cm^{-1})
$\left(\frac{dp_i}{dt}\right)_{steady-state}$	Steady state rate of pressure rise in the downstream section of the permeation cell at a fixed upstream pressure	(cmHg cm^{-1})
$\left(\frac{dp_i}{dt}\right)_{leak}$	Steady state rate of pressure rise in the downstream section of the permeation cell under vacuum	(cmHg cm^{-1})

Appendix 2

DESIGN OF THE PERMEATION CELL

1. DESIGN OF PERMEATION CELL

1.1. Operational Conditions

The normal and transient operational conditions have to be specified to design the permeation cell.

1.1.1. Normal Conditions

- The operating internal pressure existing during normal operating condition should be specified. The operating pressure considered for this design was 60 bar (6 MPa). The maximum pressure is generally not more than 10 percent in excess of the operating pressure.
- The operating temperature should also be specified depending on the contained fluid in the cell. The experiments were considered to be conducted at ambient temperature; hence, there is no thermal stress that needs to be considered for the design.

1.1.2. Transient Conditions

- The transient conditions may be repetitive, for example, those occurring during starting up and shutting down. It is necessary to know the anticipated modes of operation, including rates of changes of internal pressure, and possible emergency loads due to sudden pressure rise in the section.

1.2. National Codes

A number of National Codes which specify requirements of design, fabrication, inspection and testing of unfired pressure vessels are available. In most countries the National Codes have the force of law and strict adherence to their rules is required. It is therefore desirable that any design, regardless of the method adopted, should be checked with the standard code. In the current design, the code used was BS 5500-2003.

1.3. Material Selection for High Pressure Vessels

Ductility is an essential requirement in steel for use as a pressure vessel and should guide the choice of steel and its heat treatments. Ni-Cr-Mo are the most common steels are used for high pressure vessels. The stainless steel SS316 was used to design the permeation cell to conduct the gas permeation experiments. The nominal data sheet for 316 stainless steel was summarised in the following table.

Table I 1 The nominal data sheet for 316 stainless steel.

Chemical Composition			**Mechanical Properties (Annealed Condition)**	
Cr	16 – 18		Ultimate Tensile Strength	90,000 psi
Ni	10 – 14		0.2% Offset Yield Strength	40,000 psi
Mo	2 – 3		Percent Elongation in 2"	50%
Mn	2	max	Hardness Rockwell	B80
C	0.03	max		
Si	1.00	max		
S	0.03	max		
P	0.045	max		

1.4. Stress Calculation

The main loading in the shell is due to the internal pressure. The stresses across the shell thickness due to pressure are not uniform. The stresses due to other load (e.g. dead loads), are comparatively smaller in magnitude and, therefore, were ignored. Three principal stresses are produced in the wall of the shell du to high pressure, which are:

- Tangential (circumferential or hoop) stress
- Radial stress

- Longitudinal (axial) stress.

The tangential stresses are of high magnitude. According to Lame's analysis (assuming a fully elastic cylinder) the variation of tangential and radial stresses along the radius, R, of the shell is given by following equations.

$$\text{Tangential stress} \quad f_p = A + \frac{B}{R^2} \tag{I.1}$$

$$\text{Radial stress} \quad f_R = A - \frac{B}{R^2} \tag{I.2}$$

$$\text{Longitudinal stress} \quad f_a = A \tag{I.3}$$

where A, B are the constants.

The tangential stress may either be tensile or compressive depending on the relative magnitude of the internal pressure. The radial stress is always compressive and the axial stress is tensile. It is assumed that the axial force due to pressure is wholly carried by the wall.

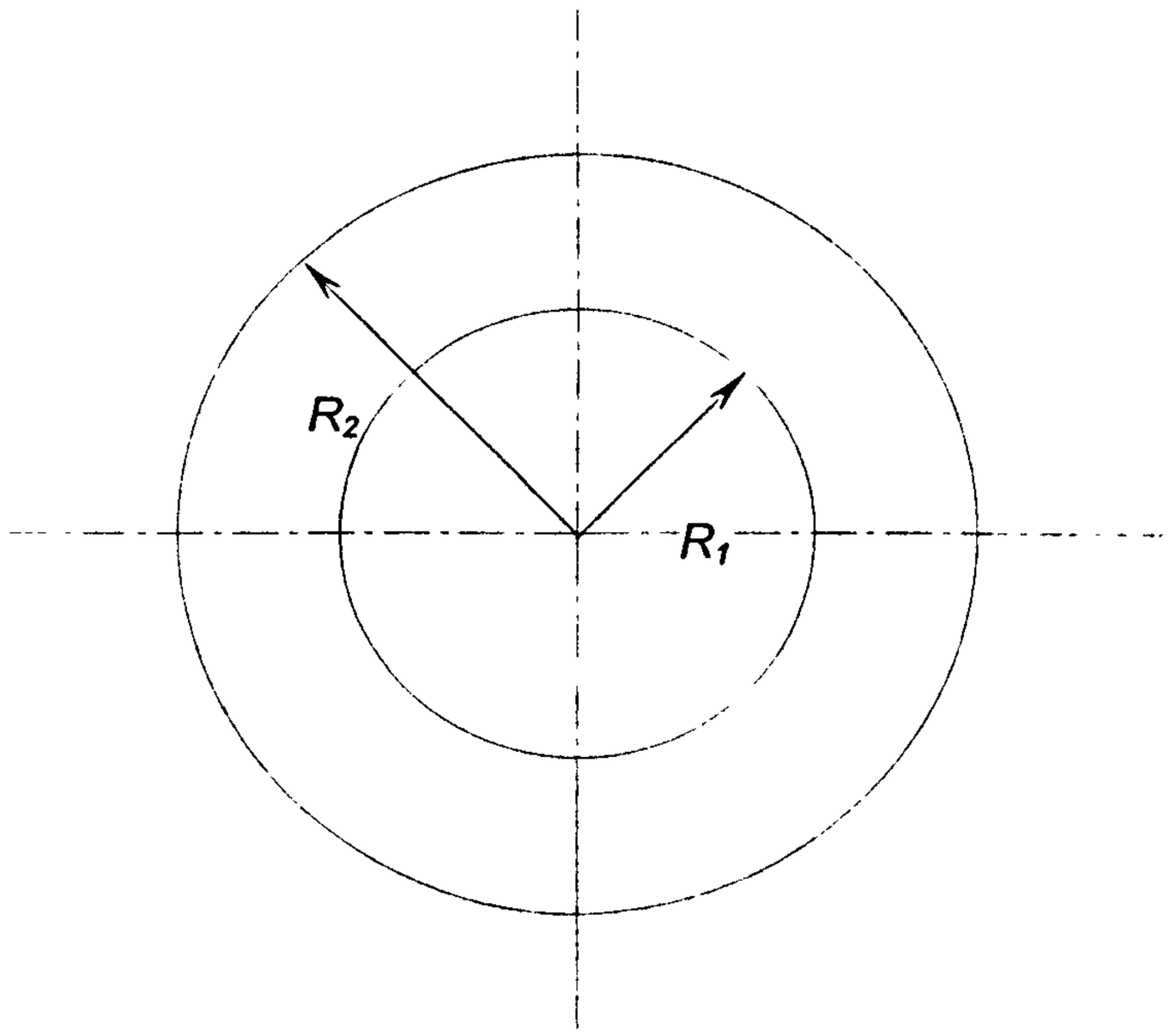

Figure I 1 Schematic of the high pressure permeation cell.

If the inner radius of the pressure vessel is R_1, the pressure p_1, and at the outer radius R_2, the pressure is p_0 (see Figure I-1), the constant A and B can be determined as;

$$A = \frac{R_1^2 \cdot p_i - R_2^2 \cdot p_o}{R_2^2 - R_1^2} = \frac{(p_i - p_o) \cdot K^2}{K^2 - 1} \qquad (I.4)$$

where, $K = \frac{R_2}{R_1}$

$$B = \frac{(p_i - p_o) \cdot R_1^2 \cdot R_2^2}{(R_2^2 - R_1^2)} = \frac{(p_i - p_o) \cdot K^2 \cdot R_1^2}{K^2 - 1} \qquad (I.5)$$

It is important to note that the tangential and radial stresses consist of a pure shear stress ($q = -B/R^2$) with a superimposed hydrostatic stress, A. The maximum values of stresses depend only on the ratio of the radii and not on the absolute magnitude. In many cases only the internal pressure, p_i, is present and the above equations I.1 and I.2 at the inner surface (i.e. $R = R_1$) are therefore simplified to;

$$f_p = A + \frac{B}{R^2} = \frac{R_1^2 \cdot p_i}{R_2^2 - R_1^2}\left(1 + \frac{R_2^2}{R_1^2}\right) \qquad (I.6)$$

$$f_R = A - \frac{B}{R^2} = \frac{R_1^2 \cdot p_i}{R_2^2 - R_1^2}\left(\frac{R_2^2}{R_1^2} - 1\right) \qquad (I.7)$$

$$f_a = A = \frac{R_1^2 \cdot p_i}{R_2^2 - R_1^2} \qquad (I.8)$$

1.5. Application to Permeation Cell Design

1.5.1. Design based on Tangential Stress

The thickness of the cylinder can be determined on the basis of the maximum tangential stress at inner surface of the cylinder. The equation I.6 can be written in terms of thickness (i.e. $t = R_2 - R_1$) as;

$$f_{p(max)} = \frac{p_i}{t}\left(\frac{R_1^2 + R_2^2}{R_1 + R_2}\right) \qquad (I.9)$$

If f_p is taken as the allowable tensile stress, f, then;

$$t = R_1\left(\sqrt{\frac{fJ + p_i}{fJ - p_i}} - 1\right) \qquad (I.10)$$

where J is the joint efficiency.

The above equation I.10 was used to calculate the thickness of the permeation cell based on tensile stress at the inner surface of the cylinder. The joint efficiency, J, was assumed to be 0.9 for the welded cylinders. For the maximum operating internal pressure, p_i, 60 bar (6 MPa), and internal radius, R_1, 4 cm, the thickness of the permeation cell is;

$$t = 4\left(\sqrt{\frac{620.528 \times 0.9 + 6}{620.528 \times 0.9 - 6}} - 1\right) = 0.0432 \text{ cm}$$

1.5.2. Design Based on Shear Stress

The another approach to design is based on the maximum shear stress produced at any point on the wall of the permeation cell, which is given by;

$$f_{s(max)} = \frac{1}{2}(f_p - f_R) \qquad (I.11)$$

The limit of elastic action occurs when

$$f_s \text{ (at yield point)} = \frac{1}{\sqrt{3}} f_{yp} \text{ (direct tensile stress at yield point)} \qquad \text{(I.12)}$$

If the cylindrical shell is to be designed within the limits of elastic action, the maximum internal pressure at the inner radius is given by;

$$p_{max} = \left[\frac{1}{\sqrt{3}} f_{yp} \cdot \frac{K^2 - 1}{K^2}\right] \qquad \text{(I.13)}$$

For purpose of design a factor of safety should be used to get the allowable stress. The value of K can then be determined as;

$$K = \sqrt{\frac{f}{f - p_i\sqrt{3}}} \qquad \text{(I.14)}$$

and

$$t = R_1 (K\text{-}1) \qquad \text{(I.15)}$$

from the above equation I.14, the value of K is;

$$K = \sqrt{\frac{620.528}{620.528 - 6 \times \sqrt{3}}} = 1.00848$$

and the thickness of the permeation cell is (from the equation I.15);

$$t = 4 \text{ x } (1.00848 - 1) = 0.0339 \text{ cm}$$

1.6. Gasket

Gasket, also known as static seal, was used to make a pressure-tight joint between upstream and downstream of the permeation cell. Flat ring rubber gaskets were cut from a Buna rubber sheet were interposed between the upstream and downstream sections and were held tight by six M10 bolts and nuts.

1.7. Threaded Fasteners

Bolts and nuts were used for fastening and making detachable joints between upstream and downstream sections of the permeation cell. In the current design, M10 bolts and nuts were used to fasten upstream and downstream section. The size of the bolt is specified by the external diameter of the thread and the length is measured under the head.

The minimum bolt load and the number and size of the bolts were determined from the following equations (in terms of the size of the gasket);

At atmospheric conditions

$$W_{m_1} = A_g \, x \, Y_a = \pi \, x \, b \, x \, G \, x \, Y_a \qquad (I.16)$$

where, b is the effective gasket surface width, G is diameter of gasket load reaction, and Y_a is the gasket seating stress.

At operating conditions

$$W_{m_2} = A_g \, x \, Y_p + A_h \, x \, p = \pi \, 2b \, Gmp + (\pi/4) \, G^2 p \qquad (I.17)$$

where m is the gasket factor, $2b$ is the effective gasket surface width under pressure and p is the design pressure.

The bolt loads W_{m_1} or W_{m_2} will create a tensile stress in the cross-section of the bolt.

$$A_{m_1} = \frac{W_{m_1}}{f_a} \quad \text{(I.18)}$$

and

$$A_{m_2} = \frac{W_{m_2}}{f_b} \quad \text{(I.19)}$$

where, A_{m_1} and A_{m_2} are the cross-section of the bolt, f is the permissible tensile stress, and the subscripts a and b are for under atmospheric and operating conditions, respectively.

Further,

$$A_{m_1} \text{ or } A_{m_2} = A_m \times \textit{Number of bolts} \quad \text{(I.20)}$$

where A_m is the area of the bolt.

The values of W_{m_1} and W_{m_2} were (calculated using equations I.16 and I.17, respectively) 1477.77 N and 51385.51 N, respectively.

In this design, M10 bolts were used to fasten the upstream and downstream sections. Hence, the required number of bolts, calculated using equation I.20, were ~2.

In order to make the design safe for the extended operation pressure range, the thickness of the permeation cell was extended to 10 mm and the number of the bolts used was 6.

Appendix 3

CALIBRATION OF PERMEATE SECTION VOLUME

1. CALIBRATION OF PERMEATE SECTION VOLUME

The permeate (downstream) volume was determined with high accuracy using a Manometric Method, and the measured value was confirmed by conducting a single gas permeation measurement with a standard PDMS membrane with known permeability, under similar operating conditions.

1.1. Manometric Method

The operational procedure to measure the downstream volume of the permeation cell using Manometric method is described in details in Section 5.3.2.2.1 (see Chapter 3). The experiment was performed with two sample gas cylinders (10 and 25 cm^3), and equation 3.3 (see Chapter 3) was used to calculate the permeate section volume.

For experiment with V_1 = 10 cm^3 sample gas cylinder:

- The pressure in the downstream section (after evacuating the section for 12 hours) before opening the Valve (g), p_0, was 0.733 cmHg.
- The atmospheric pressure, p_1, monitored at the time of the experiment was 75.95 cmHg (at 18 C).
- The pressure monitored in the permeate section after opening the Valve (g), p_2, was 14.921 cmHg.

The permeate section volume (calculated by equation 3.3) was 49.161 cm^3. However, to evaluate the actual volume of the permeate section, the additional volumes (e.g. tubing and internal volume of the pressure transducer) were deducted from the calculated value. After precise

measurements and data obtained for the internal volume of the transducer from the pressure transducer manufacturing company, the actual volume of the permeate (downstream) section was 30.0829 cm^3.

The experiment repeated for with another sample gas cylinder (V_1 = 25 cm^3). The permeate section volume obtained with 25 cm^3 sample gas cylinder was 48.837 cm^3, and the actual downstream section (after deducting additional volumes) was 29.8815 cm^3.

The values obtained via Manometric method correspond to the geometrical volume of the downstream (permeate) section volume, which is 29.1855 cm^3.

1.2. Gas Permeation Method

To confirm the value obtained for permeate section volume by Manometric method, a single gas permeation test was conducted using a standard circular PDMS membrane having selective PDMS layer thickness 2 µm with the method described in Section 5.3.2.2.2 (see Chapter 3). Nitrogen was used as a permeating gas to conduct an experiment at 2 bar (0.2 MPa) upstream (feed side) pressure and ambient temperature (20 C). The permeability coefficient of nitrogen through PDMS membrane, used to calculated downstream volume, was 240 Barrer (obtained from the manufacturer (GKSS, Germany)).

The downstream section volume was calculated using the equation 3.4 (see Chapter 3). The downstream (permeate) section volume obtained with gas permeation method was 31.1628 cm^3, which is also in a close proximity of the geometrical volume of the permeate section.

Appendix 4

CALCULATING POLYANILINE YIELD

CALCULATING THE YIELD OF POLYANILINE POWDER

The percentage yield of the as-synthesised polyaniline powder was calculated by using the following equation.

% yield = (weight of the polymer produced) / (weight of aniline used) x 100

The weight of the aniline (monomer) used to synthesise polyaniline was 9.313 g. The weight of polyaniline produced in the first batch (polymerisation reaction temperature = 21 C) is 6.43 ± 0.5 g.

The percentage yield of the polyaniline powder was calculated from the above equation;

% yield = (6.43 / 9.313) x 100 = 69.04 %

The weight loss during the washing the polyaniline powder was assumed to be ± 0.5 g for each polyaniline batch, which represents 7% error in the percentage yield calculation.

Appendix 5

ESTIMATING POLYANILINE FILM THICKNESS

ESTIMATING THE POLYANILINE FILM THICKNESS

In this work, 1-methyl, 2-pyrrolidone (NMP) was used as a suitable solvent to prepare polyaniline (EB) membranes. The glass petri dishes (20 cm diameter) were obtained from Glasgerätebau Ochs GmbH, Germany, and used to prepare uniform layers of polyaniline membranes.

The polyaniline films having desired thicknesses were prepared by pouring a known amount of 1% by weight polyaniline emeraldine base solution in NMP onto a glass petri dish followed by evaporating the solvent in a clean vacuum oven. In this work, several polyaniline films having polyaniline layer thicknesses between 14.389 μm and 0.166 μm were prepared. The following Figure IV.1 shows the relationship between amount of 1% by weight polyaniline solution in NMP used and polyaniline membrane thickness.

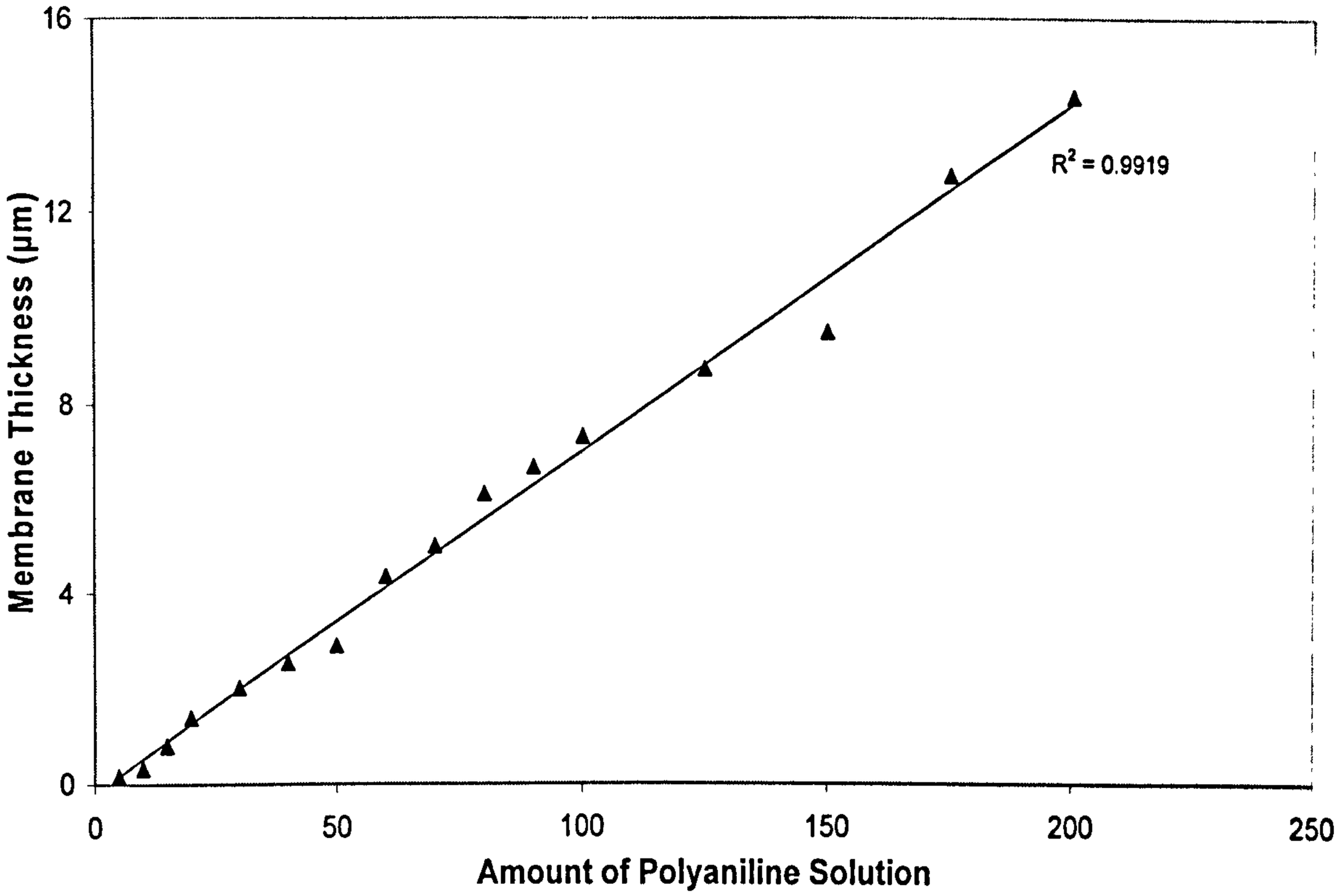

Figure IV 1 Graph of polyaniline membrane thickness (µm) *vs* amount of 1% by weight polyaniline solution used to prepare films.

Approximately, 0.16 ml/cm^2 of 1% by weight polyaniline solution in NMP was required to prepare a 1 µm thick film.

Appendix 6

CALCULATING PERMEABILITY, IDEAL (PURE GAS) AND REAL (MIXED GAS) SEPARATION EFFICIENCY

1. PERMEABILITY COEFFICIENT

The permeability coefficient of a permeating gas was calculated by using the equation 2.58 (see Chapter 2) that is;

$$P_i = \frac{1}{p_{i,o}} \times \frac{V_d \cdot t_m}{R \cdot T \cdot A_m} \times \left[\left(\frac{dp_i}{dt} \right)_{steady-state} - \left(\frac{dp_i}{dt} \right)_{leak} \right] \qquad \text{(VI.1)}$$

where V_d is the down stream volume of the permeation cell *(cm^3)*, t_m is membrane thickness *(cm)*, $p_{i,o}$ is the feed side penetrant pressure maintained in the permeation cell, R is the gas constant ($0.278\ cm^3 \cdot cmHg / cm^3_{STP} \cdot K$), and T represents the absolute temperature *(K)*. A_m is the membrane surface area *(cm^2)*, and $(dp_i/dt)_{steady\text{-}state}$ and $(dp_i/dt)_{leak}$ are the steady-state rates of pressure rise *(cmHg/s)* in the downstream (permeate) volume at a fixed pressure and under vacuum , respectively.

For example, the permeability coefficient for nitrogen (as a permeating gas through self-supported polyaniline film having thickness 2.89 μm) can be calculated by substituting all the known parameters, which are;

$V_d = 48.8365\ cm^3$

$t_m = 2.89\ \mu m = 2.89 \times 10^{-4}\ cm,$

$p_{i,o} = 2\ bar = 150.0126\ cmHg$

$R = 0.278\ cm^3 \cdot cmHg / cm^3_{STP} \cdot K$

$T = 293.65\ K$

$A_m = 7.068\ cm^2$

$(dp_i/dt)_{steady\text{-}state}$ is the gas permeation rate, which was calculated from the graph of rise in the pressure in the downstream section *vs* time, and the $(dp_i/dt)_{leak}$ was assumed to be zero for all permeation coefficient calculations.

The accumulation (permeation) rate (calculated from the graph of rise in downstream pressure *vs* experiment time) for nitrogen through self-supported polyaniline membrane was 1.041×10^{-5} cmHg/s.

These values were substituted in the above equation in order to calculate the permeability coefficient for nitrogen through self-supported polyaniline membrane (selective polyaniline film thickness = 2.89 μm).

$$P_{N_2} = \frac{1}{150.0126} \times \frac{48.8365 \times 0.000289 \times 0.00001041}{0.278 \times 293.65 \times 7.068}$$

$$= 1.71 \times 10^{-11} \left(\frac{cm^3_{STP} \cdot cm_{polymer}}{cm^2_{polymer} \cdot s \cdot cmHg} \right)$$

The permeability coefficient is often expressed with the unit Barrer,

$$1 \text{ Barrer} = 10^{-10} \left(\frac{cm^3_{STP} \cdot cm_{polymer}}{cm^2_{polymer} \cdot s \cdot cmHg} \right)$$

Hence, permeability coefficient value of nitrogen through self-supported polyaniline membrane was calculated to be 0.0171 Barrer.

2. IDEAL (PURE GAS) SEPARATION EFFICIENCY

The ability of the polymeric membrane to separate gases is characterised by the separation efficiency. Since the downstream pressure is negligible relative to the upstream pressure, the selectivity is commonly expressed by the ratio of the pure gas permeability coefficients for individual components of two gases.

$$\alpha_{i,j} = \frac{P_i}{P_j} \qquad \text{(VI.2)}$$

The permeability coefficients of pure (individual) gases were calculated from equation VI.1. The pure gas permeability of oxygen and nitrogen were 0.098 and 0.0176 Barrers, respectively.

The ideal (pure gas) selectivity for oxygen and nitrogen was calculated from the equation VI.2 as follows;

$$\alpha_{O_2/N_2} = \frac{0.098}{0.0176} = 5.56$$

The pure gas selectivity for oxygen over nitrogen indicates that the oxygen permeates 5.56 times faster than nitrogen through a self-supported undoped polyaniline film.

3. MIXED GAS SEPARATION EFFICIENCY

For mixed gas permeation system, the downstream pressure can not be ignored, henceforth, the real (mixed gas) separation efficiency can be defined by;

$$\alpha_{i,j} = \frac{y_i / y_j}{x_i / x_j} \qquad \text{(VI.2)}$$

where, y_i, x_i and y_j, x_j refer to the mole fraction of component *i* and *j* in the product and feed streams, respectively.

For oxygen/nitrogen mixed gas system, molar fractions of oxygen and nitrogen in the permeate side were monitored by the mass spectrometer. The molar fractions of oxygen and nitrogen were calculated from the feed composition. Oxygen and nitrogen molar fractions in the feed (calculated from the feed composition) were 0.467 and 0.533, respectively. The molar fractions for oxygen and nitrogen measured in the permeate were 0.834 and 0.166, respectively. The separation efficiency for oxygen/nitrogen mixed gas system was calculated by using equation VI.2 as follows;

$$\alpha_{O_2/N_2} = \frac{y_{O_2} / y_{N_2}}{x_{O_2} / x_{N_2}} = \frac{(0.834/0.116)}{(0.467/0.533)} = 5.012$$

Appendix 7

CALIBRATION OF MASS SPECTROMETER

The permeation behaviour of a pure gas through membrane depends mainly on the properties of the gas and membrane as well as the feed conditions. In the mixed gas system, the gas transport of a penetrant gas through polymer membrane is affected by the presence of other competitive penetrant gas. In this work, the sampling interface (mass spectrometer) was used for mixed gas experiments (O_2-N_2, CO_2-O_2, and CO_2-N_2 mixed gas systems). The calibration curves for N_2, O_2 and CO_2 relating the mass spectroscopic intensity and the injected standard gas concentration under the fixed conditions were constructed, and the concentration of the permeating gas (from the spectroscopic intensity) was precisely calculated from the calibration curve. The following Figures VI.1, VI.2 and VI.3 show the relationship between the spectrometer intensity and the concentration of the injected standard gas (N_2, O_2 and CO_2) sample in the feed gases.

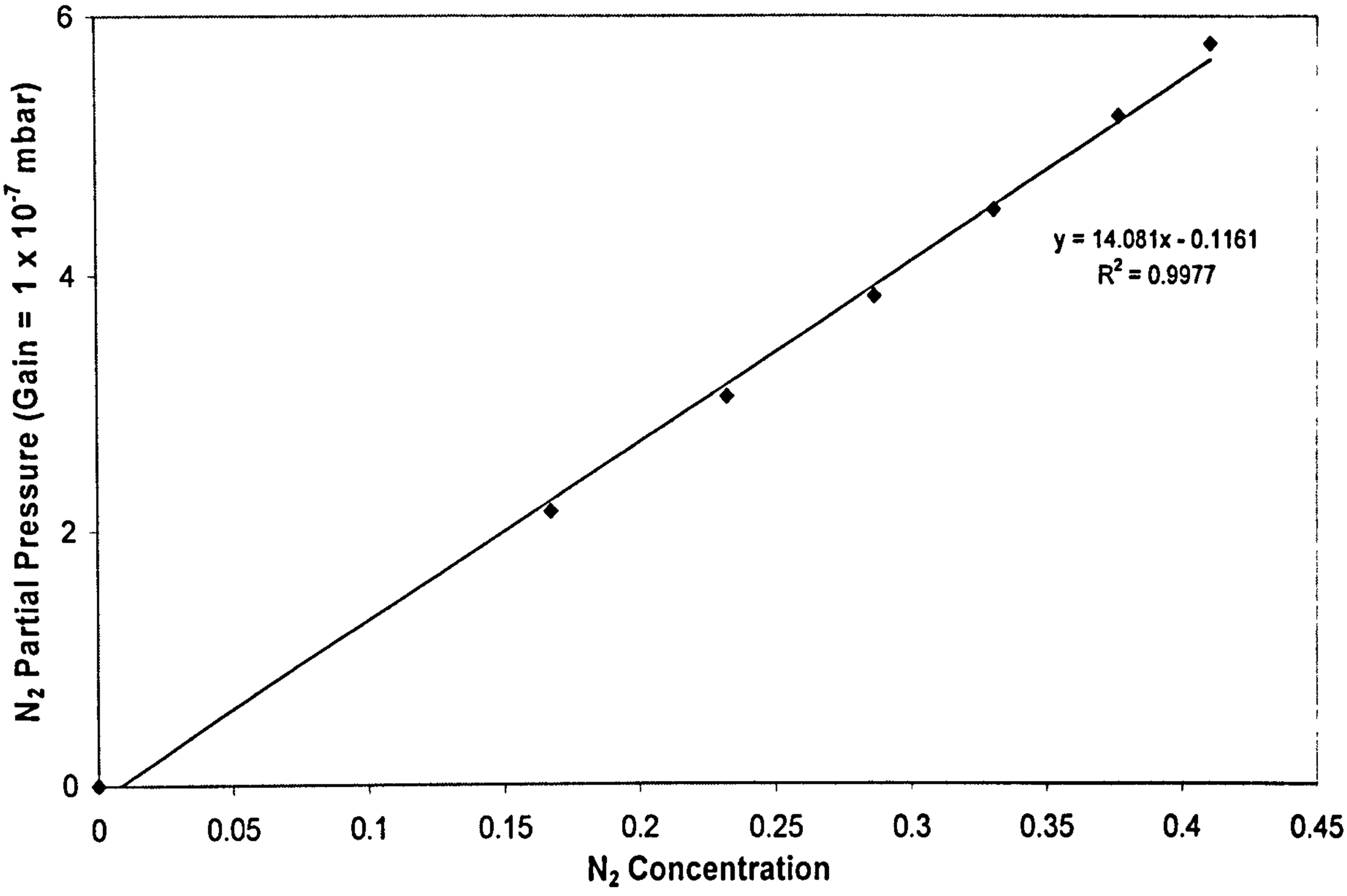

Figure VI 1 Straight line plot of N_2 partial pressure *vs* concentration of N_2 in the feed gases.

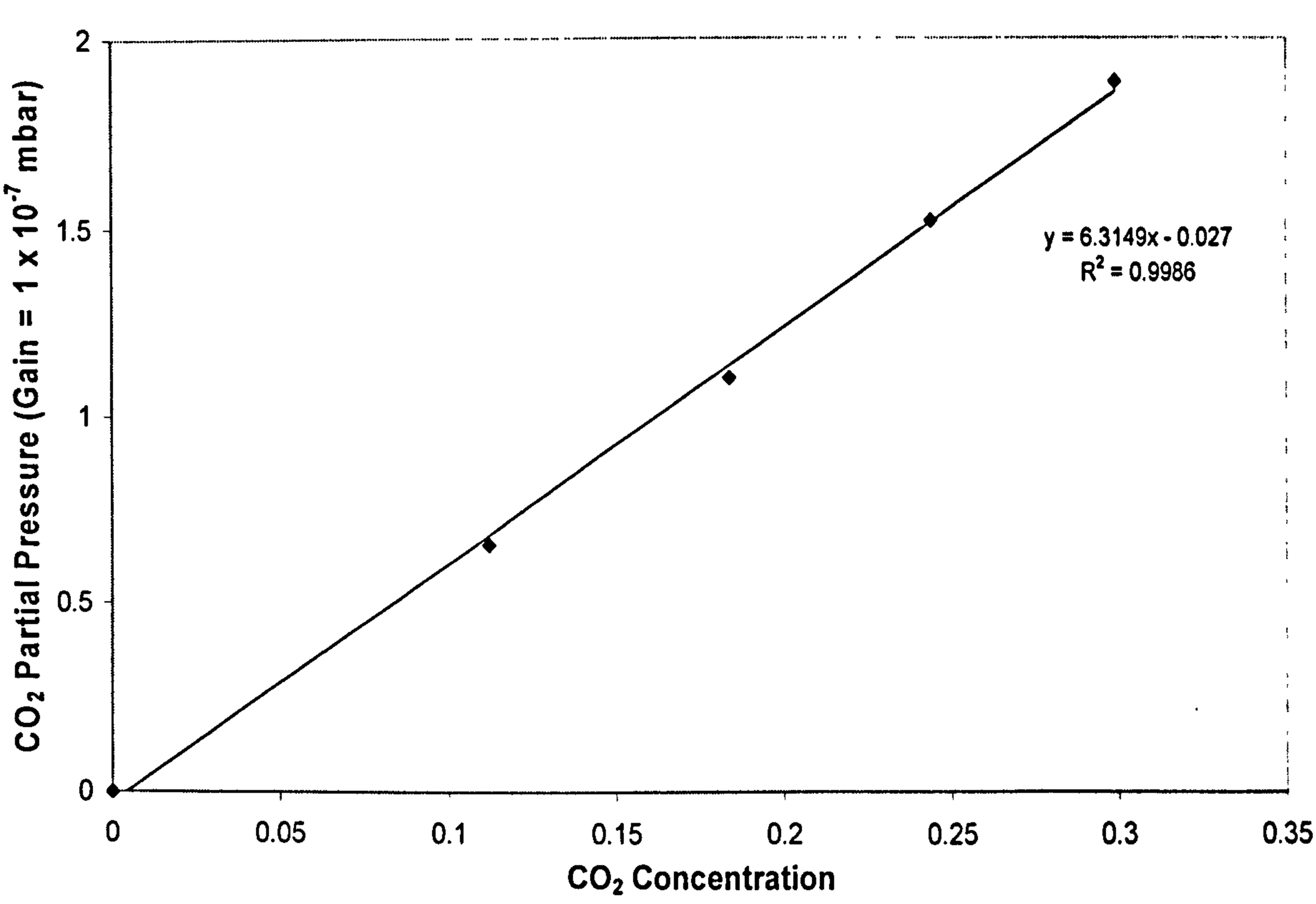

Figure VI 2 Straight line plot of N_2 partial pressure *vs* concentration of N_2 in the feed gases.

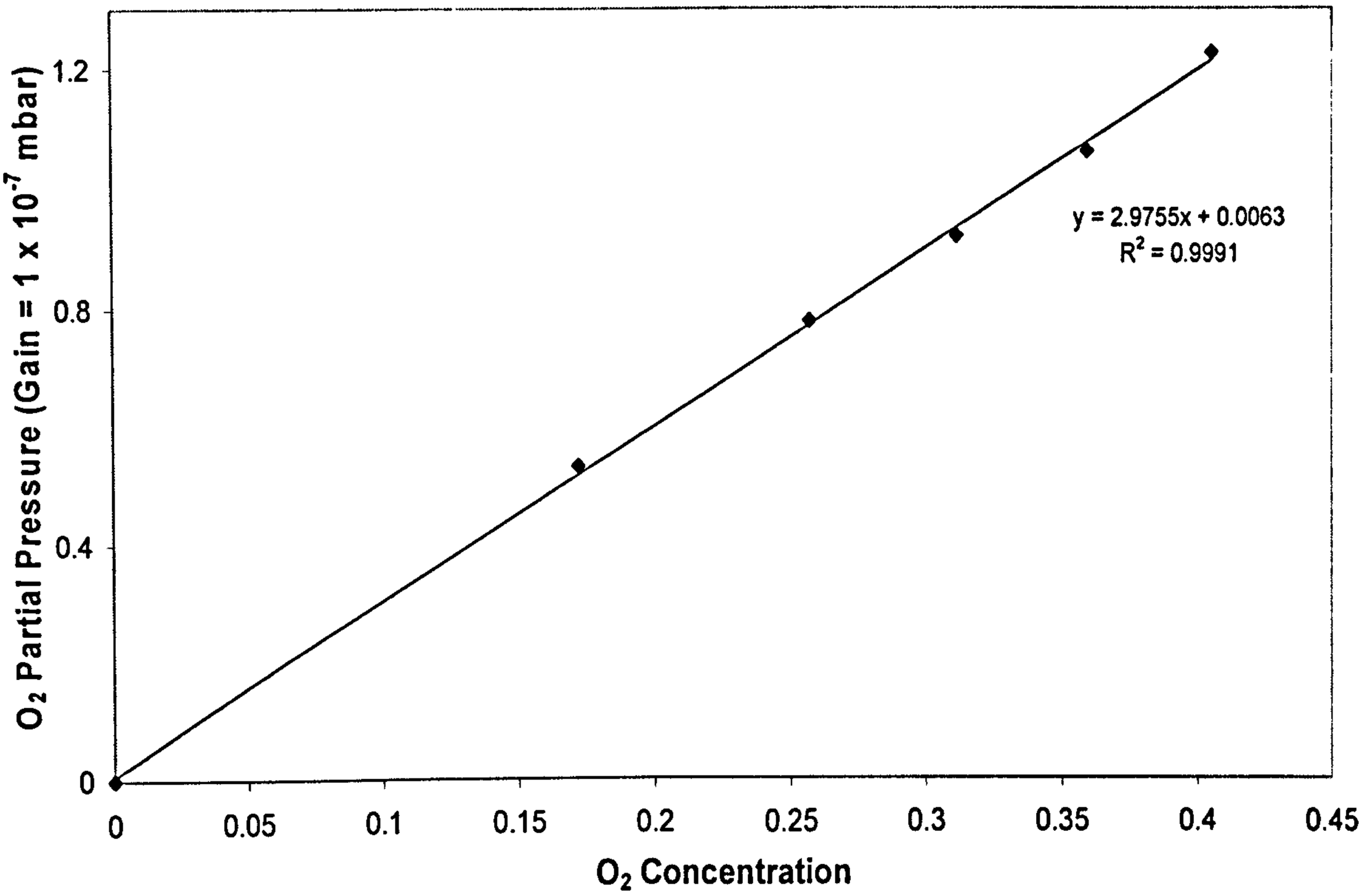

Figure VI 3 Straight line plot of N_2 partial pressure *vs* concentration of N_2 in the feed gases.

Appendix 8

LIST OF PUBLICATIONS

Journals *(Refereed)*

1. Y. Gupta, K. Hellgardt, R.J. Wakeman (2006), "Enhanced permeability of polyaniline based nano-membranes for gas separation", *J. Memb. Sci.*, **282**, 60.
2. Y. Gupta, R.J. Wakeman, K. Hellgardt (2006), "High-productivity, nanostructured polyaniline membranes for gas separation", *Desalination*, **199**, 474.
3. Y. Gupta, R.J. Wakeman, K. Hellgardt (2006), "Synthesis and gas transport studies of nano-structured polyaniline membranes", *J. Nanoscience and Technology*, (submitted).

Conferences *(Proceedings)*

1. R.J. Wakeman, Y. Gupta, K. Hellgardt (2007), "Polyaniline nano-membranes for gas separations – structure and performance", FILTECH – 2007, Wiesbaden, Germany.
2. Y. Gupta, R.J. Wakeman, K. Hellgardt (2006), "The potential of polyaniline nano-membranes for gas separations", The 10th Nordic Filtration Symposium, The Nordic Filtration Society, Norwegian University of Science and Technology, Trondheim, Norway.

Technical Conference Presentations

1. Y. Gupta, R.J. Wakeman, K. Hellgardt (2006), "Enhanced permeability of polyaniline based nano-membranes for gas separation", Advanced Membrane Technology III, Engineering Conferences International Inc., Cetraro, Italy.
2. Y. Gupta, R.J. Wakeman, K. Hellgardt (2006), "Synthesis and gas transport studies of nano-structured polyaniline membranes", 5th Annual Research Symposium, Fluid Separation Subject Group, IChemE, Sunbury, UK.
3. Y. Gupta, R.J. Wakeman, K. Hellgardt (2006), "High productivity, polyaniline nano-film membranes for gas separations", 17th Annual Meeting, North American Membrane Society, NAMS – 2006, Chicago, USA.

Technical Poster Presentations

1. Y. Gupta, R.J. Wakeman, K. Hellgardt (2005), "Enhanced permeability of polyaniline based nano-membranes", 7th World Congress of Chemical Engineering – Incorporating 5th European Congress of Chemical Engineering, Glasgow, Scotland.